

2

**DEVELOPMENT AND TESTING OF A DEVICE
CAPABLE OF PLACING MODEL PILES BY
DRIVING AND PUSHING IN THE CENTRIFUGE**

John J. Gill, Capt, USAF, PhD.

May 1989

Final Report

Approved for public release; distribution unlimited.

AD-A209 872



**A
F
W
L**

DTIC
ELECTE
JUL 10 1989
S E D

**AIR FORCE WEAPONS LABORATORY
Air Force Systems Command
Kirtland Air Force Base, NM 87117-6008**

This final report was prepared by the Air Force Weapons Laboratory, Kirtland Air Force Base, New Mexico under Job Order 2302Y202. Captain John J. Gill (NTES) was the Laboratory Project Officer-in-Charge.

When Government drawings, specifications, or other data are used for any purpose other than in connection with a definitely Government-related procurement, the United States Government incurs no responsibility or any obligation whatsoever. The fact that the Government may have formulated or in any way supplied the said drawings, specifications, or other data, is not to be regarded by implication, or otherwise in any manner construed, as licensing the holder, or any other person or corporation; or as conveying any rights or permission to manufacture, use, or sell any patented invention that may in any way be related thereto.

This report has been authored by an employee of the United States Government. Accordingly, the United States Government retains a nonexclusive, royalty-free license to publish or otherwise reproduce the material contained herein, or allow others to do so, for United States Government purposes.

This report has been reviewed by the Public Affairs Office and is releasable to the National Technical Information Service (NTIS). At NTIS, it will be available to the general public, including foreign nations.

If your address has changed, if you wish to be removed from our mailing list, or if your organization no longer employs the addressee, please notify AFWL/NTES, Kirtland AFB, NM 87117-6008 to help us maintain a current mailing list.

This technical report has been reviewed and is approved for publication.

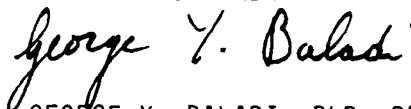


JOHN J. GILL
Capt, ISAF, PhD
Project Officer



THOMAS A. BRETZ, SR
Lt Col, USAF
Chief, Applications Branch

FOR THE COMMANDER



GEORGE Y. BALADI, PhD, PE
Technical Advisor
Civil Engrg Rsch Division

DO NOT RETURN COPIES OF THIS REPORT UNLESS CONTRACTUAL OBLIGATIONS OR NOTICE ON A SPECIFIC DOCUMENT REQUIRES THAT IT BE RETURNED.

UNCLASSIFIED

SECURITY CLASSIFICATION OF THIS PAGE

REPORT DOCUMENTATION PAGE

1a REPORT SECURITY CLASSIFICATION UNCLASSIFIED			1b RESTRICTIVE MARKINGS		
2a SECURITY CLASSIFICATION AUTHORITY			3 DISTRIBUTION / AVAILABILITY OF REPORT Approved for public release; distribution unlimited.		
2b DECLASSIFICATION DOWNGRADING SCHEDULE			4 PERFORMING ORGANIZATION REPORT NUMBER(S) AFWL-TR-89-36		
4 PERFORMING ORGANIZATION REPORT NUMBER(S) AFWL-TR-89-36			5 MONITORING ORGANIZATION REPORT NUMBER(S)		
6a NAME OF PERFORMING ORGANIZATION Air Force Weapons Laboratory		6b OFFICE SYMBOL (if applicable) NTES	7a NAME OF MONITORING ORGANIZATION		
6c ADDRESS (City, State, and ZIP Code) Kirtland Air Force Base, NM 87117-6008			7b ADDRESS (City, State, and ZIP Code)		
8a NAME OF FUNDING, SPONSORING ORGANIZATION AF Engrg and Services Center		8b OFFICE SYMBOL (if applicable)	9 PROCUREMENT INSTRUMENT IDENTIFICATION NUMBER		
8c ADDRESS (City, State, and ZIP Code) Tyndall Air Force Base, FL 32403			10 SOURCE OF FUNDING NUMBERS		
			PROGRAM ELEMENT NO	PROJECT NO	TASK NO
				2302	Y2
			WORK UNIT ACCESSION NO	02	
11 TITLE (Include Security Classification) DEVELOPMENT AND TESTING OF A DEVICE CAPABLE OF PLACING MODEL PILES BY DRIVING AND PUSHING IN THE CENTRIFUGE					
12 PERSONAL AUTHOR(S) Gill, John J., Capt, USAF					
13a TYPE OF REPORT Final		13b TIME COVERED FROM Mar 87 TO Apr 88		14 DATE OF REPORT (Year, Month, Day) 1989 May	15 PAGE COUNT 322
16 SUPPLEMENTARY NOTATION Dissertation					
17 COSATI CODES			18 SUBJECT TERMS (Continue on reverse if necessary and identify by block number)		
FIELD	GROUP	SUB-GROUP	Centrifuge, Impact.		
13	03		Piles, Granular soil, JET		
14	02		Pile-driving, Pile Drivers.		
19 ABSTRACT (Continue on reverse if necessary and identify by block number) Elastic wave propagation and the practical aspects of pile driving are discussed to develop an understanding of which aspects of pile driving must be modeled most precisely in the centrifuge. The scaling laws are developed. Design and construction of a 5 g-ton (110 g) centrifuge are presented. Construction details of the model pile placement device are discussed. The placement device has the capability of driving individual piles and can model the energy input of any single acting pile driver. The placement device can also push individual and group piles through the application of up to 1.5 million scale pounds. Static load tests can be conducted with the device. All computer software necessary for the driving, pushing, and load testing of model piles is outlined. Discussion includes all related software for model pile calibration (strain gage response to loading) and load test interpretation (deBeer method). A method of strain gaging the model piles is presented. A test series is conducted at 69.8 and 86.0 g's involving the pushing of individual, group of four, and group of five model piles based on a 35-foot long prototype pile (group) (over)					
20 DISTRIBUTION / AVAILABILITY OF ABSTRACT <input checked="" type="checkbox"/> UNCLASSIFIED/UNLIMITED <input type="checkbox"/> SAME AS RPT <input type="checkbox"/> DTIC USERS			21 ABSTRACT SECURITY CLASSIFICATION UNCLASSIFIED		
22a NAME OF RESPONSIBLE INDIVIDUAL JOHN J. GILL, Capt, USAF, PhD			22b TELEPHONE (Include Area Code) (505) 846-6471		22c OFFICE SYMBOL NTES

DD FORM 1473, 84 MAR

83 APR edition may be used until exhausted
All other editions are obsolete.SECURITY CLASSIFICATION OF THIS PAGE
UNCLASSIFIED

19. ABSTRACT (Continued)

driven 30 feet into saturated fill. All model tests are conducted on dry granular soil with relative density varying between 45 and 70 percent. All models are load tested with several being subjected to tensile pullout tests. Individual model piles are driven permitting the comparison between the load-bearing capacity of drive and pushed models.

The placement device is shown to be precise and accurate in the measurement of pile displacement and resistance to penetration. Driven individual model piles are found to have lower initial loading moduli but similar ultimate capacity to those of the pushed models. Differences are attributed to disturbance of the model during placement of load cell on the model butt prior to load testing. Bearing capacity of the model pile tips are not altered by scale effects; however, skin friction on the sidewalls decreases exponentially as test g level is increased. The model group piles demonstrate an efficiency of 1.17 with a group efficiency of 1.0 being considered conservative for group models placed in granular soils.

Accession For	
NTIS GRA&I	<input checked="" type="checkbox"/>
DTIC TAB	<input type="checkbox"/>
Unannounced	<input type="checkbox"/>
Justification	
By _____	
Distribution/	
Availability Codes	
Dist	Avail. and/or Special
A-1	



ACKNOWLEDGMENTS

An effort of this scope cannot be accomplished without the cooperation of many people and I would like to thank my many friends who helped make it possible. I am indeed fortunate to be the person to receive the credit for and benefit of all of their selfless assistance. I credit my committee for the conception of and technical assistance throughout the course of this research. Dr. Frank Townsend consistently challenged me during my brief stay at the University and thus fed my desire to pursue higher goals. I appreciate his confidence and trust in me to achieve the technically difficult project undertaken.

My utmost thanks go to Dr. David Bloomquist for his friendship, time, and encouragement, all of which were freely given. As my mentor, he provided the example of what it means to be an engineer and professional. His attitudes and approach to complex problems will serve me for years to come. I am sincerely indebted to both Drs. John Davidson and Michael McVay for their vital assistance in the proper and meaningful interpretation of the data obtained. Lastly, I thank Dr. David Jenkins for his help in providing important details on the operation of some of the finer instruments involved in this research.

I am thankful for the monetary assistance of both the United States Air Force and the Florida Department of Transportation as none of our achievements would have been possible without such help. I am most thankful to the Air Force for providing me the opportunity to pursue my education to its current level.

I wish to thank my family for their constant support, especially my sister, Dr. Barbara Carnes, for her wise counsel during this effort. Their individual contributions have helped me in ways they may not even be aware of.

My co-workers and friends at the University have helped smooth the often rocky path of these past few years. Niels Kofoed earned my admiration and respect for his finesse with the computerization of the model pile placement device operations. Jay Gabrielson and Charlie Manzione deserve much credit for their help and comic relief. I hope I may have been able to repay them in kind. Likewise, credit goes to Ken Knox and Gregory Coker for their friendship.

I take this opportunity to thank my many friends working in the civil engineering department and the engineering shop. Mr. Ed Dobson helped tremendously in the initial setup of the centrifuge. Anita Cataldo and Cheryl Holland guided me pleasantly through the financial and administrative systems. I thank Candace Leggett for her tolerance during the final weeks of typing of this dissertation. Charles Simmons, Marc Link, and Dale Wilcox were of great assistance to me at the EIES Shop. Danny Richardson, Bill Studstill, and Kirk Waite have all been willing helpers.

My wife, Carole, and daughter, Sarah, gladly shouldered the burden of my long hours at school and the many additional hours of "at-home" absence. Their patience during this process has only increased my love and respect for them.

Lastly, I thank the many people to whom I am deeply indebted yet cannot mention for lack of space. Without their assistance, this research would not have been quite as fruitful. I thank them all.

TABLE OF CONTENTS

	<u>Page</u>
ACKNOWLEDGMENTS.....	iii
LIST OF TABLES.....	viii
LIST OF FIGURES.....	ix
ABSTRACT.....	xiv
CHAPTERS	
1 INTRODUCTION.....	1
1.1 General.....	1
1.2 Objectives.....	3
1.3 Scope of Work.....	4
1.4 Review of Previous Research.....	5
2 IMPACT DRIVING OF PILES, CAPACITY PREDICTION, AND CAPACITY VERIFICATION.....	16
2.1 Introduction.....	16
2.2 Pile Placement by Impact Driving.....	17
2.2.1 Elastic Wave Propagation in Solids.....	17
2.2.2 Hammer-Pile Impact.....	23
2.2.3 Hammer-Pile-Soil Interaction.....	30
2.3 Practical Aspects of Pile Driving.....	37
2.3.1 Hammer-Cushion-Cap Interaction.....	37
2.3.2 Pile Forces Developed During Driving and Loading.....	41
2.3.3 Errors in Placement and Driving Affecting Static Capacity.....	46
2.4 Static Capacity Verification.....	48
2.5 Pile Group Behavior.....	49
3 SIMILITUDE REQUIREMENTS.....	52
3.1 Similitude Theory.....	52
3.2 Selection of Dependent and Independent Variables.....	53
3.3 Development of Scaling Laws.....	56
3.4 Experimental Requirements.....	58

4	EQUIPMENT DESIGN, FABRICATION, AND OPERATION.....	59
4.1	Model Pile Design and Instrumentation.....	60
4.1.1	Model Material Selection.....	60
4.1.2	Model Size Determination.....	61
4.1.3	Strain Gage Placement.....	64
4.1.4	Pile (Group) Cap Fabrication and Lead Wire Protection.....	74
4.2	Model Placement Device Design.....	74
4.2.1	Specimen Container, Placement Device Protec- tive Canister, and C-Channel Support Beam.....	31
4.2.2	Stepper Motor.....	86
4.2.3	Ball Screw Assembly.....	38
4.2.4	Guide Tube.....	96
4.2.5	Electromagnet.....	96
4.2.6	Model Pile Hammers.....	98
4.2.7	Model Pile Cap as an Alignment Tool.....	101
4.2.8	Proximity Device.....	104
4.2.8.1	Charge pump proximity device.....	108
4.2.8.2	Phase comparator proximity device.....	113
4.2.9	Load Cells.....	117
4.3	Centrifuge Design.....	117
4.3.1	In-Place Equipment.....	119
4.3.2	Shroud Construction.....	120
4.3.3	Main Arm Modification.....	123
4.3.4	Cover Construction.....	123
4.3.5	Slip Ring Placement.....	127
4.3.6	Rotational Speed Monitoring.....	129
4.3.7	Specimen Platform Construction.....	132
4.3.8	Closed Circuit Television.....	136
4.4	Model Pile (Group) Set-Up Procedure.....	138
4.5	Computer Control of the Equipment.....	145
4.5.1	Hardware.....	146
4.5.1.1	Hewlett-Packard 9000 series, model 216 computer.....	146
4.5.1.2	Hewlett-Packard 6940B multiprogram- mer and 59500A interface unit.....	146
4.5.2	Software.....	155
4.5.2.1	Main Programs.....	157
4.5.2.2	Subroutines.....	167
4.6	Data Collection and Recording Equipment.....	173
4.6.1	Hardware.....	173
4.6.1.1	Hewlett-Packard 3497A Data Acquisi- tion/Control Unit.....	173
4.6.1.2	Transducers.....	173
4.6.2	Software.....	195
4.7	Equipment Limitations.....	195
5	SPECIMEN PREPARATION, TEST RESULTS, AND DISCUSSION.....	211
5.1	Soil Description and Specimen Characterization.....	212
5.2	PUSHPILE and PUSHGROUP Test Results.....	217
5.2.1	Qualitative Discussion of Pushed Model Pile Test Results.....	217

5.2.2	Quantitative Discussion of Pushed Model Pile Test Results.....	238
5.3	DRIVEPILE Test Results.....	254
5.3.1	Qualitative Discussion of Driven Model Pile Test Results.....	254
5.3.2	Quantitative Discussion of Driven Model Pile Test Results.....	264
5.4	Reproducibility of Results.....	267
5.5	Modeling of Models.....	269
5.6	Comparison with a Prototype.....	270
5.7	Strain Measurement.....	272
6	CONCLUSIONS AND RECOMMENDATIONS.....	276
6.1	Conclusions.....	276
6.2	Recommendations.....	281
APPENDICES		
A	PI TERM DERIVATION AND SCALING LAW DEVELOPMENT.....	283
B	NUMBER THEORY AND DIGITAL, OCTAL, AND DECIMAL CONVERSION ALGORITHMS.....	293
REFERENCES.....		296
BIOGRAPHICAL SKETCH.....		303

LIST OF TABLES

<u>Table</u>	<u>Page</u>
3-1 Independent and Dependent Variables.....	55
3-2 Scaling Relationships.....	56
4-1 Model Pile Dimensions and Scale Factors.....	62
4-2 Model Hammer Weights and Dimensions.....	100
4-3 Platform Specifications and Factor of Safety Computations....	137
4-4 Multiprogrammer Operating Mode Codes.....	151
4-5 Stepper Motor Response to Commanded Rotation at Test g-Levels.....	206
5-1 Pushed Pile (Group) Model Test Series.....	223
5-2 Pushed Pile (Group) Load Test Results.....	246
5-3 Pile Group Factors Based on deBeer Capacities.....	249
5-4 Initial Loading Curve Slope, Elastic Deformation Curve Slope and Resulting Soil Response for Individual and Group Model Piles.....	251
A-1 Pissets Input Matrix.....	284
A-2 Pi Terms.....	285
A-3 Scaling Law Derivation.....	286

LIST OF FIGURES

<u>Figure</u>	<u>Page</u>
2-1 Propagation of an Elastic Wave.....	20
2-2 Idealized Reflections of an Elastic Wave. a) Reflection from Stress-Free End Rods; b) Reflection from Fixed End Rods.....	24
2-3 Idealized Hammer and Pile Before Impact.....	25
2-4 Mechanism of Impact of a Cylindrical Hammer on a Finite Cylindrical Rod.....	28
2-5 Effect of Impedance Ratio on the Theoretical Wave Shape for Same Hammer Mass and Drop.....	31
2-6 Finite Difference Pile Representation.....	34
2-7 Finite Element Mesh Pile Representation.....	36
2-8 Definition of Pile Cap Terminology.....	38
4-1 Model Piles. a) Individual Model Piles (Left to Right--49.3, 57.5, 69.3 and 86.0 g models); b) Model Pile Groups (Left 69.8 g., Right 36.0 g).....	63
4-2 Micromasurements EA-06-015LA-120 Strain Gages.....	66
4-3 Strain Gage Application Technique.....	67
4-4 Alternate Technique for Placement of First Pair of Strain Gages When Multiple Pairs are Needed.....	70
4-5 Suggested Gage Positions and Position Designations for Individual Driven and Pushed Piles (8 Strain Gage Channels Available). a) Driven Pile, Four Pair of Strain Gages; b) Pushed Pile, Four Pair of Strain Gages and Load Cell.....	72
4-6 Suggested Gage Positions and Position Designations for Driven and Pushed Pile Groups (Load Cell Placed on Top After DRIVEPILE; Load Cell In Place During PUSHPILE).....	73
4-7 Pile Cap Assembly for Individually Driven Model Piles.....	75

4-3	Pile Cap Assembly for Driven Model Pile Groups.....	76
4-9	Pile Cap Assembly for Individually Pushed Model Piles.....	77
4-10	Pile Cap Assembly for Pushed Model Pile Groups.....	78
4-11	Specimen Container, Placement Device Protective Canister, and C-Channel Support Beam.....	30
4-12	Top View of Canister and Placement Device Configuration. a) Configuration Used for Video Recording; b) Normal Configuration.....	33
4-13	Platform Mechanical Stops.....	35
4-14	Stepper Motor Transformer and Variable Power Resistors.....	39
4-15	Bodine Type THD-1830E Adjustable Motion Control.....	39
4-16	Stepper Motor Control Circuit and Slip Ring Channel Assignments.....	90
4-17	Ball Screw Assembly, Thrust Bearings, and Reaction Clamp.....	93
4-18	Electromagnet Actuator Circuit and Slip Ring Channel Assignments.....	99
4-19	Pile Cap, Hammer, and Electromagnet Configuration for Driving Sequence.....	102
4-20	Guide Rod Length Determination (69.8 g's).....	103
4-21	Charge Pump Proximity Device Schematic Drawing.....	109
4-22	Charge Pump Proximity Device.....	110
4-23	Charge Pump Proximity Power and Output Signal Circuit and Slip Ring Channel Assignments.....	112
4-24	Phase Comparator Device Schematic Drawing.....	114
4-25	Basic Phase Locked Loop Circuit.....	115
4-26	Load Cell Power and Output Signal Circuit and Slip Ring Channel Assignments.....	118
4-27	Centrifuge Main Power Transformer.....	121
4-28	Parajust AC Motor Speed Control.....	121
4-29	Hand-Held Centrifuge Speed Control.....	122

4-30	Centrifuge Main Circuit Breaker and Resistive Speed Brake....	122
4-31	Completed Centrifuge Shroud.....	124
4-32	Pillow Block Bearing Support Plates Fastened at the Ends of Each Arm.....	124
4-33	Centrifuge Cover, Access Opening and Slip Ring Housing.....	125
4-34	Centrifuge Power Requirements and Performance Characteristics.....	126
4-35	Electric and Hydraulic Slip Ring Assembly.....	128
4-36	Slip Ring Assembly In-Place.....	130
4-37	Pulse Generator and Slotted Disk.....	130
4-38	Rotational Speed Monitoring and Control Circuit.....	131
4-39	Equipment for Monitoring Centrifuge Rotational Speed. a) Photoelectric Tachometer; b) Display Unit.....	133
4-40	Orthographic Projection of Centrifuge Platform.....	134
4-41	Completed Platform.....	135
4-42	Platform In-Place.....	135
4-43	Closed Circuit Television Power Supply and Output Signal Circuit and Slip Ring Channel Assignments.....	139
4-44	Hewlett-Packard 9000 Series, Model 216 Computer.....	147
4-45	Hewlett-Packard 59500A Interface Unit and 6940B Multiprogrammer.....	149
4-46	Computer Variable Designations.....	158
4-47	Model Pile Calibration Equipment. a) Model Pile Calibration Accessories; b) In-Place.....	166
4-48	Hewlett-Packard 3497A Data Acquisition/Control Unit.....	174
4-49	Resistance Circuit Element.....	181
4-50	Wheatstone Bridge Circuit.....	182
4-51	Three-Wire Circuit for Strain Measurements.....	186
4-52	On-Board Bridge Completion Circuit for Strain Gages (8 Channels Available).....	188

4-53	On-Board Bridge Completion Unit and Slip Ring Channel Assignments.....	190
4-54	Cross Section of a Linear Voltage Differential Transformer (LVDT).....	192
4-55	LVDT Power Supply Circuit and Signal Output.....	194
4-56	Maximum Payload Operating Capacities vs. RPM.....	197
4-57	Stepper Motor and RVDT in Test Position.....	205
4-58	Placement Device and LVDT in Test Position.....	208
4-59	Ball Screw Response to Stepper Motor Drive Shaft Rotational Displacement (\pm 1600 Step Displacement, 40-Step Displacement Increment).....	209
4-60	Ball Screw Response to Stepper Motor Drive Shaft Rotational Displacement (\pm 200 Step Displacement, 1-Step Displacement Increment).....	210
5-1	Specimen Preparation "Chimney" and Associated Tools.....	214
5-2	Specimen Containers.....	216
5-3	Pile Penetration vs. Load, Single Pile, PG69812072, PG69812073.....	219
5-4	Pile Penetration vs. Load, Single Pile, PG69812151, PG69812154.....	221
5-5	Pile Penetration vs. Load, Single Pile, PG86012153, PG86012181.....	222
5-6	Pile Penetration vs. Load, Single Pile, PG69804013, PG69804011, PG69804021.....	224
5-7	Pile Penetration vs. Load, Single Pile, PG86004014, PG86004012, PG86004022, PG86012172.....	226
5-8	Group Penetration vs. Load, Group of Four PG69802251, PG69802252, PG69802253.....	228
5-9	Group Penetration vs. Load, Group of Four, PG86002244, PG86002243, PG86002242.....	230
5-10	Group Penetration vs. Load, Group of Five, PG69804023, PG69804051, PG69802254.....	232
5-11	Group Penetration vs. Load, Group of Five, PG86002231, PG86002232, PG86002241.....	234

5-12	Change (%) in Total Frictional Resistance to Pull-Out With Respect to the Change (%) in Model Pile-Soil Contact Area (Referenced to Single 86.0 g Model).....	239
5-13	Bearing Capacity of Single Pile, deBeer, 04013LOAD, 04011LOAD, 04021LOAD.....	240
5-14	Bearing Capacity of Single Pile, deBeer, 04014LOAD, 04012LOAD, 04022LOAD, 12172LOAD.....	241
5-15	Bearing Capacity of Pile Group, deBeer, Group of Four, 02251LOAD, 02252LOAD, 02253LOAD.....	242
5-16	Bearing Capacity of Pile Group, deBeer, Group of Four, 02244LOAD, 02243LOAD, 02242LOAD.....	243
5-17	Bearing Capacity of Pile Group, deBeer, Group of Five, 04023LOAD, 04051LOAD, 02254LOAD.....	244
5-18	Bearing Capacity of Pile Group, deBeer, Group of Five, 02231LOAD, 02232LOAD, 02241LOAD.....	245
5-19	deBeer Method Model Pile Capacity vs. Specimen Relative Density.....	247
5-20	Butt Deflection (inches) at Failure vs. Failure Load (kips) Using the deBeer Method of Capacity Determination.....	252
5-21	Per Cent Increase in Soil Stiffness vs. Increase in Number of Piles.....	253
5-22	Pile Penetration vs. Number of Hammer Blows, Single Pile, DG69803171.....	255
5-23	Pile Penetration vs. Number of Hammer Blows, Single Pile, DG69803282, DG69803181.....	257
5-24	Pile Penetration vs. Number of Hammer Blows, Single Pile, DG69803251, DG69803281.....	258
5-25	Pile Penetration vs. Number of Hammer Blows, Single Pile, DG69803291, DG69803292, DG69832182.....	260
5-26	Butt Deflection vs. Load, Single Pile, DG69803293.....	261
5-27	Hammer Blows (100% Efficiency, 20 Gram Hammer) for 30 Scale Feet of Penetration vs. Specimen Relative Density.....	265

Abstract of Dissertation Presented to the Graduate School
of the University of Florida in Partial Fulfillment of the
Requirements for the Degree of Doctor of Philosophy

DEVELOPMENT AND TESTING OF A DEVICE CAPABLE OF PLACING MODEL
PILES BY DRIVING AND PUSHING IN THE CENTRIFUGE

By

John Joseph Gill

August 1988

Chairman: Frank C. Townsend
Major Department: Civil Engineering

Elastic wave propagation and the practical aspects of pile driving are discussed to develop an understanding of which aspects of pile driving must be modeled most precisely in the centrifuge. The scaling laws are developed. Design and construction of a 5 g-ton (110 g) centrifuge are presented. Construction details of the model pile placement device are discussed. The placement device has the capability of driving individual piles and can model the energy input of any single acting pile driver. The placement device can also push individual and group piles through the application of up to 1.5 million scale pounds. Static load tests can be conducted with the device. All computer software necessary for the driving, pushing, and load testing of model piles is outlined. Discussion includes all related software for model pile calibration (strain gage response to loading) and load test interpretation (deBeer

method). A method of strain gaging the model piles is presented. A test series is conducted at 69.3 and 86.0 g's involving the pushing of individual, group of four, and group of five model piles based on a 35-foot long prototype pile (group) driven 30 feet into saturated fill. All model tests are conducted on dry granular soil with relative density varying between 45% and 70%. All models are load tested with several being subjected to tensile pullout tests. Individual model piles are driven permitting the comparison between the load-bearing capacity of drive and pushed models.

The placement device is shown to be precise and accurate in the measurement of pile displacement and resistance to penetration. Driven individual model piles are found to have lower initial loading moduli but similar ultimate capacity to those of the pushed models. Differences are attributed to disturbance of the model during placement of load cell on the model butt prior to load testing. Bearing capacity of the model pile tips are not altered by scale effects; however, skin friction on the sidewalls decreases exponentially as test g level is increased. The model group piles demonstrate an efficiency of 1.17 with a group efficiency of 1.0 being considered conservative for group models placed in granular soils.

CHAPTER 1 INTRODUCTION

1.1 General

Piles have been used to provide for a suitable foundation for man-made structures for over 12,000 years. Their suitability as a foundation has been left to chance, sometimes inferred from empirical relationships, less often determined by some fairly scientific method relying on known soil properties, and, least of all, determined by full-scale on-site testing. These approaches have led to outright failure, unacceptable performance, or overconservative design of many of the successful pile foundations. While full scale testing may provide the most accurate information regarding pile performance at the construction site, it is undeniably the most expensive and time consuming method. Additionally, only a limited number and type of tests can be performed on the prototype.

The mechanisms of soil behavior are still subject to interpretation as evidenced by the wide variety of pile capacity prediction techniques available. Furthermore, the variability of soil deposits limits the accuracy with which capacities can be predicted. The nonstandardization of some sampling techniques and their interpretation contributes to the uncertainty and sometimes leads to errors in the determination of the properties on which capacity predictions are based. Lastly, there is a lack of sufficient data regarding the performance of pile foundations and the properties of the soil on which they are founded. The high cost

of obtaining such information and the few sites suited to provide useful results are limiting factors (Harrison, 1983).

Geotechnical engineers rely on theoretical and empirical relationships to aid in the design of pile foundations. Using these relationships requires an accurate knowledge of subsoil conditions. This knowledge is becoming more readily available from increasingly accurate in situ testing; however, the in situ soil properties can change dramatically as a result of placement of the foundation.

Researchers have made use of prototype data, but the lack of information has made the investigation of models attractive. Initial investigations involved pile performance using miniature models in a one-gravity environment. These efforts have been expanded to include the investigation of scale model pile performance in a high gravity environment. This high gravity environment is most frequently generated by the use of a centrifuge. Recent developments in small-scale testing present several alternatives to the problems described above. Piles as small as 1/100 the size of the prototype have successfully been tested in high gravity environments which reproduce the same unit stresses at equivalent locations in the model as are experienced by the prototype. Furthermore, various in situ tests are being adapted for use in the centrifuge through innovative research. This combination of modeling and the ability to characterize the soil adjacent to the model permits the engineer to conduct parametric studies revealing more about how changing soil properties affect the bearing capacity, deformation, and load transfer mechanism of piles subjected to static loads.

Several significant aspects must be considered for one to attempt strict modeling of pile performance at a reduced scale. First, scaling

Laws must be developed allowing the engineer to construct a model which will react both dynamically and statically to a scale load as would the prototype. The scaling laws, based on similitude, are needed both for the design of the model and interpretation of the model response. Second, strict modeling of piles requires that a dynamic pile driver be developed to ensure the piles are placed in the same way as in the prototype. This stipulation lessens the current need to infer results from load tests on piles that have been inserted statically (pushed) rather than driven. Lastly, a method must be developed to measure the load transfer from the pile to the soil during placement as well as loading.

The ability to perform the aforementioned tasks will permit parametric studies of a variety of pile types over a wide range of soil conditions. This is very advantageous as the soil conditions of the prototype are quite often impossible to reproduce exactly in the model. Furthermore, a large number of tests can be conducted at an insignificant cost when compared to prototype testing. Interaction between the individual piles of a group and group response can also be studied. This report documents the development and testing of the equipment designed to accomplish the aforementioned goals. The results of all tests conducted in association with the development of the model pile placement device will be presented.

1.2 Objectives

The objectives of this research program are as follows:

- 1) To design and build a device capable of driving and load testing model piles (groups) in-flight in the artificially high gravity environment generated in a centrifuge. The device must also be

capable of pushing model piles (groups) into place and load testing the pile (group) after placement.

- 2) To develop the computer software necessary to control the pile placement device.
- 3) To instrument the model piles (groups) and develop the means of measuring butt deflection and residual stress development in the model subjected to static loading at design gravity level.
- 4) To drive or push model piles (groups) into homogeneous, dry, granular soils and compare the differences, if any, between static capacity, residual stress development during placement, and load shedding to the soil during subsequent loading.
- 5) To discern the effects of various gravity levels on the accuracy of the model by conducting tests on scale models at 69.8, and 36.0 gravities. The validity of the scaling laws used evaluated in this manner and possible effects on the contribution of relative grain size to the modeled capacity are explored.
- 6) To determine the feasibility of using the device to predict prototype pile capacity by modeling a well-instrumented pile group.

1.3 Scope of Work

The wave equation used in the development of pile stress, strain, and particle velocity magnitudes during driving is presented. The theoretical effects of variation of hammer and pile configurations are explored. The practical aspects of pile driving are presented to foster an understanding of the system parameters which must be most closely modeled. Scaling relationships are developed permitting the determination of performance capabilities of the placement/loading device.

A complete pile placement (both driving and pushing) and loading device and associated computer control hardware/software system are designed, built, and tested. Data measurement, recording, and presentation techniques are developed. A "gravity-level independent" means of testing and data capture is employed to permit the use of this device for testing of a variety of scale models.

Model piles (groups) are driven and pushed in the range of 70 to 90 gravities and subsequently loaded statically. Static resistance developed versus deflection of the butt (cap) is measured and ultimate capacity is recorded. The validity of the scaling relationships is verified.

1.4 Review of Previous Research

Two major areas of interest exist in the centrifugal modeling of piles and pile groups. First, the centrifuge must be shown to be a valid tool for use in the modeling process. Second, the technical aspects of building, placing, and testing the models must be understood. The earliest pile model studies involved placement and load testing of miniature piles at one gravity. Results from these studies indicated the need to recreate stresses at the model pile-soil interface that were similar to the stresses experienced by the prototype. This is most easily accomplished in a centrifuge. Initial centrifuge studies were concerned with the placement of model piles at one gravity with subsequent load tests being conducted at the design test gravity level. Several research efforts have since been conducted regarding the in-flight placement of model piles with subsequent load tests.

Early tests conducted on miniature piles in the United States, Whitaker (1957), Saffery and Tate (1961), and Sowers et al. (1961), provided only qualitative results and a cursory understanding of pile-group load factors. Model piles for these tests were typically nine to twelve inches long, pushed into the tests specimen, and loaded incrementally to failure. Results of these tests could not be directly related to prototype performance using available scaling laws (Rocha, 1957) because the unit stresses at the tip and along the side walls of the piles were *not being reproduced*. Additionally, the previously stated irregularities inherent in soil deposits made modeling of prototype soils infeasible. Scott (1977) conducted tests on model piles pushed into a silt at one gravity and laterally loaded after being accelerated to 50-70 g's. Results were reproducible and internally consistent in the sense that stiffer soils resulted in a model with greater resistance to lateral displacement. However, no prototype was available for comparison. Similitude and the use of scaling laws was not verified. Most significantly, this research demonstrated the feasibility of conducting load tests on miniature piles in the centrifuge. Hougnon (1980) demonstrated similitude by modeling the response of individual and group tapered wooden piles subjected to axial and lateral loads. The wooden piles, 0.2 in. in diameter, were tested at 70 g's. The models were scaled to represent the prototype wooden piles driven 35 feet into the ground at Lock and Dam #26, near Alton, Illinois. Problems associated with the development of a functional loading device limited the applicability of the results. Furthermore, the five-unique soil layers of the prototype were replaced in the model by a homogeneous, uniform specimen supposedly having strength characteristics

similar to the average strength characteristics of the prototype. Problems associated with the preparation of uniform soil specimens limited the applicability of the results; however, useful data was obtained concerning the qualitative effects of pile taper and soil density on the capacity of the model piles. Centrifugal tests investigating the axial capacity of modeled steel cylindrical piles, Ryan (1983), United States Department of Transportation/Federal Highway Administration (USDOT/FHWA, 1984c), and Millan (1985), refined the techniques associated with pile placement and data retrieval. Results of those studies further established the centrifuge as a valid tool for use in the investigation of prototype pile capacities. Problems associated with the construction of model piles, application of scale loads, and measurement of resulting displacements will now be discussed.

Model piles used in the investigation of prototype response to axial loading have progressed from relatively crude noninstrumented cylindrical tubes, Whitaker (1957), and Saffery and Tate (1961), to fairly complex machined aluminum tubes of scale proportions and instrumented to measure stresses and strains at various depths while being statically loaded in the centrifuge, (USDOT/FHWA, 1984a, 1984b, 1984c; Millan, 1985). That progression will now be outlined.

Although Scott (1977) has been credited with conducting some of the earliest centrifugal pile capacity tests in the United States, Hougnon (1980) is among the first to attempt verification of scaling laws. Models were miniature (1/70th scale) replicas of tapered wooden piles and were constructed of wood with strength properties similar to those of the prototype. The models were not individually instrumented to

measure stresses developed during loading. Rather, the pile was loaded using a hydraulic cylinder with displacement being measured by a linear variable differential transformer (LVDT). This technique provided information regarding butt deflection versus applied load but difficulties in modeling the prototype soil conditions made comparison of the model response with the prototype inappropriate.

Harrison (1983) pioneered a technique which subsequently became the standard for the manufacture of model piles. His method consisted of removing half of an aluminum tube exposing the inside which then permitted the placement of strain gages along the shaft. Two halves with opposing strain gages were then glued together forming an instrumented model pile. Harrison tested models placed in granular soil at one gravity and loaded after being accelerated to 50 g's, concluding the presence of the seam along the length of the model influenced both axial and lateral response to loading. Significant departure from the prototype response resulted from the model's splitting during placement (by hydraulic cylinder) and loading. Harrison cited the smallness of the available gage sites on the inside of the model pile halves as the limiting factor in the use of the split-tube method of strain gage application. Furthermore, he concluded the presence of the epoxied seams, where the model halves were joined, influenced the model's response to lateral loading to a greater extent than the response to axial loading. Ryan (1983), Ko et al. (1984), and the USDOT/FHWA (1984c), and Millan (1985) conducted further tests making models using the split-tube technique.

Ryan (1983) conducted the preliminary work for Millan at the University of Florida. Ryan's work involved the construction, calibration,

and preliminary testing of 0.25 inch outside diameter, five-inch long aluminum tubes which had five pairs of strain gages installed. The models were not scaled down from a chosen prototype. Rather, the one size pile was to be tested at 30, 45, and 60 g's. Significant difficulty was encountered in the construction of the instrumented model piles. Strain gages which appeared to be properly installed did not provide accurate and reproducible readings. The epoxy used to glue the halves together was found to stiffen with time precluding the determination of a repeatable calibration curve. Rather, the piles had to be calibrated before each test to determine model response to loading. Lastly, the calibration of such models at one gravity with the model being unsupported over the five-inch length disclosed the susceptibility of the model to be influenced by stress concentrations at the butt and tip. Some reduction in the variation in strain during static loading was accomplished by the introduction of a load-eccentricity-reducing support at the tip and butt during calibration. Strain gage readings during in-flight testing were found to be adversely affected by the need to transmit the strain gage response through the slip rings prior to bridge circuit completion. Additionally, vibration and strain of the gage leads was found to influence the accuracy of the readings obtained.

Ko et al. (1984) achieved greater success with the split tube technique and tested model piles at 50 and 70 g's in granular soil. Individual piles were pushed in either at one gravity or the appropriate test gravity level and results of load tests conducted for both at the test g-level compared. The relative accuracy of the results indicated the need to both place and load test the model pile at the design test g-level. Subsequent tests involved the insertion and loading of an

individual pile in one continuous flight of the centrifuge and comparing the load test results with a model pile inserted during one flight and loaded after stopping and restarting the centrifuge. The results indicated that interrupting the insertion and loading cycle by stopping the centrifuge had no significant effect on pile capacity. Ko concluded that in granular soils similar to those tested, it is important to conduct both insertion and load testing at the appropriate test gravity level to ensure that self-weight soil stresses on the model are geometrically similar to those developed on the prototype. Results of this study indicated the potential for studying pile groups by sequential insertion of individual piles and load testing after the piles had been capped.

The FHWA tests were conducted in granular soils using instrumented piles at 70 g's (split-tube method of strain gage installation) with several noninstrumented piles being tested at 50 and 100 g's to verify modeling of models. Specially manufactured miniature "coupons" were inserted between the pile and hydraulic cylinder to measure the force required to insert and load the piles. Deflection measurements were taken by an LVDT attached directly to the pile butt. Strain gages were placed in the tip and at the butt of the pile permitting separation of tip capacity from the total force required to push and load the pile. Side wall frictional forces were inferred by subtracting the measured tip capacity from the total force required to push the pile. The strain gages placed at uniform intervals along the shaft indicated the side wall unit friction increased only slightly, but uniformly as the model pile depth of penetration increased. Between 70% and 95% of the total capacity was derived from the tip for the individual piles tested

(USDOT/FHWA, 1984a). Tests by the FHWA involving the insertion of models at test gravity levels, stopping the centrifuge, and restarting before load testing, supported the findings of Ko et al. It was concluded that stopping the centrifuge had no effect on the subsequent performance of the pile embedded in sand when the load test was conducted at the appropriate g-level.

Millan (1985), using piles similar to those tested by Ryan, conducted load tests in granular soils with the same size pile being tested at 30, 45, and 60 g's. The specimens were created by suspending the model piles within the centrifuge bucket and raining soil into the container. This was done to avoid the potential damage to the model resulting from pushing the pile in at the test g-level. Millan scaled the results at the three test g-levels to prototype capacity concluding modeling of models was a valid means of verifying the scaling relationships. Furthermore, the scaling relationships appeared to be valid as pile capacities were within $\pm 20\%$ of the predicted prototype capacity using the capacity prediction method of Meyerhof (1976). Differences between the actual and predicted capacities were attributed to the instrumentation shortcomings outlined by Ryan and the method of placement of the model.

Harrison (1983), Ko et al. (1984), and the USDOT/FHWA (1984c), and Millan (1985) all recognized the sensitivity of ultimate model pile capacity to changes in the relative density of the granular soil specimen. The increase in bearing capacity resulting from an increase in the relative density of the specimen was noted regardless of the method of placement of the pile in the soil as long as the model capacity was measured at the appropriate test gravity level. Ryan

(1983) and Millan (1985) mention the impracticality of creating a specimen with the exact values of prototype relative density and coefficient of friction as limiting factors in the use of centrifugal models for the prediction of specific prototype pile (group) capacities. The use of parametric studies over a suitable range of soil conditions is suggested. The variability of naturally occurring soil deposits further supports the need for parametric studies.

The insensitivity of ultimate model pile capacities to temporary pauses in the rotation of the centrifuge makes the study of group piles possible by the progressive insertion of individual piles in the appropriate group pattern with subsequent capping prior to load testing. This technique was used by Harrison (1983), Ko et al. (1984) and the USDOT/FHWA (1984c). Each recognized the progressive increase in resistance to penetration of individual piles due to the presence of the pile(s) which had already been placed. After all the piles had been placed, the groups were capped by bolting a multipiece cap in place which rested on and clamped around the individual butts. The inability to model the proper connection between butt and cap has been perceived to alter the results (Harrison, 1983). Tightening of the cap pieces around the piles inevitably led to the exertion of a lateral load on some or all of the piles. This resulted in improper or inefficient transfer of axial load to the piles. Pile groups capped in this manner were pushed between 6 and 12 scale inches further into the specimen prior to load testing in order that proper seating could be assumed. The desired reduction in lateral forces has not been verified. Each pile in the groups tested was inserted through a spacing template which rested on the specimen surface, the intent being to ensure the piles

were precisely spaced in all tests of the same group configuration. Excavation of the soil from around the model group subsequent to load testing was used to provide a qualitative input to the data obtained.

Ryan (1983) and Millan (1985) attempted to reduce the development of lateral forces on the individual piles of a group by manufacturing a one-piece cap and attaching the individual piles to the base of the cap. As mentioned previously, specimens were then created by raining soil around the suspended cap and piles. Millan reported relatively low group efficiencies (less than 1.0) while the USDOT/FHWA, (1984a) reported higher than expected group efficiencies (greater than 1.0). The author suggests the lower efficiencies reported by Millan are due to the method of placement of the pile group and the higher efficiencies of the FHWA may be attributed to the incomplete erasure of the lateral stresses induced by placement of the multipiece cap. Millan (1985) reported scouring directly under the cap due to wind turbulence during testing. The effect of the removal of soil from around the cap base was not determined.

The most significant remaining variable in the study of pile capacity using the centrifuge as a modeling tool is the degree of realism achieved by inserting the pile rather than driving as is normally done with the prototype. Field piles are driven by a variety of weights falling a specified distance to impart a certain impact energy on the pile butt. A wide variation is found in the means of imparting this energy, for example, falling weights, single- and double-acting diesel hammers, etc.

Researchers suggest the difference in method of model pile placement may have a significant effect on the ultimate capacity of the

model. The variation has been attributed to the creation of stresses at the pile-soil interface which are dependent on the method of placement.

Ko et al. (1984, p.167) cited the relative density and coefficient of friction of the soil specimen "in the zone of disturbance of the pile" as the controlling factors determining ultimate model pile capacity. Ryan (1983) and Millan (1985) noted that the soil properties at the pile-soil interface may not bear any resemblance to the original properties after placement of the pile and the degree of disturbance due to the pile placement method may alter the ultimate capacity. The difference between insertion of a model pile either prior to or during acceleration of the specimen and driving of the model under the influence of centrifugal acceleration is speculated to affect the type and magnitude of soil disturbance and lateral stresses around the pile.

The installation of the pile by the steady jacking force likely created a zone of disturbed soil adjacent to the pile. The disturbance produced by the pile installation probably affected the structure of the sand for a distance of approximately one diameter around the pile circumference as shown by Vesic (1977) for dense sand. The method of pile installation, i.e., a steady jacking force versus dynamic repeated blows, could affect the nature and extent of soil disturbance.

(USDOT/FHWA, 1984c, p. 66)

Researchers agree the effect on pile behavior from different methods of placement should be investigated (Ko et al., 1984; USDOT/FHWA, 1984a, 1984c; Millan, 1985). Such an investigation requires the development of a device to dynamically drive the pile in the centrifuge until the desired penetration is achieved. Model load tests equivalent to those performed on prototype individual and groups of model piles could then be interpreted more closely in accordance with established methods. Parametric studies of model piles driven in-flight may prove

to be a significant step in the determination of prototype pile (group) capacities by modeling. Additionally, the ability to drive model piles in-flight will provide a greater understanding of the sensitivity of pile performance to changes in soil properties at the pile-soil interface.

CHAPTER 2
IMPACT DRIVING OF PILES, CAPACITY PREDICTION,
AND CAPACITY VERIFICATION

2.1 Introduction

The transfer of energy from hammer to pile during driving is a complex occurrence involving elastic and inelastic deformations, energy losses, nonhomogeneity in the soil medium, deformation and deformation rate-dependent soil response, and transient phenomena, including soil consolidation and dissipation of pore pressure (Holloway, 1975). Developing a mathematical model which incorporates all of the important variables of the driving process is extremely complex as evidenced by the computer programs which model wave propagation. Extending that model to predict the capacity of the driven pile introduces yet another order of complication. It is necessary to understand the concepts of how individual events occur before an investigation of the complete process can be conducted. Simplifying assumptions are necessary even if the process is broken down into smaller events. This chapter will present wave mechanics theory as it applies to impact driving, practical considerations of that theory concerning the impact driving of piles, and a discussion of how those forces result in the development of residual stresses during driving.

2.2 Pile Placement by Impact Driving

2.2.1 Elastic Wave Propagation in Solids

The initial assumption regarding the transfer of energy from the hammer to the pile is that only one dimension (length) be considered in the analysis. This assumption simplifies the proposed mechanism of energy transfer in that energy to the pile is transmitted in the form of a planar wave. In other words, the planar cross sections of the hammer and pile remain planar during the transmission of the strain pulse and the resulting stress over the section is uniform. These assumptions permit the simplest of solutions, commonly referred to as the one-dimensional wave equation, (Kolsky, 1963; Richart et al., 1970; Palacios, 1977). That equation is expressed by the following partial differential equation:

$$\frac{d^2u}{dt^2} = c^2 \frac{d^2u}{dx^2} \quad \text{Eq. 2-1}$$

where

u = displacement in the direction of the wave front

t = time

$c = \sqrt{\frac{E}{\rho}}$ = longitudinal wave propagation velocity

x = distance along the rod

when

E = Young's Modulus of elasticity

$\rho = \gamma/g$ = mass density

γ = unit weight

g = acceleration due to gravity

The assumption that lateral inertial forces are negligible in the derivation of the wave equation implies the longitudinal wave must be long with respect to the cross-sectional dimension of the transmitting medium. Kolsky (1963) showed the wave equation to be valid when the wave length is at least five times the diameter of the medium (rod) through which the wave is propagating. This condition is always met in the practical situation of driving piles (Krapps, 1977).

The solution of the differential equation has the following form:

$$u = f(x + ct) + h(x - ct) \quad \text{Eq. 2-2}$$

The letters f and h represent arbitrary functions such as $\sin w$, e^w , w^n , etc., where w is either $(x + ct)$ or $(x - ct)$.

The general form of the arguments of Equation 2-2 indicates the x - t plane is divided into regions of constant compression and velocity by disturbance lines of constant slope. The slope of these lines is defined as the characteristics. The left-hand term in the above equation ($f(x + ct)$) represents a wave traveling in the negative x direction with velocity c . The remaining term denotes the wave traveling in the positive x direction with velocity c as shown below.

$$\text{Let } f(x + ct) = 0$$

Therefore,

$$u = f(x - ct) \quad \text{Eq. 2-3}$$

The passage of a nonattenuating elastic wave is depicted in Figure 2-1. Since $u = s$ when $t = t_1$ and $x = x_1$, and also when $t = t_2$ and $x = x_2$, the rate of wave propagation with respect to the x axis is as shown below.

$$c = (x_2 - x_1)/(t_2 - t_1) \quad \text{Eq. 2-4}$$

Since

$$s = f(x_1 - ct_1) = f(x_2 - ct_2) \quad \text{Eq. 2-5}$$

then

$$(x_1 - ct_1) = (x_2 - ct_2) \quad \text{Eq. 2-6}$$

With the understanding that $t_2 > t_1$ and c is constant, x_2 must be greater than x_1 indicating the term $h(x - ct)$ refers to the wave traveling in the positive x direction. A similar manipulation of the left-hand term of Equation 2-2 indicates that term refers to the wave traveling in the reverse direction.

When considered independently, each term represents a valid solution to the wave equation. When the terms are used together, a valid solution is still obtained, indicating Equation 2-2 is a simple partial linear differential equation. The significance is that the separate effects of the two solutions may be added together at any instant to determine the net effect of the passage of the waves.

Kolsky (1963) and Richart et al. (1970) have shown that the speed, c , at which a stress wave propagates in a medium is dependent on the material properties of the medium, namely, the Young's modulus of elasticity and density of the medium.

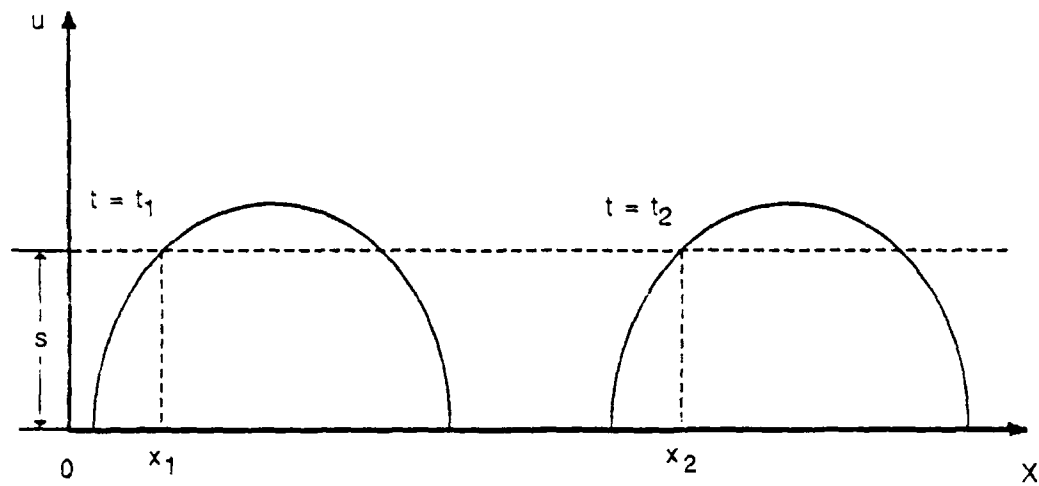


Figure 2-1 Propagation of an Elastic Wave

$$c = \sqrt{\frac{E}{\rho}} \quad \text{Eq. 2-7}$$

Several other equally important wave parameters are dependent on the magnitude and type of input wave. Particle velocity and stress are two such parameters which are directly proportional to one another. Particle velocity (V_p) is the partial derivative of displacement with respect to time. In a compression wave, the particle velocity and wave propagation are in the same direction. In tension waves, the particle velocity is opposite the direction of wave propagation. The particle velocity is always less than c in the propagation of elastic waves. Krapps (1977) and Richart et al. (1970) have shown the particle velocity to be proportional to longitudinal wave speed and stress, and inversely proportional to Young's modulus of elasticity as follows:

$$V_p = \frac{\sigma c}{E} = \frac{\sigma}{\rho c} \quad \text{Eq. 2-8}$$

Likewise, stress can be determined if the particle velocity is known.

$$\sigma = \rho c V_p \quad \text{Eq. 2-9}$$

Since dynamic force (F) equals the stress times the cross-sectional area of the medium,

$$F = \frac{A E}{c} V_p = \rho c A V_p \quad \text{Eq. 2-10}$$

The product ρc is referred to as the "characteristic impedance" (Z_0) and is dependent on the material properties of the medium. A scalar value of impedance (Z) results when the characteristic impedance is multiplied by the cross-sectional area of the medium. The impedance of each component in the pile driving system affects the transfer of energy from the hammer to the pile and thus the total amount of energy available to the pile to be used for penetration. System impedance will be discussed following a brief summary of boundary condition limitations.

The preceding presentation has been limited to the propagation of elastic waves in a uniform, geometrically regular medium of infinite length. These assumptions were necessary to simplify the solution of the wave propagation equation and develop a general understanding of this form of energy transfer. The necessity of driving piles of finite length and using system components of complex geometry requires that the boundary conditions and their effect on the dynamic system also be understood. The influence of end conditions on the magnitude and stress sense of the reflected wave will be considered before the effects of system geometry.

The elastic wave discussed in previous examples propagates at a constant velocity in a freely suspended geometrically uniform rod without changing shape. Assume the wave reaches the boundary of the medium (i.e., the end of a rod) and is reflected. If the end of the rod is unsupported and free to vibrate in the direction of the propagating wave, the incident stress wave is reflected from the free end with the same magnitude but having the opposite stress sense. A compression wave reflects as a tension wave and vice versa. The free end implies a zero

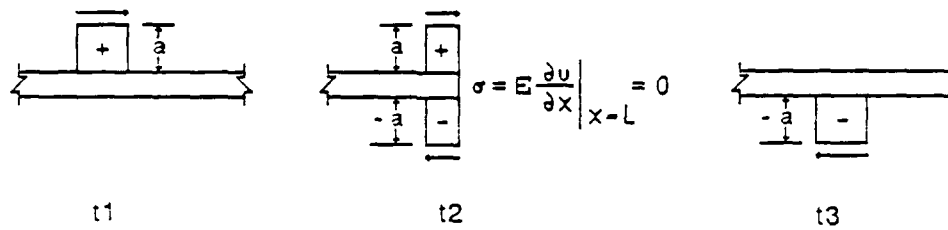
stress state at the boundary as shown in Figure 2-2(a). The opposite occurs when the wave impinges on a fixed boundary (Figure 2-2(b)). In this situation, the stress wave is reflected as a wave of equal magnitude and stress sense. This causes the stress wave to double in magnitude, either compressive or tensile, at the fixed boundary. Most practical applications of these two limiting boundary conditions require the determination of intermediate boundary conditions based on empirical results.

2.2.2 Hammer-Pile Impact

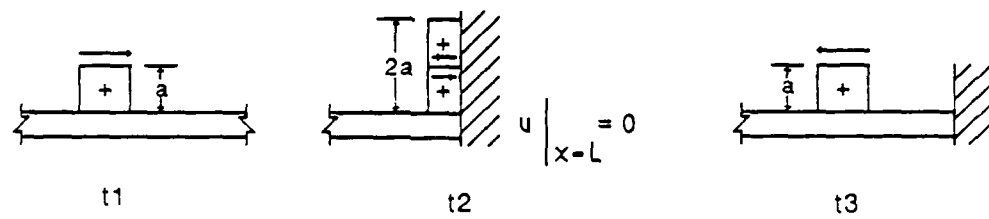
The impedance of two bodies plays a significant role in the efficiency of the transfer of energy as one impacts the other. Consider the hammer-pile system depicted in Figure 2-3. The variables A and a refer to the cross-sectional areas of the hammer and pile, L and l to the length of the hammer and pile, and V to the impact velocity of the hammer. The contacting ends of the hammer and pile are assumed flat and contact is made across the full cross-sectional area of the rod during impact. Two initial assumptions are needed for this generalization to be valid. The force in the hammer equals the force in the pile. Likewise, the velocities of the contacting hammer and pile faces are equal while the two are in contact. Let σ_h denote the stress in the hammer and σ_p the pile stress. Regarding the initial assumption that the forces in the hammer and pile are equal, the relationship between the impedance of each and the stress in each is readily determined. Using Equation 2-10,

$$\text{Force} = \text{Stress} (\text{Area})$$

$$\text{Eq. 2-11}$$



a) Reflection from Stress-Free End Rods



b) Reflection From Fixed End Rods

Figure 2-2 Idealized Reflections of an Elastic Wave.
 a) Reflection from Stress-Free End Rods;
 b) Reflection from Fixed End Rods

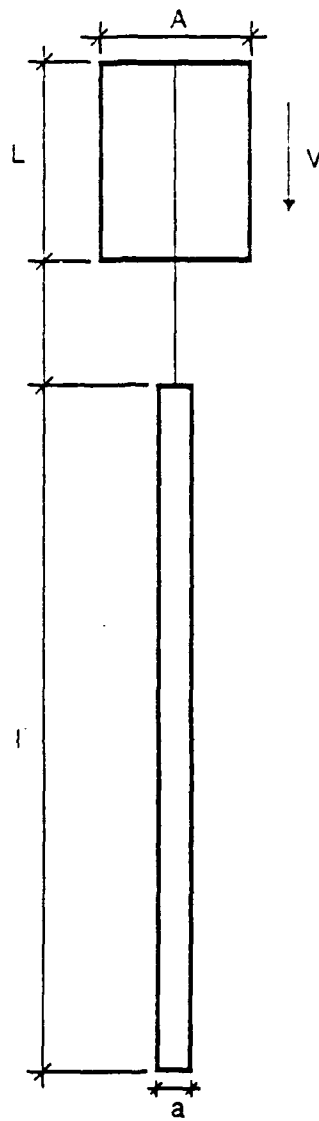


Figure 2-3 Idealized Hammer and Pile Before Impact

$$\rho_p c_p V_{po} A_p = \rho_h c_h V_{ho} A_h \quad \text{Eq. 2-12}$$

From Equation 2-10, the impedance of each component is ρcA . Thus,

$$Z_p V_{po} = Z_h V_{ho} \quad \text{Eq. 2-13}$$

The quantity termed the characteristic impedance ratio (r) is derived by dividing the characteristic impedance of the struck body by that of the striking body as presented below.

$$r = \frac{Z_p}{Z_h} = \frac{\rho_p c_p A_p}{\rho_h c_h A_h} \quad \text{Eq. 2-14}$$

The characteristic impedance ratio is simply a function of the areas of the hammer and pile if the two are made of the same material.

Consider the second assumption which requires the velocities of the striking end of the hammer and the struck end of the pile to be equal.

Let V be the hammer velocity. Thus,

$$V - V_{ho} = V_{po} \quad \text{Eq. 2-15}$$

when

V_{ho} = the velocity with which the hammer face particles are compressed backwards relative to the unstrained portion of the hammer yet to recognize that impact has occurred. The hammer velocity (V) is uniform. uniform.

V_{20} = the velocity with which the pile butt particles are compressed relative to the unstrained portion of the pile.

Palacios (1977) solves Equations 2-13, 2-14, and 2-15 for V_{ho} and V_{20} in terms of the hammer velocity and impedance ratio.

$$V_{ho} = \left(\frac{r}{1+r} \right) \quad \text{Eq. 2-16}$$

$$V_{20} = \left(\frac{r}{1+r} \right) \quad \text{Eq. 2-17}$$

Palacios continues his development of the impact based on the findings of Fairhurst (1961):

As impact continues, the strained region in both members extends away from the interface at the propagation velocity c so that, at a given instant, the strain wave has covered the same length of hammer and rod (Figure [2-4b]). The particle velocity within this region is constant at values V_{ho} and V_{20} , respectively. Upon reaching the free end of the hammer after time $t = L/c$, the compression wave will be reflected as an equal tension pulse which combines with and cancels the outgoing compression wave, giving the particles a total velocity of $2V_{ho}$ away from the interface.

Thus, as the tension wave returns, the hammer is progressively released from strain, such that the absolute spatial velocity (V_1) of the unstrained portion (Figure [2-4d]) is given by:

$$V_1 = V - 2V_{ho} \quad \text{[Eq. 2-18]}$$

At the instant $t = 2L/c$ that the reflected wave reaches the hammer [pile] interface, no strain exists in the hammer (Figure [2-4e]) and it is traveling with uniform velocity, V_1 . The hammer velocity at the interface is thus abruptly changed at time $t = 2L/c$ as V changes suddenly to V_1 .

(Palacios, 1977, p. 46)

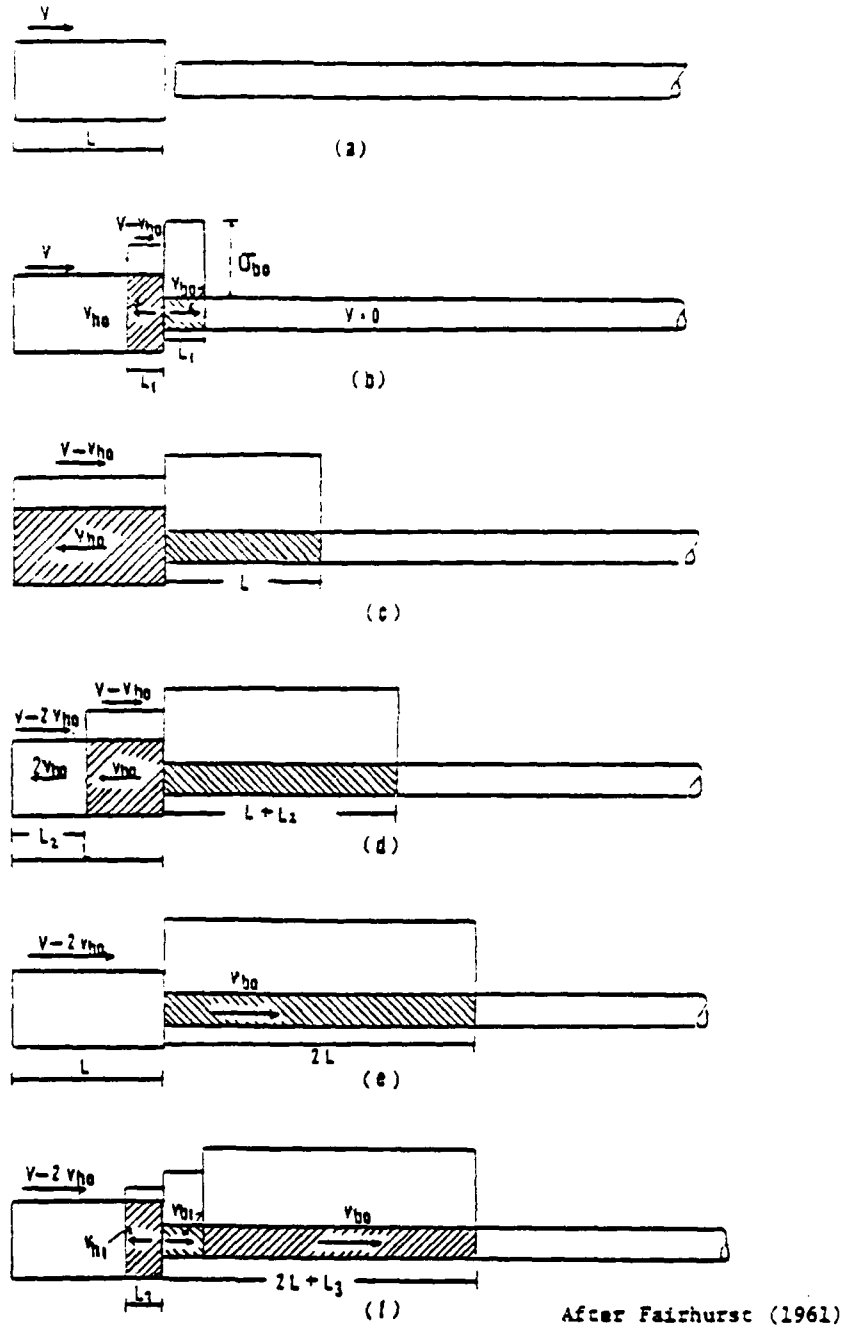


Figure 2-4 Mechanism of Impact of a Cylindrical Hammer on a Finite Cylindrical Rod. After Palacios (1977)

The change in hammer velocity from V to V_1 implies new boundary conditions and the process is repeated using the new boundary conditions for each complete cycle of compression and reflected tension wave traversing the hammer. Palacios concludes

$$V_{pn} = V_{po} \left(\frac{1-r}{1+r} \right)^n \quad \text{Eq. 2-19}$$

when

$$\frac{2nL}{c} < t < \frac{2(n+1)L}{c} \quad \text{Eq. 2-20}$$

Note that $V_{po} = \frac{V}{1+r}$ Eq. 2-21

Additionally,

$$\sigma_{pn} = \sigma_{po} \left(\frac{1-r}{1+r} \right)^n \quad \text{Eq. 2-22}$$

Note also that $\sigma_{po} = \rho c \left(\frac{V}{1+r} \right)$ Eq. 2-23

When the hammer and pile are made of the same material and have the same cross-sectional area, $r = 1$ and

$$\sigma_{po} = \frac{1}{2} \rho c V \quad \text{Eq. 2-24}$$

The energy is thus transferred from the hammer to the pile in a stepped waveform with the hammer decelerating incrementally and the pile butt accelerating likewise. The hammer and butt separate when the

velocity of the butt exceeds that of the hammer. The energy transmitted to the pile is used productively for penetration and/or dissipated as heat, vibration, etc. This separation typically occurs when the wave reflected from the pile-soil interface returns to the contact face. Palacios concluded the theoretical maximum stress is uniform for the duration of contact when the impedance ratio is 1.0. An incremental decrease in the impedance ratio (with hammer mass and drop height held constant) results in increasingly higher theoretical maximum stresses acting over increasingly smaller time periods as shown in Figure 2-5. The total time required for the complete transfer of hammer energy increases as the impedance ratio decreases with total time required being in excess of twice that which is necessary when the impedance ratio equals 1.0.

2.2.3 Hammer-Pile-Soil Interaction

The preceding discussion has been concerned with the propagation of elastic waves which were not altered in their passage through a uniform medium. This situation is possible in an experimental setup but is too limited for accurate representation of the transmission of energy from hammer to pile. Several factors complicate the simple model presented thus far. Dispersion, interaction between the hammer, cushion, and pile, and soil-pile interaction all affect the transmission of energy.

Dispersion results from two frequency dependent aspects of wave propagation. Both wave velocity and amplitude attenuation occur more rapidly for higher frequency waveforms. A waveform may appear uniform over a short time; however, monitoring the progression over a suitable distance reveals the composite waveform is made up of various high and

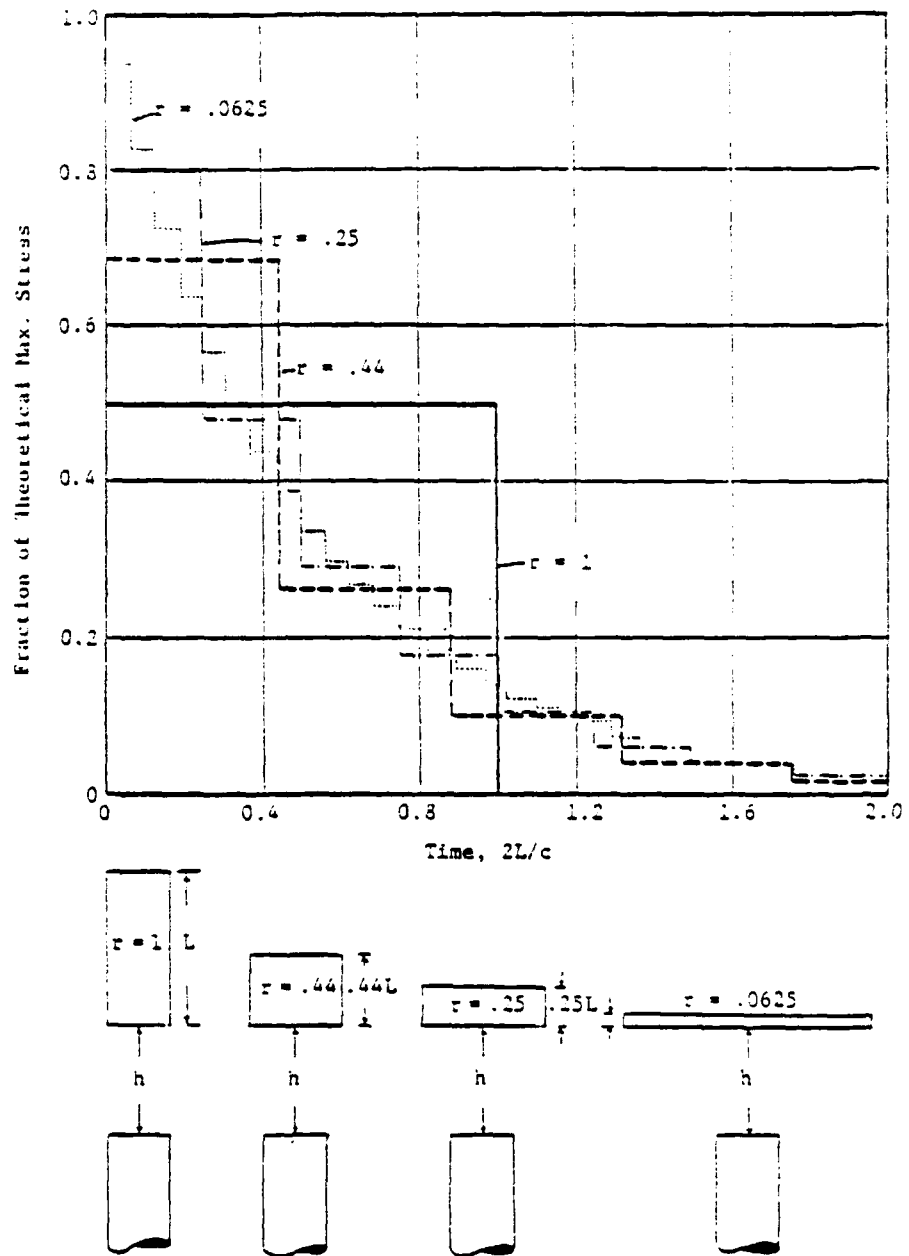


Figure 2-5 Effect of Impedance Ratio on the Theoretical Wave Shape for Same Hammer Mass and Drop. After Palacios (1977)

low frequency components. The high frequency components proceed relatively quickly through the medium followed by the waveforms of successively lower frequency components. It is also apparent that the higher frequency waveforms attenuate and slow down more quickly than the lower frequency components. The low frequency waveforms never "catch up." Rather, the high frequency portions dissipate at some point while the low frequency portion continues to propagate for a relatively large distance. Thus, a waveform changes during propagation and has a different energy content dependent on the instant at which the wave is observed. Dispersion is not usually a problem in the practical application of driving piles (Palacios, 1977). However, it is an important consideration if waveform analysis is to be performed. After several cycles of reflection of the initial wave from the ends of the pile, the now separate high and low frequency portions interfere with one another's passage and can dramatically alter the predicted energy content.

The aspect which has more practical bearing on the transmission of available energy from the hammer to the pile is interaction between the hammer, cap/cushion, and pile itself. When an elastic wave impinges on a boundary between two media, reflection and refraction occur. In the most general case, two distinct waves are generated each time an individual wave passes the boundary; one reflected and one refracted (Kolsky, 1963). As the two new waves can have only as much energy as the initial wave, the refracted wave (moving in the same general direction as the initial wave) has lost the amount of energy contained in the reflected wave. Reflection, refraction, and energy loss occur at every interface between the hammer face and the pile and can be significant.

The interaction between the pile and soil changes with depth of penetration, soil conditions, and the remaining energy which is available to be productively used for penetration as the stress wave progresses. Attempts to understand this aspect and its contribution to the development of residual stress and static capacity have resulted in several mathematical models. The most frequently used models are the finite difference and finite element methods.

The finite difference method discretizes the physical problem into small segments as shown in Figure 2-6 (Smith, 1960; Holloway, 1975). The pile is approximated by a series of short longitudinal segments. Each segment is a discrete mass connected by springs of known deformation constants which approximate similar deformation characteristics between the mass centroids of the segments and the equivalent portion of the pile. This model, developed by Smith (1960), can be solved by integrating element displacement and velocity with respect to time. Total displacement can be determined by integration over small time increments from known initial conditions. This method has been modeled on digital computers with moderate success. Particular care must be taken in the selection of the time increment of integration. Too small an interval results in an inordinately large number of calculations being performed and possible magnification of small numerical errors in the model. A large time increment could permit the bypass of an element and subsequent instability in the solution (Holloway, 1975; Smith, 1960). The time increment is sometimes determined simply by dividing the length of the pile segment by the stress wave velocity (E/ρ) in a freely suspended rod made of the same material as the pile. Inelasticity of the system components, most notably the pile cushion, has a

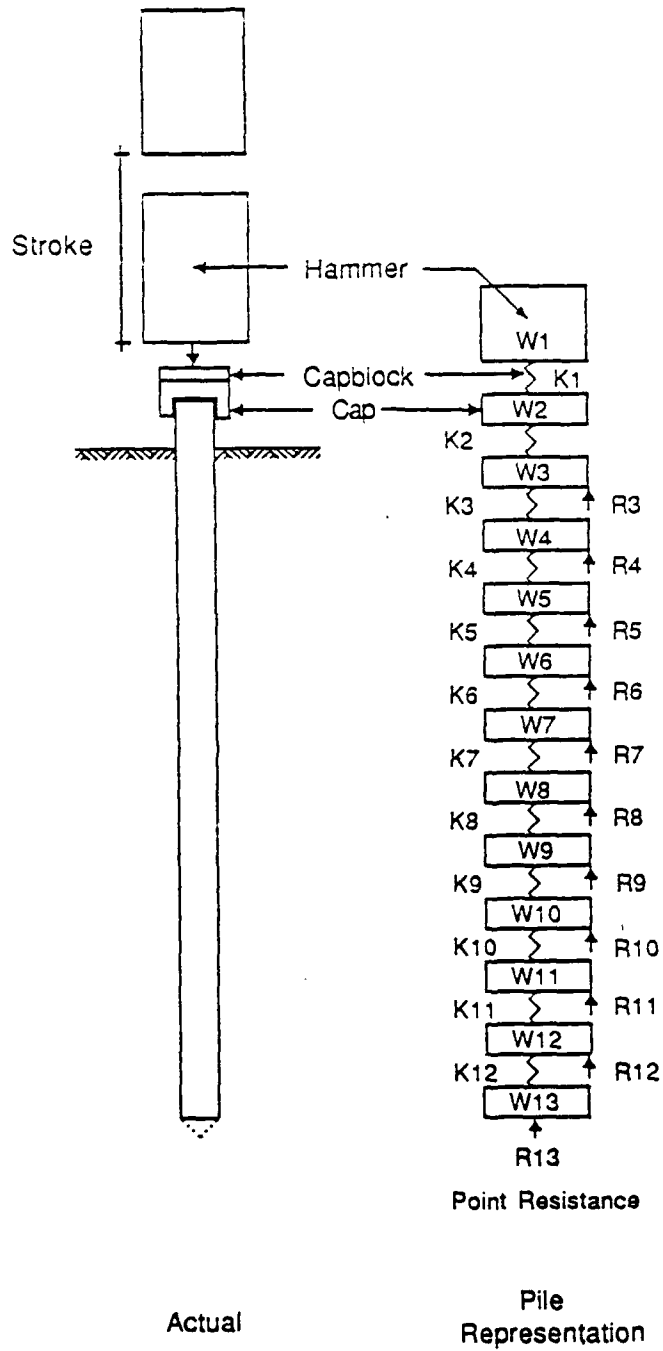


Figure 2-6 Finite Difference Pile Representation.
 Smith's Lumped Parameter Representation.
 After Smith (1960).

profound effect on the transmission of energy in the prototype and model. Permanent deformation of the cushion introduces energy losses which reduce the efficiency of the transfer. Soil strength and resistance were highly simplified in this model as less was known about in situ conditions contributing to pile strength.

The finite element method was the successor to the finite difference solution. This method relies on an axisymmetric idealization of the three-dimensional pile-soil model. The elements suggested by Desai and Abel (1972), project as wedge segments when the model pile representation (Figure 2-7) is viewed from above. The first analysis of pile soil interaction using the finite element method was conducted by Ellison (1969). This method has since become the subject of several texts (Zienkiewicz, 1971; Desai and Abel, 1972). Deformation is concentrated at the nodes and is equal for the pile and soil at the interface. The pile material strength parameters are usually well known and the soil parameters conform to a tri-linear approximation based on either lab tests or in situ test results. The soil strength is mobilized until it exceeds the Mohr-Coulomb strength parameters at which time it is considered to have developed ultimate strength. The soil continues to deform if the stress is increased; however, no additional strength is mobilized. The deformation "envelope" simply grows larger. This method provides acceptable results in static loading predictions as the relative motion between the pile and soil is small. It is less applicable for analysis of dynamic situations because of the difficulty of modeling the interaction (and differential displacement) between the pile and soil. A knowledge of the propagation mode of both compression and shear waves is very helpful in the initial determination of the

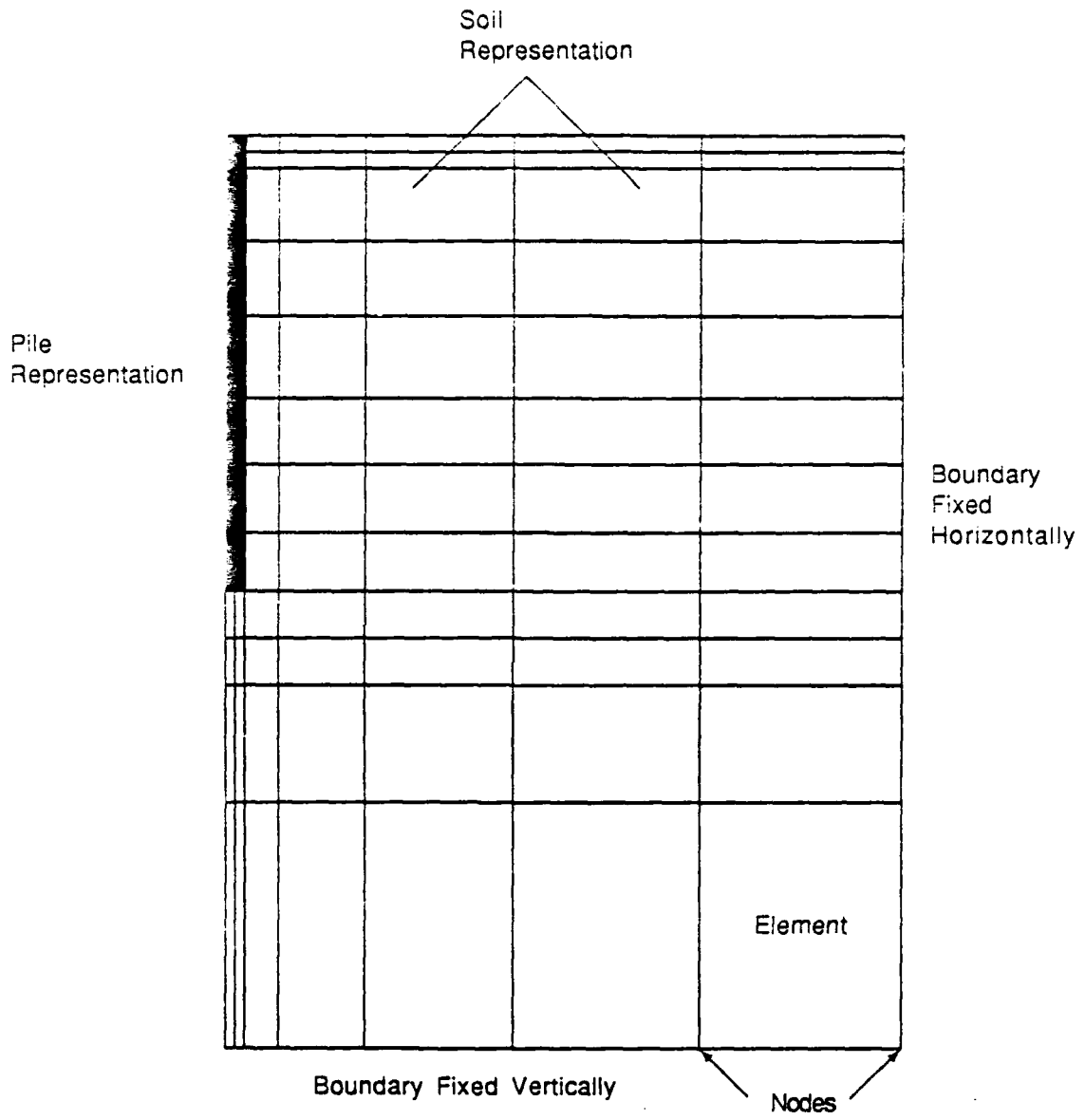


Figure 2-7 Finite Element Mesh Pile Representation

nodes and elements, yet this is the type of information the finite element investigation is supposed to provide. Holloway (1975) correctly predicted this method would continue to receive emphasis as a research tool for quite some time.

2.3 Practical Aspects of Pile Driving

The practical considerations of prototype pile installation will be presented as a guide for determining the aspects which must be modeled most accurately. Pile installation considerations include the interaction of the hammer, cushion, and cap (or helmet), as equally important members of the system needed to drive the pile. Pile forces experienced during driving will be discussed. Errors in the placement and driving of piles affecting capacity will be detailed.

2.3.1 Hammer-Cushion-Cap Interaction

Similarities between the energy transmission from the hammer to the Standard Penetration Test (SPT) sampler and the hammer to the pile permit several conclusions to be drawn from research conducted on SPT rigs. The need to have the relatively simple SPT rigs energy calibrated (Schmertmann, 1977) prior to interpreting and comparing results underscores the necessity of viewing the hammer, cushion, and pile cap system (Figure 2-8) as a whole when determining the amount of energy being transmitted to the pile.

The ram weight and impact velocities are generally the most important variables with respect to pile penetration for a given pile-soil system. Heavier rams generally give more penetration than lighter rams with the same kinetic energy at impact. Note that the heavier ram has more momentum at impact than the lighter ram in this case and the transmitted stress wave generally has a longer wavelength. Heavier rams are generally more efficient

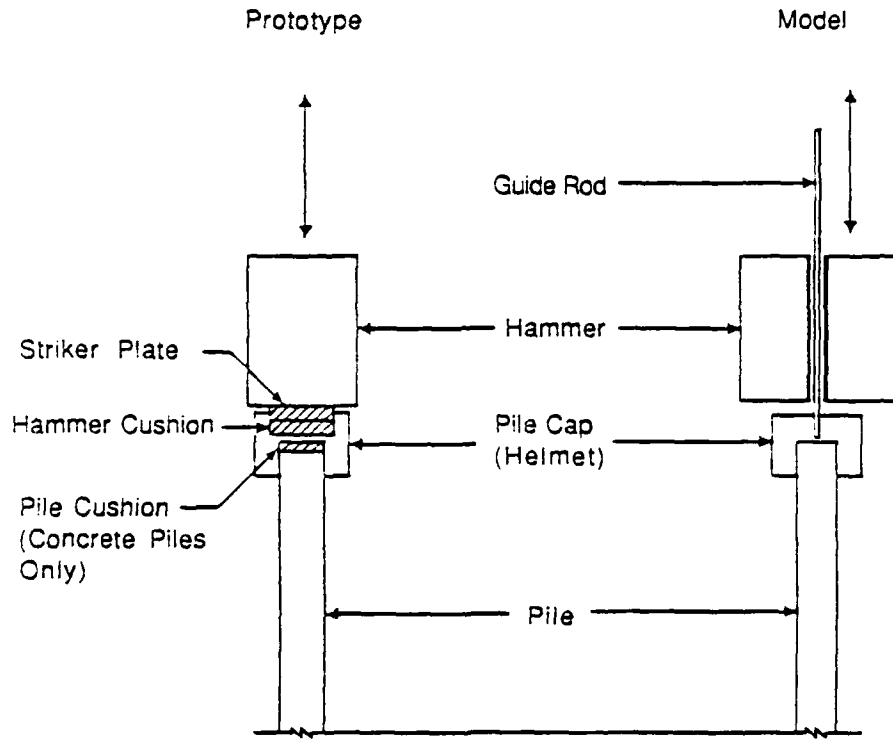


Figure 2-8 Definition of Pile Cap Terminology

with respect to utilization of kinetic energy than lighter hams.

(Knapp, 1977, p. 49)

The dramatic effect of these variables on energy transmission are underscored by the efficiency of some pile drivers, which can range from 30 to 95% (American Society of Civil Engineers (ASCE) Committee on Deep Foundations, 1984). The hammer weight and lift height are simply a measure of the energy available to be transmitted to the pile during an individual impact.

Energy transfer from hammer to pile is less dependent on the degree of tilt (or list) of the driver than if the driving components are misaligned. Palacios (1977) determined that the concentrically aligned hammer and rods could be tilted as much as three degrees before causing a decrease in transmitted energy.

Full understanding of the hammer, cushion, and cap interaction is vitally necessary prior to modeling of the driving process. The characteristics of these components should be chosen to satisfy the following two criteria (Peck, Hanson, and Thornburn, 1974). The components must be able to transfer the amount of peak driving force at least equal to the desired ultimate capacity of the pile being driven. Unless this criterion is satisfied, the pile cannot penetrate far enough to develop the desired capacity. Refusal will occur first. The components must also transmit as much of the available energy from the hammer as possible. This criterion is more flexible than the first. It is important only for economy in driving. The lift height or hammer weight can, and must, be modified if their standard configuration would overstress the pile. Stresses in the pile and determination of the amount of energy

transferred from an impact can be directly measured by the appropriate instrumentation (i.e., strain gages and accelerometers), however, this method is not used on a widespread basis. Computerized wave equation analysis is more frequently used to find the best combination of hammer, cushion, and cap for a given hammer and pile combination (ASCE Committee on Deep Foundations, 1984). These methods suffer from the need to make assumptions regarding the chosen components.

The cap distributes the hammer blow to the butt of the pile and can also serve to hold the butt in place during the initial stages of driving. A close fit should be maintained between the cap and butt to prevent buckling of the pile or bulging of the butt itself. The bearing surface of the butt or cap should be machined to assure proper fit. The cap should be sufficiently massive to provide efficient transfer of energy to the butt. An insufficiently massive cap may separate prematurely from the butt effectively stopping the flow of energy from the hammer.

Historically, hammer cushions were made of hardwoods cut to fit snugly within the cap, but they are now usually made of aluminum or micarta. The relatively soft hardwoods transmit an initial compressive wave of lower frequency and magnitude to the pile for a given hammer and cap combination. Additionally, the hardwoods have revealed their tendency to catch on fire as the amount of energy transferred from the hammer has increased. The coefficient of restitution (COR) of hardwood is only 0.5. Aluminum and micarta have the advantage of a higher COR (0.8), more nearly linear elastic properties, and greater and more consistent energy transmission characteristics than the hardwoods. The significant improvement in the use of aluminum and micarta lies in their

more predictable elastic properties and reduction of energy losses. Excessively high compressive and tensile forces in the pile are controlled by proper selection of these components. Pile penetration per impact may be controlled somewhat by selection of cushions with different elastic properties.

2.3.2 Pile Forces Developed During Driving and Loading

Tubular steel shell piles were the only type of piles considered in this research. This type of pile can develop high capacities, but the limiting criteria for pile selection is usually the pile's ability to withstand the significant stresses experienced during driving. The pile must be of adequate cross-sectional area to provide the necessary driveability characteristics and thus be able to achieve proper penetration. The driving force a pile can withstand is dictated by the impedance of the pile (refer to Section 2.2.1), the limitation being that the pile material should remain within the boundaries of elastic deformations during driving. Increasing the impedance, and thus the driveability, can be accomplished by changing the strength characteristics of the pile material, increasing the cross-sectional area, or both. A reasonable balance must be maintained between the resulting pile size and available driver. The increase in impedance will provide the added benefit of greater pile capacity given adequate soil conditions.

The driving stresses in a pile are usually relatively insensitive to driving resistance (dependent on soil properties) for a given hammer, cushion, and cap. The stresses then would be equal in a given pile regardless of the soil type in which it is driven. The variation would be in the amount of penetration per impact. The amount of tip resistance experienced by the pile also affects the driving stresses

developed. Excessive resistance at the tip contributes to crushing of the tip if driving is continued. If the pile tip rests in a soft soil, a tensile wave is reflected from the free end which may exceed the tensile strength of the pile. Fracture can result. This is usually a concern only in concrete piles. Thus, forces developed at the tip depend on the stress transmission characteristics of the hammer and cap assembly, the impedance of the pile, and the general pattern of distribution of soil resistance at the tip and along the side. A better understanding of the relative contributions of the tip and side resistances will provide valuable information regarding ultimate pile capacity.

The aforementioned stresses of both driving and static loading can be measured by a variety of methods. Displacement of the tip and side walls can be measured directly or inferred from the readings of strain gages appropriately located on the interior of the pile. The strain gages will also provide information concerning the unit pressures and total loads felt by the walls and tip. Tell-tales can be mounted along the inside wall of the pile to monitor movement of the tip and walls during static loading. An inclinometer will permit determination of the accuracy of placement of the tip as well as deviations from the intended placement along the pile length.

Strain gages are the most frequently used instruments to measure stress distributions along the pile shaft. They are easily mounted on the interior of the pile, durable if suitably protected, easy to interpret, and accurate. Strain gages measure strain directly; however displacement, unit stress, and thus total load can be inferred from the readings. Properly attached gages provide information regarding the

passage of elastic compression and tension waves during the driving process. Recording the variation in these waves at regular intervals during driving can reveal where the input driving energy is spent during penetration and how much energy is stored in the pile as residual stress. Likewise, recording the magnitude of static stresses developed in the pile at regular intervals during driving provides a record of the development of residual stresses. Continued recording of the pile stresses during loading aids in determination of the load shedding characteristics of the pile-soil system and the mechanism by which the soil mobilizes its strength to support the pile. Measuring the residual stresses over time will reveal how the residual stresses are redistributed either due to changes in the soil (movement of the water table or changes in lateral effective stresses) or movement of the pile itself.

Tell-tales, or indicator rods with one end attached to specific points along the interior wall and the other brought to the surface, directly measure the displacement of the pile at the attached point. Movement of the pile relative to the butt is measured. Total displacement of a pile section can be determined if the movement of the butt is measured from a separate reference. The tell-tales can be used in conjunction with strain gages, as verification of the readings of one another, or independently. The tell-tales cannot give information concerning the dynamic response of the pile.

The tip load can be inferred from placement of strain gages in close proximity to the tip or measured directly using a specially installed load cell. A ring of strain gages at the tip will reveal the tip load if the elastic modulus of the pile material and tip dimensions are known. Measurement of the tip pressure by a load cell dictates

separation of the tip from the pile walls to ensure the load cell is subjected entirely and only to the load at the tip. This determination requires a specially manufactured pile and extra precaution to ensure the integrity of the tip is maintained during driving.

Inclinometers provide information regarding the "trueness" of the pile with regard to its intended placement. Typically, the channel or track for the inclinometer is placed in the pile during manufacture and the inclinometer readings taken after driving. Such measurements reveal the degree of tilt of the pile either from vertical or with respect to the intended degree of slope of a batter pile. Furthermore, departure of the pile tip from its desired position can be determined if a complete record of the pile inclination is obtained. Such information is important especially if there is a question of exceeding the bearing capacity of the soil at the tip of an end bearing pile.

The effects of residual stress on static capacity became important to researchers only ten years ago (Davisson, 1978). These effects had not been considered in pile load capability estimates and may have resulted in significantly higher actual tip and friction stresses. Neglecting these effects may also have contributed to unknowingly unconservative designs. Early attempts (1960-65) to investigate the development of residual stresses and their contribution to static capacity indicated unit tip bearing capacity and skin friction increased with depth until some critical depth was attained (ten to twenty pile diameters). Further penetration did not increase either unit stress capacity (Vesic, 1970). Subsequent field testing with 16- to 18-inch diameter piles driven in sand indicated the tip and side wall unit capacities increased linearly until a penetration of ten diameters had

been achieved. The unit capacities then became constant after tip penetration of twenty diameters with the zone between ten and twenty diameters being a zone of smooth transition between the unit capacities (Vesic, 1970). The three studies previously mentioned indicated the final values of tip and skin capacities appeared to be dependent on the initial relative density (D_r) of the sand. Vesic suggested the following ultimate tip and side wall unit capacities.

$$q_p = 4(10^{2.4})D_r^3 \quad \text{Eq. 2-25}$$

$$q_s = 0.08(10^{1.5})D_r^4 \quad \text{Eq. 2-26}$$

The subscripts p and s refer to point and side wall, respectively.

The suggestion that residual stresses might influence the ultimate capacity of statically loaded piles led to further research. The time dependence of residual stress relaxation was also investigated using the measurement techniques discussed in the preceding paragraphs. Such efforts have provided the current understanding of pile behavior. The distribution of friction along the pile wall appears to be parabolic (Vesic, 1970). Other researchers have also recognized this distribution of pressures along the shaft. The overall participation of the shaft in carrying the total pile load is proportionately greater in the early stages of loading for the end bearing pile as well as the friction pile. The side walls make some initial contribution to supporting the applied load before the tip makes its initial contribution. Application of additional load results in mobilization of friction capacity along the walls until the ultimate capacity is progressively achieved at

increasing depth along the shaft. The total load at the tip increases during mobilization of the skin friction and increases linearly in conjunction with the applied load after skin the friction component has been fully mobilized (Marcuson and Bieganousky, 1977a). The skin friction component is not necessarily fully mobilized in all cases. Either the pile is conservatively designed and will never reach its full capacity in service or end bearing failure occurs prematurely and the pile is rejected.

Cyclical loading of piles can have a significant effect on the distribution of stresses along the shaft. Initially the pile may distribute residual stresses from driving resulting in latent movement of the tip even before the design loading is applied to the butt. Load transfer in piles has been found to be sensitive to small changes in soil strain and pile compression (Lundgren, 1978). Loading and unloading can cause irreversible changes in the distribution of effective lateral pressures along the shaft. What was originally positive skin friction contributing to the ultimate capacity of the pile has, in limited cases, been found to reverse itself over time thus contributing to the ultimate load of the pile (Brierly, Thompson, and Eller, 1973).

2.3.3 Errors in Placement and Driving Affecting Static Capacity

The static capacity of an individual pile or group can be influenced by several factors during initial placement and subsequent driving. Each factor and its effect on static capacity will be considered individually; however, it is not uncommon to have more than one error in a driven pile with the effects being either compounded or cancelled.

Axial misalignment results from an initial misalignment of the pile and driver components, field layout errors, trying to drive a flexible pile, driving in the proximity of a subsurface obstruction, uneven ground compaction, excessive surcharge placement after driving, or penetration of a sloping hard strata. Pile misalignment can result in problems at the tip as well as the butt. Butt misalignment problems are found most often in slender piles carrying large loads and least often in mat foundations supported by piles as the loads are relatively lighter and carried by many piles. Proper axial alignment is most important where the butt enters or is encased by the pile cap. Misalignment leads to stress concentrations which may quickly exceed the design stresses. This error is easily checked and can be corrected by modifying either the pile or the cap, or both, to reduce stress concentrations. The most critical applications may require redesign of the foundation once the actual butt locations are known. Likewise, misalignment at the tips of group piles can overstress the soil causing local failure (ASCE Committee on Deep Foundations, 1984).

Significant overstress can result even when the pile is placed within the normal design tolerances, usually ± 3.0 inches. Davisson (1978) found one instance in which the load of an individual pile had been increased 24% although all piles in the group had been placed within design tolerances.

Severe axial misalignment, which sometimes results in bending of the pile, is not necessarily cause for rejection. Several analytical capacity prediction methods are available (ASCE Committee on Deep Foundations, 1984) and load testing is a viable alternative.

Static capacity can be reduced in two ways due to misalignment of the hammer and pile cap elements. Visible damage and failure can result from the concentric overloading of thin-walled pipe piles such as those modeled in this research. High hammer impact velocity contributes to "rolling" of the butt (Dismuke, 1978). Damage may be severe enough to warrant rejection of the pile. Should the pile be judged suitable for service, its capacity may have been reduced as the stiffness of the shaft usually decreases due to deformation. Piles adjacent to the damaged one must carry a larger share of the load.

2.4 Static Capacity Verification

Static load tests are conducted to verify the design capacity of a placed pile and determine the suitability of the pile type selected. Although many variations exist in the conduct of the load test, all involve the static loading of the pile in increasing increments with various measurements being made of the settlement of the pile at the butt. Appropriately instrumented piles will render data concerning displacement and load at the instrumentation points. Consult ASTM D-1143 for specific criteria regarding pile capacity verification.

After placement of the test pile (group), a framework is constructed above the pile. This framework serves to provide the reaction load against which the pile is jacked. A hydraulic jack is usually placed between the pile and reaction framework and load is applied by increasing the fluid pressure in the jack. Load can also be applied simply by placing iron ingots or even soil in a suitable box mounted directly on the butt.

An independent framework is also constructed which serves as the reference against which settlement readings are made. In most instances, a dial gage is installed on the reference beam with the indicator stem resting on the test pile butt. Redundancy is important and gages are usually installed on opposite sides of the butt to determine average settlement. ASTM D-1143 stipulates two independent systems be used to determine settlement. The backup system sometimes consists of a taut wire stretched between two posts placed in the ground beyond the zone of influence of the pile or its reaction load. Readings are taken visually from a ruler and mirror placed on the butt.

The pile is loaded incrementally up to as much as twice the design load and settlement of the pile butt is measured for a specified period of time after placement of each load increment. The time period between placements of the test load is determined by the size of the load and the type of soil in which the pile is placed. Maximum load can be held for up to two days before the load test is considered complete.

The test load is removed incrementally and rebound readings are made. The readings taken after the load has been removed give an indication of the total settlement of the pile and its ultimate capacity. Rebound readings should be made after the removal of each increment for a sufficient amount of time to ensure rebound has stopped before the next increment is removed.

2.5 Pile Group Behavior

The behavior of statically loaded individual piles has often been the basis for predicting the capacity of pile groups given the same type pile and soil stratification. This approach has led to the development

of efficiency formulas whereby the capacity of a pile group equals the capacity of an individual pile times the number of piles in the group multiplied by an efficiency factor (ASCE Committee on Deep Foundations, 1984). This approach most closely approximates the true bearing capacity of pile groups spaced at 2 to 3 diameters and deriving their principal support from granular media. The efficiency formulas do not account for the time effects which can manifest themselves as excessive settlements. ASTM D-1143 recognizes that capacities and settlements of pile groups cannot usually be inferred from the test of an individual pile in a like mass of soil. Due to the relatively short time span over which the load test is conducted on the individual pile, the positive skin friction resulting from driving may not have time to redistribute itself and can lead to a higher perceived capacity than the pile can maintain over its lifespan. If the pile group is underlain by a compressible layer, even at a significant depth, the entire foundation may settle subsequently to the consolidation of that layer. This type of failure will not be apparent from measurements taken from nearby reference piles as the reference piles are settling with the pile group. The piles may not be settling with respect to the soil in which they have been driven.

Group pile response to loading may vary significantly from that of individual piles due to the different zones of influence created by each foundation. It is important to consider the relative contribution of skin friction and point bearing to the overall capacity. A single pile can derive a large part of its capacity from skin friction with a proportionately smaller part being derived from end bearing. The pile group stresses the soil in such a way that the entire block of soil

contained within the group boundary transfers a relatively larger portion of the load to a lower stratum. Additionally, a rigid cap serves to transfer a greater proportion of the total load to the outer piles. This may contribute to the total mobilization of the friction capacity of the outer piles with the inner piles being only slightly stressed. In a group configuration, the piles act more as end bearing than friction piles (Peck, Hanson, and Thornburn, 1974). Thus, the zone of influence created by individual piles contributes to the overall influence of the group when a number of piles are driven as a group. The interaction between piles of a group becomes more pronounced as the Poisson's ratio of the surrounding soil decreases (Butterfield and Banerjee, 1971).

The behavior of the group may vary significantly from that of the individual pile. This variation makes the prediction of group behavior dangerous and difficult when based on only individual pile load tests even if the bearing soil is the same. Regarding group settlement in granular soils, the major portion of settlement occurs immediately. The shape of the load-deflection curve is similar to that for individual piles; however, the proportion of immediate settlement is generally smaller for a group than for the individual pile (Butterfield and Banerjee, 1971).

CHAPTER 3 SIMILITUDE REQUIREMENTS

3.1 Similitude Theory

Driving model piles in an artificially induced high gravity environment is a complex task which does not lend itself easily to analytical solutions based on mathematical models. As discussed previously, conducting tests with miniature piles at one gravity does not accurately model the prototype stresses experienced at the soil-pile interface. Uncertainties are introduced if the results are extrapolated to prototype depth as soil has stress-dependent mechanical properties that vary with depth (e.g., strength, moduli, wave propagation velocity, etc.). Whitaker (1957), Saffery and Tate (1961), and Sowers et al. (1961) produced qualitative results in their studies of miniature pile (group) response to loading at 1-g. Collectively, these efforts served to verify the findings of Rocha (1957) that the results of 1-g tests cannot be scaled up to re-create or predict pile performance. The model must be subjected to stresses equivalent to those experienced by the prototype. Scott (1977) demonstrated the ability to conduct pile load tests in a high gravity environment by cyclically loading piles inserted in silt. There was no prototype and thus no standard with which to compare the model performance.

It is necessary to create equivalent self-weight-induced stresses at similar points of interest in the model as in the prototype. This is accomplished by subjecting a properly scaled model and soil mass to a

gravity level sufficiently high to produce the desired stress. This acceleration is provided most simply by a centrifuge.

Scaling relationships permit the design of the pile and driver for the proposed gravity levels and interpretation of the data obtained by operation of the device at its design gravity level. Testing in a high-gravity environment requires the energy input of the miniature pile driver to be scaled down in some manner to insure equivalency with the prototype. Likewise, the pile capacities and stresses developed during placement and loading must be scaled up for comparison with the prototype. The scaling relationships are derived by dimensional analysis.

Dimensional analysis is a method by which we deduce information about a phenomenon from the single premise that the phenomenon can be described by a dimensionally correct equation among certain variables.

(Langhaar, 1951, p. 17)

As the number of variables affecting a process increases, it becomes progressively more difficult to determine the function which relates the experimentally controlled inputs (independent parameters) to the response being investigated (dependent parameters). By creating dimensionless parameters relating the most easily controlled experimental parameters to the ones being measured, ratios can be defined which relate model response to prototype response. These dimensionless ratios, called Pi (π) terms, were first developed by Buckingham and presented in 1914.

3.2 Selection of Dependent and Independent Variables

The choice of independent and dependent variables is of most critical importance in the development of the Pi terms.

If variables are introduced that really do not affect the phenomenon, too many terms may appear in the final equation. If variables are omitted that logically may influence the phenomenon, the calculations may reach an impasse, but, more often, they lead to incomplete or erroneous results.

(Langhaar, 1951, p. 19)

The selection of basic units for the Pi terms is also very important. The mass, length, time (MLT) system was selected for this research as unit mass does not change in multiple gravity environments and the MLT system appears to be favored in previous references (Nielsen, 1983; Bradley et al., 1984; and Tabatabai, 1987).

Table 3-1 presents the researcher's choice of independent and dependent variables considered pertinent to this investigation. The first three variables are the independent parameters which are considered easily controlled experimentally. The choice of which three variables were used was subject to the restrictions that, among the three, each of the basic units had to be used at least once, and the variables had to be independent among themselves to ensure independent solutions. The remaining variables were chosen to represent the material and physical properties considered to be important in the process being modeled. Certain properties of each of the materials used are important, such as modulus, compression wave speed, and strength. However, as the units for any one of those parameters are the same for each material under consideration, the collection of like parameters is represented by one generic term. Thus, Young's modulus of elasticity, E , is included only once in the collection of variables and not once for each material. Material properties relating to the presence of water in

the soil were included as the model piles were designed to be capable of being driven into saturated soils.

Table 3-1 Independent and Dependent Variables

Variable		Units	
<u>Independent</u>			
Length	L		L
Density	γ		M/L ³
Modulus	E		M/LT ²
<u>Dependent</u>			
π_1	Stress	σ	M/LT ²
π_2	Acceleration	a	L/T ²
π_3	Impact Energy	E_n	ML ² /T ²
π_4	Impulse	I	ML/T
π_5	Cohesion	C	M/LT ²
π_6	Dynamic Time	T	T
π_7	Wave Speed	P	L/T
π_8	Yield Strength	F	M/LT ²
π_9	Displacement	D	L
π_{10}	Area	A	L ²
π_{11}	Permeability	K	L/T
π_{12}	Hydrodynamic Time	T_h	T ²

The Pi terms were developed using the program PISETS written by Theodore Self at the University of Florida in 1983. PISETS was available on the Commodore SuperPET microcomputer as well as the Northeast

Regional Data Center (NERDC). Bradley et al. (1984) and Bradley (1983) present the method of setting up the input matrix for use with PISETS. Appendix A presents the derived Pi terms and verification that each is dimensionless.

3.3 Development of Scaling Laws

Scaling laws were formulated by taking the derived Pi terms and equating the model Pi term to its equivalent prototype Pi term. The scale length factor was used to change geometric properties by an appropriate factor of n . Like materials in the model and prototype permitted the cancellation of material properties in the equivalent Pi terms. The scaling laws were derived as presented in Appendix A and are summarized below in Table 3-2.

Table 3-2 Scaling Relationships

Property	Prototype	Model
Length	1	$1/n$
Density	1	1
Modulus	1	1
Stress	1	1
Acceleration	1	n
Impact Energy	1	$1/n^3$
Impulse	1	$1/n^3$
Cohesion	1	1
Dynamic Time	1	$1/n$
Wave Speed	1	1
Yield Strength	1	1
Displacement	1	$1/n$
Area	1	$1/n^2$

Dimensionless quantities such as strain and Poisson's ratio remain dimensionless and scale 1:1. Quantities not specifically derived above can be determined by combining the appropriate Pi terms. The two remaining pertinent scaling laws, permeability and hydrodynamic time, will be derived as examples.

Permeability (k) has units of length/time. Model permeability equals prototype length times the scaling factor $1/n$ divided by the prototype time multiplied by its scaling factor, $1/n$. The scaling factors (in this example) cancel one another indicating that model permeability equals the permeability of the prototype. This is a predictable result considering the requirement to utilize like materials in the prototype and model.

Hydrodynamic time (T_h) is determined by a similar method. The equation for hydrodynamic time is derived from Terzaghi's one-dimensional consolidation differential equation which provides a nondimensional time T called the time factor (Lambe and Whitman, 1969). The time factor equals the coefficient of consolidation, C_v , multiplied by real (hydrodynamic) time, T_h , and divided by the square of the drainage path, H . The equation for hydrodynamic time and its units are provided below.

$$T_h = \frac{T H^2}{C_v} \quad \text{Eq. 3-1}$$

$$T_h = \frac{T L^2}{L^2/T} = T^2 \quad \text{Eq. 3-2}$$

The units of hydrodynamic time are T^2 . Thus, model T_h equals prototype T_h multiplied by the square of the dynamic time scale factor ($1/n$), or $1/n^2$. The two scaling laws derived are summarized below. The subscripts m and p designate the model and prototype variables, respectively.

$$k_m = k_p \quad \text{Eq. 3-3}$$

$$T_{hm} = T_{hp} 1/n^2 \quad \text{Eq. 3-4}$$

3.4 Experimental Requirements

Care must be exercised in the application of the scaling laws to the development of the model pile driver. Consider the impact energy imparted by the hammer striking the pile. The scaling factor which relates the prototype energy to the amount of energy input by the model driver is $1/n^3$. Modeling the 50,000 ft-lbs of work needed to lift the prototype hammer (5,000 pounds with a drop height of 10 ft) at 70 g's requires the model pile driver input 0.146 ft-lbs. The model driver input can likewise be determined by considering the hammer weight and drop height independently. The ram weight of 5000 lbs divided by n^2 equals 1.02 lbs and the fall height is reduced to 0.143 ft. The product of these two properly scaled values is the required 0.146 ft-lbs. However, the hammer weight required during driving is the weight of the hammer mass at 1 g multiplied by the gravity level at which the test is conducted. The model hammer weight is then 1.02 lbs divided once more by the gravity scale factor, n . Thus, a model hammer weighing 0.233 ounces at 1 g is sufficient to model the 5,000-lb prototype hammer when subjected to 70 g's.

CHAPTER 4 EQUIPMENT DESIGN, FABRICATION, AND OPERATION

This chapter documents the design of the system developed to place the model piles. Computer control of the system and data recording techniques are presented. Pertinent fabrication methods are discussed.

The model pile sizes were determined prior to the system design as all critical dimensions of the placement device are predicated on the model dimensions. Designing the piles to be used as models required an understanding of the type of pile to be modeled, the loading regime under which the prototype pile was tested, and the modeling techniques used by previous researchers. The higher stresses experienced by the model pile during driving predicated a significant departure from the existing techniques.

The placement device was designed to permit the pushing and driving of model piles and groups permitting the comparison of the residual stresses developed in each model resulting from the different methods of placement. Design required an understanding of the prototype pile driver performance capabilities.

The centrifuge was designed to permit positioning of the specimen and placement device with sufficient clearance to allow all tests to be safely performed. The uses of the Hewlett-Packard 6940B Multiprogrammer and 3497A Data Acquisition/Control Unit are also detailed. Several limitations in the use of the pile placement device are presented in the final section of this chapter.

1.1 Model Pile Design and Instrumentation

The pile system modeled resembled the Hunter's Point group of five piles (O'Neill, 1986). This system was designated as the prototype although there were limitations in modeling of the axial stiffness and soil properties. Each pile was 35-ft long tubular steel with a wall thickness of 0.375 in. The outside diameter of the piles was 10.75 in. When driven in a group, the piles were arranged in an 'x' pattern with a pile in the center and one at each corner. The corner piles were 3 ft from the center pile. The cap was made of concrete having a thickness of 5.0 ft. The pile butts were embedded 2.0 ft into the cap leaving 3.0 ft of cover. The bottom of the cap was 3.0 ft above the ground surface. Nominally, the cap was 6.0-ft square. Total driven depth was 30.0 ft.

4.1.1 Model Material Selection

Similitude theory is simplified by the understanding that models will be made of the same material as the prototype to ensure the same stresses are developed in the model as in the prototype during testing. Use of the same material in the model was important in this application because the transfer of forces from the pile to the soil was investigated. As soil strength is mobilized by the slight movement of the pile surface relative to the surrounding soil, a variation in this relative movement would alter the load bearing capacity of the model pile as well as the load-deformation curve. However, strict adherence to similitude would have necessitated the use of a thin-walled steel tube as the pile model. The wall thickness would have varied between 6.3 and 4.7 thousandths of an inch for tests at 60 and 80 g's. Model piles with this wall thickness would have been crushed during driving due to lack of axial stiffness or the inability of the model driving device to strike

the pile perfectly in flight. Furthermore, the available steel tubes which could reasonably be considered as potential models had wall thicknesses far in excess of the desired amount. This would have resulted in an axial stiffness too great to permit accurate modeling of the stress transfer (load shedding) between the pile and soil. Therefore, various materials were considered which had lower strength moduli and were available in small tubular shapes. The axial stiffness of the prototype could be accurately modeled if the scale cross-sectional area of the model pile was increased by a factor equal to the modulus of the steel prototype (30,000,000 psi) divided by the modulus of the model material being considered. Aluminum was chosen as a suitable modeling material and has been used successfully in several previous studies (Millan, 1985; Ko et al., 1984; Harrison, 1983). Aluminum has a Young's modulus of 10,000,000 psi requiring that the scale cross-sectional area of the model pile be three times that of the prototype. Theoretically, the model pile would strain the same amount under the same scale load as the prototype thereby having the most potential of accurately mobilizing the same soil strength.

4.1.2 Model Size Determination

Limitations in the availability of tubular aluminum and the difficulty of manufacturing models with accurately scaled dimensions forced the need for a compromise between the modeling of pile diameter (and thus scale surface area) and axial stiffness. All tests were conducted with the models having the correct scale outside diameter and length. Because the available tubular aluminum had thinner walls than required for correct modeling, the scale axial stiffness of these models was lower than that of the prototype. This approach correctly modeled

the scale surface area of the model pile as well as the scale area of the tip; however, the model piles were less stiff (axially) when compared to the prototype stiffness.

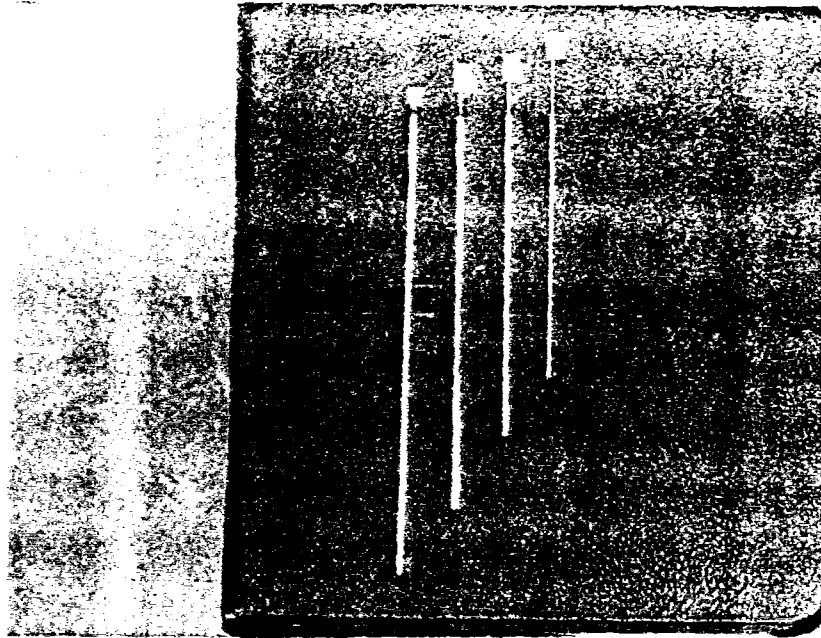
The gravity level of testing for pile models with scale geometric proportions (outside diameter and length) was determined by dividing the outside diameter of the prototype by that of the available model material. The length of the model was then the prototype length divided by the gravity factor. Table 4-1 provides the model dimensions and scale factors.

Table 4-1 Model Pile Dimensions and Scale Factors

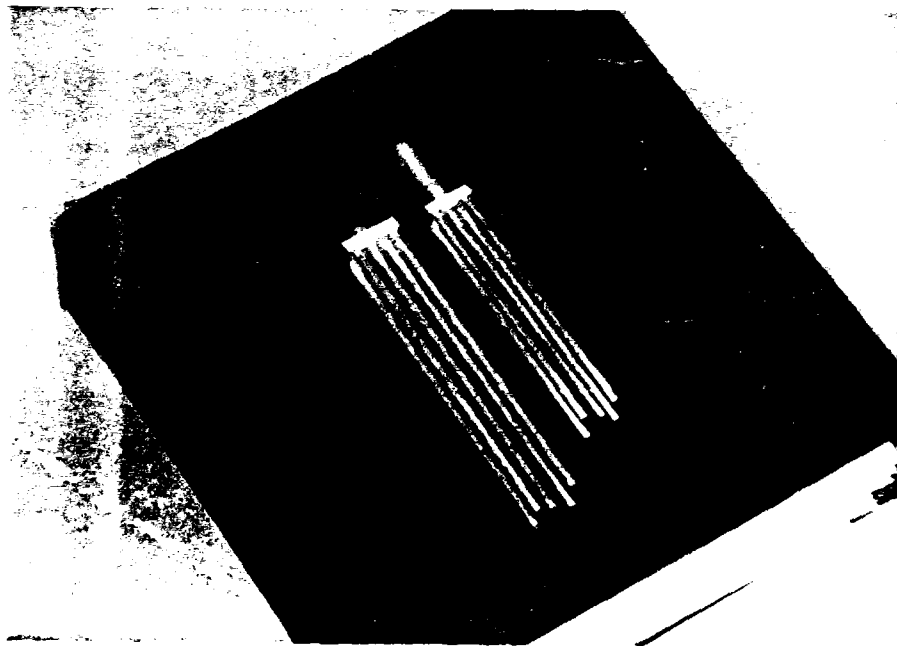
Controlled by Geometry (Outside Diameter)					
	Prot.	A	B	C	D
O.D. (in.)	10.75	0.125	0.154	0.187	0.218
g-level (g's)	1	86.0	69.8	57.5	49.3
Length (in.)	420	4.88	6.02	7.39	8.52
Stiffness (%)	100	95.4	73.8	66.6	57.5

NOTE: The axial stiffness of the model piles is given as a percentage of that of the prototype.

In summary, four suitable aluminum tubes were found for the manufacture of model piles. Scaling factors based on the outer diameter of the tubes yielded four pile sizes to be tested at g-levels between 49.3 and 86.0 g's. There was no manufactured aluminum tube which accurately modeled both the outer diameter and axial stiffness. Figure 4-1(a) depicts the individual model piles and associated gravity levels of testing. Figure 4-1(b) depicts the model pile groups and test gravity levels.



a) Individual Model Piles (Left to Right--49.3, 57.5, 69.3 and 86.0 g models)



b) Model Pile Groups (Left 69.8 g., Right 86.0 g)

Figure 4-1 Model Piles. a) Individual Model Piles (Left to Right--49.3, 57.5, 69.8 and 86.0 g models)
b) Model Pile Groups (Left 69.8 g., Right 86.0 g)

4.1.3 Strain Gage Placement

Research has been conducted using aluminum tubes which were split in half to permit the placement of strain gages, then glued together prior to pushing them into the modeled soil (Millan, 1985; Harrison, 1983). The difficulty of obtaining a strong bond between the two pile halves frequently resulted in the model piles splitting and exhibiting irregular butt deflection patterns during loading. The significantly greater stresses required for driving the pile prevented the reuse of this technique as only continuous tubular stock could be expected to withstand the driving process. The most significant drawback in the use of continuous stock is the difficulty of placing strain gages inside the model pile.

The method of placing the strain gages had to satisfy three criteria; the bond between gage and model had to be complete and permanent, the gages had to be positioned precisely, and the gages had to be able to perform after completion of driving. In addition to the above criteria, the gages had to be placed with leads already soldered on. Connection of the leads to the gages after placement was not possible without exceptionally sophisticated equipment.

Each strain gage, regardless of its working environment, must be placed on a clean, chemically prepared site. Proper cleaning ensures the gage can be bonded as intimately as possible with the material being measured. Preparing the sites inside the models was accomplished in accordance with Micro-Measurements Instruction Bulletin B-130-2. Fine grade emery paper was rolled into a small tube and inserted in the model. Being a soft metal, the aluminum required little sanding to smooth the interior and expose clean metal at the sites. An acid

solution (Micromasurements M-Prep 5) was used to etch the metal during cleansing. The site was neutralized with the appropriate solution, Micromasurements Neutralizer. Preparation was completed by pushing small wads of lint-free cotton material down the pile shaft in one direction only to prevent recontamination of the cleaned sites. The cleansing process was repeated until the cotton wads emerged dirt-free from the model pile interior.

Suitably sized strain gages (Micromasurements EA-06-015LA-120, Figure 4-2) were then prepared for placement. These gages were chosen because the lead terminals were large with respect to the field and were placed above the field in such a way that they presented a narrow plan view. This was important as the gage had to conform to rather tight radii on the insides of the models. The minute gage size required the leads be soldered on while being viewed under magnification. Consequently, the gages were sent to a laboratory where suitable equipment was available.

The strain gages with leads attached were prepared using the following procedure. Excess gage backing material was removed as indicated in Figure 4-3(a) to make the gage as tall and slender as possible. Gage resistance and continuity were checked to determine if damage had occurred during the trimming process. A piece of Micromasurements nonstretch tape was cut to the width of the length of the strain gage field. This tape was affixed to the two strain gages holding them in the same position relative to one another (Figure 4-3(c)). Special care was taken to ensure the principal strain measuring axes of both gages were parallel and the gages were the correct distance from one another. The distance between the two gages was predicated on the inner diameter

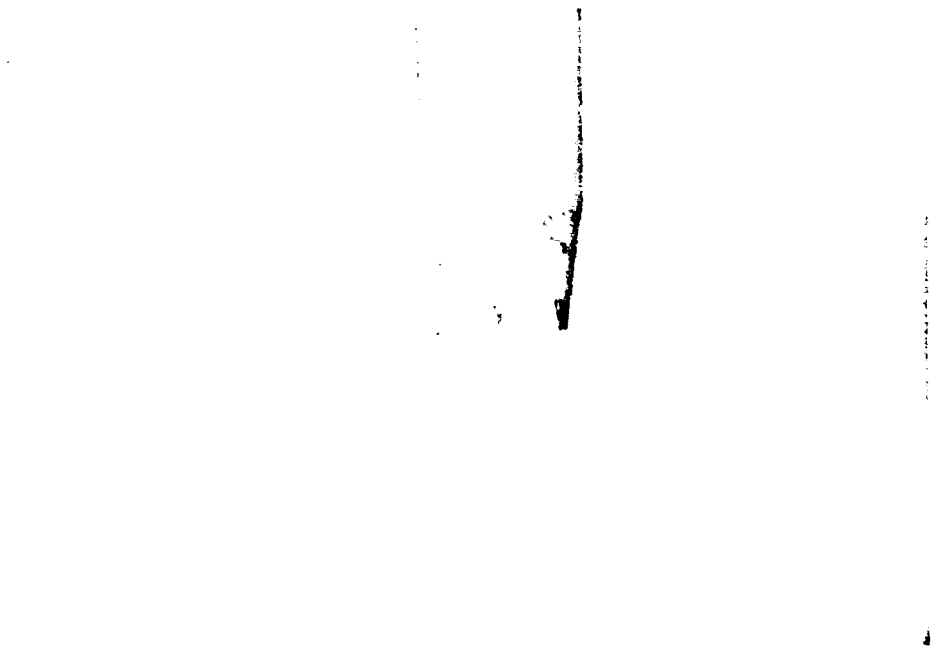


Figure 4-2 Micromerements EA-06-015LA-120 Strain Gages

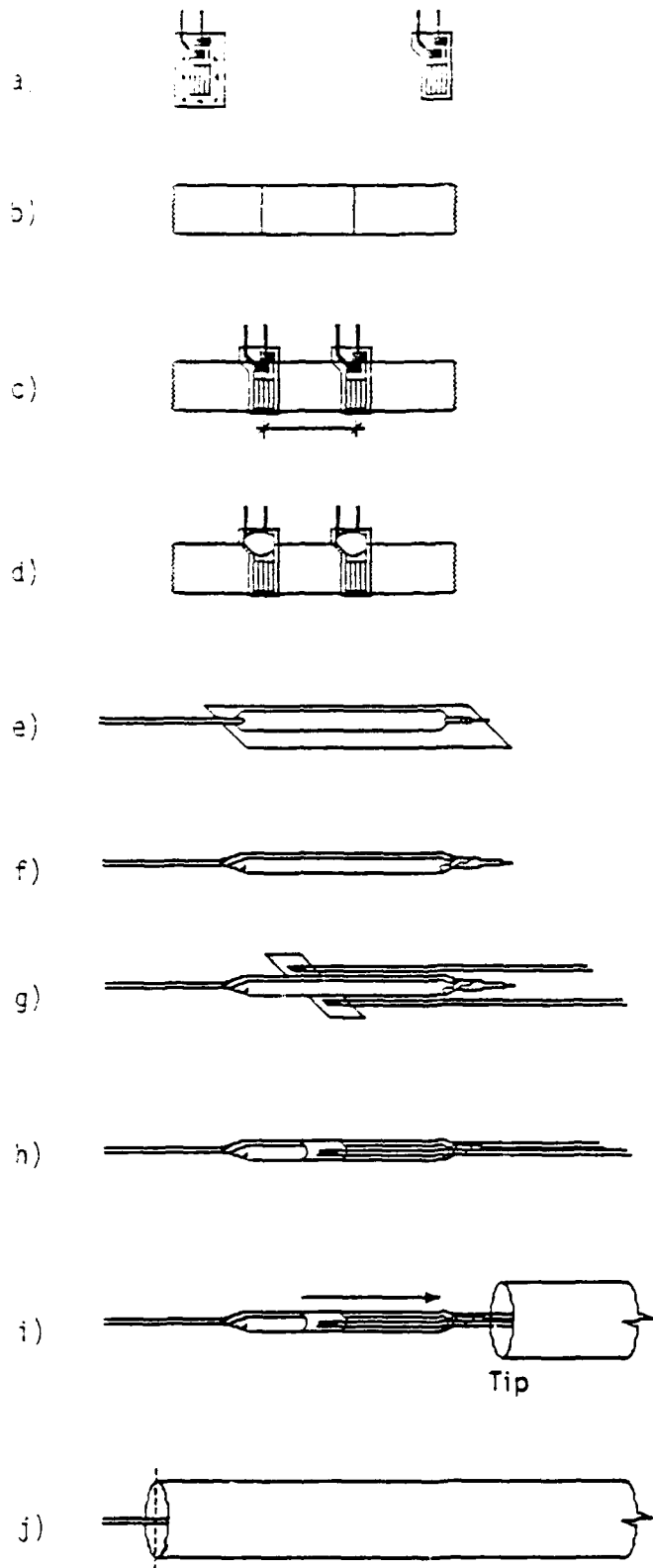


Figure 4-3 Strain Gage Application Technique

of the pile model in which the gages would be placed. The correct distance equaled one-half of the inner circumference of the model. A small amount of rapid-curing epoxy was applied as a sealer to the leads, gages, and tape as shown in Figure 4-3(d). This assembly was set aside to dry while the insertion device was prepared.

A Coronary Balloon Dilatation Catheter served as the insertion device. The catheter is fitted with a balloon which expands to a specific diameter upon pressurization. The balloon was wrapped with Teflon tape as shown in Figures 4-3(e) and 4-3(f) while the epoxy was drying. The gages and tape assembly was then wrapped 'gages out' around the catheter balloon (Figure 4-3(h)). Gage resistance was rechecked at this time to ensure only functional gages were inserted into the model. The small size of the deflated balloon permitted the catheter and gages to be inserted as a unit down the shaft of the pile (Figures 4-3(i) and 4-3(j)). The lead wires were inserted first, into what was to eventually become the pile tip. They were followed by the gages and balloon assembly which was advanced by pushing the pressure line leading to the balloon. Proper positioning was accomplished by marking the pressure line at the correct depth of insertion and inserting the assembly up to the mark. Each pair of gages became successively more difficult to insert as the leads from the previously placed gages interfered with feeding the new leads through. When in the proper position, the balloon was inflated, pressing the gages into the preplaced bonding material at the site. The balloon remained inflated until the bonding material had cured at which time the balloon was deflated and removed. The wrap of Teflon tape prevented the balloon from being bonded to the gages.

Placement of the gages had to be accomplished in a specific order. Models requiring strain gages only at the tip were produced using the previously described technique of inserting the lead wires into the tip and following with the balloon and gage assembly. Models requiring the placement of multiple pairs of gages underwent a slightly modified placement procedure to simplify the placement of the first pair. The balloon was first inserted through the model pile before being wrapped with teflon tape and having the gage assembly attached (Figure 4-4). This method improved the placement success rate of the butt gages by requiring they be pulled back into the model a short distance rather than being pushed through the length of the model before bonding. The balloon was deflated and withdrawn after placement in the same manner as when the gage pair is placed by being pushed through the model. The resistance of each gage was measured after being placed in the model. Variation of the gage resistance by more than 5.0% of the specified factory value of 120 ohms was cause for rejection of the gage and noted in the model pile construction log. There was no way to replace the gages if they were rejected. After placement of the final pair, the butt was sealed with a silicone cap reducing the chance of the leads breaking off of the gage during driving and testing.

The model was completed by fitting the tip with an individually machined cap which was inserted into the model plugging the tip. The outside diameter of the plug was equal to the model diameter. Each cap was held in place by pressure fit and sealed on the inside with silicone sealer to prevent the intrusion of water. This technique and the aforementioned procedures yield a fully instrumented waterproof pile capable of withstanding the stress of driving.

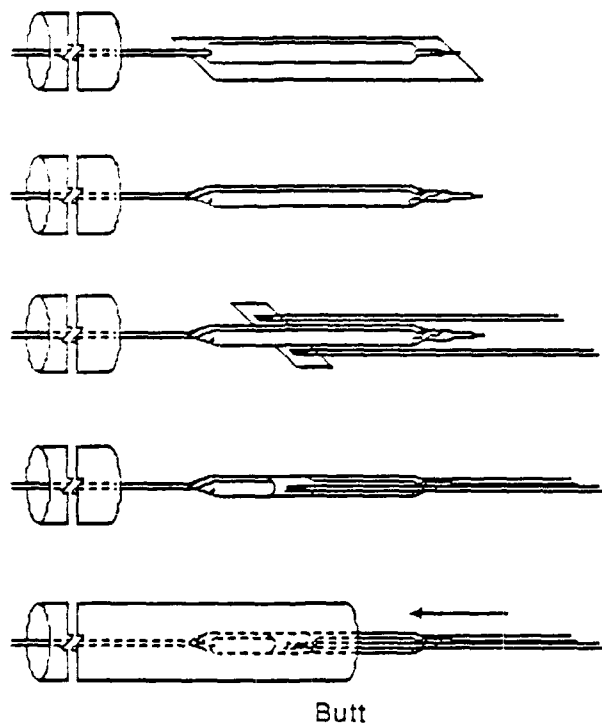


Figure 4-4 Alternate Technique for Placement of First Pair of Strain Gages When Multiple Pairs are Needed

Strain gages were positioned in the instrumented models at the tip and butt only. Initial tests were conducted on pushed piles with one pair of strain gages at the tip ($0.97d$ with d being the distance the model was pushed into the soil). Instrumented driven models (Figure 4-5(a)) should have pairs of strain gages placed at the one-third points and tip. The uppermost pair (gages 4A and 4B) serve to measure the total resistance of the pile to penetration due to both tip capacity and skin friction. The pushed models use a load cell to measure the total resistance to penetration and can therefore have four pair of gages placed at the quarter-points and tip (Figure 4-5(b)). Individual piles fitted like the one in Figure 4-5(a) should be used for measurement of the tip and side friction capacity in driven models. Again, the gage pair at the top (butt) of the model is required because the load cell could not remain in-line when models were driven. Positioning of the gage pairs at the butt in individually instrumented driven piles permits the immediate conduct of loading after the pile is driven.

Figure 4-6 depicts the suggested placement of gage pairs when instrumented model groups are driven and pushed. After being driven, the centrifuge must be stopped to fit the top of the group with a load cell. Load tests are then conducted after the centrifuge has been spun up to the required test rpm. When the group has been pushed in, loading is conducted immediately as the load cell is already in place.

Provision was made to protect the leads during driving and loading as will now be discussed. This method of protection was also used to prepare all models pushed into the soil with only slight modifications of the caps depending on whether the model was driven or pushed.

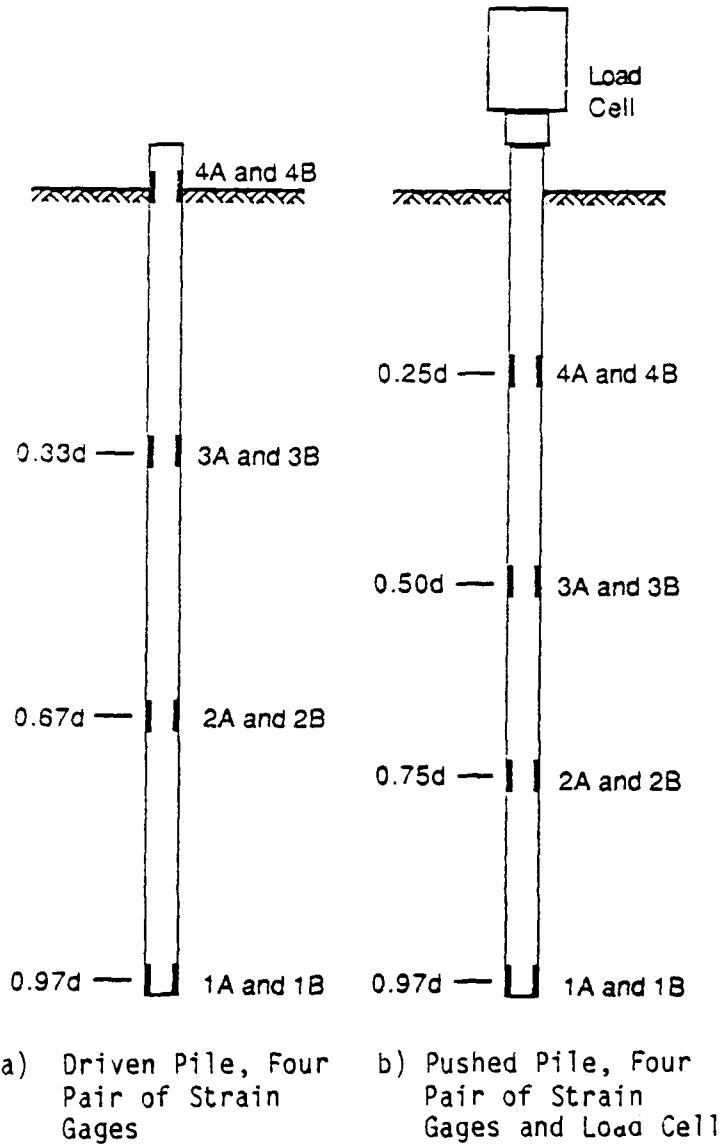


Figure 4-5 Suggested Gage Positions and Position Designations for Individual Driven and Pushed Piles (8 Strain Gage Channels Available). a) Driven Pile, Four Pair of Strain Gages; b) Pushed Pile, Four Pair of Strain Gages and Load Cell

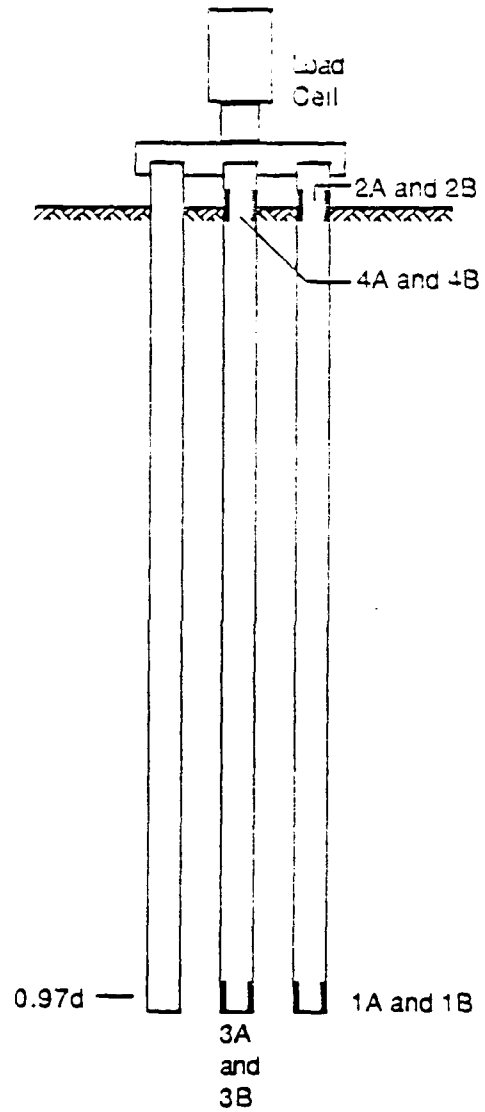


Figure 4-6 Suggested Gage Positions and Position Designations for Driven and Pushed Pile Groups (Load Cell Placed on Top After DRIVEPILE; Load Cell In Place During PUSHPILE)

4.1.1 Pile (Group) Cap Fabrication and Lead Wire Protection

An important consideration in pile driving is the protection of the butt of the pile from the potentially damaging blows of the hammer. This was accomplished using a pile cap as discussed in Section 2.3.1, Hammer-Cushion-Cap Interaction. A similar method was used in the driving of the models. Figures 4-7 through 4-10 show the types of caps developed for driving and pushing the model piles (groups). The caps served to protect the model as well as the strain gage lead wires while permitting the models to be interchanged quickly between tests. The lead wires were terminated in miniature connectors mounted on the support arm shown in Figures 4-7 through 4-10. When only one connector was necessary, the weight of the connector and shielded leads to the side of the specimen container was counterbalanced by the placement of a suitable weight at the end of the support arm extension through the other side of the slotted cast acrylic guide tube. This precluded the development of excessive moment at the top of the model when under the influence of the design gravity level. The model pile, cap, lead wires, and connectors are thus a complete unit capable of being plugged into the placement device as necessary for testing. This permits the models to be reused and interchanged quickly between tests.

4.2 Model Placement Device Design

The placement device needed for this investigation was required to lift a considerable variety of weights, provide accurate feedback regarding position of the lifted weight, and accurately raise the lifted weight a predetermined height above an object whose position changed with every impact. All of these activities were to be performed in an

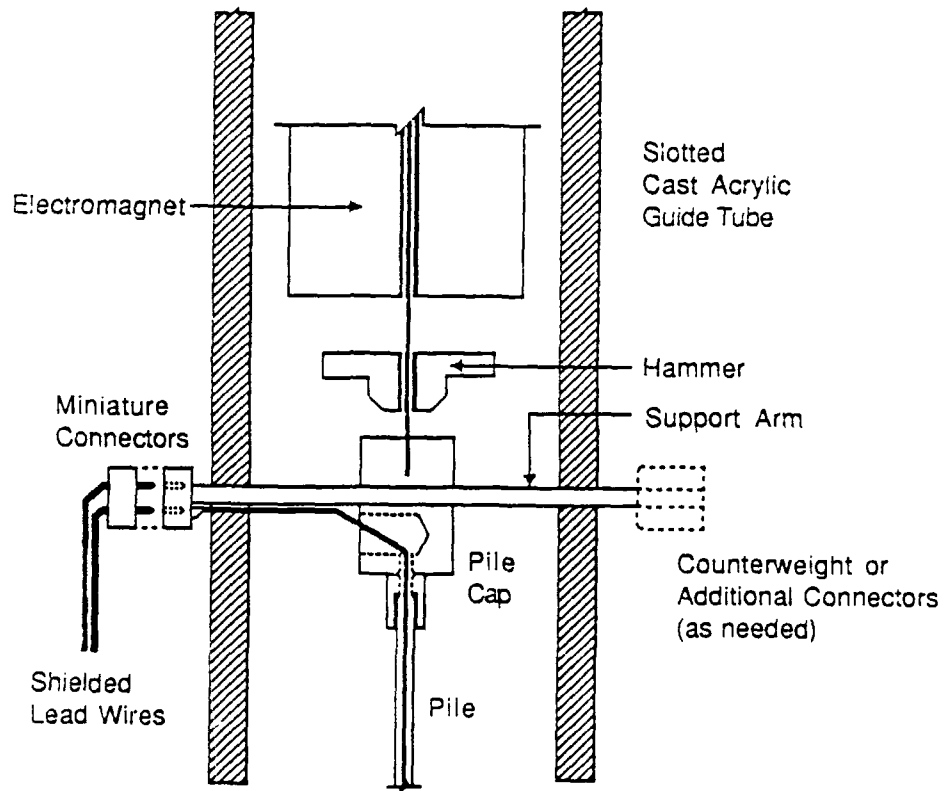


Figure 4-7 Pile Cap Assembly for Individually Driven Model Piles

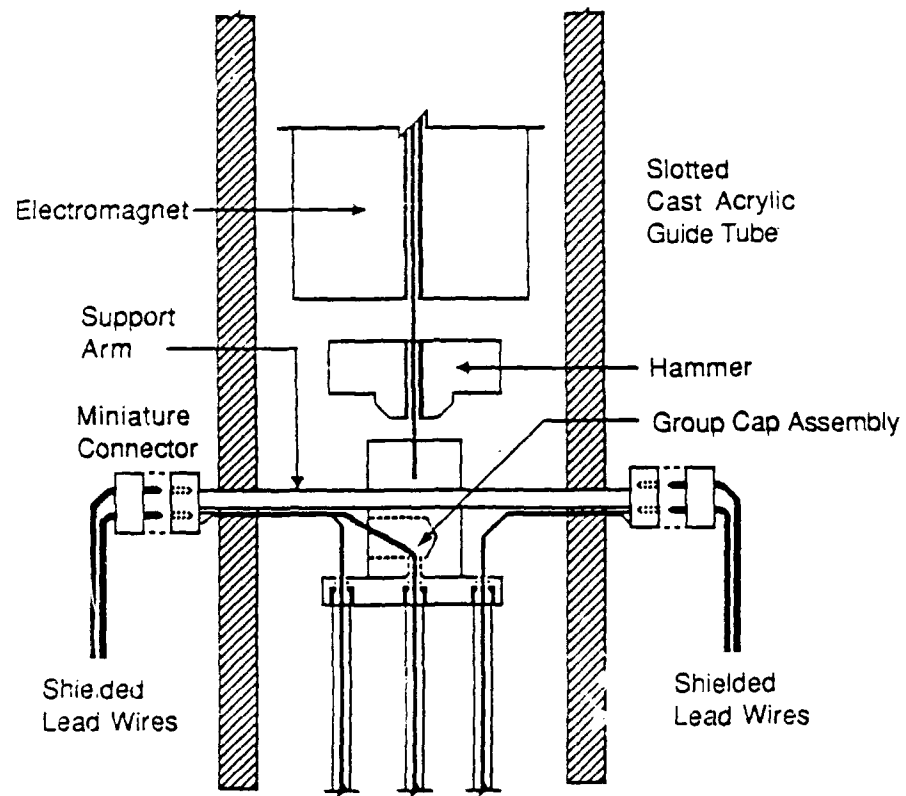


Figure 4-8 Pile Cap Assembly for Driven Model Pile Groups

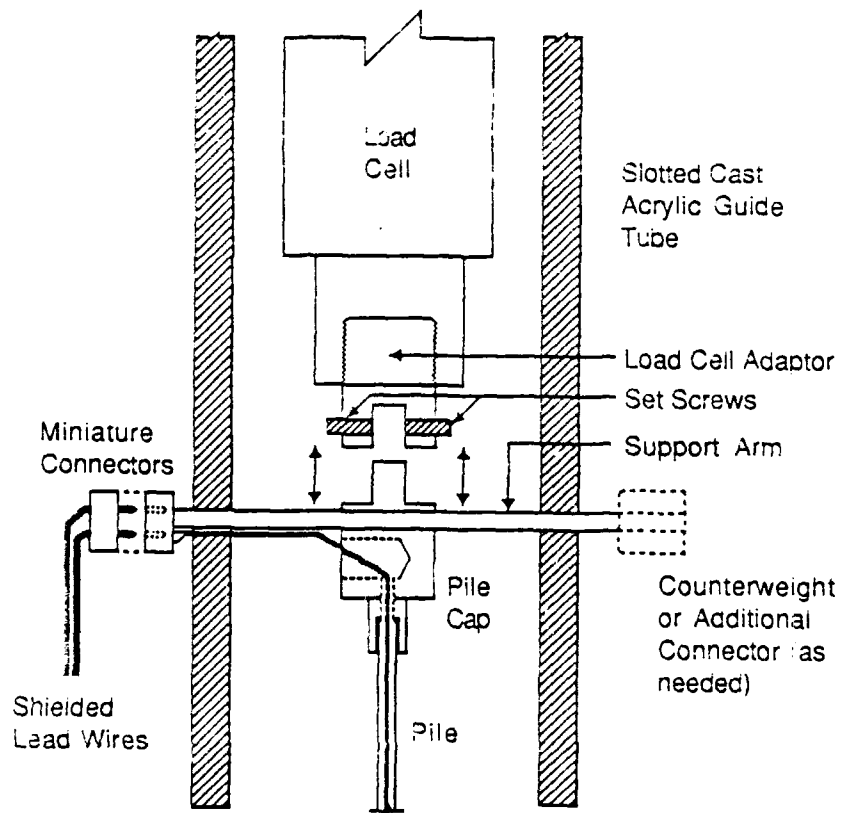


Figure 4-9 Pile Cap Assembly for Individually Pushed Model Piles

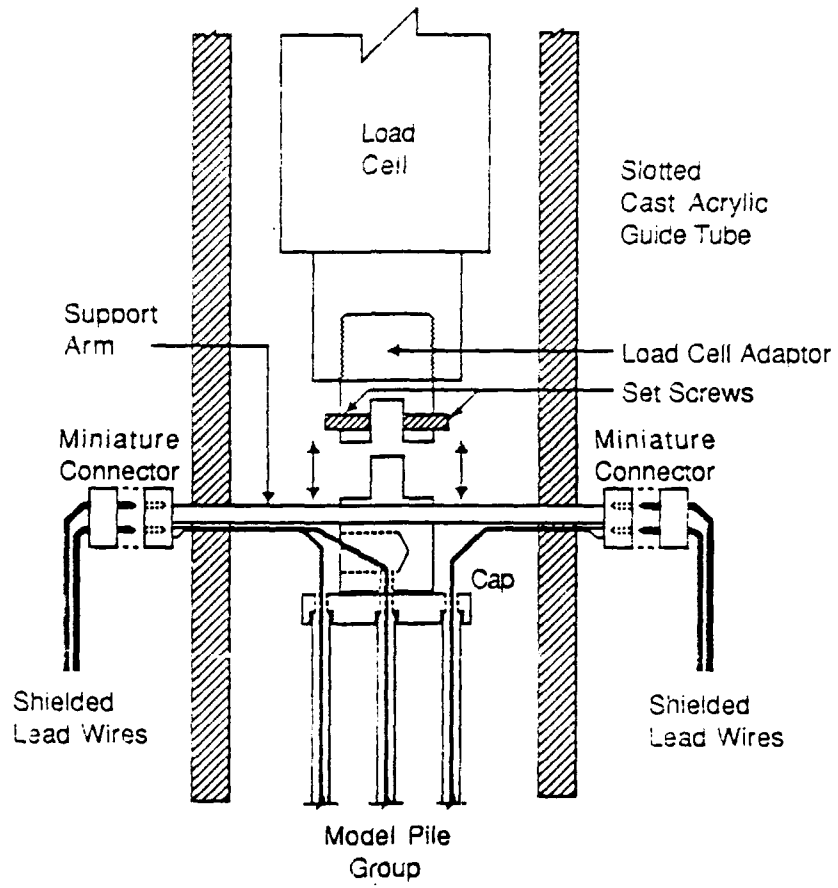


Figure 4-10 Pile Cap Assembly for Pushed Model Pile Groups

environment whose gravity level was high and subject to variation during the course of an experiment. The system developed was chosen after exhaustive elimination of many other mechanical methods, several gas/fluid hydraulic systems, and even a purely electromagnetic device. The main objection to some of the preceding systems was their inability to "follow" the model pile (group) as it advanced through the soil and their reliance on awkward position monitoring devices which would have affected the dynamic response of the system. Compounding the difficulty of building the device was the limitation imposed by the lack of clearance above the platform. A suitably sized soil specimen with a model pile on the surface and the placement device above requires a relatively deeper centrifuge than that needed for experiments with compact specimens. Furthermore, the system must be designed with a low center of gravity. An alternative design considered the driving device being mounted statically on the arms of the centrifuge with the specimen swinging into position for driving. However, pile placement accuracy could not be guaranteed with this design. The chosen configuration consisted of a soil specimen container with the driving device mounted above in a protective canister.

The system chosen (Figure 4-11) consists of a stepper motor geared through a ball bearing screw assembly (ball screw) to a support shaft which lifts an electromagnet and pile hammer when individual piles and groups are driven. Rotation of the ball nut (the housing around the ball screw which contains the ball bearings) either raises or lowers the ball screw to which the electromagnet is attached. During driving, the electromagnet is advanced (downward) until it comes within 0.005 in. of the ram. The closeness of approach is determined by a proximity device.

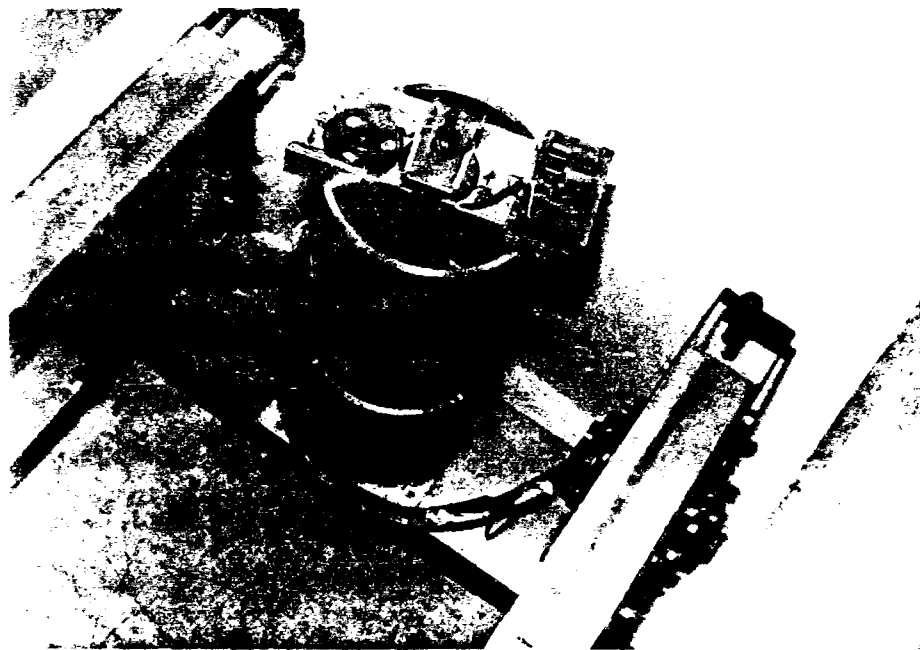


Figure 4-11 Specimen Container, Placement Device Protective Canister, and C-Channel Support Beam

The electromagnet is then energized. Reverse rotation of the stepper motor retracts (upward) the magnet and ram to the predetermined drop height. The magnet is then de-energized allowing the weight to fall and impact on the pile cap.

The predetermined lift height is achieved by rotating the stepper motor a known number of "steps". Counting the number of steps which the magnet is lowered to regain contact with the ram permits the determination of the number of steps the device has penetrated the soil. That number of steps is easily and accurately converted to a vertical distance. The process then repeats itself with the energizing of the magnet and the retraction of the magnet and ram assembly to a newly determined lift height. This system offers the advantages of accuracy and control of the height to which the ram is lifted, repeatability, a free falling weight, the capability of following the device as it penetrates the soil, and no bulky displacement measuring devices to alter the dynamic performance of the system.

When piles (groups) are pushed, the electromagnet and hammer are replaced by an in-line load cell which fastens directly to the base of the ball screw. During pushing, the pile (group) is advanced into the soil with readings being taken from the load cell at frequent intervals.

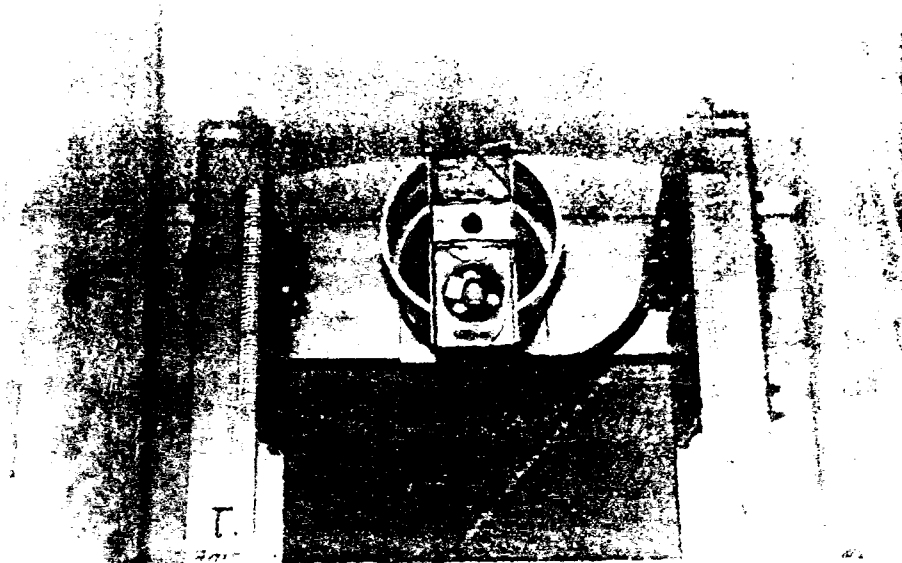
Load tests are conducted as will be presented in Section 4.5.2, Software. The major components of the system will now be presented.

4.2.1 Specimen Container, Placement Device Protective Canister, and C-Channel Support Beam

Support for the device consists of a circular specimen container machined from high-strength aluminum and welded to a square base plate. The square base plate is bolted to the swinging platform on the end of the centrifuge arm (Figure 4-11). The base plate can be mounted in four

configurations, with any given side being able to be positioned at 0, ± 90 , and 180 degrees with respect to the center line of the platform. The top of the soil specimen container has a groove machined around the rim. This groove serves as the male end which fits snugly into the female groove machined into the base of the placement device canister. The grooves hold the canister in place above the specimen container while permitting rotational flexibility. The top of the canister supports the aluminum c-channel which is the main frame of the placement device components. The c-channel has limited positioning capability which permits the placement of the ball screw directly above the center of the canister centerline as well as in any position within approximately 2 in. of the centerline. This flexibility permits the driving of pile groups by individual piles as with the prototype. The combination of the back and forth freedom of movement of the c-channel with the rotational freedom of the canister top provides substantial positioning freedom within the specimen container.

The capability of mounting the specimen container base plate in four unique positions was included in the design to ensure the least stress was exerted on the platform support arms during testing. Figure 4-12(b) shows how the canister and placement device should be configured. The intent is to decrease the eccentricity of the load on the platform due to the placement of the stepper motor. Figure 4-12(a) shows the configuration of the canister and stepper motor when video recording of the placement process is necessary. This position exposes the placement mechanism to the camera through a port in the side of the canister when the platform and canister have rotated to horizontal. A mirror is needed for the video camera to view the placement device.



a) Configuration Used for Video Recording



b) Normal Configuration

Figure 4-12 Top View of Canister and Placement Device Configuration.
a) Configuration Used for Video Recording;
b) Normal Configuration.

However, this is the least desirable configuration and was used only when necessary. In this position, the concentrated load of the motor (close to the vertical centerline of the platform) will force overrotation of the platform. This configuration would ultimately cause the payload to fall off into the bottom of the centrifuge housing if the payload were not properly fastened to the platform or if the platform were not fixed against overrotation. Rotation of the canister until the stepper motor is almost in line with the horizontal centerline of the platform (Figure 4-12(b)) will decrease the tendency of the platform to overrotate. However, video recording of the placement process is not possible because the line of sight is blocked by the canister side. Rotation of the canister until the stepper motor is above the center line of the platform will induce underrotation, another obviously unacceptable occurrence. The combination of stepper motor positioning which caused the least stress on the platform bearings was the position which developed a slight tendency to overrotate just pushing the platform arms against mechanical stops installed on the centrifuge arms (Figure 4-13). This was the configuration used most often. Once this position was established, the driving of second and subsequent piles in a group could be accomplished by pushing the stepper motor slightly closer to the central axis of the specimen container. The shift in placement would be equal to the scale distance between multiple piles. Shifting the stepper motor towards the central axis of the specimen container would then serve to decrease the eccentric loading induced by the motor. For subsequent piles, the specimen container would be rotated ninety degrees underneath the stationary canister.

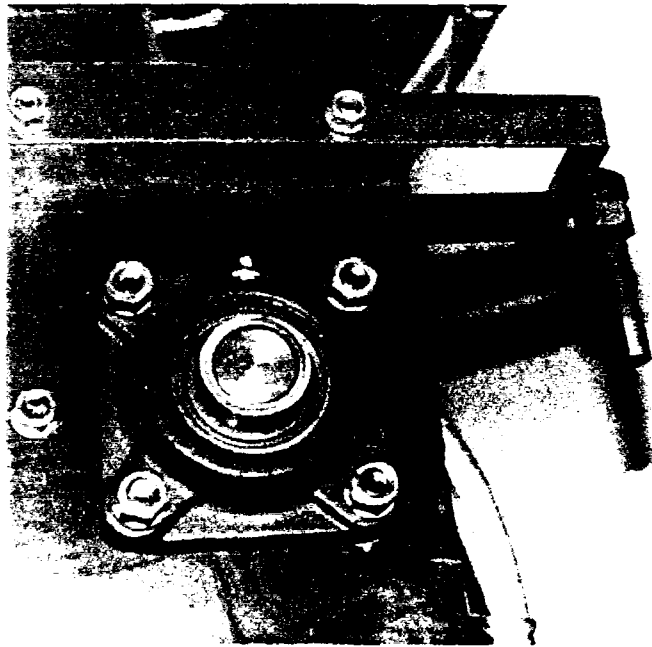


Figure 4-13 Platform Mechanical Stops

4.2.2 Stepper Motor

The stepper motor is a versatile and relatively important member of the system. It provides both precisely controlled incremental positioning and high static and dynamic torque. The name stepper motor is derived from the discontinuous motion of the driveshaft as each pulse received initiates acceleration, precise rotational displacement, and deceleration of the drive shaft. Thus, there is no continuous shaft motion, only short steps in the desired direction. Controlling the number of pulses determines the amount of rotational displacement. Controlling the frequency of the pulse input determines the "speed" at which the drive shaft rotates. Initialization of the drive shaft position will permit the accurate determination of the shaft orientation at any time if the input pulses have been accurately accounted for. One revolution of the drive shaft requires 200 pulses, or steps. Thus, each step results in a shaft rotation of 1.8 degrees.

Proper use of the stepper motor requires an understanding of the amount of time required to perform a given rotational command, the necessary static and dynamic accuracy, settling time required to achieve that accuracy, and the total system friction and inertia. These parameters must be determined before the stepper motor can be chosen. Considering the type of experiment being conducted, the first three concerns are minor. The stepper motor frequency was chosen to ensure the motor would accurately perform the desired rotational displacement. A low frequency (200 pulses per second) was chosen for initial tests. The motor control circuitry was configured to provide input pulses at this frequency as prior research has not even suggested a time dependence on pile driveability vs. the frequency of impact in the granular soils

being investigated. Therefore, for control purposes, the stepper motor was driven at the rotational speed which offered the optimum combination of lifting capacity and step accountability--the latter being the primary concern.

According to the manufacturer, a low performance system, i.e., low rotational speed, can provide accurate stepping under an inertial load of approximately nine times the rotor inertia. This is true under normal gravity. However, rotation of the stepper motor drive shaft under a higher inertial load, as was necessary in the centrifuge tests, could result in missed steps. One or more steps could be lost or gained due to inertial "coasting" of the motor after pulses have stopped. Thus, it was necessary to verify the stepper motor was performing the commanded rotations under the proposed test gravity levels. Verification of the accuracy of the rotational displacement is presented in Section 4.7, Equipment Limitations.

Operating the motor at a low rotational speed minimized the potential for dynamic overshoot of the desired number of steps. Dynamic accuracy concerns settling time, or the amount of time it takes the stepper to return to its commanded position after a given rotation. Settling time was also reduced by operating the motor at a low frequency. Regarding this application, the settling time was negligible.

Static accuracy is dictated by the amount of control desired over the lift height of the ram and is adjustable by several means. A direct linkage between the stepper motor and ball screw assembly provides the simplest relationship governing the number of steps versus the vertical displacement of the rack gear and magnet load cell. Vertical displacement of the ball screw for each step equals the "lead" of the ball screw

assembly divided by the number of steps per complete revolution of the stepper motor drive shaft (200 for the stepper motor used). Finer control of the vertical displacement can be achieved by the introduction of a gear reduction assembly between the stepper motor and ball screw assembly. Accuracy of the vertical displacement can be improved by a factor equal to the reduction gearing. The reduction gearing likewise increases the lifting (or pushing) capacity of the driving device by a like factor. Alternatively, the stepper motor can be configured to advance only 0.9 degrees per step (called half-stepping) effectively doubling the accuracy of the system, however, the dynamic and static torque available decrease as a result of this reconfiguration.

Manufacturers' literature should be consulted prior to use of a stepper motor to familiarize the operator with the unique power and control requirements of the system. The required 24-volt power is provided by an appropriately sized transformer. A Bodine THD-1830E Adjustable Motion Control provided precise control of the direction and speed of rotation. Figure 4-14 shows the transformer and adjustable power resistors required to power the stepper motor. The motion control is shown in Figure 4-15. The slip ring assignments for power and control leads are shown in Figure 4-16. Control is switchable from manual to external (computer) by toggling a single pole double throw switch fitted to the side of the stepper motor controller.

4.2.3 Ball Screw Assembly

The ball screw assembly consists of threaded shaft (ball screw) fitted with a cylindrical housing and collar (ball nut). Contact between the ball screw and ball nut is maintained by small ball bearings which facilitate rotation of the ball nut even with the ball screw under

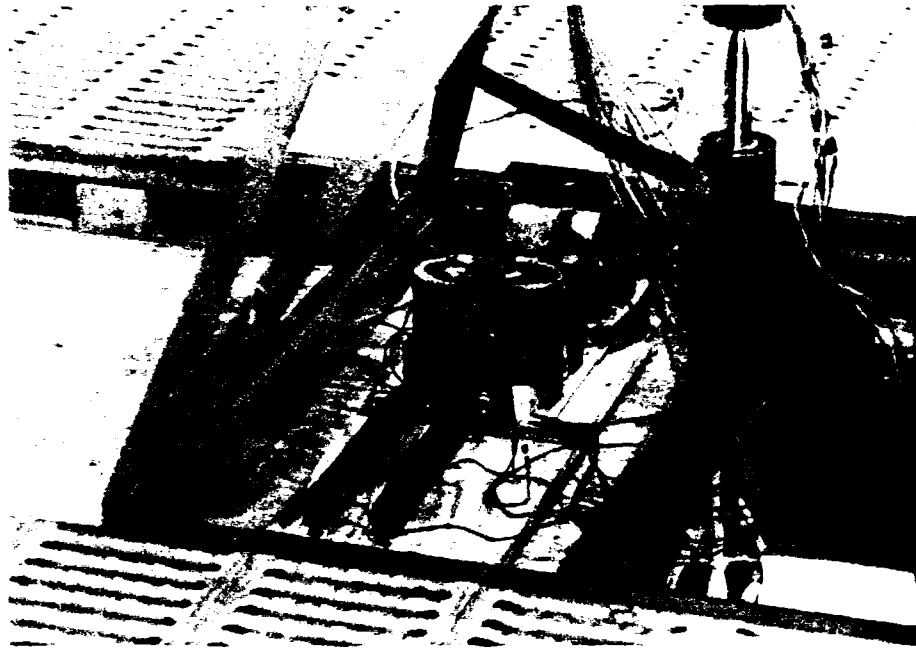


Figure 4-14 Stepper Motor Transformer and Variable Power Resistors

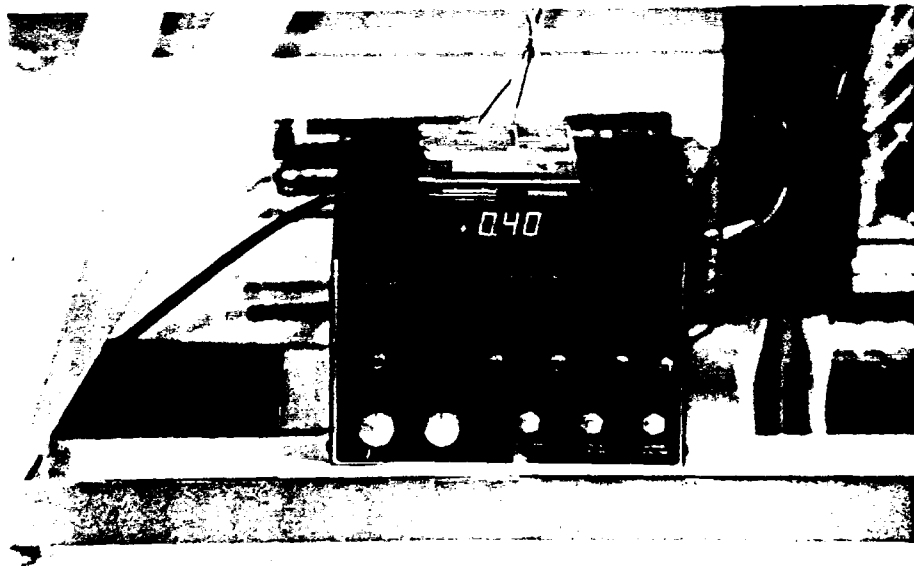


Figure 4-15 Bodine Type THD-1830E Adjustable Motion Control

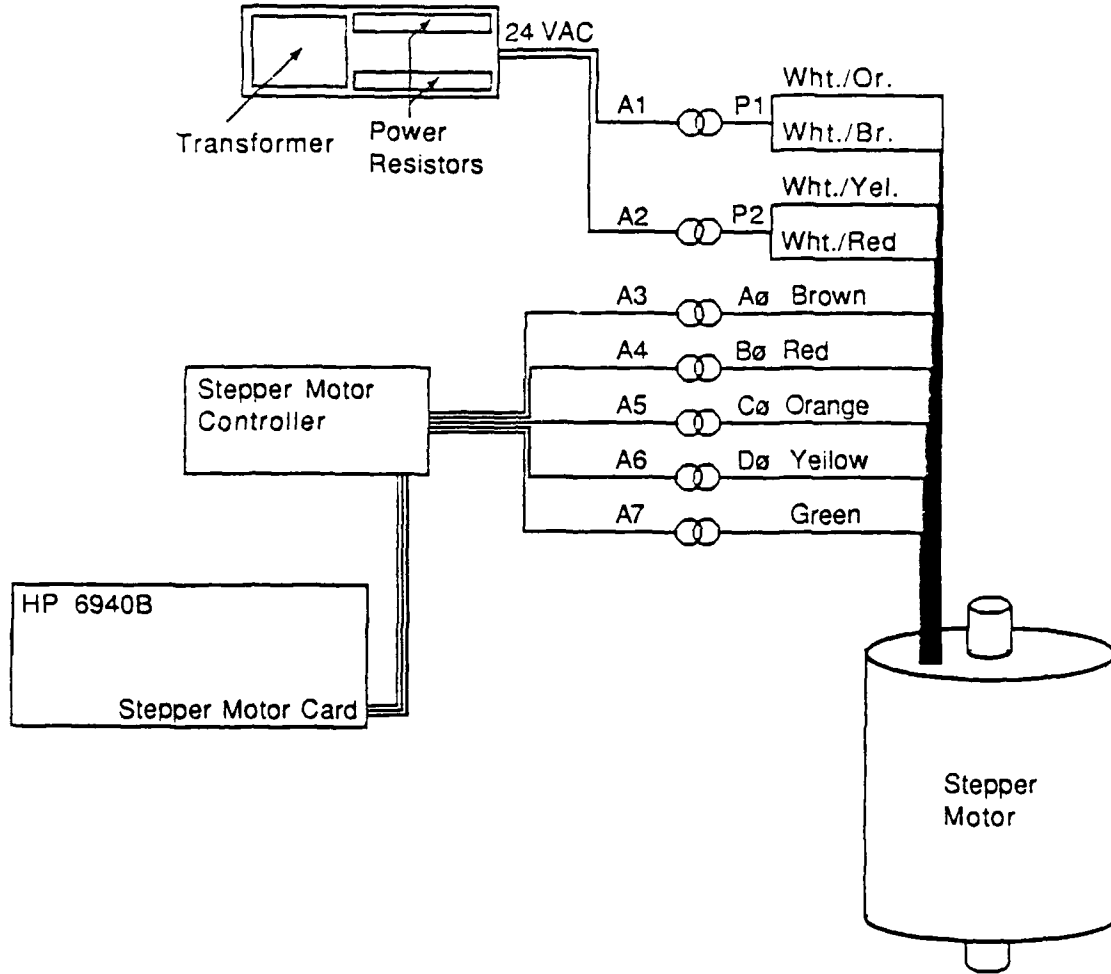


Figure 4-16 Stepper Motor Control Circuit and Slip Ring Channel Assignments

substantial axial load. The ball screw and nut are supported by a custom manufactured support ring which fixes the ball screw assembly against lateral movement. The stepper motor driveshaft torque is transmitted to the ball nut by identical gears on the driveshaft and ball nut. The driving gear is located on the stepper motor drive shaft and the driven gear on the support ring. The gears have a diametral pitch of 54, the finest available from the manufacturer. Gears of this pitch have 64 teeth at the pitch diameter for every inch of diameter. These gears are the largest available of the stated pitch diameter. The pitch diameter was chosen because the finer teeth provide smoother meshing and less backlash due to meshing errors. Furthermore, there is less play between the teeth when the direction of rotation is reversed. The large (3.0-inch pitch diameter) gears are suitable for several reasons. First, the centerline of the stepper motor must be at least 2.90 in. from the centerline of the ball screw shaft in order to be mounted in the configuration shown. This configuration was the most compact with regard to height. Secondly, the larger the pitch diameter of the chosen gear, the smaller the stress on the individual teeth in contact. This is an important consideration as the gears of this size are available only in brass, a relatively soft metal.

The driving gear was bored out to fit snugly over the stepper motor drive shaft and fitted with three set screws to lock the gear onto the motor shaft. The driven gear required extensive machining. It was placed in custom made lathe chuck teeth to hold the gear by the teeth while the center of the gear was removed. The remaining ring gear was press fitted onto the support ring shoulder of matching diameter and held in place by a pressure ring. The shoulder was necessary to keep

the driven gear and ball screw assembly in concentric alignment. This support ring connecting the driven gear and ball screw rests on a precision thrust bearing. Likewise, the support ring is sandwiched between a similar thrust bearing which provides a reaction for the pushing of piles. The ball screw assembly, thrust bearings, and support ring are held in position by a clamp attached to the supporting c-channel. Figure 4-17 depicts the assembly devised to transform rotational displacement of the stepper motor into vertical displacement of the ball screw.

The ball screw device located on top of the support ring is the means of converting the rotation of the stepper motor drive shaft into vertical displacement of the ball screw. As mentioned, there is no physical contact between the screw and nut as they have matching grooves (or races) which contain ball bearings. As either the screw or nut rotates, the rolling balls reach the end of their travel within the nut and are then recirculated by a return tube outside of the nut. A significant advantage of the rolling contact between ball and screw is the elimination of "stick slip" normally encountered when two surfaces slide across one another. Rolling contact improves the precision and repeatability of the positioning of the screw. Most commonly, the screw rotates and the nut moves back and forth along the shaft. The nut is attached to whatever object is being moved. Precise placement of the object is controlled by monitoring the rotation of the screw from some known orientation. In this application, the screw is restrained from rotation while the nut is rotated. This results in translation of the screw through the nut. The same degree of precision and load capacity is maintained as in the standard configuration. The ball screw assembly

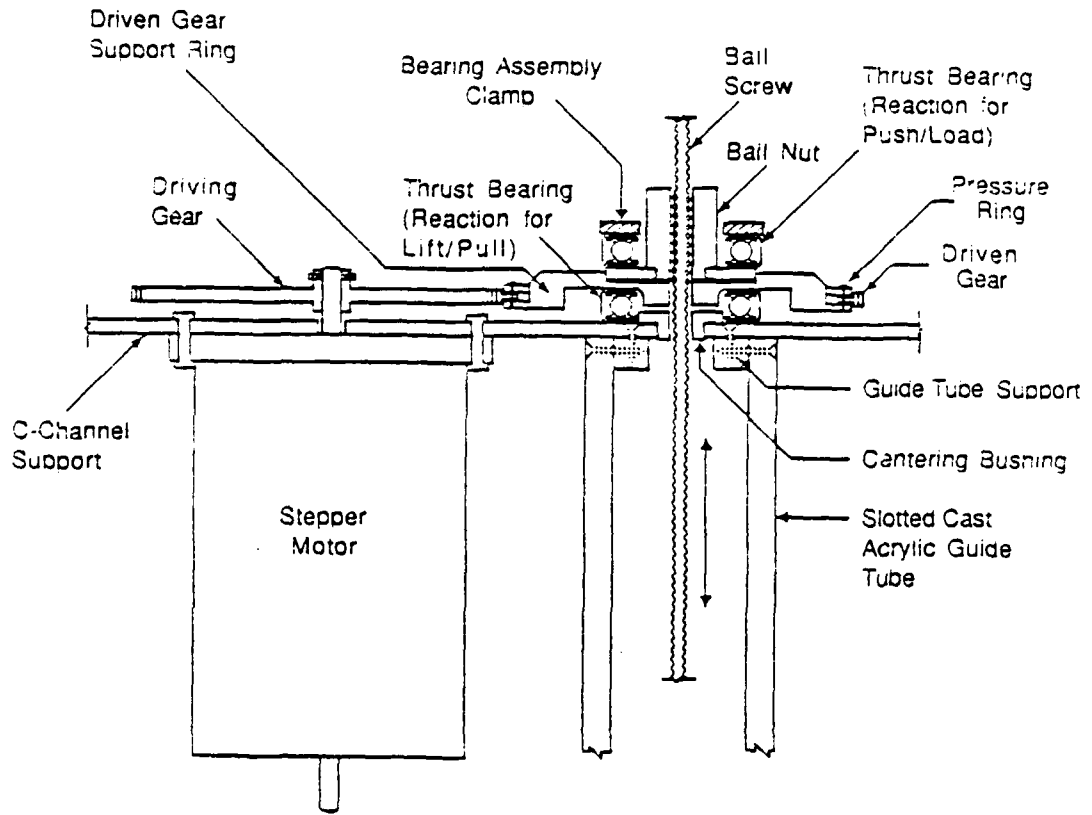


Figure 4-17 Ball Screw Assembly, Thrust Bearings, and Reaction Clamp

is highly efficient, with over 90% of the input power being converted to linear motion. This high efficiency permits the use of a smaller stepper motor for a given system. The rolled thread ball screw is machined to 0.0005 in. and case hardened giving high accuracy and repeatability throughout the life of the ball screw. The assembly used in this application was fitted with oversize balls to decrease the amount of backlash to 0.003 in.

Nominally, the screw traveled 0.125 in. for every rotation of the nut. This is called the "lead" of the screw and is significant because the ability of the ball screw assembly to transmit power is dependent on the lead. When changing rotary power to linear, the following expression is used to find the ultimate lifting capacity when given the available torque input and screw lead (Rockford Ball Screw Form Number RBS-101-B, 1986).

$$P \text{ (lbs)} = \frac{5.65 (T)}{L} \quad \text{Eq. 4-1}$$

where T = Torque input in inch-lbs.

L = Screw Lead

$$P = \frac{5.56 (28.125)}{0.125} \quad \text{Eq. 4-2}$$

$$P = 1,250 \text{ lbs}$$

The ball screw assembly was subjected to a maximum load of approximately 250 lbs during the operation of the placement device.

As previously mentioned, the precision placement characteristics of the ball screw are enhanced by the use of ball bearings as opposed to the standard metal to metal sliding contact between a conventional screw and nut. For a standard screw and nut configuration, the displacement of the nut is equal to the lead of the screw times the number of rotations (or portion thereof) of the screw. Rotation of a screw with a lead of 0.125 in. for 8 turns displaces the nut 1 in. However, the presence of the ball bearings between the screw and nut introduces a "planetary ratio" which slows down the advance of the nut for a given rotation of the screw. The name planetary ratio is derived from the motion of the ball bearings around the screw. The revolutions of the ball nut needed to move the screw 1 in. is the product of the planetary ratio and the threads per inch (N).

$$\text{Planetary Ratio} = \frac{R + S}{R} \quad \text{Eq. 4-3}$$

where $R = \text{Rolling Diameter in Nut} = 0.600 \text{ in.}$

$S = \text{Rolling Diameter in Screw} = 0.003 \text{ in.}$

$$\text{Planetary Ratio} = 1.005$$

Therefore, the nut must be rotated 8.04 times to advance the screw 1 in. Conversely, one rotation of the nut advances the screw 0.124 in. One rotation requires 200 steps of the stepper motor giving an accuracy of 0.0006219 in. per step. Determination of the travel of the screw under various operational circumstances required experimental verification. The screw was fitted with a Linear Voltage Differential

Transformer (LVDT) which provided a highly accurate measure of displacement of the screw for a given rotation of the shaft. Experimentally, the ball screw was found to displace 0.0000217 in. for each step of the stepper motor. See Section 4.7, Equipment Limitations, for verification of the accuracy of vertical displacement for a given rotation of the stepper motor.

4.2.4 Guide Tube

A guide tube for the electromagnet, hammer, and other associated placement components was fastened to the supporting c-channel adjacent to the stepper motor. The guide tube was clear cast acrylic to permit the viewing of the pile during placement and also to facilitate alignment of the pile placement components. The inner diameter was $1 \frac{7}{8}$ in. and the outer diameter was $2 \frac{3}{8}$ in. Two longitudinal slots were machined in the tube walls, one each down opposing sides. The purpose of these slots was to provide an opening for the strain gage and electromagnet leads to exit the tube and also to provide a means of preventing rotation of the electromagnet while it moved up and down. The guide tube was long enough to reach top of the soil and served to keep each piece within the tube (magnet, ram, and pile) aligned. The base of the tube was fitted with a guide to center the pile (group) as it exited the placement device. The centering pieces were individually machined for the pile (group) being tested to prevent scouring around the model pile(s).

4.2.5 Electromagnet

An electromagnet is fastened to the bottom of the ball screw during the driving sequences. As manufactured, it is 2 in. tall with a 1.00-inch diameter core. The windings are encased in epoxy which is housed

in a metal casing with a diameter of 1.75 in. The top of the casing is predrilled and tapped to accept a 0.25-inch diameter, 14 thread per inch bolt. Rated capacity of the magnet is 140 lbs with a voltage input of 12V DC, 125 milliamps. The two leads exit the casing on the side at the top as manufactured. However, the electromagnet was modified extensively for use in the driving device.

The leads were required to exit the top of the casing for the magnet to fit properly within the guide tube (1 $\frac{7}{8}$ in. I.D.). Therefore, sufficient material was removed from the casing to permit the lead wires to be placed as required. A plastic guide washer was fastened to the top of the casing to serve as a spacer between the walls of the guide tube and the magnet casing. The washer was thick enough (0.25 in.) to permit two opposing holes to be drilled from the circumference towards the center of the ring. A brass electrode was then forced into each of the holes. The leads from the electromagnet were soldered to the electrodes so the electrodes could then be inserted through the milled slots in the side of the guide tube and be connected to a power source outside the tube. The milled slots were larger than the diameter of the electrodes. Brass bushings were manufactured to slip around the electrodes where they passed through the guide tube to help keep the electromagnet centered within the tube and also to provide a rolling bearing surface as the magnet traveled up and down. The guide tube was fixed to the bottom of the c-channel and thus, the passage of the electrodes through the side of the guide tube prevented the magnet from rotating. The guide tube then also served the purpose of insuring that the rotation of the ball nut resulted in the vertical motion of the electromagnet.

A second set of bushings were fitted onto the electrodes. Power was supplied to the magnet by leads attached to this second set of bushings. The bushings permitted the leads to hang in a natural position as the magnet traveled up and down reducing the stress on the magnet and tube. Figure 4-13 shows the electromagnet actuator circuit and slip ring assignments for the power leads.

The tapped shaft at the top of the casing was not modified. Rather, the tip of the ball screw was modified to be screwed into the casing. When screwed tightly into the magnet casing, the ball screw could not rotate either, but only travel up and down.

4.2.6 Model Pile Hammers

The hammers had to be individually machined for tests at a specific gravity level. Initially, the hammer weight for driving individual piles was determined by dividing the prototype hammer weight by the appropriate gravity level to the third power as discussed in Section 3.4, Experimental Requirements. This resulted in hammer weights of 3.30 and 4.45 grams for the driving of individual piles at 69.8 and 86.0 g's, respectively. Considering the system being modeled, weights of this small size would have to be lifted almost 500 times to drive the model to the desired 30 ft depth of penetration. This was deemed unrealistic as one impact cycle required approximately 20 seconds. The total time to drive a model pile would have been almost three hours. Furthermore, the measurement of insignificant model penetration after each impact could introduce significant cumulative errors in the determination of total penetration. Therefore, the model hammer weight was increased arbitrarily by a factor of approximately 2.5. The intent was to drive the pile (group) as quickly as possible decreasing the wear on the

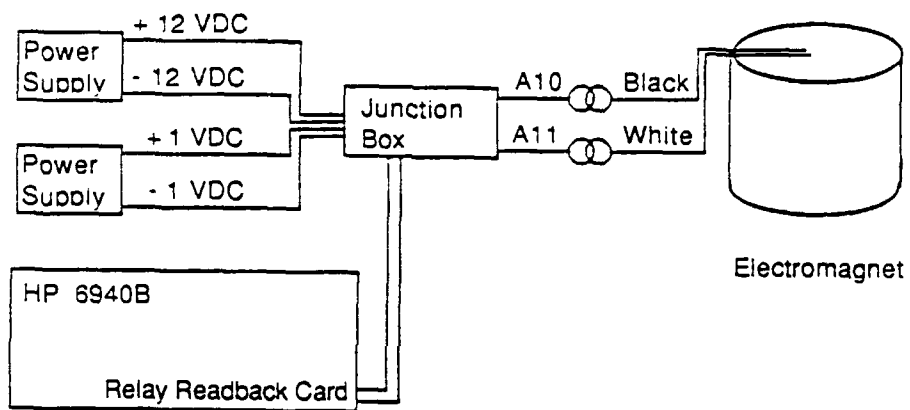
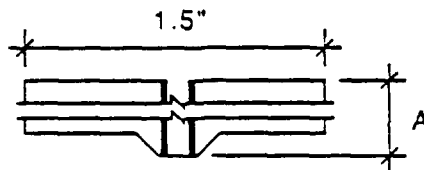


Figure 4-18 Electromagnet Actuator Circuit and Slip Ring Channel Assignments

centrifuge and placement device while increasing the number of tests which can be conducted. This served as a starting point in the determination of the optimum weight to be used for driving individual model piles. Noninstrumented models were first driven to determine the suitability of the weight and to ensure the instrumented models would not be destroyed by impact of the hammer. The hammer weight for driving group piles was determined by multiplying the factored weight required for driving the individual piles by five. Again, initial tests were conducted on noninstrumented groups to assess their survivability during driving. Table 4-2 provides the hammer weights for driving individual and group model piles determined by this process. The hammer dimensions were determined based on the hammer having a diameter approximately equal to that of the electromagnet. The intent was to provide a large face for the development of capacitance between the electromagnet and hammer. The dimple at the bottom of the hammer decreased the contact area between the hammer and pile cap and also the magnetic attraction between the two.

Table 4-2 Model Hammer Weights and Dimensions



G-Level	Hammer Weight/"A"	
	Individual Piles	Group Piles
69.8	20.0/0.125	100.0/0.625
86.0	10.7/0.060	53.5/0.300

NOTE: Weight and Dimension (A) are provided in grams/inches.

The hammer dimensions suggested above assume the hammer is manufactured from cold rolled steel stock as was commonly available at the University Machine Shop. Being ferrous and dense, this metal was the obvious choice of hammer material.

4.2.7 Model Pile Cap as an Alignment Tool

The model pile cap served the functions attributed to the prototype (Section 2.3.1, Hammer-Cushion-Cap Interaction) and others based on the requirements of the placement system. Figure 4-19 shows the standard design of the pile cap used during driving. The most significant function of this cap was to guide the hammer down to the center of the pile butt. A guide rod extending up through the hammer, then through the magnet, and into the center of the ball screw shaft fulfilled this purpose. Additionally, the guide rod ensured the magnet returned to the center of the hammer after impact and helped keep the magnet and hammer faces parallel during the approach of the magnet. The length of the guide rod was dictated by the hammer length (variable), magnet length (constant), and lift height (variable). Thus, each test g-level stipulated the use of a specific guide rod length. Figure 4-20 shows how the length of the guide rod and depth of drilled hole within the ball screw shaft were determined for the 65 g tests. This is the worst case as the hammer length, lift height, and guide rod length all decrease when testing at higher g-levels.

The model cap served the purpose of the prototype cap and hammer cushion. The cap was machined to fit snugly over the butt of the pile and protect it from the potentially damaging blows of the hammer. Being made of aluminum, the cap deformed slightly under the repeated impact of the hammer. The cap head was kept large enough to provide adequate area

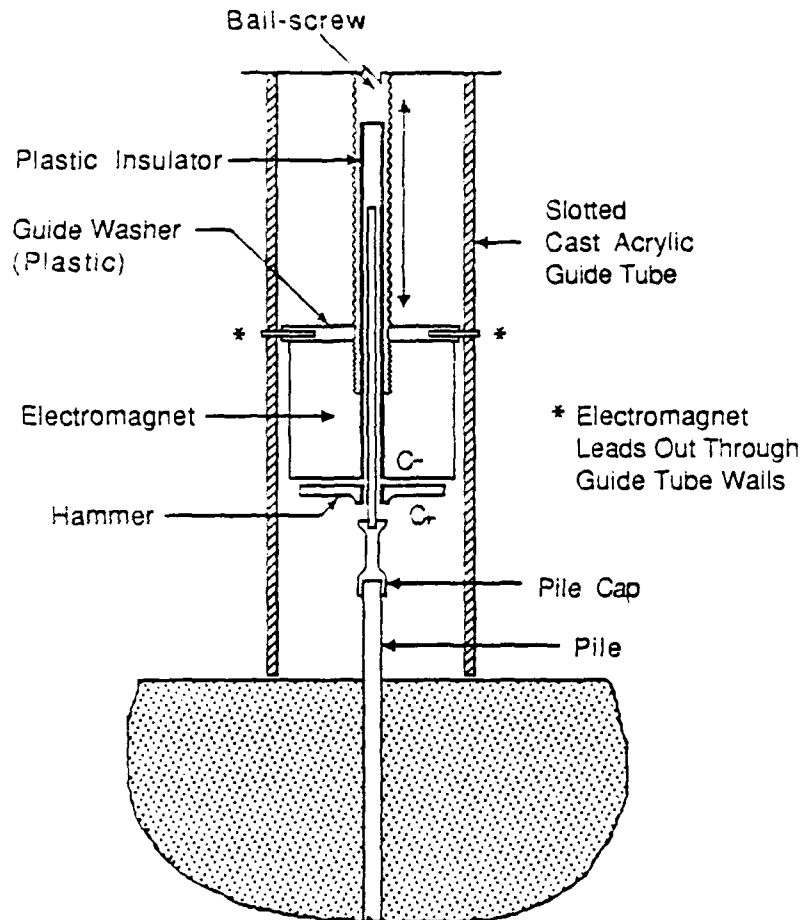
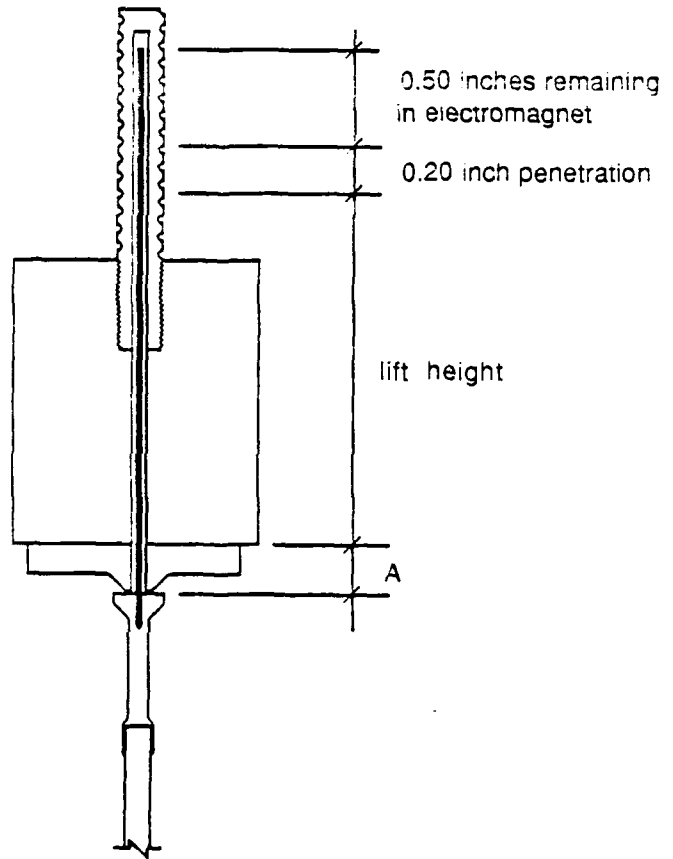


Figure 4-19 Pile Cap, Hammer, and Electromagnet Configuration for Driving Sequence



Hammer thickness ("A" for group)	0.40 in.
Lift height (200% efficiency)	2.40 in.
Allowance for penetration (per blow)	0.20 in.
Allowance for guide rod remaining in magnet	<u>0.50 in</u>
	3.50 in.

Figure 4-20 Guide Rod Length Determination (69.8 g's)

for the hammer to strike and transfer energy efficiently to the pile butt. Keeping the area of the cap head relatively large with respect to the pile butt also helped ensure the head was perpendicular to the longitudinal axis of the pile at hammer impact. An alternate cap design was necessary for the driving device to be able to push piles and groups.

The alternate design for the pile cap to be used during the pushing of piles (groups) included the capability for the model pile to be inserted in an adaptor screwed into an in-line load cell. The force of pushing the pile (group) was transmitted through the load cell. This was important also in the conduct of the load tests. Each test conducted by pushing the pile was accomplished with the load cell in place. Loading the model pile after pushing was accomplished without stopping the centrifuge. The electromagnet and hammer were replaced by a load cell before load tests were conducted on driven piles (groups). The load cell capabilities are presented in more detail in Section 4.2.9, Load Cells.

4.2.6 Proximity Device

The ability to use this device as a pile driver was predicated on the capability of being able to determine when the electromagnet had been lowered just to the point of contact with the hammer. If the electromagnet were not brought down close enough to the hammer after impact, the magnet would not have been able to engage and lift the hammer for succeeding impacts. Alternatively, if the electromagnet continued its downward travel past the point where it had made contact with the hammer, the device would push the pile further into the soil and possibly alter the creation of the desired soil stresses adjacent to the pile.

The capability of measuring the proximity of the magnet to the hammer was important for the above reasons as well as in the determination of the penetration of the pile after impact. Using the stepper motor in its capacity as a precision positioning device, the displacement of the pile could be measured by counting the number of "steps" the pile had advanced after impact. Thus, a proximity device was necessary to ensure the magnet was engaged for successive impacts, to prevent the electromagnet from pushing the pile into the soil, and to permit the use of the stepper motor as a device to measure penetration of the pile.

The electrical property of capacitance was chosen as the basis of design for the proximity device. A capacitance circuit produces a current proportional to the time derivative of the voltage across the capacitive element. The constant of proportionality is called the capacitance. Expressed quantitatively, the current is

$$i = C \frac{de}{dt} \quad \text{Eq. 4-4}$$

where $\frac{de}{dt}$ is the time derivative of the voltage

The element voltage (e) can be found from the above equation.

$$e = \frac{1}{C} \int i dt \quad \text{Eq. 4-5}$$

Since the instantaneous current (i) in a circuit equals a change in electrical charge (q) over some time period (t), one can denote the instantaneous current as follows.

$$i = \frac{dq}{dt} \quad \text{Eq. 4-6}$$

Integrating, we find that

$$q = \int i dt \quad \text{Eq. 4-7}$$

Substituting Equation 4-7 into 4-5, the element voltage is

$$e = \frac{q}{C} \quad \text{Eq. 4-8}$$

and thus

$$C = \frac{q}{e} \quad \text{Eq. 4-9}$$

The proportionality constant (C) is the charge storing property of the element and is referred to as capacitance. With q expressed in coulombs and e in volts, the resulting capacitance is expressed in farads (F). Capacitance is most often expressed in microfarads (μf), or 10^{-6} farads.

A fixed capacitor usually consists of a pair of metallic plates separated some known constant distance by a dielectric. One of the plates is positively charged and the other is charged negatively. The plates discharge alternately at a constant frequency if a resistor is introduced in series with the capacitor and the capacitance is held constant. The frequency of discharge is directly related to the "characteristic time" of the resistance-capacitance, or r-c, circuit. The product of resistance times capacitance is time (characteristic time) and the frequency of discharge is found easily by taking the inverse of

this time. The characteristic time (and frequency) can be varied by changing either the resistance of the circuit or the capacitance. Increasing either increases the characteristic time and thus decreases the frequency of discharge. This relationship between capacitance and frequency of discharge serves as the basis for operation of the proximity device.

The capacitance of the magnet and hammer couple was the variable capacitance of the design r-c circuit. The bottom face of the electromagnet was the negatively charged face of the capacitor and the top of the hammer the positively charged face. Capacitance between the two faces could exist only if the faces were electrically insulated from one another. The method of insulation chosen was to insert a plastic tube through a hole drilled through the center of the hammer. This prevented the guide rod and cap from coming in contact with the hammer unless the hammer was resting on the top of the cap (after impact). Likewise, a hole was drilled through the center of the electromagnet and up through the center of the ball screw shaft. This hole was also fitted with a thin-walled plastic tube. Thus, the pile, cap, guide rod, and hammer were totally insulated from the electromagnet and ball screw shaft, a vital consideration when measuring the capacitance between the two. When resting on the pile cap, the bottom of the hammer made electrical contact with the cap. This was necessary as the hammer was required to be positively charged to serve as one face of the variable capacitance proximity device. The model, cap, and hammer were positively charged by a lead wire fastened to the miniature connectors used to protect the strain gage lead wires. Similarly, the bottom of the electromagnet had to be electrically charged. This was accomplished by attaching the

negatively charged lead wire to the c-channel support which was always in intimate contact with the bail screw and thus the electromagnet. The capacitance across the two faces could exist only if they did not come in physical contact. Therefore, they were insulated from one another by covering the top of the hammer with a layer of cellophane tape.

Two proximity devices based on capacitance were considered. The device used in this research was an electron charge pump proximity device. It included several features which were improvements on its predecessor, a phase comparator proximity device. Each device will be discussed.

4.2.8.1 Charge pump proximity device

The proximity device consisted of a crystal reference oscillator and divider, which alternately charged and discharged the variable capacitor made up of the bottom face of the electromagnet and top face of the hammer. The quantity of charge stored and subsequently discharged from the two faces is a function of the distance between them. The discharge served as the input to an integrating microchip which transformed the discharge into a unique value of current determined by the distance between the plates. This current was passed through a precision resistor resulting in a measurable variable voltage across the resistor. The output voltage was compared to a reference voltage which was adjustable based on the desired closeness of approach of the variable capacitor faces. Figure 4-21 shows the schematic drawing of the device. Figure 4-22 depicts the proximity device before mounting on the c-channel support.

The reference system voltage output was constant depending on the adjustment of a precision potentiometer. Increasing the capacitance of

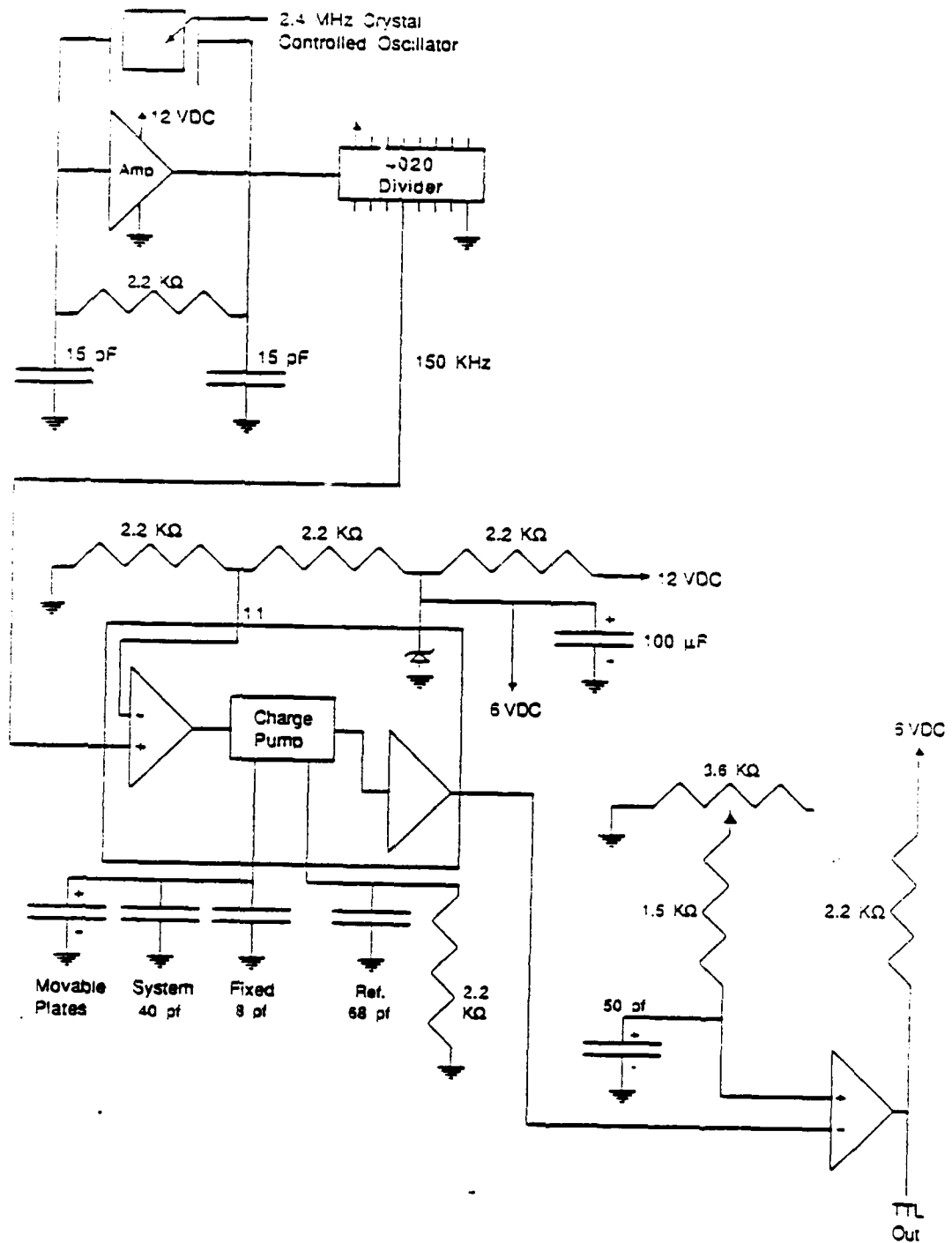


Figure 4-21 Charge Pump Proximity Device Schematic Drawing

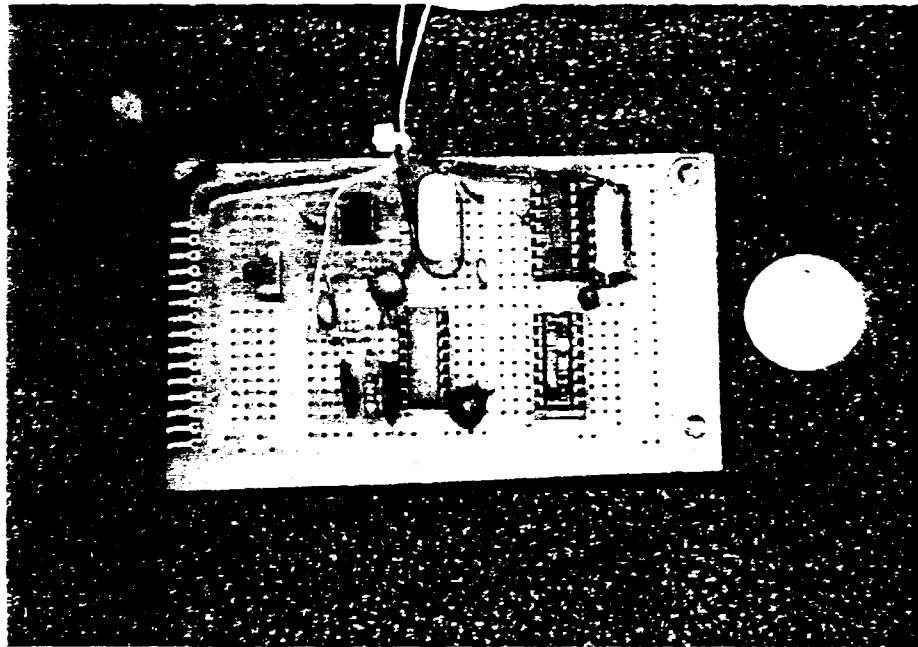


Figure 4-22 Charge Pump Proximity Device

the local circuit increased the charge storing capability of the circuit during the fixed time interval and thus also the amount of discharge when the Electron Charge Pump (ECP) was de-energized. Thus, the voltage representation of the output increased as the electromagnet and hammer approached one another. When the voltage from the variable capacitance circuit exceeded the reference voltage, a transistor in the voltage comparator microchip changed its output from a low state of 0 volts to a high state of 5 volts. Thus, the approach of the magnet to the hammer closer than some preset distance is signified by an instantaneous change in the output of the device from 0 to 5 volts.

A crystal reference oscillator was chosen to "drive" the device because of its inherent accuracy. The divider reduced the circuit frequency to a nominal value of 150 kHz from the crystal frequency of 2.4 MHz. The reason for this reduction will be explained shortly. The output from the reference oscillator powered a microchip which contained an ECP. With the ECP energized, the variable capacitor faces would store charge. De-energizing the ECP caused the capacitor to discharge. The divider was necessary to increase the amount of time available for the capacitor to store charge. The resulting discharge was larger in magnitude and more easily compared between the two circuits. Adjustment of the reference system output permitted the determination of the distance between the electromagnet and hammer at which the comparator output changed. The output from the comparator was connected to the high-speed analog to digital converter in the multiprogrammer to notify the computer the electromagnet had found the hammer.

Figure 4-23 shows the electron charge pump proximity device circuit and slip ring channel assignments for the power and output signal leads.

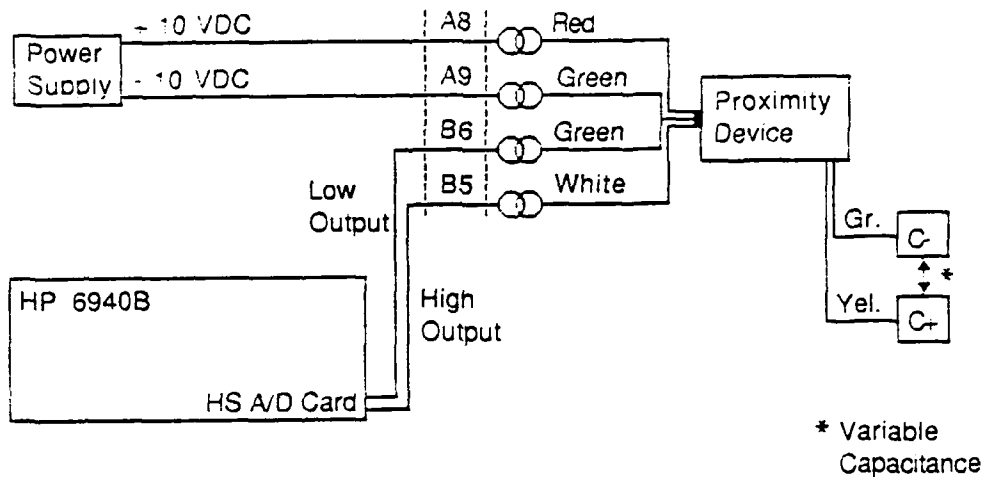


Figure 4-23 Charge Pump Proximity Power and Output Signal Circuit and Slip Ring Channel Assignments

4.2.3.2 Phase comparator proximity device

The alternate design was very similar in principle but relied on the comparison of the frequencies of two r-c circuits rather than the measurement of voltage output from a current integrating microchip. Figure 4-24 depicts the phase comparator device schematic. Knowing the approximate capacitance of the canister, magnet, and ram system, a similar r-c circuit was constructed which oscillated with a frequency of 490 Khz. This was termed the reference oscillator. By varying the distance of the electromagnet from the hammer, the capacitance of the "local" oscillator could be changed. Altering the capacitance likewise changed the frequency of discharge of the system. This frequency, and the constant frequency of discharge of the reference oscillator were simultaneously input to a frequency comparator. When the frequency of the local oscillator equaled that of the reference oscillator, the voltage comparator triggered a transistor to change its output from zero to five volts. Changing the frequency of the reference oscillator (using a precision adjustable resistor) changed the distance at which the transistor output changed from zero to five volts. The device was adjustable to a gap of approximately three thousandths of an inch but could not repeatedly provide accurate results.

The most significant drawback of this proximity device was the use of a phase-locked loop (PLL) in the local oscillator circuit. The PLL is a noninductive, tunable, active filter with an adjustable bandwidth (Buchsbaum, 1973) suitable for use in communications devices and servo controlled motor systems. The basic PLL circuit consists of a voltage controlled oscillator, phase detector, and loop filter (Figure 4-25).

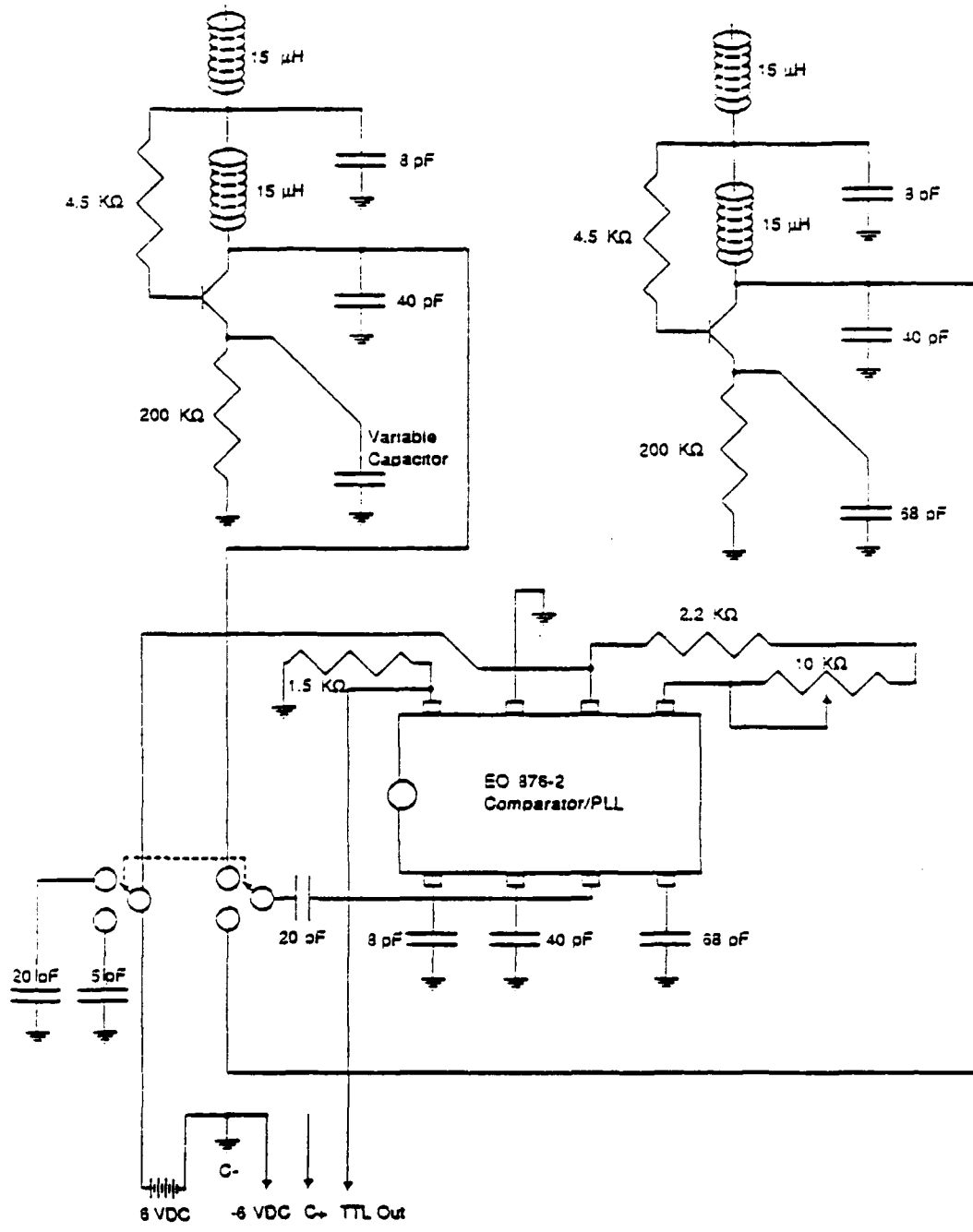


Figure 4-24 Phase Comparator Device Schematic Drawing

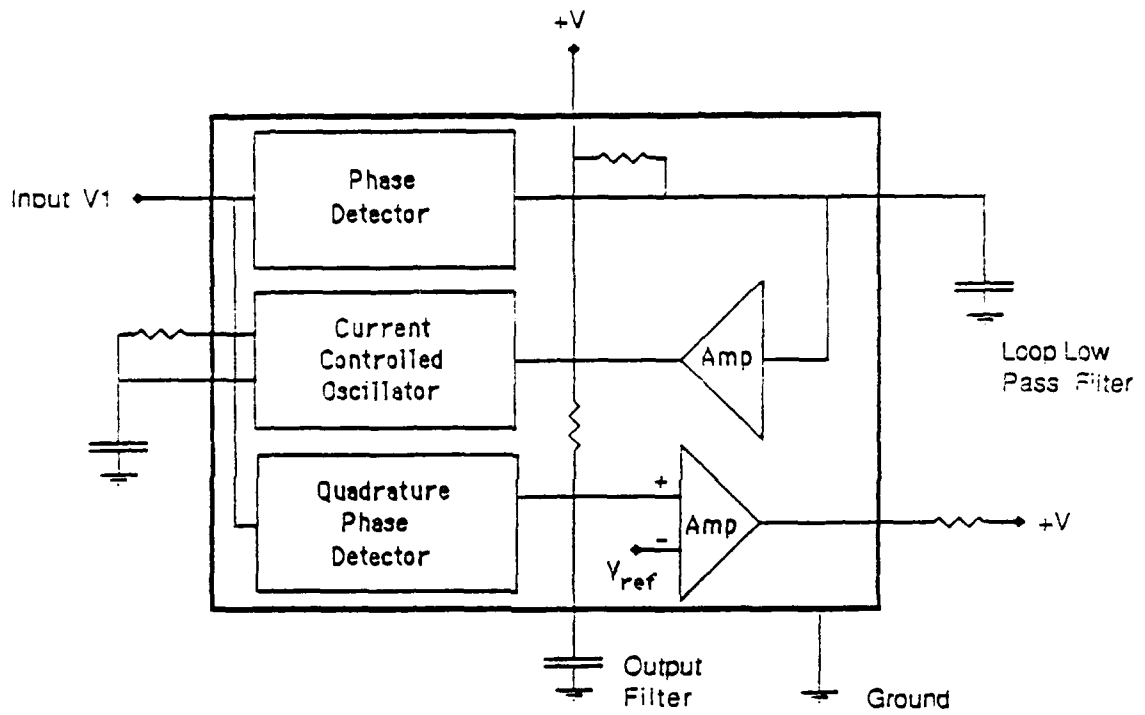


Figure 4-25 Basic Phase Locked Loop Circuit

The phase loop is considered locked when the difference between the input signal (from the local oscillator in this application) and the VCO output signal is constant. A variation in either the input signal phase or the VCO output phase generates an "error" voltage from the phase detector which is proportional in both magnitude and polarity to the phase shift. This error voltage serves to modify the VCO output until it is again in phase with the reference signal. The range over which the circuit can keep itself in phase with the reference circuit is referred to as the lock range. Regarding the use of this circuit in the proximity device, as the electromagnet approached the top of the hammer, the capacitance of the local oscillator circuit increased, which served to decrease the circuit's frequency of discharge. As this frequency fell within the lock range of the PLL circuit, the reference oscillator frequency would lock onto and follow the frequency variations of the local oscillator circuit. Thus, any additional changes in capacitance (or variation in the distance between the electromagnet and hammer) would be masked by the ability of the PLL circuit to lock onto and follow the frequency variation.

The inability to accurately adjust the frequency output of the local oscillator also hampered the operation of the device. The PLL circuit was incorporated into the frequency determining network for the reference oscillator. Variation of the PLL circuit output thus affected the reference frequency output negating the use of the circuit as a true reference. The reference circuit capacitance also varied in response to the nearness of the tools needed to adjust the precision potentiometer in the reference r-c circuit. Thus, it was not possible to achieve a predetermined, stable reference oscillator frequency with the device and

the PLL circuit precluded the precise and repeatable determination of the proximity of the electromagnet to the hammer.

4.2.9 Load Cells

Two load cells were used in this research. The load cell used for pushing and loading individual piles had a static capacity of 200 lbs. This load cell was also used to conduct load tests on individual piles which had been driven. The load cell used to push and load group piles had a static capacity of 500 lbs. Load tests on pile groups were conducted with the 500-lb capacity load cell. Each load cell had a calibration factor provided in the form of millivolts output per volt of input power. Millivolt output per pound of force was determined as follows. The calibration factor (1.9961 mv/v for the 200 pound capacity load cell) is multiplied by the load cell input voltage (10 volts in this example). The resulting maximum output voltage (19.961 millivolts) is divided by the static capacity of the load cell. The 200-lb capacity load cell output is thus .0998 millivolts per pound. The calibration factor for the 500 pound capacity load cell was determined to be 0.0397 millivolts per pound. The load cell power and signal circuit is shown in Figure 4-26. Slip ring channel assignments are included in the figure.

Each load cell had leads which exited from the side of the casing. These leads were passed through the side of the cast acrylic guide tube and helped to prevent the ball screw, load cell, and model from rotating during placement and loading.

4.3 Centrifuge Design

Conduct of this research required the development of a new centrifuge facility and associated testing equipment. This section of the

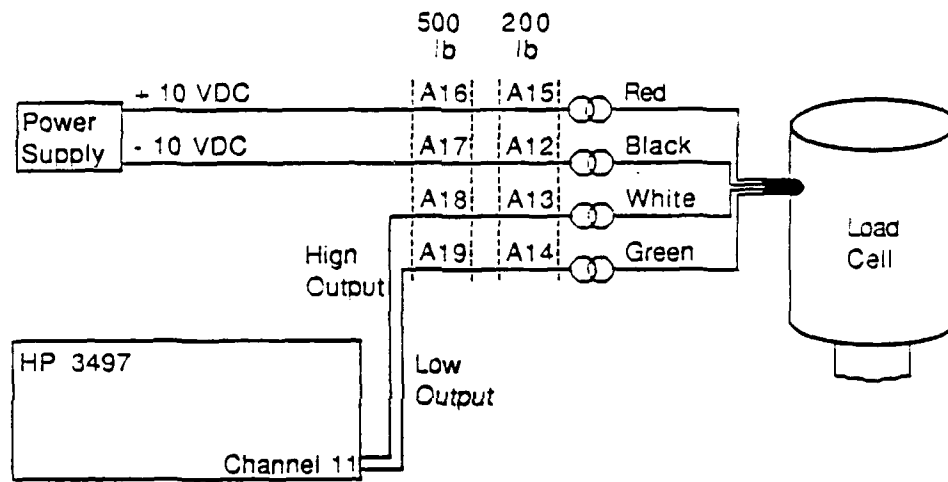


Figure 4-26 Load Cell Power and Output Signal Circuit and Slip Ring Channel Assignments

report presents the specifications of the new centrifuge facility as well as capabilities of the equipment to be used for high gravity level testing.

1.3.1 In-Place Equipment

The equipment in-place at the beginning of this research consisted of a fifteen horsepower electric motor mounted in the center and below the floor of an 11 1/2-foot square room having a height of 4 ft. The top of the centrifuge enclosure was at floor level in the basement of the Weil Hall addition, Reed Laboratory. Nominally, the motor was capable of 1200 rpm. Other pertinent motor specifications are as provided in Appendix B. The drive shaft (3.0-inch diameter) stood to a height of 3 ft within the enclosure and was linked to the motor through a Holloshaft 5.077:1 speed reducer thereby limiting the rotational speed of the centrifuge arms to 236 RPM. Initial testing revealed that 1281 rpm of the motor resulted in only 201 rpm of the arms indicating the rotational speed was being reduced by a factor of 6.373. Inspection of the pulleys on the motor shaft and centrifuge drive shaft accounted for the additional reduction by a factor of 1.25. The pulley on the motor shaft was 8.87 in. in diameter and the pulley on the reduction gearbox driveshaft was 11.09 in. in diameter. The reduction gearbox driveshaft pulley was replaced by a pulley similar to the one on the motor driveshaft thereby correcting the total reduction to the desired 5.077:1. One-hundred g's could then be consistently achieved with the arm rotating at 241 rpm, depending on the radius at which the desired gravity level was measured.

Arms had already been mounted on the driveshaft. The arms and mounting plates were made of T-6061 high strength aluminum having a

yield strength of 42,000 psi. High strength bolts were used throughout the construction. Lastly, for aerodynamic reasons, each of the arms had had material removed from the web to reduce turbulence during rotation. Each pair of arms has a nominal cross-sectional area of 14.90 square in.

A main power transformer (Figure 4-27), and Parajust AC Motor Speed Control (Figure 4-28) constitute the dedicated circuit which powers the centrifuge. Rotational speed control is provided either by a precision potentiometer housed in the hand-held control shown in Figure 4-29 or by the variable direct current voltage input (from 0 to +10.24 volts) from the multiprogrammer (Section 4.5, Computer Control of the Equipment). A rotary switch mounted on the side of the Parajust speed control permits the operator to switch control from the hand-held speed control to the external control (multiprogrammer) and back. The main circuit breaker for the centrifuge is mounted directly above the transformer adjacent to the resistive speed brake shown in Figure 4-30.

4.3.2 Shroud Construction

The initial modification consisted of building a shroud to encase the arms thereby providing a more suitable housing for them during rotation. The inside radius of the shroud was constructed at 68.5 in. from the center of the drive shaft as this was the largest circular wall which could be built within the confines of the centrifuge housing. The wall of the shroud is 0.25 in. smooth finish plywood sheeting supported by a 2x4 frame which is in turn mounted on 0.75-inch thick plywood forms fastened to the floor and walls. Two support beams were fastened in place above the centrifuge equidistant from the center of the drive shaft and spaced at a width of 34.0 in. The purpose of the beams was to provide solid support for the cover to be placed on the centrifuge,

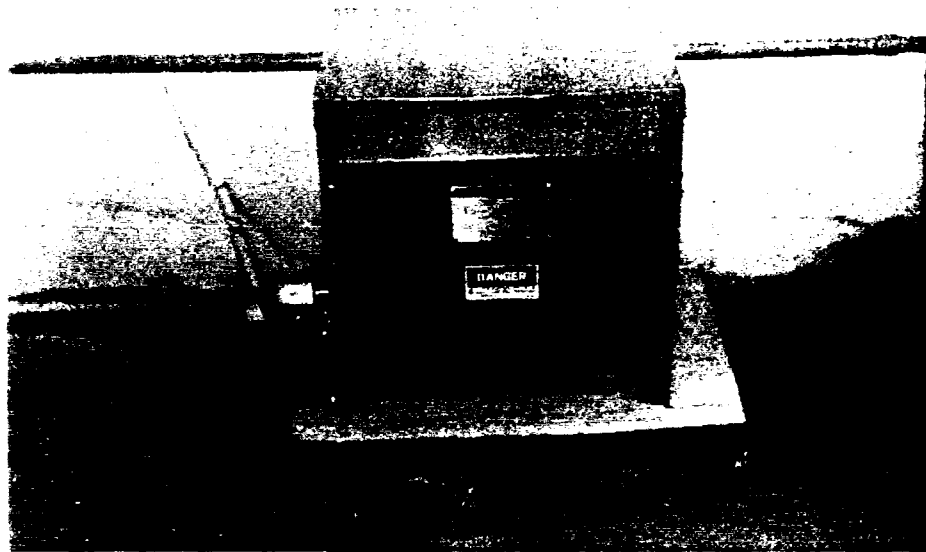


Figure 4-27 Centrifuge Main Power Transformer

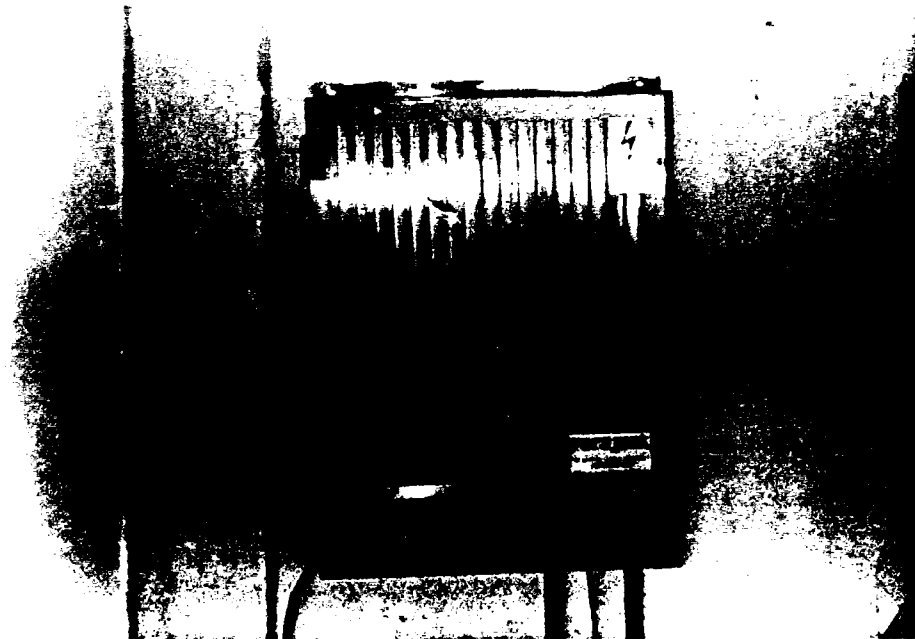


Figure 4-28 Parajust AC Motor Speed Control

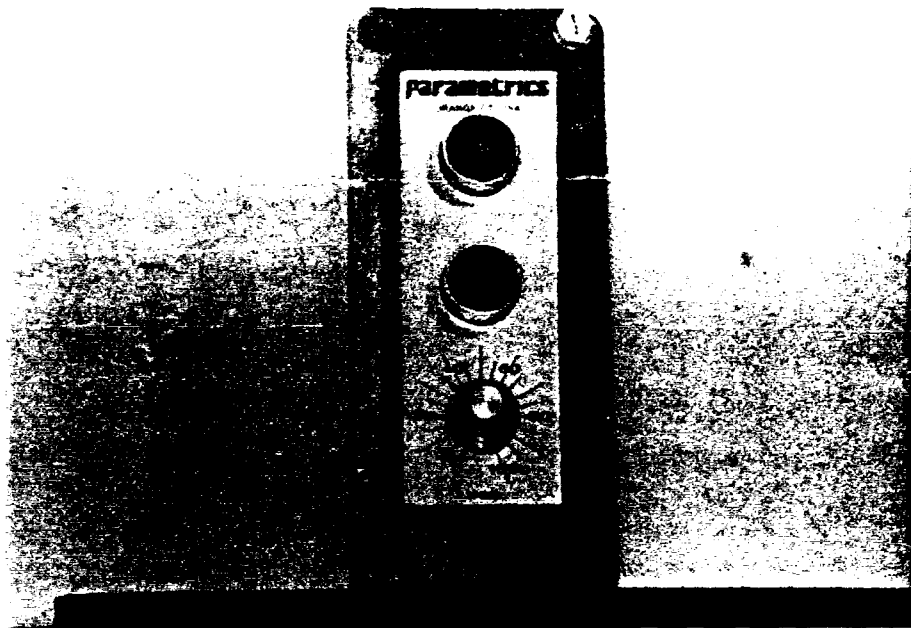


Figure 4-29 Hand-Held Centrifuge Speed Control

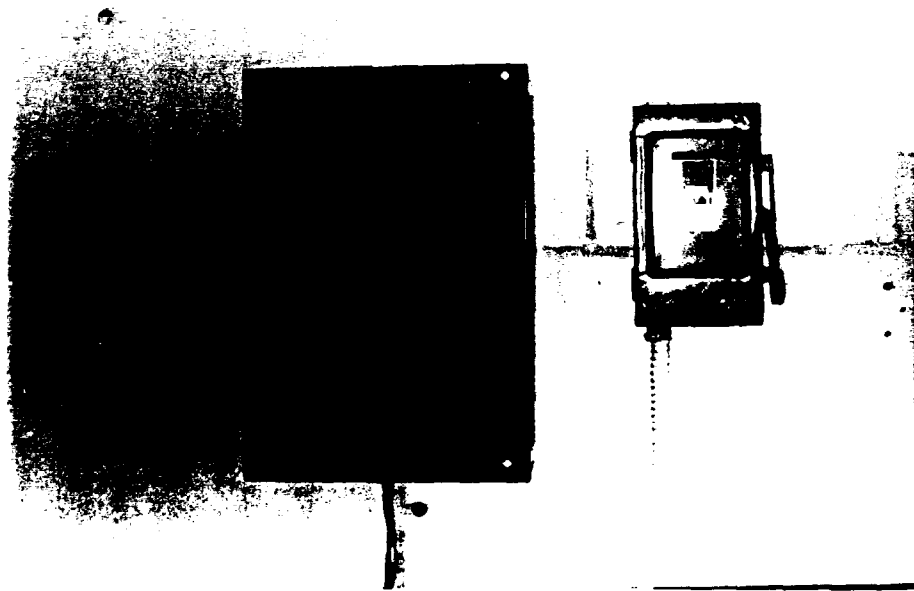


Figure 4-30 Centrifuge Main Circuit Breaker and Resistive Speed Brake

provide a platform which could support the slip ring housing eventually mounted above the drive shaft, and to serve as a track along which could be rolled a portable hoist to be used for transferring buckets to and from the centrifuge arms. The completed shroud, support beams, and slip ring housing are shown in Figure 4-31.

4.3.3 Main Arm Modification

The original arms were removed and taken to the University of Florida Machine Shop where a 12 in. by 12 in. by 0.5 in. high strength aluminum and 12 in. by 12 in. by 0.25 in. steel plate was fastened to the end of each arm (Figure 4-32). These plates served as the attachment points for the pillow-block bearings which supported the platform arms. The plates were welded in place and bolted with high strength bolts for redundancy in case of weld failure during flight.

4.3.4 Cover Construction

After replacing the arms, the centrifuge roof was closed with sheets of 0.75-inch thick plywood and interlocking pieces of heavy gage pressed steel floor grating (Figure 4-33). A distributed load of 2000 pounds was temporarily placed on the roof with no adverse effects. The inside of the centrifuge housing was then caulked and painted to provide a smooth inner surface. The cover had an access opening of 30 by 40 in. as shown in the foreground of Figure 4-33 through which the main arms can be removed if necessary.

The current draw of the main motor at full speed was reduced 44% (from 41.5 amperes to 23.2 amperes) after placement of the shroud and cover. Figure 4-34 shows the current draw (per phase) for a given rotational speed of the centrifuge and includes the voltage input to the

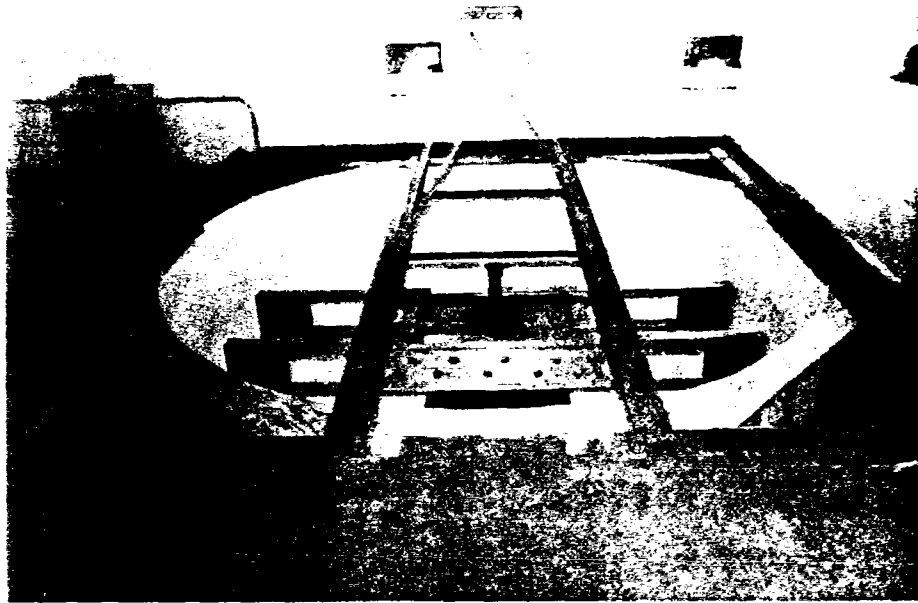


Figure 4-31 Completed Centrifuge Shroud

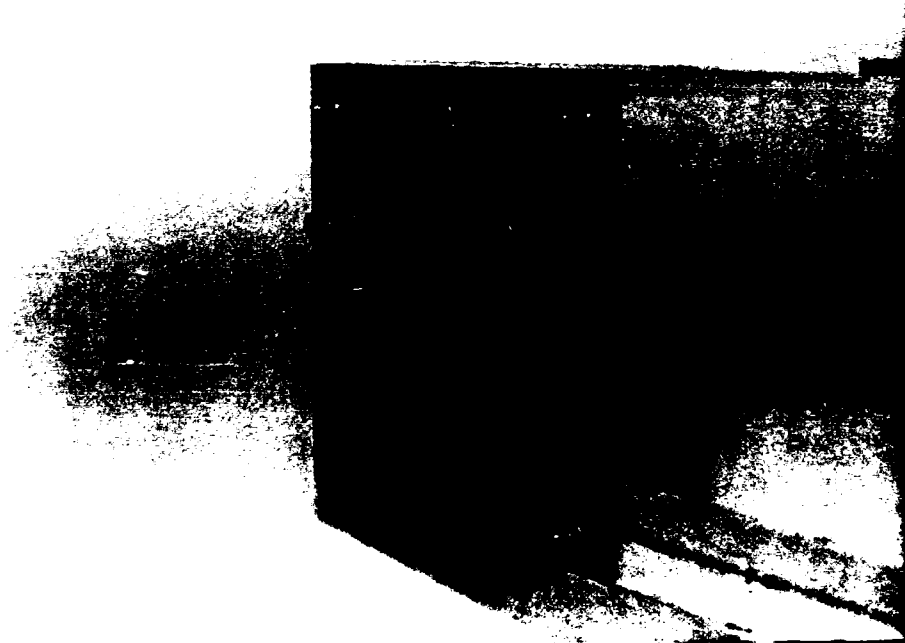


Figure 4-32 Pillow Block Bearing Support Plates Fastened at the Ends of Each Arm

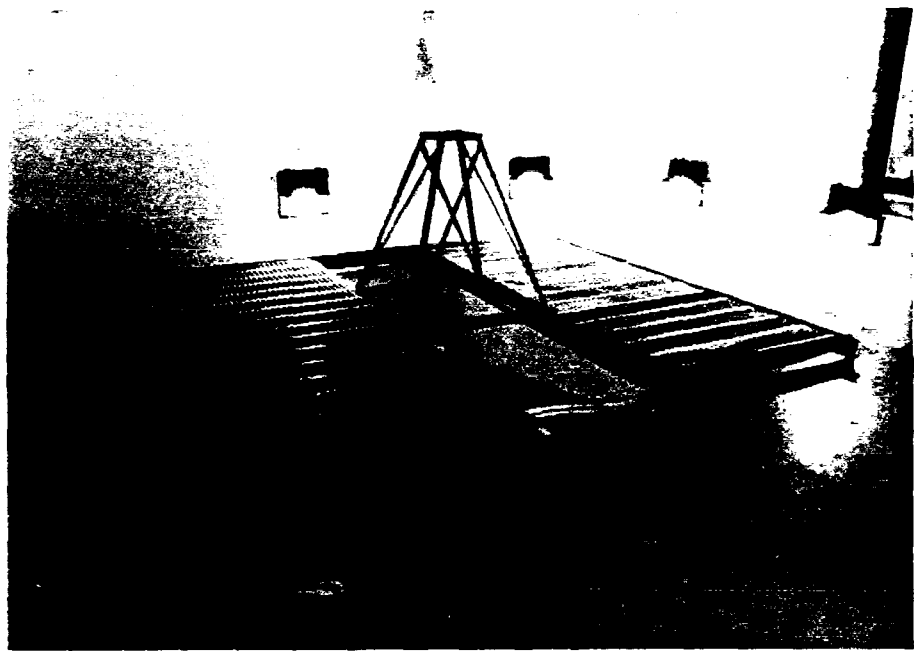


Figure 4-33 Centrifuge Cover, Access Opening and Slip Ring Housing

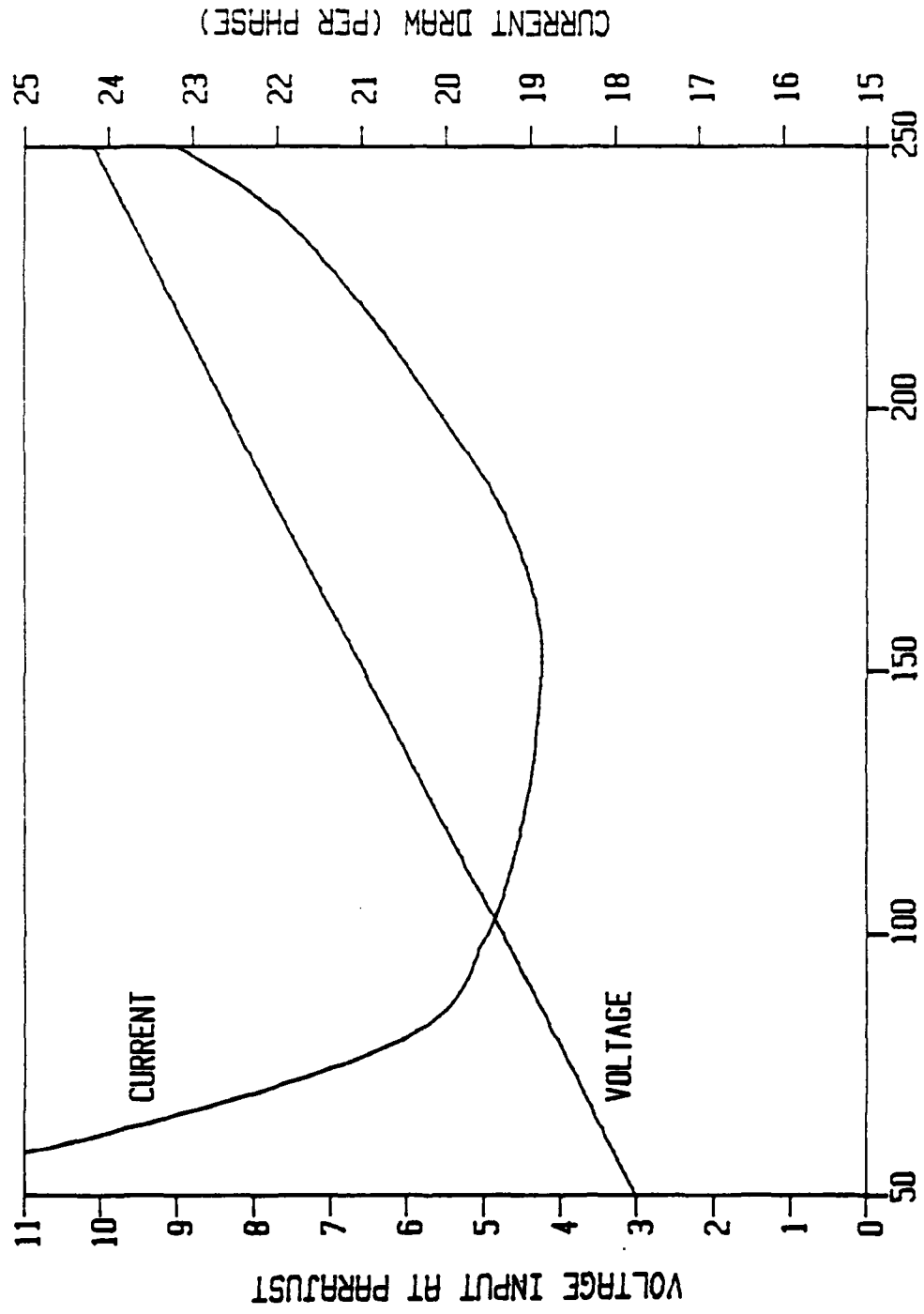


Figure 4-34 Centrifuge Power Requirements and Performance Characteristics

Parajust Speed Controller necessary to achieve the desired rotational velocity.

4.3.5 Slip Ring Placement

Equipment control input and data capture dictated the use of electric slip rings and rotating hydraulic unions. The mounting of the slip rings was the next modification. A pyramid shaped frame of angle-iron (Figures 4-31 and 4-33) was fabricated with a base large enough to span the support beams and with a housing at the top to permit the firm but flexible restriction of the rotating hydraulic union assembly. Flexibility was needed to accommodate the unavoidable vibration associated with the operation of the centrifuge. The hydraulic slip ring was fastened to the housing by four large eye-bolts and springs which gave the necessary flexibility while also permitting lateral adjustment of the entire slip ring assembly to ensure trueness during rotation. Figure 4-35 depicts the electric and hydraulic slip ring assembly with mounting device already in-place on top of the large rotating hydraulic union. The bottom of the slip ring assembly was fastened to the top of the drive shaft via a Wood's No. 6J universal joint. The universal joint consisted of two metal end pieces with a short, hard rubber, fine-toothed coupling sandwiched between them. This type of joint was selected for its ability to transmit power smoothly with a minimum of vibration. An adjustable cap was manufactured and placed over the top of the main drive shaft serving as a connector between the shaft and universal joint at the bottom of the slip ring assembly. The stainless steel central shaft of the slip ring assembly was mounted directly on top of the universal joint. This shaft supports the electric and hydraulic slip rings and is hollow to permit the passage of shielded

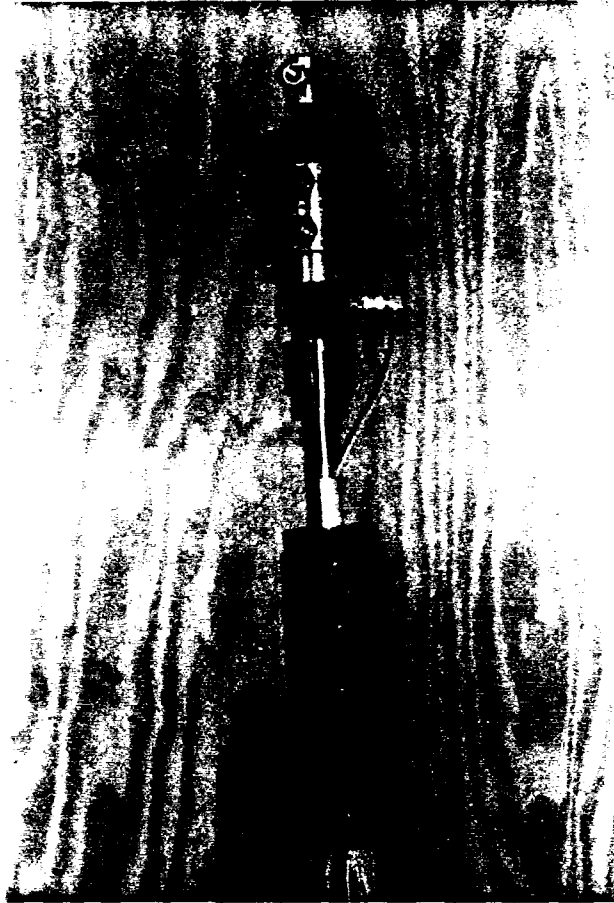


Figure 4-35 Electric and Hydraulic Slip Ring Assembly

cables and hydraulic pressure lines. Sufficient room was available for the passage of 30 shielded cables and two hydraulic pressure lines. Figure 4-36 shows the completed slip ring housing with the electric and hydraulic slip rings in-place. The top slip ring unit is designated "A" and the bottom unit "B".

4.3.6 Rotational Speed Monitoring

Following placement of the slip rings, a pulse generator was fixed atop the single rotating hydraulic union (Figure 4-37). The pulse generator consisted of a small light source and reader on opposing sides of a small c-shaped fitting. The source and reader were fixed to the stationary outer casing of the union. A slotted disk was fitted to the rotating central shaft of the union such that the slots passed between the arms of the c-shaped fitting. Rotation of the centrifuge, and thus the central shaft of the union, caused the slotted disk to intermittently interrupt the path of light between the source and reader. Each passage of an opening between the two resulted in the generation of a 5 volt pulse. The frequency of the pulse is directly related to the rotational speed of the centrifuge. The pulses are transmitted to the multiprogrammer and counted by a pulse counter card over some predetermined time period. This permits the computer to determine the rotational speed of the centrifuge. Comparison of the actual rpm with the desired rpm causes the computer to adjust the output of the digital to analog voltage converter card which commands the rotational speed of the centrifuge. Figure 4-38 shows the rotational speed monitoring and control circuit developed to permit control of the centrifuge by either the multiprogrammer and computer or manual means. The specific



Figure 4-36 Slip Ring Assembly In-Place

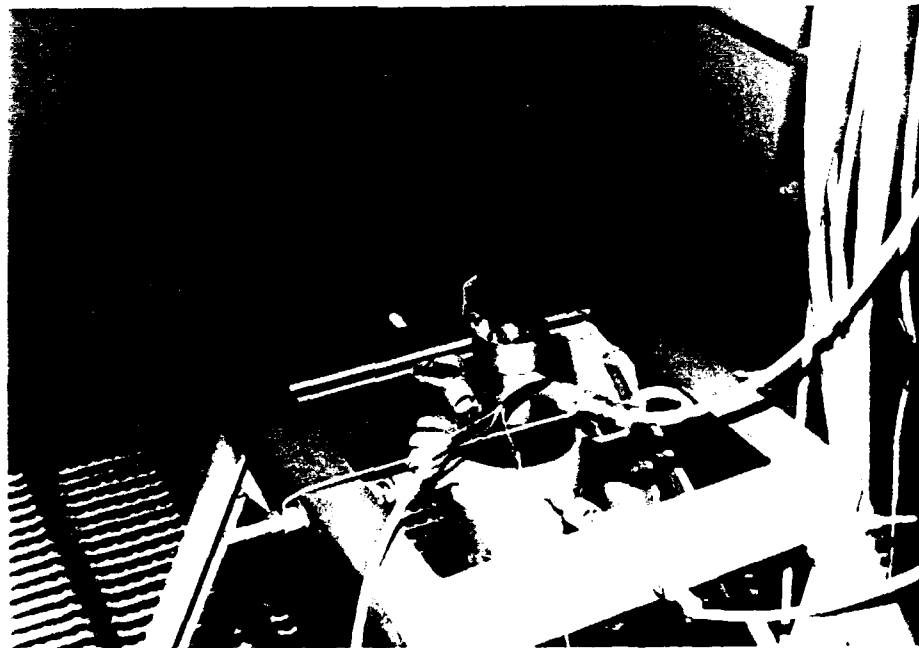


Figure 4-37 Pulse Generator and Slotted Disk

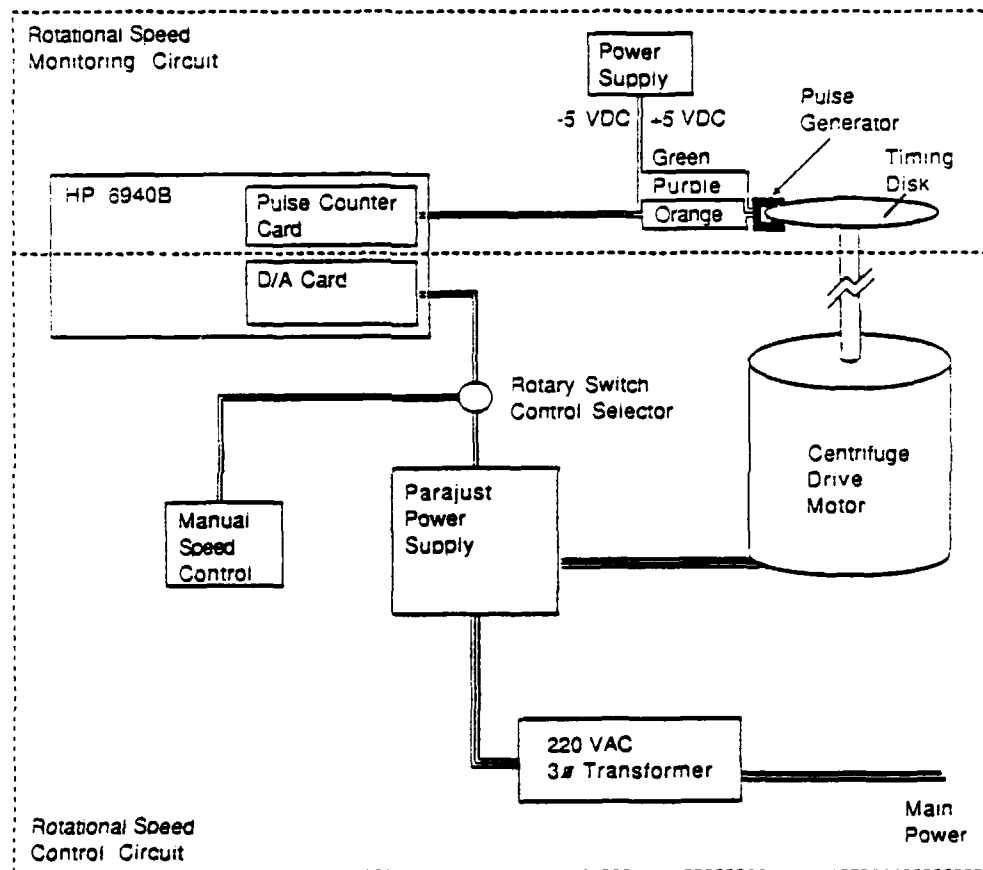


Figure 4-38 Rotational Speed Monitoring and Control Circuit

functions of the computer system components and software will be presented in Section 4.5, Computer Control of the Equipment.

Figure 4-39 shows the photoelectric tachometer and display unit which was used for monitoring the centrifuge rotational speed with the motor under manual control. This attachment also served as a backup system when the centrifuge speed was controlled by the computer and multiprogrammer.

4.3.7 Specimen Platform Construction

Identical platforms were built for each arm. The major consideration was to provide similar capacity for each arm permitting the simultaneous performance of like tests during one flight of the centrifuge. Balance of the arms was accomplished by placing equal weight payloads on each platform. The orthographic projection of each platform is presented in Figure 4-40. Figure 4-41 depicts one of the fabricated platforms. The $1 \frac{3}{16}$ -inch diameter hole bored in the end of each support arm permitted the passage of a steel pin. The pin was supported on either side by pillow-block bearings mounted on the main arms (Figure 4-42 shows a platform in-place). Special consideration was given to ensure the base was as far as practically possible from the drive shaft (during flight) to provide the highest g capability.

The platform arms were spaced at 28 in. (inside spacing) predicated on their being mounted adjacent to the outer face of the inner pillow block bearing plate. The pillow block bearing bolts which would have interfered with the swinging up of the platforms were countersunk. Thin plastic washers were placed between the platform support arms and centrifuge main arms permitting unrestricted rotation of the platforms.



a) Photoelectric Tachometer



b) Display Unit

Figure 4-39 Equipment for Monitoring Centrifuge Rotational Speed.
a) Photoelectric Tachometer; b) Display Unit

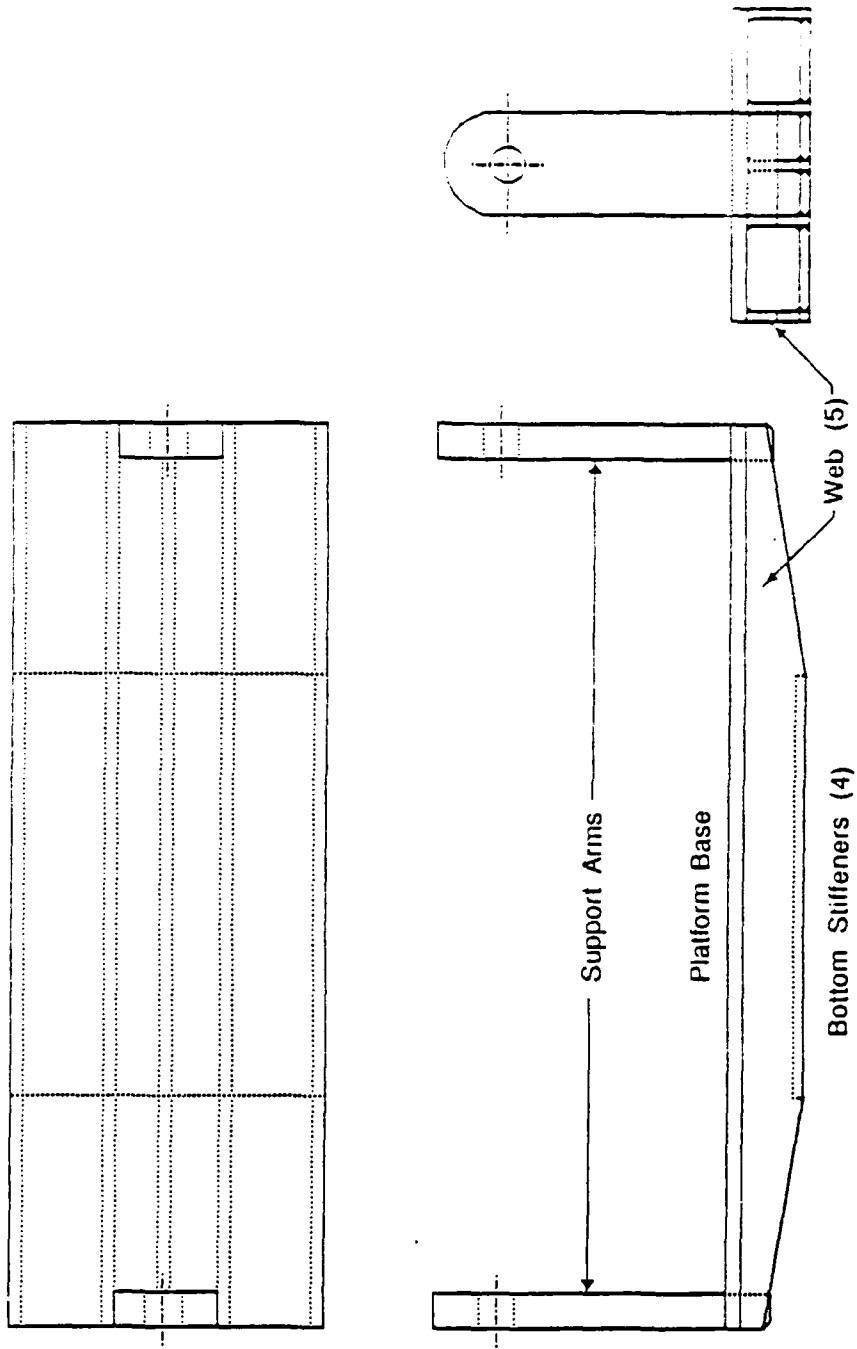


Figure 4-40 Orthographic Projection of Centrifuge Platform

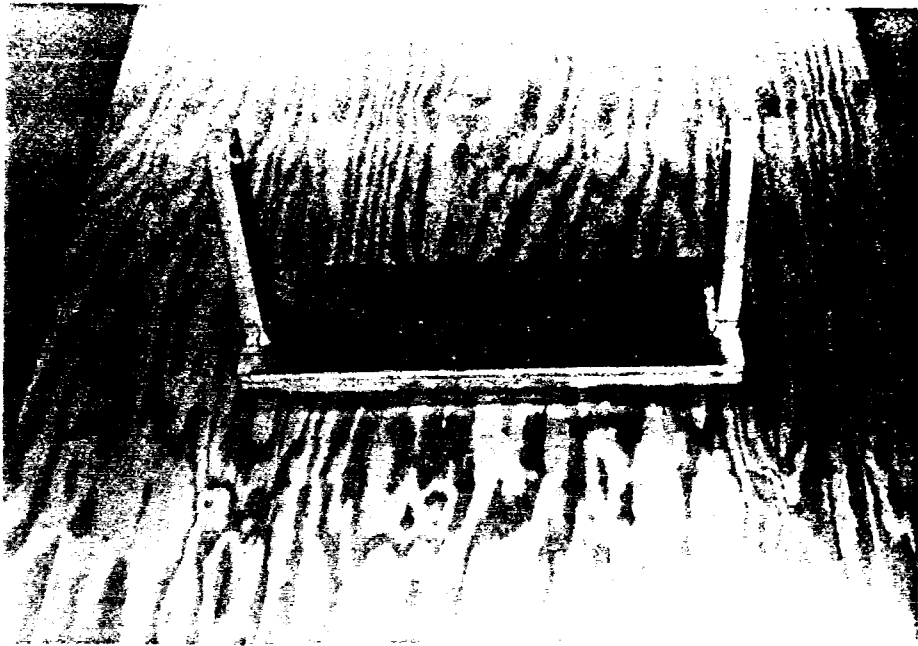


Figure 4-41 Completed Platform



Figure 4-42 Platform In-Place

The washers also prevented lateral displacement of the platforms during spin up.

The base of the platforms were reinforced with lengthwise ribs of 0.25-inch thick high strength aluminum to achieve a satisfactory moment of inertia. Five ribs were required. The spacing of the ribs introduced difficulty in fabrication as the welding tool could not fit between the ribs once they were tacked in place. Therefore, the center rib was the only one to have fillet welds on both sides. The remaining four ribs had fillet welds only on the side away from the center rib and had to be mounted in outward succession starting from the center rib. The eccentric welding required the placement of a tie-strip at the extreme fiber of the ribs to resist their tendency to bend outwards under load. The tie-strip increased the depth of the platform to 2.25 in. which resulted in an in-flight clearance of 0.75 in. between the shroud wall and bottom of the platform. This was considered the minimum permissible as there are minor irregularities in the shroud. Table 4-3 provides the pertinent specifications of the base and includes factor of safety calculations.

4.3.8 Closed Circuit Television

A television monitor was mounted on the centrifuge main shaft between the two plates which support the main arms. This monitor provided black and white live coverage of the tests in-progress. The flexibility of the mount permitted either the top of the placement device to be viewed or, by use of an appropriately adjusted mirror, viewing of the driving, pushing, and loading processes. The camera was not adjustable during the flight of the centrifuge. It performed very well throughout the research at up to 90 g's.

Table 4-3 Platform Specifications and Factor of Safety Computations

	Unit (lbs)	per platform	Total (lbs)
Pillow Block Bearing Static Capacity	3,250	4	13,000
Support Arm Capacity* at Pillow Block Bearing Pin	15,250	2	30,500
Weld Capacity* Where Support Arm is Connected to Platform Base	30,000	2	60,000
Platform Base Capacity*†	29,750	1	29,750

NOTE: - Ultimate platform capacity (13,000 lbs) is based upon the limiting strength of the pillow block bearings. Centrifuge capacity is thus 6.5 g-tons.

- Pillow block bearings can be safely used with a factor of safety of 1.0. The ball bearings begin to deform their races only when the ultimate capacity is exceeded. The pillow block housing still has a factor of safety of 5.0 when the bearing is subjected to its ultimate load.

* High strength aluminum (T6061, yield strength 32,000 psi) was used throughout construction. Welding decreases the strength to 8,000 psi. Conservatively, the limiting strength of 8,000 psi was used in the determination of member strengths whether they were welded or not.

† Platform base capacity based on 8.2 in.⁴ moment of inertia, yield strength of 8,000 psi, and a distance to external fiber (y) of 2.20 in. Moment determined using worst case conditions; concentrated load at mid-span with pinned connections.

Figure 4-43 depicts the closed circuit television circuit and slip ring channel assignments. An in-line power supply filter was used to decrease the interference in the output signal caused by the nearby discharge of the speed control capacitors. The output signal was shielded to enhance monitor display.

4.4 Model Pile (Group) Set-Up Procedure

The following procedures were followed in the set-up of each model specimen. This procedure presumes a suitable specimen has been created in accordance with the method presented in accordance with Section 5.1, Soil Description and Specimen Characterization. The platform stops at the end of the main arms must also have been adjusted with the platform empty to ensure the platform will be stopped in the appropriate position during testing.

The multiprogrammer (Hewlett-Packard 6940B) must be connected to the pulse generator, Parajust Motor Speed Control, and Stepper Motor Motion Control by the provided plugs. The Data Acquisition/Control Unit (Hewlett-Packard 3497A) must also be connected to the load cell and strain Gage output slip rings by the provided plugs.

1. Mount the appropriate specimen container and fasten with the four bolts provided. The bolts should be tightened slightly more than finger tight, just enough to ensure there is no looseness which would permit the specimen container (and placement device canister) to rock back and forth during centrifuge spin-up.
2. Rest the placement device protective canister on the lip of the access hatch opening. Ensure the canister is well supported as the attached umbilical cords protecting the wire leads tend to pull

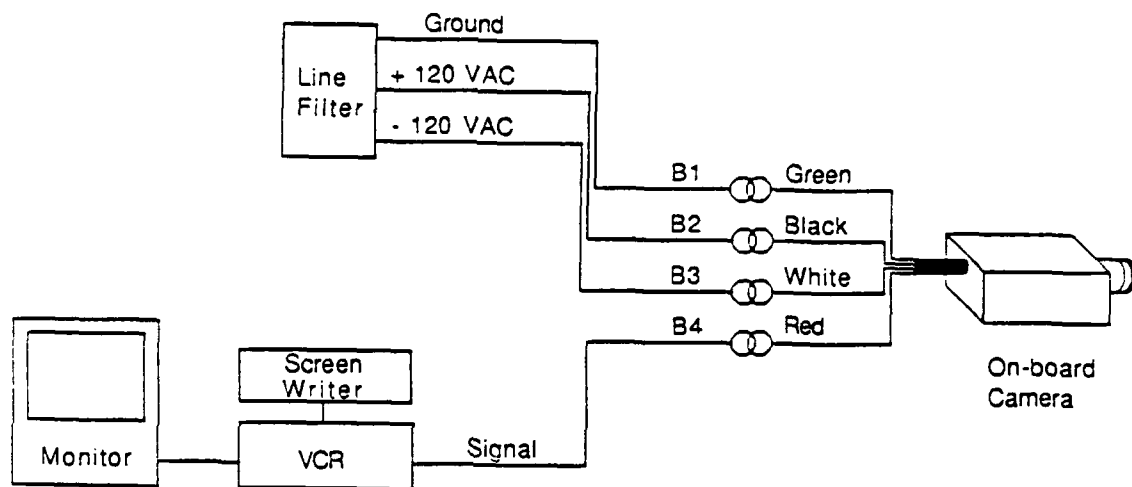


Figure 4-43 Closed Circuit Television Power Supply and Output Signal Circuit and Slip Ring Channel Assignments

the canister into the centrifuge. Experience will teach the operator the best position in which to rest the canister.

3. Advance the ball screw until the tip is within approximately 2.0 in. of the bottom of the slotted cast acrylic guide tube.
4. Fasten either the electromagnet or the appropriate load cell in position at the tip of the ball screw. The ball screw can be screwed into the magnet/load cell at this time because the ball screw is restricted from rotating only after being tightened down into the magnet/load cell.
5. Retract the ball screw several inches upward either by manual rotation of the driving gear or by energizing the stepper motor and inputting the necessary command at the motion control.
6. a) For driving; Choose the appropriate model. Slip the necessary hammer over the guide rod which extends from the cap. Insert the guide rod into the plastic insulator tube inside the electromagnet. The model must be held in place either by light pressure upward on the pile tip or by lifting gently on the connector support arm which extends through the slotted cast acrylic guide tube. A piece of tape fixed underneath the connector support arm serves this purpose.
b) For pushing; Choose the appropriate model. Insert the top of the cap into the load cell adaptor and tighten the set screws which hold the model in place when strain gaged models are used.

Models are simply screwed in if no strain gages are used.

7. Place the guide washer in the base of the guide tube and fasten with the clamp provided.

3. Retract the model until the pile tip(s) is (are) adjacent to the end of the guide tube.
9. Place the canister on top of the specimen container being careful not to disturb the specimen surface by drawing the umbilical cords across the soil. Rotate the canister to the final position and fasten with a wrap of duct tape. Adjust the supporting c-channel to its final position and tighten the locking bolt underneath the proximity device housing until the stepper motor just lifts off of its support. Loosen the locking bolt until the stepper motor is lowered back onto its support. This degree of "tightness" is sufficient to hold the placement device in position during testing.
10. Advance the pile (group) until the model tip(s) contact the soil surface or continue until the desired depth of insertion is achieved.
11. Measure the distance from the butt(s) of the pile (group) to the top of the centrifuge platform. This distance equals the depth of the specimen container plus 0.25 in. (the thickness of the base of the specimen container) plus the height of the butt(s) above the soil surface. Measure the distance from the top of the electromagnet to the bottom of the slotted guide tube support. This is the maximum available lift height which must be compared to the computed lift height displayed during execution of PILEDRIVE. Furthermore, this lift height is subject to the limitations depicted in Figure 4.20, Guide Rod Length Determination.
12. Attach the appropriate miniature connectors.
13. Ensure the top of the ball screw has sufficient clearance to permit one full rotation of the payload. One rotation is required to

develop sufficient acceleration to cause the bucket to rotate outwards.

14. Balance the centrifuge by placement of a suitable payload on the opposing platform.
15. Close the centrifuge access hatch and place both cover locking bars in position.
16. Energize the following power supplies.
 - a) Pulse generator (5 volts)
 - b) Strain gage bridge completion unit (Two power supplies at 3 volts each)
 - c) Load cell (10 volts)
 - d) Electromagnet (when necessary) (Two power supplies, one at +12 volts and the other at -1 volt.)
17. Start the small portable fan which cools the stepper motor power resistors. This is critically important as the resistance of the power resistors changes as they heat up. If the resistance changes sufficiently, the stepper motor could be damaged.
17. Connect and turn on the closed circuit television equipment.
18. Load the appropriate program into the computer. Press "run" and input the requested information. This is referred to as "initialization" of the program. Follow the provided instructions until the plotter and printer have completed their initial graphs/listings.
19. Verify the output voltage of all power supplies and adjust as needed.
20. Check again to ensure the centrifuge access hatch cover is securely fastened.

21. Energize the stepper motor power supply. The transformer must be turned on first followed by the toggling of the switch which powers the stepper itself. This switch is in-line between the transformer and Bodine adjustable motion control. Check the small toggle switch on the side of the motion control. It must be set on "computer".
22. Toggle the circuit breaker which supplies power to the centrifuge main motor and enable the hand held speed control as follows. Push the red "reset" button and then the green "start" button. The "start" button must be depressed for approximately 2 seconds. The Parajust motor speed control will generate a high pitched whine.
23. "Continue" the program. The computer will automatically spin the centrifuge, conduct the requested tests, record and plot the data, and shut off the centrifuge. Appropriate instructions will be displayed on the monitor. IMPORTANT: If it becomes necessary to stop the test, turn the multiprogrammer off. This will interrupt power to the Parajust AC Motor Control. The program will not be continuable from this point and must be "run" again. If it is important to stop the progress of the test only momentarily, push the "pause" key on the keyboard. This will stop progress of the test until the pause key is depressed again. The program will then continue execution. Follow the instructions displayed on the monitor until pile placement and load testing is complete. The load test will be conducted automatically when the pile (group) has been pushed in. If the model is driven, the centrifuge will automatically shut down after driving is complete to permit the load cell to be placed in-line with the model. As the centrifuge is

decelerating (the Parajust will be silent), turn off power to the stepper motor (see 24 below) and the centrifuge main power. This is done to enhance operator safety while the load cell is being fitted. After the load cell is in place, close the centrifuge safety cover, energize the stepper motor. Centrifuge main power and load cell power supply. Enable the hand-held speed control and "continue" the program. The load test will be conducted automatically.

24. As the centrifuge is decelerating after load testing (the Parajust will be silent), de-energize the stepper motor circuit. The toggle switch between the transformer and Bodine motion control must be opened first. If the transformer is turned off first, the charged capacitors within the stepper motor will discharge back through the controller circuitry possibly damaging the motor or controller. Turn off the transformer after the stepper motor has been de-energized. The stepper motor is de-energized with the centrifuge still rotating to give the motor the best opportunity to cool after testing.
25. After the centrifuge has stopped, turn off the remaining power supplies. Allow the small fan to cool the stepper motor power resistors for approximately 10 minutes.

Performing consecutive tests on similar models is much simpler than trying to perform a variety of tests on different ones. For example, the placement device should be configured to push individual piles and a series of such tests should then be conducted. The placement device can then be reconfigured for pushing groups or driving models prior to the next series of tests being conducted. Consecutive tests of similar

nature can be started within 30 minutes of the stopping of the centrifuge from the previous test. The pushing and loading tests can be conducted in approximately 20 minutes. Driving and loading model piles requires approximately 30 minutes.

4.5 Computer Control of the Equipment

Several aspects of the final model pile placement device design required the use of computer controlled equipment. The two most significant aspects requiring computer control and feedback were the rotation of the stepper motor and control and monitoring of the rotational speed of the centrifuge. The stepper motor served the dual purpose of lifting the electromagnet and hammer to the predetermined lift height and subsequently determining the amount of penetration after impact. Penetration of the pile altered the successive lift height of the hammer. The rotational speed of the centrifuge was monitored and adjusted, when necessary, at several intervals throughout the conduct of every test. Several other secondary functions were performed by the computer and multiprogrammer such as voltage measurement, voltage output, pulse counting, analog to digital and digital to analog voltage conversions, and relay switching. Each of these functions was made possible by the installation of the appropriate "card" in a multiprogrammer. A Hewlett-Packard 6940B multiprogrammer was available for use and configured to perform the desired functions. This multiprogrammer was used in conjunction with the Hewlett-Packard series 9000, model 216, computer which is programmable in the BASIC language. The pertinent specifications of the computer will be presented in Section 4.5.1.1, Hewlett-Packard 9000 series, model 216 computer. The specifications and

operating characteristics for each of the multiprogrammer cards used will be presented individually following a broad description of the use of the multiprogrammer. The three main programs developed, one each for a) pile driving, b) pile (group) pushing, and c) model pile calibration will then be presented in Section 4.5.2, Software.

4.5.1 Hardware

The information presented has been extracted from the Hewlett-Packard 9000 Series, Number 216 Computer User's Guide and 6940B Multiprogrammer's User's Guide as well as the operating and service manuals for the individual cards. The User's Guides should be consulted for more detailed information.

4.5.1.1 Hewlett-Packard 9000 series, model 216 computer

The computer shown in Figure 4.44 consisted of a combined central processing unit and monitor with an attached disk drive and keyboard. The users manual should be consulted for pertinent specifications. Transmission of data between the computer and multiprogrammer will be presented in the following section.

4.5.1.2 Hewlett-Packard 6940B multiprogrammer and 59500A interface unit

The multiprogrammer permits the computer to read inputs from various electrical/electronic devices/transducers and command the action of other devices based on the provided inputs. The multiprogrammer and cards serve to translate the input/output from the attached devices into a format understood by the computer and vice versa. The multiprogrammer communicates using 16-bit words which are normally transmitted via a General Purpose Input/Output (GPIO) interface. However, the existing system has a Hewlett-Packard Interface Bus (HP-IB) interface which communicates using 8-bit American Standard Code for Information Interchange



Figure 4-44 Hewlett-Packard 9000 Series, Model 216 Computer

ASCII coded characters. Therefore, use of the 6940B multiprogrammer with the HP-IB interface required the use of a 59500A interface unit to convert the ASCII characters to the 16-bit words required by the multiprogrammer. Likewise, the interface unit translates the 16-bit multiprogrammer words into the 8-bit ASCII characters recognized by the controlling computer. The 59500A Interface Unit and 6940B Multiprogrammer are shown in Figure 4-45.

The multiprogrammer must be established as the listening device before any communication can take place. This is especially important if more than one multiprogrammer is being used. However, since one multiprogrammer was sufficient for the number of cards required, the standard select code and multiprogrammer address of "723" was used to address the multiprogrammer. This address, followed immediately by a semicolon (;), alerts the multiprogrammer to listen for subsequent commands.

Three types of codes (words) can be sent during computer-to-multiprogrammer exchanges. Only one type can be received during multiprogrammer-to-computer exchanges. These words will be recognized by the multiprogrammer only after it has been properly addressed as discussed in the preceding paragraph. The three output (computer-to-multiprogrammer) words are either control words, data words, or address words. Control words are usually the first words sent to the multiprogrammer system. They consist of six control word characters which are transmitted and obeyed in the order written. The first of the six digits is the control word tag which tells the 6940B the information which follows defines the control mode and internal unit address, or slot. The address character (first character) is "0" for the

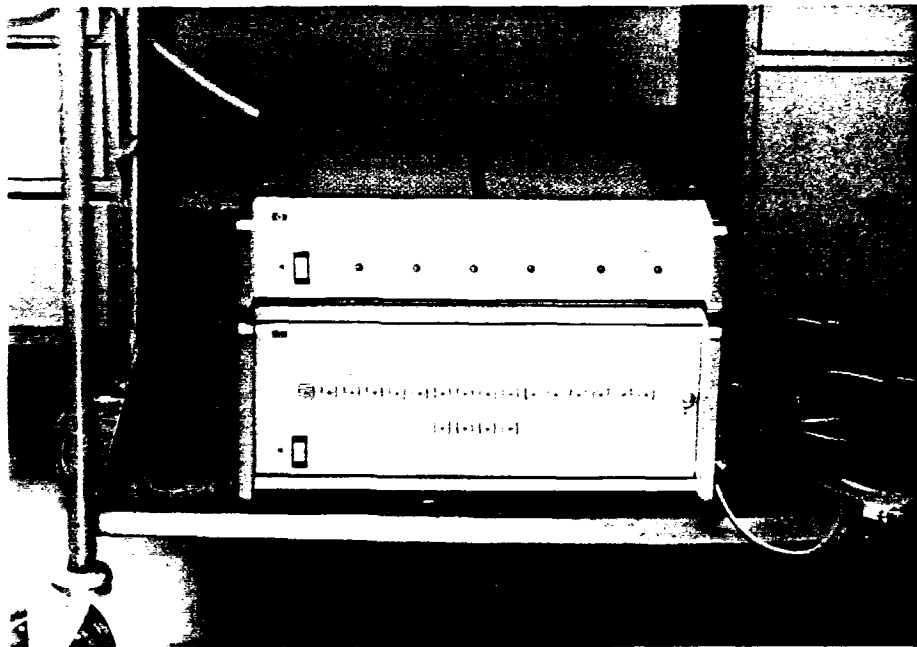


Figure 4-45 Hewlett-Packard 59500A Interface Unit and 6940B Multiprogrammer

multiprogrammer system being described. The next four characters are the data field consisting of four octal numbers (see Appendix B, Number Theory and Decimal, Octal, and Binary Conversion Algorithms). The left-most digit, D4, is always zero in the control word. The operating mode is then specified by the following two digits, D3 and D2. Digit D2 serves a dual purpose, though, as it is also used in conjunction with D1 to specify the unit address. The operating mode and unit address must be considered independently before the correct data field can be determined. Table 4-4 shows the most common data field codes for the two multiprogrammer operating modes.

After selecting the desired operating mode from Table 4-4, the complete control word can be determined by adding (in octal) the unit address to the previously selected operating mode. Since only one multiprogrammer was required to conduct the research, the only unit address used was 00. Thus, the correct control words are as shown above. The control word is followed by either a data word or an address word.

Data words select and control output cards within the mainframe previously specified by a control word. The four most significant digits of the data word specify the address of the multiprogrammer card which will execute the specified command. The remaining 12 digits are the computer's input to the card. The 12 digit data portion of the word is then stored on the card and executed on command resulting in rotation of a stepper motor, closure of a solenoid, output of a specified current, etc.

An address word is used to select the input card that is to send data back to the calculator. Only the four most significant digits of

Table 4-4 Multiprogrammer Operating Mode Codes

Multiprogrammer Operating Mode		Data Field
Output Mode	Input Mode	
SYE Off		0000
SYE On		0040
DTE,SYE On		0140
DTE,SYE,TME On		0160
	ISL,SYE On	0240
	ISL,SYE,TME On	0260
	IEN,SYE,TME On	0460

NOTE: Data field codes shown are in octal and assume a unit address of 00.

SYE - System Enable; Absence of this signal automatically deactivates certain cards to a "safe" state.

DTE - Data Transfer Enable; Controls data transfer and timing signals on certain output cards.

TME - Timing Mode Enable; Modifies action of the handshake logic by suppressing the automatic flag and causing the FLA signal to follow the state of the CTF (Common Timing Flag) signal. FLA (Leading Edge of Flag) is a signal returned to the calculator to indicate a process has begun.

ISL - Input Select Mode; Terminates output data in the mode gates, thereby permitting input data to be returned to the controller from an addressed input card.

IEN - Interrupt Enable; Used in conjunction with TME to modify the action of the handshake logic during input operations.

the address word are recognized by the input card. The remaining 12 digits are ignored. An example of a control word and associated data or address word is shown below.

```
10  SPOLL (723)
20  OUTPUT 723;"00160TC.....
```

The calculator output words requiring a slightly modified format will be discussed when the appropriate card is presented.

A return data word is sent from a specified input card to the calculator when the input card is addressed from the controller output register with an address word. The return data word is composed of 12 digits representing the system property being monitored by the card.

In general, a Serial Poll (SPOLL) is conducted to clear the multiprogrammer and prepare it for the following command. Then, a control word is sent to specify the mainframe and its mode of operation. The control word is followed either by a data word or address word. The data word selects and controls a specified output card whereas the address card designates an input card which must then transmit its stored information back to the calculator. The word the input card sends back is called a data return word. The multiprogrammer Users Guide should be consulted regarding specific requirements concerning the multiprogrammer word formats. Both output and input words were required in the use of the multiprogrammer and their specific formats will be presented in the following discussion of each card used during this research.

Stepping motor control card, 69335A. This card is programmable to generate between 1 and 2047 squarewave pulse trains at either of two

output terminals. When the pulses are received by a stepping motor controller they are translated into either clockwise or counterclockwise rotation of the motor shaft thereby permitting the use of the stepper motor as a precision positioning device. The direction of rotation is dictated by the output terminal used. Octal outputs up to 3777 (decimal 2047) will be output from pin number one. Adding any value to this number shifts the output to pin number two (reversing the direction of rotation) and results in a pulse train of up to 2047 pulses in the opposite direction (octal 7777). Rotation of the motor more than 2047 pulses in one direction requires simple software modifications. This card has two operating modes. The first mode, Automatic Handshake, provides no indication to the user's program that the output pulse train has been completed. The second, or Timing Mode, provides the user's program an indication from the multiprogrammer that the output pulse train has been completed. The timing mode was used in this application as the physical rotation of the motor drive shaft was the limiting factor in the amount of time needed to drive a pile. The timing mode permitted the processing of additional information in conjunction with the rotation of the motor. Essentially, the electromagnet was kept in oscillating vertical motion during the driving sequence. The frequency of the output pulse train was dictated by a resistor placed across terminals C3 and R12 located on the card. The frequency equals 213 pulses per second (pps). This frequency was chosen, after testing several resistors, as the value which permitted the most rapid raising and lowering of the electromagnet without any loss of steps.

Digital to analog (D/A) voltage converter card, 69231B. This card is programmable to provide an output of from -10.240 to +10.235 volts direct current in increments of five millivolts. Use of this card requires the installation of a 69351B Voltage Regulator Card which supplies the necessary $\pm 15V$ bias voltages to the D/A converter. The output from the D/A card was used to control the rotational speed of the centrifuge. The voltage output from the card was input across terminals 2 and 3 within the Parajust Motor Controller Housing. This card was used in conjunction with a pulse counter card to establish a feedback loop between the output from the D/A converter and the rotational speed of the centrifuge.

Pulse counter, 69435A. This card counts pulses incrementally or decrementally in the range of 0 to 4095. A 'borrow' pulse is generated if the count goes above or below these values to permit significant counting capacity by cascading multiple cards. One card was sufficient in this application as the card was used to count the pulses output by the pulse generator monitoring the rotation of the centrifuge drive-shaft. Pulses were counted for a specific time period permitting the accurate determination of rpm by the appropriate software.

Relay output with readback, 69433A. This card is programmable to provide twelve, independent, normally open, Single Pole-Single Throw relays. Output data from the card is in the form of contact closures. The readback option on the card permits the computer to determine the status of each of the relays before and/or after any of the relays are changed. This cards primary purpose was the energizing and de-energizing of the electromagnet used to lift the pile hammer via closure

of a relay. The relay switches can pass a current of up to 500 milliamperes with a maximum voltage potential of 100 volts.

Analog to digital (A/D) voltage converter card, 69421A. This card, also called a Voltage Monitor Card, is programmable to monitor analog direct current voltage inputs and return a digital input to the multi-programmer interface indicating both polarity and magnitude of voltage. Three voltage ranges are available on the card; $\pm 102.35V$, $\pm 10.235V$, and $\pm 1.0235V$. Use of this card requires the installation of a Voltage Regulator Card, 69351B, which supplies the required 15V bias voltage necessary for the operation of the A/D converter card. The converter card was used in conjunction with an additional Relay Output with Readback Card (69433A) to monitor the output of the proximity device which sensed the closeness of the electromagnet face to the top of the pile hammer. The proximity device used TTL logic and thus had an output of either 0 or +5V permitting the A/D converter to be used at the factory setting of $\pm 10.235V$.

4.5.2 Software

Two main programs were developed to control the centrifuge and placement device in this investigation. DRIVEPILE was developed to drive individual model piles. PUSHPILE was a simplified program developed for the pushing of individual model piles. Both programs include a loading subroutine which conducts the required load test, plots, and then stores the results. Each program consists of a series of questions which the user answers to initialize the computer before testing. The initializing portion of the program has certain safeties built in which prevent the placement device from being used in a manner

which might be damaging. Furthermore, constraints are built into the program which ensure a minimum of 10 scale feet of clearance is provided between the bottom of the model pile and base of the specimen container. This portion of the program also displays the required rotational speed of the centrifuge on the monitor to give the user an indication of whether or not the computer is controlling the test properly. The rpm shown by the photoelectric tachometer display box should be equal to the value displayed on the monitor. After initialization, each program plots and prints the necessary forms and then pauses, waiting for the user to check all connections and voltages before continuing the test. The programs will not spin the centrifuge until the user has performed the specific tasks covered in Section 4.4, Model Pile (Group) Set-Up Procedure. However, the programs have not been made safe against simple errors of omission or errors in data entry which can potentially damage the device. It is the users responsibility to ensure all tests conducted are within the capacity of the placement device. Refer to Section 4.7, Equipment Limitations, for a summary of those limitations.

The programs include commands to interrupt the power from the Parajust Motor Speed Control to the centrifuge upon completion of the desired tests. Subsequent running of the program clears all previous inputs and reinitializes the system. Specific aspects and the logic of each program will be presented in Section 4.5.2.1, Main programs.

Each program refers to a series of subroutines which will be presented and discussed in Section 4.5.2.2, Subroutines. New programs can be developed relatively simply by changing the order in which the subroutines are utilized. The device can be quickly adapted to perform the types of research suggested in Section 6.2, Recommendations.

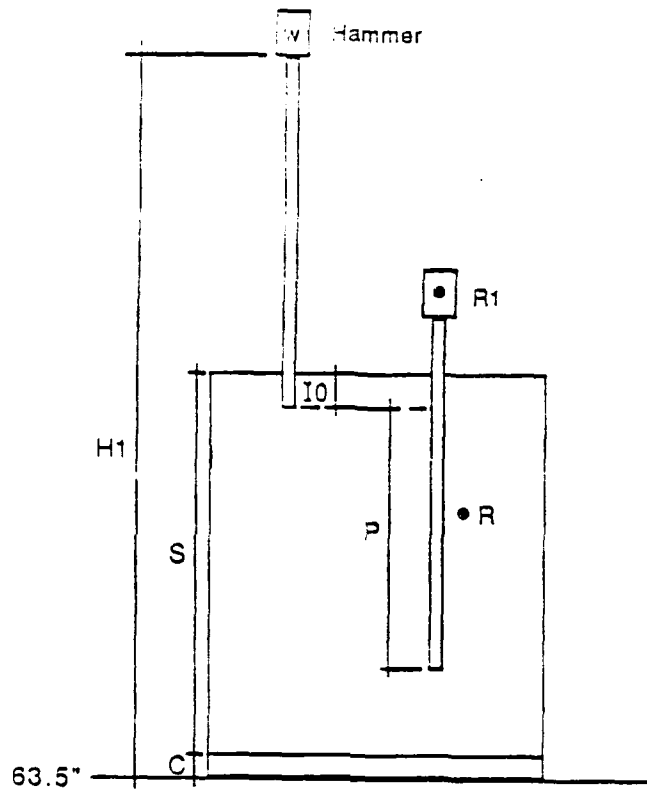
The program PUSHGROUP, a derivative of PUSHPILE, was developed to push model pile groups and will not be discussed as a separate program. The only significant differences are a change in the calibration factor of the load cell output, as the 500-lb. capacity load cell is used when groups are pushed, and modification of the plotting subroutine due to the increased load output. Rather, the programs are considered the same and presented under the heading PUSHPILE. The program developed to calibrate each of the model piles, CALTEST, is presented following the discussion of the two main programs.

4.5.2.1 Main programs

The initialization of each main program is similar with only slight modification of the DRIVEPILE program which provides the user a suggested hammer weight. Both programs, all associated subroutines, and CALTEST, are listed in Programs Developed for Use in the University of Florida Geotechnical Centrifuge (GEOCENT) (Gill and Kofoed, 1988).

Each program requests the following inputs during initialization; prototype pile length (LO), prototype depth of tip at termination of placement (TO), soil specimen density (Gamma), depth of soil in the specimen container (S), height of the model butt above the top face of the centrifuge platform (H1), thickness of the specimen container base (C), and proposed gravity level at which the test is to be conducted (N). Each input will be discussed separately. Refer to Figure 4-46.

The prototype pile length and depth of tip at termination of placement are the two most basic parameters. Initially, the two inputs are reduced by a factor of N and stored as L1 and T1, respectively, for later use in the determination of whether the specimen container is



C = thickness of specimen container base	inches
E = efficiency of energy transfer	%
E1 = prototype energy at impact (100% efficiency)	ft-lbs
Gamma = soil unit weight	pcf
g = g-level at midpoint of hammer	g's
H1 = Height of top of model above centrifuge platform base	inches
I0 = depth of model pile insertion	inches
I = cumulative number of impacts	integer
K0 = prototype hammer lift height	feet
L0 = length of model pile	inches
n = g-level of test	g's
P = penetration of model pile	inches
P1 = penetration per impact	inches
R0 = centrifuge rpm	rpm
R1 = radius at midpoint of hammer	inches
R = radius at midpoint of full penetration	inches
S = depth of soil in specimen container	inches
W0 = weight of prototype hammer	lbs
W = weight of model hammer	grams
X1 = commanded step rotation to the stepper motor	integer

Figure 4-46 Computer Variable Designations

suitable for the test being performed and when penetration of the model pile is finished.

The dry unit weight of the specimen, as determined using the procedure outlined in Section 5.1, Soil Description and Specimen Characterization, is input and called Gamma. The program determines void ratio and relative density using the algorithms also presented in Section 5.1. The program assumes all tests are conducted on Reid-Bedford sand in the determination of the aforementioned parameters. Values obtained are then saved for use in the plotting of results.

The depth of soil in the specimen container (S) is used in the determination of the suitability of the container to be used for the proposed test. The program includes an arbitrary limit on the clearance between the tip of the pile and base of the specimen container of 10 scale feet. For the piles being modeled (10.75-inch outside diameter), the minimum distance between the tip and container wall is $11.16 d$. The test will not be performed if the computer determines there is insufficient clearance. This determination is based on the program's assumption the specimen container is filled to the top.

The height of the butt above the top of the platform base (H1) is the most important input assuming all other inputs have been made correctly. It is used in the determination of the depth the model has been inserted in the soil prior to testing, the distance the model will be driven or pushed before the load test is conducted, and the rotational speed of the centrifuge. Depth of insertion (I0) is determined by adding the thickness of the specimen container base (C), soil depth, and the model pile length (L1). The value of H1 is subtracted from the sum

of the three inputs to give the value of IO . The resulting value can be either positive or negative. If positive, the pile has been inserted and the tip physically rests within the soil specimen. If negative, the pile is not yet in contact with the specimen. The test will be conducted in either instance with the pile being driven or pushed until the tip achieves the desired penetration. The test will not proceed if the pile has been inserted past the desired depth of total penetration. The distance the pile is to be driven or pushed is designated P and called penetration. It is the difference between the depth of the tip at the termination of placement and the depth the pile has been inserted. At the start of the test, $P = 0$ and increases incrementally with each successive blow from the hammer or push on the model until $P + IO$ equals the desired depth of pile placement.

The rotational speed is determined based on the midheight of the final total depth of penetration of the model with respect to the height of the soil specimen. The radius of the top of the centrifuge platform is constant at 63.5 inches. Subtracting the height of the specimen container from this value and adding one half of the final total model penetration depth (in inches) provides the average radius at which the test will be conducted. This is done automatically and the proposed speed of the centrifuge is displayed on the monitor. The value of the specimen base thickness (C) is included in the computation of the average radius to ensure the desired g -level of testing is determined for exactly the midpoint of the final model placement depth.

DRIVEPILE includes additional inputs to aid in the proper conduct of pile placement. The prototype pile driver hammer weight (lbs),

nominal lift height (ft), and driver efficiency (%) are input as $K\delta$, $W\delta$, and $E\delta$. The nominal lift height is required to determine the total hammer input energy. However, the program computes a new lift height after every impact based on the position of the hammer relative to the known platform base radius of 63.5 inches. The hammer weight is computed by first determining the average radius at which the hammer will be acting during the driving process. This value equals the average of the distance of the butt from the center of rotation of the centrifuge at the start and finish of the driving process. The program accounts for the height of the cap assembly and one-half of the height of the model hammer. Knowing the proposed rotational speed of the centrifuge and the average radius at which the hammer will be acting, the average g-level at which the hammer will act is determined. The weight of the prototype hammer is divided by the cube of the average g-level (see Section 3.4, Experimental Requirements) to determine the proposed weight of the model hammer. The model hammer weight is determined in grams. This weight is considered to be the weight which most closely models the action of the prototype driver. However, model hammer weights were determined as described in Section 4.2.6, Model Pile Hammers, using the proposed model hammer weight as a starting point. DRIVEPILE requires the weight (grams) of the model hammer being used be input as W .

As mentioned, the lift height of the hammer varies with every impact. The constants used in determining the lift height are the weight of the model hammer and the prototype impact energy. The height of the butt and rotational speed of the centrifuge are known throughout the progress of the test. Thus, the g-level at the butt is known also.

Dividing the prototype impact energy (converted to inch-grams) by the g-level at the butt to the fourth power gives the required energy input of the model. Dividing that result by the known constant weight of the model hammer gives the required lift height. The lift height decreases as the model penetrates due to the increasing force of gravity as the model moves outward with respect to the central axis of the centrifuge.

The computer requests the efficiency of the prototype pile driver as a simple means of modifying the number of impacts needed to drive the pile without manufacturing a new weight. An efficiency of greater than 100% increases the lift height, and thus, impact energy of the driver. Likewise, an input efficiency of less than 100% decreases the lift height. The determination of the model hammer weight is not affected by the value of efficiency input.

DRIVEPILE. Following initialization and the plotting/printing of the initial output formats, DRIVEPILE is paused waiting for the operator to "continue" the program. The electromagnet is energized and remains energized while the multiprogrammer accelerates the centrifuge arms to the proper rpm. The electromagnet is de-energized and allowed to rest on top of the pile. Contact is re-established between the electromagnet and hammer using the FIND subroutine (it is possible the model pile has not settled into the soil due to either spinup or deflection of the placement device.) This establishes the reference point from which driving is begun and penetration measured, the total amount of penetration already having been determined in the initialization portion of the program. The lift height is determined based on the starting position of the pile butt.

The hammer is lifted off of the pile and five readings are taken from the strain gages. The average of these readings (for any given pair of gages) is the initial reading to which all subsequent strains are referenced. The hammer is then lowered onto the pile and the driving sequence begun.

The RAMBLOW subroutine performs one impact and returns the electromagnet to its starting position. The counter for the number of impacts (I) is incremented by 1 and the FIND subroutine then reestablishes contact between the electromagnet and hammer. The FIND subroutine provides the main program with the number of "steps" required to make contact. This amount is converted to penetration and added to the initial insertion and any previous penetration. Total penetration versus impact is plotted as the test progresses. If additional blows are required, a new lift height is computed and the RAMBLOW/FIND subroutines are repeated. This process continues until the model has been driven to the desired depth.

The development of residual stresses is monitored by lifting the hammer off of the pile and reading the strain gage pairs. The final residual stress readings are taken with the hammer having been lifted from the pile butt also. The program interrupts power to the Parajust AC Motor Control after the final residual stress readings causing the centrifuge to coast to a stop. With the electromagnet energized, the placement device is lifted from driven model. The appropriate load cell is then magnetically attached to the magnet using a specially manufactured metal plate and centering bolt. The "continue" key is depressed when the load cell and placement device have been properly positioned over the model and the load test is conducted.

PUSHPILE. Following initialization and the plotting/printing of the initial output formats, PUSHPILE determines the number of steps the stepper motor must rotate to push the model 3.0 scale inches into the soil. Load cell and strain gage readings are then plotted, printed, and stored on disk. Actual penetration is added to the original value of insertion and compared with the total value of desired penetration. If actual penetration exceeds desired penetration, the pushing process is considered complete. If actual penetration is less than desired, the process repeats itself until total desired penetration is achieved. The program then proceeds with the conduct of a loading test without the need of stopping the centrifuge.

The data recorded consists of total force required to push the pile for each increment, the force experienced by each pile at the cross section fitted with a pair of strain gages, and the time at which the readings were taken (provided by an internal clock on the 3497A).

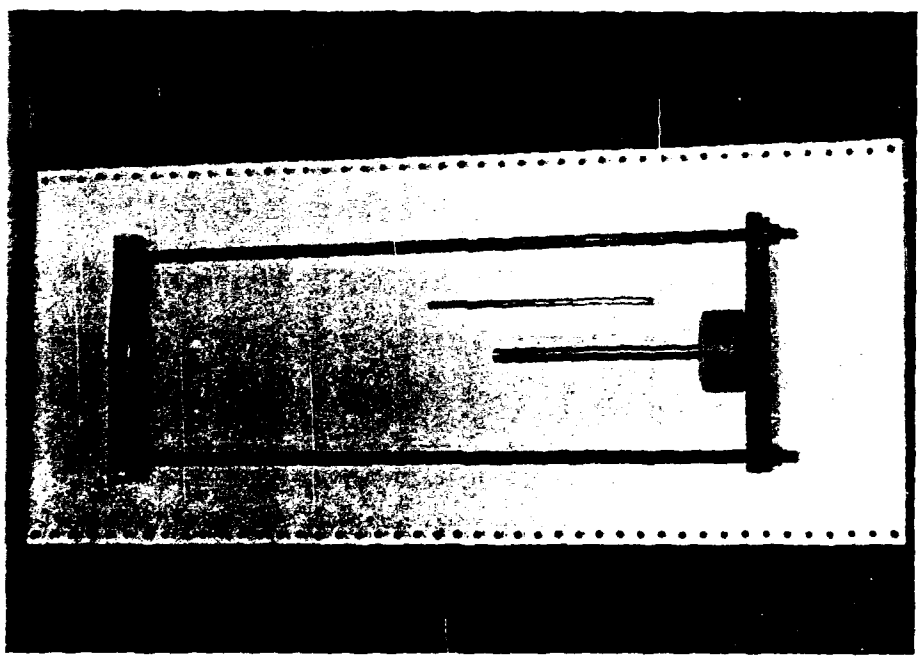
The transducers are zeroed at the start of the pushing process before any data is recorded. After the computer has spun-up the centrifuge, five readings are taken from the load cell and strain gages. These are averaged to provide the initial reading for each transducer. The difference between the actual output of the transducer and the initial reading is the measured load for a given penetration. After pushing is complete, the load is removed from the pile by backing off the load cell one "step" at a time until the load cell output equals the initial reading. The strain gages are then read and the readings taken to be the residual stress in the pile. Loading is accomplished by lowering the load cell, two steps at a time, onto the pile and pushing

the pile in two-step increments until the butt has been deflected 5.0 scale inches. Load versus butt deflection is plotted during this phase of the test. Readings taken from the strain gages during loading provide an indication of the transfer of the loading stresses to the soil down the length of the model.

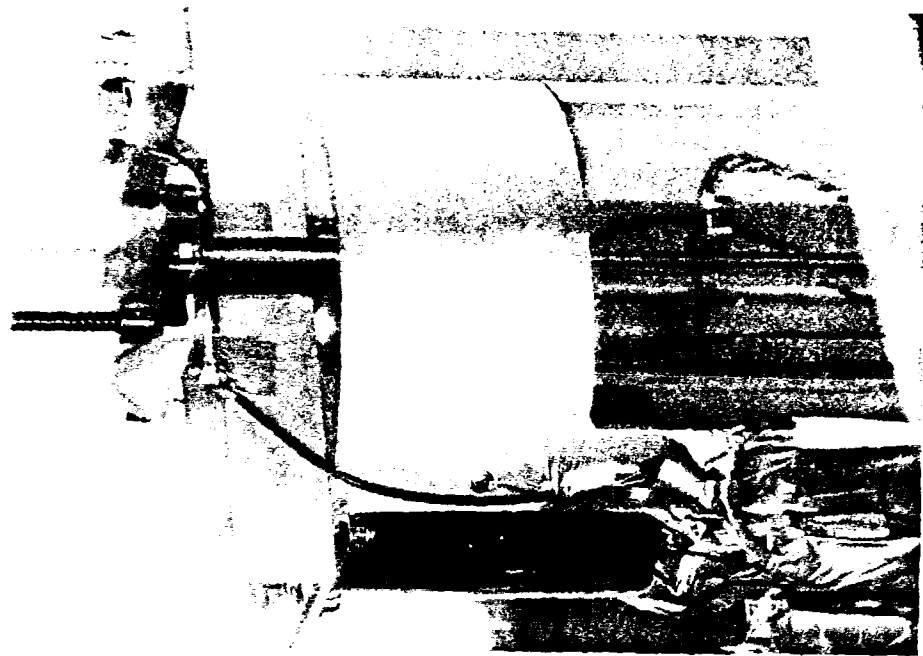
CALTEST This program is used to calibrate all individual piles and each gaged pile subsequently used as a member in a group model. The 200-lb. capacity load cell and pile to be calibrated are installed in the placement device and encased in a rigid tube to prevent buckling of the model. The base of the rigid tube provides the reaction preventing the pile tip from displacing during calibration. The base and tube are supported by a reaction beam connected to the ball screw bearing assembly clamp (Figure 4-47).

Five readings are taken from the load cell and each strain gage. The average of these readings is the initial reading for the respective transducer. The load cell is lowered onto the pile model with the load cell and strain gages being read after each step. The pile is loaded until a preset load cell reading is attained. Final readings are made from each of the strain gages and the load cell is lifted from the pile. The calibration process takes approximately five minutes once the model has been positioned in the placement device.

The program provides gage calibration factors for each gage and performs a linear regression resulting in a correlation factor. The correlation factor provides an indication of the linearity of the gage response.



a) Model Pile Calibration Accessories



b) In-Place

Figure 4-47 Model Pile Calibration Equipment. a) Model Pile Calibration Accessories; b) In-Place

All calibrations are performed through the slip rings with the system being set up as if a driving or pushing test were being conducted. Thus, the calibration factors do not change during the conduct of a driving or pushing sequence.

1.5.2.2 Subroutines

Each of the subroutines used in this research are presented below. The three main programs do not necessarily contain each of the subroutines presented.

STARTSTOP. This subroutine is used in the initial acceleration of the centrifuge to test rpm and also to interrupt power to the Parajust AC Motor Speed Control at the conclusion of testing. There is a counter in the program (35) which is set to zero when the program is started. If the counter equals zero when the subroutine STARTSTOP is used, as it will the first time the subroutine is used, the computer commands the high speed Digital to Analog converter card to incrementally increase its output voltage to the Parajust Speed Control until some predetermined voltage output is achieved. That voltage level is dependent on the value of rotational speed required for the conduct of the test. The subroutine accelerates the centrifuge to within 10 rpm of the desired speed but does not exceed the test rpm. The rate at which the centrifuge accelerates is determined by the "WAIT" command which tells the computer how long to wait, in seconds, between incremental increases of the D/A converter card output. The value of 0.025 was determined by trial and error to be the wait time which resulted in the least adverse vibration of the specimen during spin-up. After the computer had increased the D/A converter card output to the desired level, the

counter 35 was increased by 1. Subsequent reference of the program to the STARTSTOP subroutine caused the D/A converter card output to go immediately to zero and the centrifuge would coast to a stop. Anytime the counter 35 did not equal zero, the computer would change the output of the D/A converter card to zero volts.

RPM. This subroutine commanded the timer card to energize the pulse counter card for fifty 0.1 second time increments (5.0 seconds). The pulse counter card then determined the number of pulses input by the pulse generator on top of the hydraulic slip ring assembly. This value was used in the determination of the rpm based on one pulse being generated for each 15 degrees of rotation of the centrifuge arms. The actual value of rpm was compared to the rpm required for the test and the subroutine determined the difference in those rpm, whether positive or negative. Figure 4-34 shows that the centrifuge rotational speed will vary 0.143 rpm for each 5 millivolt increment output from the D/A converter card at the test rotational speeds. The difference in rpm is then divided by 0.143 to find the number of 5 millivolt increments the D/A converter card output must be increased or decreased. The subroutine adjusts the output accordingly. The subroutine is referred to twice consecutively after the STARTSTOP subroutine has brought the centrifuge up to initial rpm and subsequently in the program to monitor and adjust the rpm as needed. This program maintains the centrifuge rpm within ± 0.1 rpm.

STEPPER. This subroutine accepts the required number of steps computed by the main program ($\pm X1$) and manipulates the value into a format acceptable by the Stepper Motor Control card. The stepper card

will accept inputs no greater than 2047 steps in either direction. This subroutine was established to limit the maximum number of input steps to 2000 in either direction. If the computer determines less than 2000 steps are required for a given rotation of the stepper motor, that number is input directly to the stepper motor card. When more than 2000 steps are required, this subroutine determines the number of 2000-step increments needed. The required number of 2000-step increments are then input to the stepper card. The final increment of steps, some value less than 2000, is then input to the stepper control card. The main program resumes after those steps have been sent from the stepper control card.

ROTATE. This subroutine accepts the value of steps input by the STEPPER subroutine and commands the stepper motor to perform the desired rotation. The use of the automatic handshake mode prevented the program from continuing until the commanded rotation was complete.

RAMBLOW. This subroutine performs as described in Section 4.5.2.1, Main programs, subsection DRIVEPILE. The intent of the subroutine is to raise and lower the electromagnet as quickly as possible. Bringing the electromagnet back to its position at the beginning of the RAMBLOW subroutine establishes the reference from which incremental penetration is measured.

FIND. After the electromagnet returns to its starting position, the FIND subroutine is used to bring the electromagnet back into contact with the hammer. In this subroutine, the stepper is commanded to rotate five steps at a time lowering the electromagnet onto the hammer. The output of the proximity device is checked after every five-step

increment. When the proximity device signals the electromagnet is within three thousandths of an inch of the hammer, the electromagnet is lowered an additional 5 "steps". The total number of steps required for the electromagnet to regain contact with the hammer is the penetration from the previous blow.

MAGON/MAGOFF. This subroutine commands the exclusive closure of the mercury relays in the relay readback card which energize and de-energize the electromagnet. Closure of relay switch 1 results in the electromagnet being energized with 12 volts of direct current. Closure of switch 2 (which automatically opens switch 1) provides 1 volt direct current of the opposite polarity causing separation of the hammer from the electromagnet. Switch three is then closed permitting residual magnetic flux to dissipate from the electromagnet. Switch three remains closed until the magnet is again in close proximity with the hammer and the lifting cycle is repeated.

READ TTL. This subroutine reads the TTL (5 volt) output of the proximity device after every five-step increment taken by the electromagnet while searching for the hammer. The output is read by the analog to digital voltage converter card in the multiprogrammer.

PUSH ROUTINE. This subroutine commands the stepper to rotate far enough to push the pile (group) 3 scale inches and reads the load cell output from channel 11 of the 3497 Data Acquisition/Control Unit. This subroutine is used in the PUSHPILE program only. The required number of steps to push the model 3 scale inches is determined in the body of the main program.

LOAD TEST. This subroutine conducts the load test on the placed model. It is used immediately after the conclusion of the pushing process in PUSHPILE. However, DRIVEPILE requires the centrifuge be stopped momentarily, for the placement of the appropriate load cell on top of the driven pile, and restarted before the load test is conducted. The main program pauses itself and interrupts power to the centrifuge while the load cell is being positioned. Depressing the "continue" key causes the centrifuge to resume speed and the load test is conducted.

LOAD TEST begins by establishing the zero reading on the load cell. In DRIVEPILE, five initial readings are taken with the load cell raised above the point of contact with the pile butt. The average is the zero reading. The load cell is lowered one step at a time until the load cell reading increases to a preset level indicating the load cell has contacted the pile butt. The load cell is then lifted back off the butt until the zero reading is reestablished. In PUSHPILE, the load cell is lifted off of the model butt until the zero reading established at the beginning of the test is attained. This is the point in both programs where the pile is considered as having been placed in the soil and resting with no applied load. A reading is taken from each strain gage as an indication of the residual stresses developed in the model during pushing.

The load test consists of the load cell being lowered onto the model one step at a time until the butt has been pushed down 5 scale inches. Load cell and strain gage readings are taken after each step to provide the most accurate record of the load versus deflection performance of the model, the increase in stress above the residual stress

level, and the transfer of stresses from the pile to the surrounding soil.

Each increment of deflection (step of the stepper motor) results in a scale butt deflection of 0.043 and 0.053 in. at 69.3 and 36.0 g's, respectively.

CREATE FILE, STORE DATA, and CLOSE FILE. These subroutines are used to create the filespace on the disk, store the data as the test progresses, and close the file upon conclusion of the test, respectively. This sequence of subroutines may be used more than once by the main program as the data obtained during each phase of the test; pushing, driving, loading of the pile (group), etc., requires a separate storage file.

GRAPHICS LAYOUT/PLOT. This pair of subroutines is used to generate the initial graph upon which the results of the DRIVE ROUTINE, PUSH ROUTINE, and LOAD TEST are plotted. Plotting is accomplished in scale thousand pound (kip) increments as the test progresses to provide the user indication that the test is being performed properly.

NOTES. This subroutine permits the addition of notes to the plotter output. An individual line of notes cannot exceed thirty characters.

PRINT LAYOUT/PRINT. This pair of subroutines is used to create the printout format upon which the results of RAMBLOW, PUSH ROUTINE, and LOAD TEST are recorded. Printing is accomplished as the test is being performed.

4.6 Data Collection and Recording Equipment

This section presents the theory behind the operation of all model response measuring devices, collectively called transducers. All of the transducers were electrical in nature and provided data measurable with a Hewlett-Packard 3497A Data Acquisition/Control Unit. The operation of the unit and practical considerations to aid in the proper use of the transducers is covered in Section 4.6.1, Hardware. Section 4.6.2, Software, explains the techniques used to access the output from the transducers and transmit the information to the computer.

4.6.1 Hardware

This section outlines the operating characteristics of the Hewlett-Packard 3497A Data Acquisition/Control Unit. Also presented is the theory of operation of the transducers used to verify the performance of the placement device and to measure the model pile response to placement and loading.

4.6.1.1 Hewlett-Packard 3497A data acquisition/control unit

Figure 4-48 shows the Hewlett-Packard 3497A Data Acquisition/Control Unit. Various cards are placed in the data acquisition unit depending on the type of measurement being made. The 3497A was chosen because all circuits being monitored are kept energized between readings noted of being energized when readings were requested. This option eliminates errors in the transducer readings associated with rapid temperature changes when the transducer circuit is energized.

4.6.1.2 Transducers

The word *transducer* is used collectively to refer to an instrument or device which converts one form of energy into another. A very common



Figure 4-48 Hewlett-Packard 3497A Data Acquisition/Control Unit

type of transducer, the electrical sensor, is used to provide signals to electrical recording instrument. The devices used in this research produce an output proportional to a change in some parameter. Collectively, they are called analog electrical sensors. An analog device provides an infinite number of possible signals within the limits of the device output voltage as opposed to the discrete output of a digital device. Four basic types of transducers were used; strain gages, load cells, Linear Variable Differential Transformers (LVDT), and Rotational Variable Differential Transformers (RVDT). Each will be discussed separately.

Strain gages. The strain gages used in this research were of the electrical resistance type. These gages function by changing their electrical resistance in response to the strain of the object they are bonded to. The change in resistance of these gages is linear within the elastic limits of the gage. By applying a known constant electrical current through the gage, the resulting voltage across the terminals varies directly with the change of resistance, or strain. This voltage, when corrected using the appropriate gage factor, is the analog of the induced strain. These gages are frequently used as transducers in the static and dynamic measurement of load, torque, pressure, and acceleration. In this application, strain gages were applied to the interior of the model piles to measure the force required to insert the pile, the development of residual stresses in the pile during placement, and response of the pile to static loading.

The principles of operation of electrical resistance gages were discovered in 1856 by Lord Kelvin. He made three significant

discoveries by simply measuring the resistance of iron and copper wires subjected to various tensile forces. First, the resistance of the wires changed in response to the strain. Secondly, the different materials had different sensitivities to strain. Thirdly, a wheatstone bridge could be used to accurately measure the changes in resistance (voltage) accurately. Each of these aspects of strain measurement by electrical resistance methods will be discussed.

The resistivity of a given material is dependent on the degree of cold working of the conductor during formation, the range of strain over which the measurement of resistivity is made, the purity of the alloy being tested, and temperature. The resistance of a specific piece of material is then determined by multiplying the resistivity of the material by the length and dividing by the minimum cross-sectional area through which current will have to pass. The resistance (R) of a uniform conductor is expressed as follows:

$$R = \rho \frac{L}{A} \quad \text{Eq. 4-10}$$

where

L = length

A = area

ρ = resistivity

Differentiating the above equation and dividing by the resistance gives

$$\frac{dR}{R} = \frac{d\rho}{\rho} + \frac{dL}{L} - \frac{dA}{A} \quad \text{Eq. 4-11}$$

The term dA represents the change in the cross-sectional area of the conductor resulting from the longitudinal strain. This change is a function of the Poisson's Ratio (ν) of the material and is denoted as shown below.

$$dA = -2\nu \frac{dL}{L} A \quad \text{Eq. 4-12}$$

A tensile strain produces a decrease in cross-sectional area and a proportionate increase in resistance. The reverse is true of compressive strains. This relationship is valid for all materials commonly used in electrical resistive gages today. It also highlights the dependence of resistance on the geometric properties of the material being used as a gage filament, Lord Kelvin's first finding.

Continuing the refinement of the initial relationship between the resistance of a uniform conductor and its resistivity, one can determine the sensitivity of the strain gage filament with respect to the metallic alloy used as a conductor. Denoting the original diameter of the conductor as d_0 , the diameter after the application of some axial strain is shown below.

$$d_f = d_0 \left(1 - \nu \frac{dL}{L}\right) \quad \text{Eq. 4-13}$$

It can be shown (Dally and Reilly, 1984) that

$$\frac{dA}{A} = -2\nu \frac{dL}{L} + \nu^2 \left(\frac{dL}{L}\right)^2 \cong -2\nu \left(\frac{dL}{L}\right) \quad \text{Eq. 4-14}$$

Substituting Equation 4-14 into 4-11,

$$\frac{dR}{R} = \frac{d\rho}{\rho} + \frac{dL}{L} (1 + 2\nu) \quad \text{Eq. 4-15}$$

Rewriting the above, it can also be shown (Dally and Reilly, 1984) that

$$S_a = \frac{\Delta R/R}{\epsilon} = 1 - 2\nu + \frac{d\rho/\rho}{\epsilon} \quad \text{Eq. 4-16}$$

The sensitivity (S_a) of the metallic alloy used in the conductor is defined as the change in resistance per unit of initial resistance divided by the applied strain as shown above.

This relationship is used in the determination of the gage factor (F) as shown in Equation 4-17. The change in resistance of gage is related to the strain in Equation 4-17 as opposed to the change in the resistivity of the gage foil material as shown in Equation 4-16.

$$F = \frac{\Delta R_g/R_g}{\epsilon} \quad \text{Eq. 4-17}$$

The gage factor is directly dependent on two material properties; the change in the cross-sectional area of the conductor ($1 + 2\nu$), and the change in the resistivity of the alloy ($d\rho/\rho$)/ ϵ . In pure metals, sensitivity can range from -12.1 (nickel) to 6.1 (platinum). However, most metallic alloys used in the manufacture of electrical resistive gages have sensitivities between 2 and 4. Since the geometric factor varies between 1.4 and 1.7 for most metals, it is implied the resistivity and thus, the gage factor, can change dramatically over the range of strain for a specific measurement unless the gage foil material is selected properly.

The gages used in this research were formed of the metallic alloy Constantan, with a sensitivity of 2.1. This material is used quite commonly in resistance gages for several reasons.

1. The value of strain sensitivity is linear over a wide range of strain.

2. The value of sensitivity remains constant if the material goes plastic during testing.
3. The specific resistance of Constantan is relatively high.
4. The alloy exhibits high thermal stability.
5. The remaining small temperature induced changes in resistance of the alloy can be virtually eliminated by heat treatment or introduction of trace impurities into the alloy.

The linearity of the sensitivity implies the gage calibration constant will not change with strain level. The wide range of the linear region shows the alloy can be used in gages measuring both elastic and plastic strains in most common construction materials. The high specific resistance is important as small gages can be constructed with relatively high resistance. This permits the measurement of strain over small lengths of the material being tested. Finally, the ability to eliminate the temperature induced changes in resistance of the alloy permits the fabrication of temperature compensating gages for each material being tested.

Metal foil strain gages are manufactured almost exclusively today rather than relying on the bonded wire gages introduced in the mid-1930's. The foil method is advantageous as the grid is formed by a photoetching process. The grid is drawn in the proper configuration and then photographically reduced before photoetching on the appropriate alloy. This provides infinite flexibility in the gage configuration. More importantly, it permits the manufacture of very small gages with the shortest gage length available being less than 0.008 in. (0.20 mm).

The fragility of the etched metal alloy grid requires that it be bonded to a base material, or carrier, to aid in application of the gage. In most instances, the foil is first bonded to the carrier and then photoetched. The carrier is then bonded to the material being tested serving the additional purpose of insulating the alloy grid from the specimen. The carrier material is very stiff to ensure the transfer of strain from the specimen to the grid.

A resistance circuit element is presented diagrammatically in Figure 4-49. This type of circuit element produces a voltage across the element directly proportional to the current passing through it. Quantitatively, the voltage equals the resistance of the element times the current passing through. This relationship is known as Ohm's Law.

$$V = Ri \quad \text{or} \quad R = \frac{V}{i} \quad \text{Eq. 4-13}$$

It should be apparent that changing the resistance of the device results in a voltage output which varies in direct relation to the current. Gages used in this research had a nominal resistance of 120 ohms. This value of resistance is required to permit the gage to exhibit a measurable change in voltage output for a given strain. The voltage output is measured using a Wheatstone bridge configuration which will now be presented.

The change in resistance of a strain gage subjected to loading is commonly measured using the Wheatstone bridge depicted in Figure 4-50. This configuration is known as a "full bridge" if all of the resistors are subject to variation. More commonly, three of the resistors are kept constant and only the remaining resistor is permitted to vary.

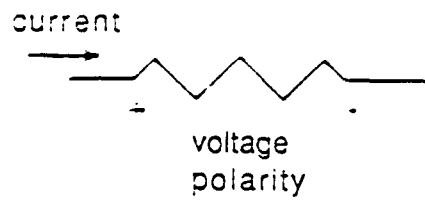


Figure 4-49 Resistance Circuit Element

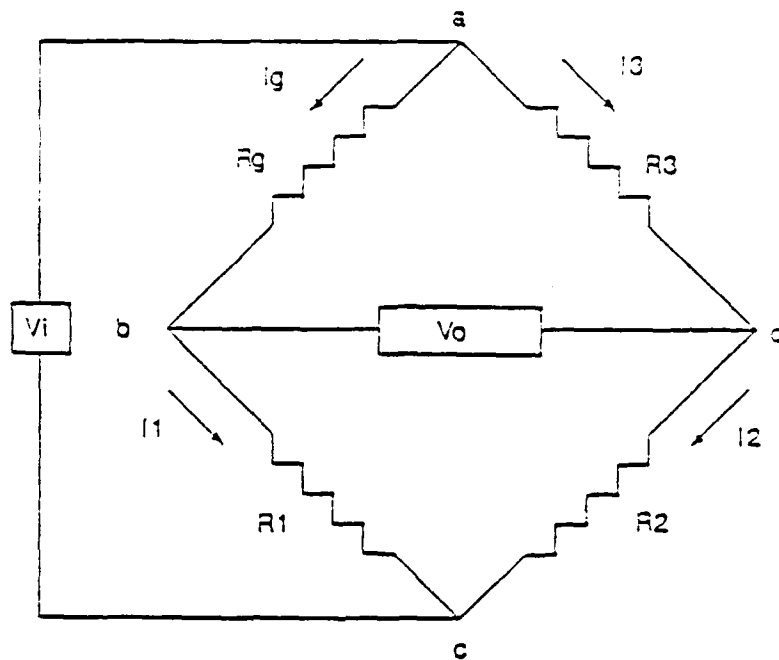


Figure 4-50 Wheatstone Bridge Circuit

This configuration is denoted as "quarter bridge" and the variable resistor is the strain gage. The "balanced bridge" method of strain calculation will be presented. This method is useful in the measurement of strains induced by static loading as was done in this research. The bridge is powered by an input voltage supply, denoted v_i . The bridge is balanced when the voltage drop across a-b is the same as across a-d. In this instance the output voltage, v_o , equals zero. Assuming R_1 , R_2 , and R_3 are equal, the voltage drop across b-c equals the drop across d-c. Stated in terms of the current through the four arms of the bridge;

$$R_g I_g = R_3 I_3 \quad \text{and} \quad R_1 I_1 = R_2 I_2 \quad \text{Eq. 4-19}$$

In the balanced condition,

$$I_1 = I_g \quad \text{and} \quad I_3 = I_2 \quad \text{Eq. 4-20}$$

Therefore,

$$R_g I_1 = R_3 I_2 \quad \text{Eq. 4-21}$$

and

$$\frac{R_g}{R_1} = \frac{R_3}{R_2} \quad \text{Eq. 4-22}$$

Continuing the development of the balanced bridge method of strain measurement, the full bridge must be balanced in the unloaded condition. This is accomplished by replacing R_1 with a variable resistor and adjusting it until V_o equals zero. After loading, the bridge is again balanced by adjusting R_1 . The difference between the two values of R_1 is used in the calculation of strain as follows.

$$\Delta R_1 = R_1(\text{loaded}) - R_1(\text{unloaded}) \quad \text{Eq. 4-23}$$

Using Equation 4-22,

$$\Delta R_g = (R_3/R_2) R_1 \quad \text{Eq. 4-24}$$

Since R_3/R_2 is a constant, the value of R_g is directly proportional to R_1 . Substituting ΔR_g into Equation 4-18,

$$\epsilon = \frac{R_3}{R_2 R F} \Delta R_1 \quad \text{Eq. 4-25}$$

Equation 4-25 is used to determine strain in balanced bridge circuits where there is sufficient time to adjust the strain indicator device to obtain a reading. This research required eight channels be read at frequent intervals during the penetration and loading of the pile. Penetration occurs too rapidly for the bridge to be rebalanced and the manual balancing of the bridges introduces a potential for error. The 'unbalanced bridge' method of calibration is presented as an alternative in the determination of pile strain.

Tabatabai (1987) and Williams and McFetridge (1983) develop the equations which provide strain measurement based on the output voltages of an unbalanced wheatstone bridge circuit. Again, ΔV_o is the change in the bridge output between the initial and strained conditions.

$$\epsilon = - \frac{4 \Delta V_o}{F(V_i + 2\Delta V_o)} \quad \text{Eq. 4-26}$$

Supply voltage, V_i , and gage factor, F , must remain constant throughout the measurement period. The relationship between strain, e , and ΔV_o is nonlinear, however, for gage factors close to two, the deviation from linear is less than 1.0% for strains less than 10,000 micro in./in. (Dove and Adams, 1964). This permits a linear approximation of Equation 4-26 as shown below.

$$e = - \frac{\Delta V_o}{F V_i} \quad \text{Eq. 4-27}$$

Strain can thus be determined by measuring the change in voltage output of the wheatstone bridge circuit from the known initial conditions. Figure 4-51 depicts how an active strain gage is typically wired into the wheatstone bridge circuit.

Three equal-length leads are needed to connect the gage to the wheatstone bridge. This is because of the relatively long distance which separates the active gage from the rest of the bridge. If the leads connecting the gage to the bridge were the only long leads, then resistance changes in the wires, due to temperature, stretching, etc., would be interpreted as strain by the strain indicator. By using equal length leads in adjacent arms of the bridge, the change in resistance of the individual leads due to the aforementioned causes is the same. Equal resistance changes in adjacent arms make equal and opposite contributions to the bridge output. Thus, the effects of temperature and strain in the lead wires cancel themselves (Dove and Adams, 1964).

Recording strain gage response from a process which occurs in the centrifuge implies the need for slip rings to pass signals from the payload to external equipment unless both the bridge completion circuit

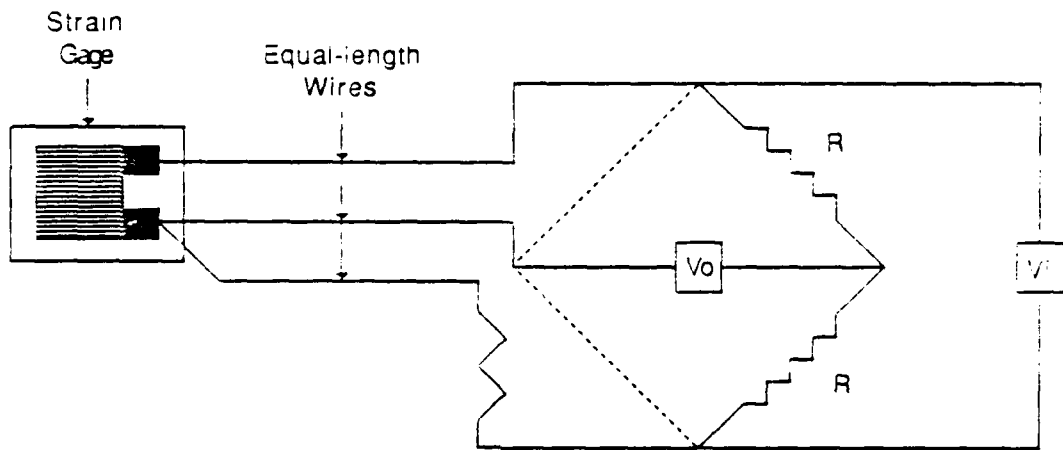


Figure 4-51 Three-Wire Circuit for Strain Measurements

and voltage measuring/recording devices are mounted on-board. Mounting the voltage measuring/recording devices on board was impossible due to the limited size of the available centrifuge. Therefore, slip rings had to be used at some point in the circuit. The change in resistance of the slip rings can be interpreted as significant strain if the slip rings are introduced between the active gage and bridge completion circuit (Tabatabai, 1987). Instead, the slip rings should be introduced between the bridge completion circuit and voltage measuring/recording devices. This implies the bridge completion unit be mounted on-board the centrifuge with the output from the individual channels being passed through the slip rings. Amplifying the output signal prior to passage through the slip rings provides a satisfactory signal-to-noise ratio depending on the gain of the amplifier.

Figure 4-52 depicts the on-board signal conditioning and amplification circuitry developed for use in the blast loading research of Tabatabai (1987). This device was designed to provide linear response at high frequency and was well suited for the static strain readings being made in this research. The INA 101 amplifiers used in each channel had a gain of 100. Modifying Equation 4-27 to include the gain of the device results in the following equation which was used to convert all voltage changes to strain.

$$\epsilon = - \frac{4 \Delta V_{oa}}{F V_i g} \quad \text{Eq. 4-28}$$

where

V_{oa} = amplified bridge output voltage

g = amplifier gain

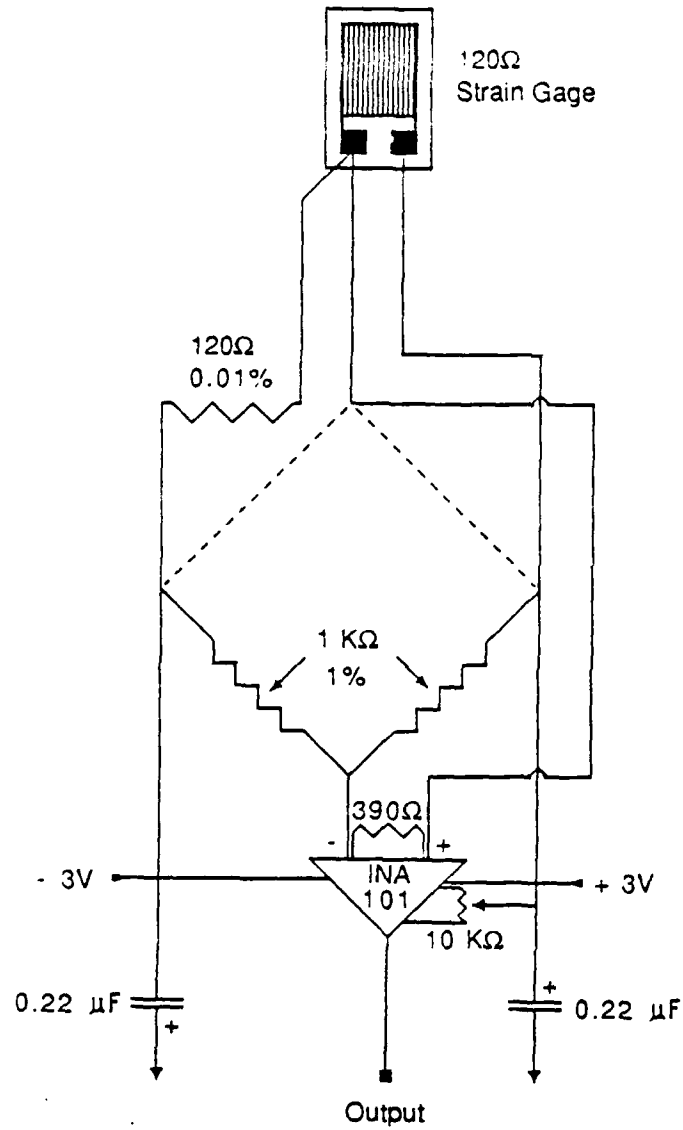


Figure 4-52 On-Board Bridge Completion Circuit for Strain Gages
(8 Channels Available)

For the conditions under which all measurements were made, $F = 2.05$, $V_i = 6.0$ volts, and $g = 100$, the following calibration factor is determined.

$$e = - \frac{1 \text{ (1 volt)}}{2.05 (6) 100} = -0.25 \times 10^{-3} \frac{\text{strain}}{\text{volt}}$$

or 3.25 microstrain per millivolt of amplifier output

The device built for Tabatabai was bench checked and mounted in the centrifuge close to the center of rotation to reduce unwanted centrifugal accelerations on the electronic components. The lead wires connecting the device to the active gages were approximately 5.0 ft long and shielded reducing the potential for noise pickup. Figure 4-53 shows the on-board bridge completion unit and slip ring channel assignments.

Load cells. The term load cell refers to a load measuring device which incorporates strain gages mounted on a protected coupon or within a suitable load carrying member. Load cells usually contain the necessary bridge completion circuitry and provide calibrated output.

Load is transmitted through the load cell by a tubular compressive/tensile member. Strain gages mounted on the member strain as the member is subjected to load. Both longitudinal (active) and transverse (dummy) gages are mounted on the member. The longitudinal gages provide the measurement of load and the dummy gages are applied to compensate for temperature or other environmental effects which could be misinterpreted as applied load.

The magnitude of the applied load can be determined when the Young's modulus and cross-sectional area of the load carrying member is known. The Young's modulus is defined as stress divided by strain.

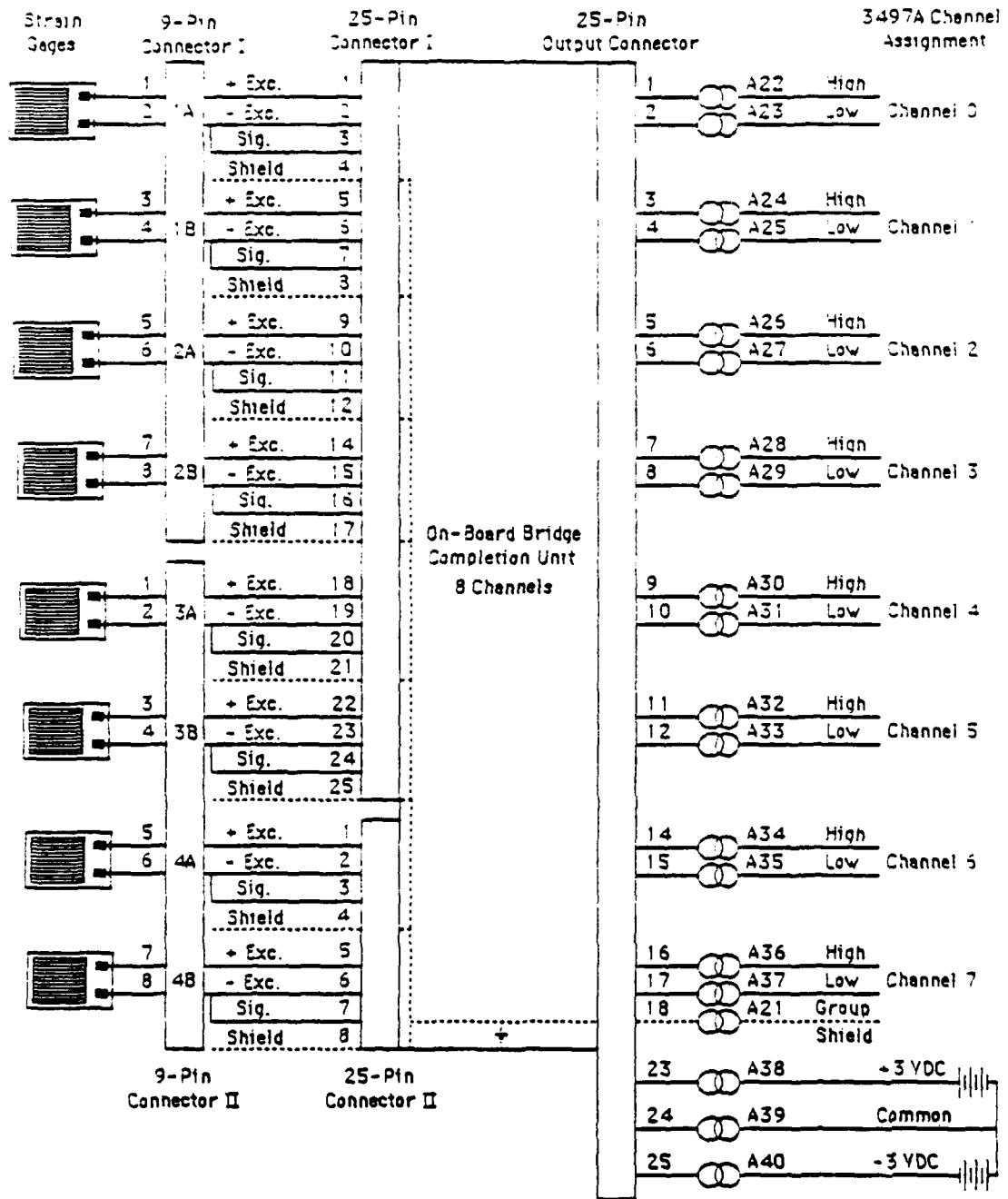


Figure 4-53 On-Board Bridge Completion Unit and Slip Ring Channel Assignments

Stainless steel, the material of preference for the member, has a young's modulus of 30,000,000 lb/in.². In terms of strain, stress then equals 30,000,000 lb/in.² times the strain of the member. That stress, times the cross-sectional area of the member is equal to the total applied load. Manufacturers do not usually supply this information with the load cell. Rather, a calibration is provided in terms of millivolt output versus voltage input as explained in Section 4.2.9, Load Cells.

Linear variable differential transformers (LVDTs). As implied by the name, this transducer provides a variable voltage output in response to some linear displacement. An LVDT with a range of ± 1.0 in. was used to measure the displacement of the ball screw in response to the commanded rotation of the stepper motor. LVDT's are generally flexible in design with operating ranges of from one millionth of an inch to over 30 in. This device consists of a central primary winding flanked by two secondary windings (Figure 4-54). The windings surround a hollow core which houses a moveable magnetic piece, or armature. The secondary windings are manufactured so that they are balanced and the current induced in them by the armature is equal and opposite when the armature is exactly in the middle of the device. Displacement of the armature to either side results in a measurable imbalance in the secondary windings output which is proportional to the displacement. Detection of this output voltage requires the secondary coils be connected to form an AC bridge (refer to the above passage concerning Strain Gages). Movement of the armature through the center position results in the output signal changing sign. The exact displacement is then found by knowing the magnitude and sign of the output voltage.

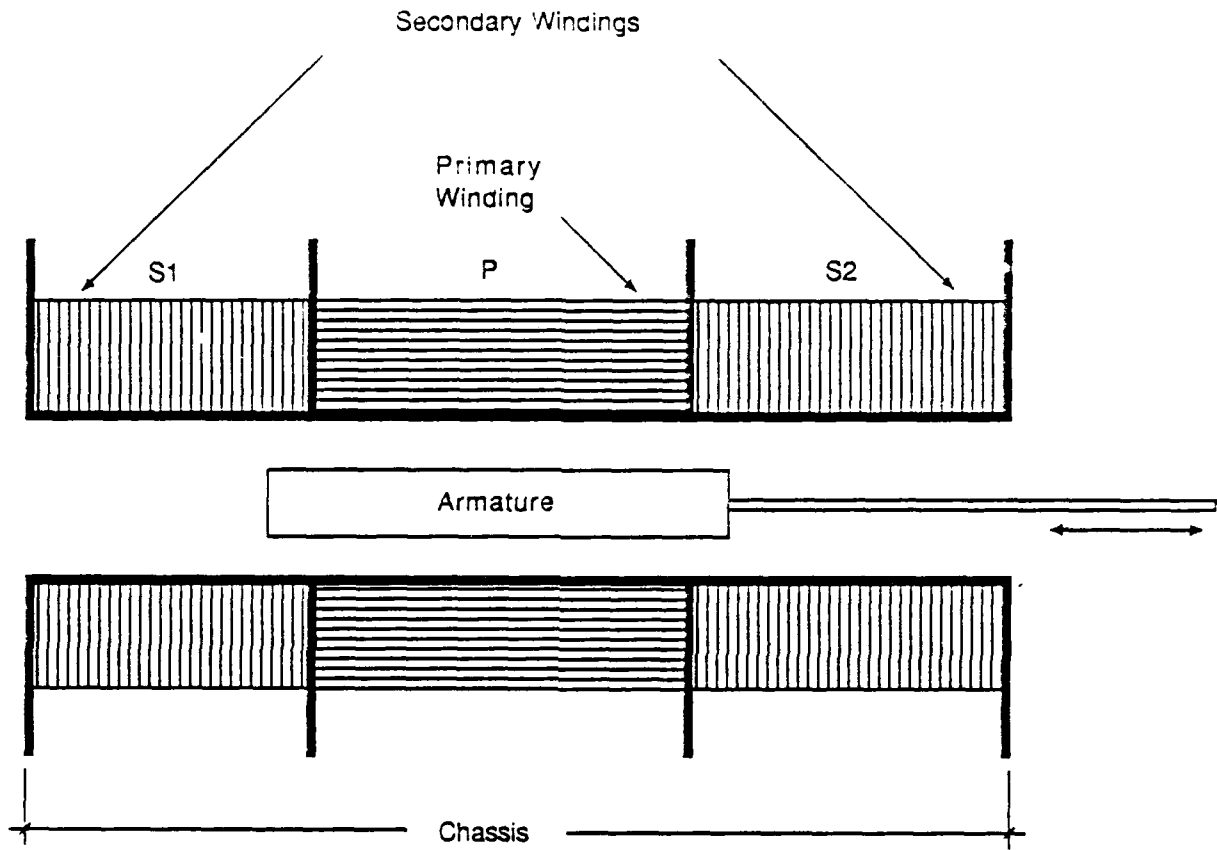


Figure 4-54 Cross Section of a Linear Voltage Differential Transformer (LVDT)

In early devices, the primary winding was excited by an alternating current (ac) generally of 1,000 to 10,000 Hz. The output from these devices was an ac signal with the same frequency as the excitation voltage, or carrier. However, dc-to-dc versions have been developed which have internal oscillators and filtering circuits to improve output voltage characteristics. Direct current power supplies can be used with these devices and the dc output signal is the analog of the armature movement. The LVDT used in this application was of the dc-to-dc type. Figure 4-55 depicts the circuit which powered the LVDT and the output signal leads.

The accuracy of the output signal depends on the stability of the power supply as the output is directly proportional to the primary winding excitation voltage. The input voltage was considered to be constant during the short period of time over which readings were taken. Use of this device, or other dc-to-dc transducers for a long period of time would require frequent monitoring of the excitation voltage or measurement of the voltage prior to each reading.

An LVDT was mounted on top of the ball screw to measure displacement of the shaft versus the commanded rotation of the stepper motor. Results of those tests are presented in Section 4.7, Equipment Limitations.

Rotational variable differential transducers (RVDTs). An RVDT precisely measures rotational displacement using the same principal of operation as an LVDT. The significant difference between the two is that the armature in the RVDT rotates within the hollow core of the wound coils as opposed to being displaced linearly. Although the

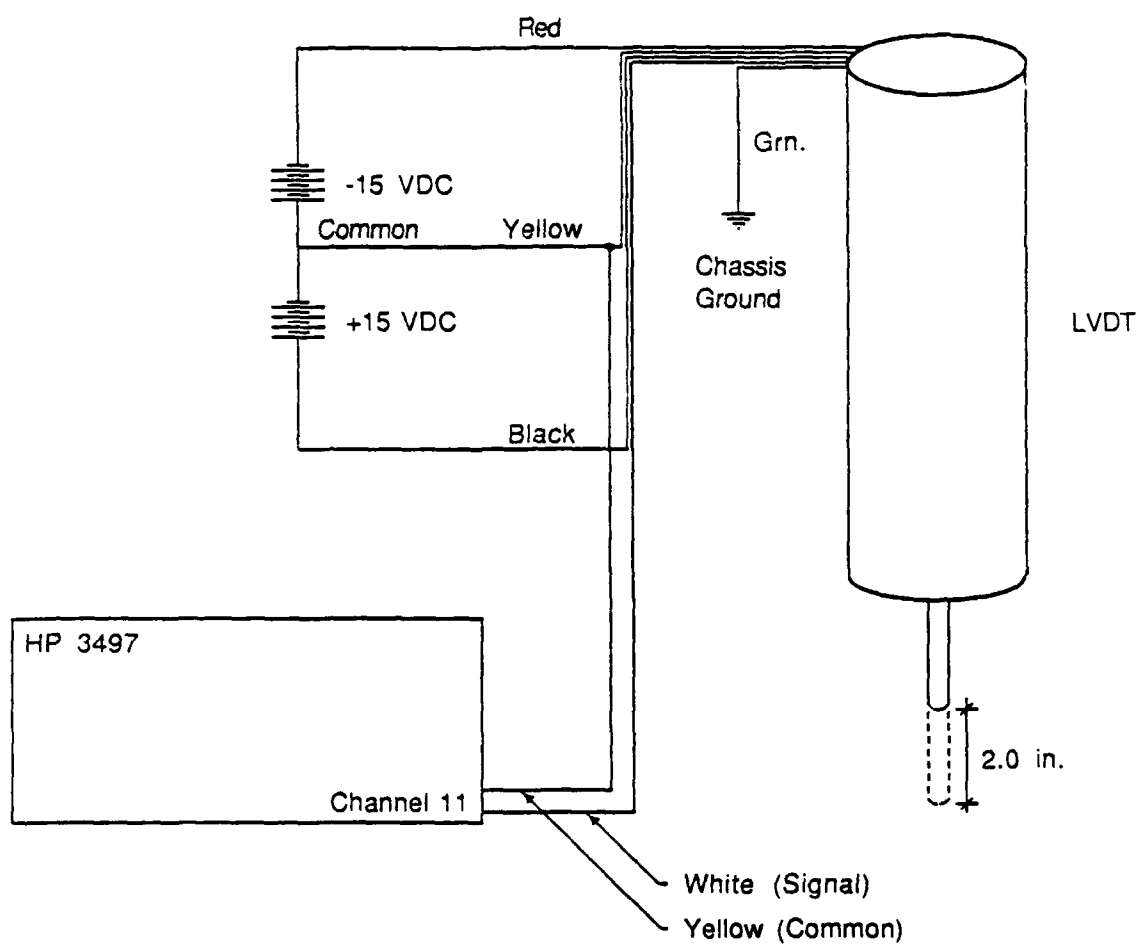


Figure 4-55 LVDT Power Supply Circuit and Signal Output

armature is free to rotate within the RVDT housing, RVDT's cannot be manufactured to provide a unique voltage output for a complete revolution. Rather, they are designed to provide a highly accurate, linear response over a predetermined degree of rotation. The RVDT used in this application provided a linear response up to ± 30 degrees from its center point. It was used in preliminary tests to determine the degree of precision with which the stepper motor could perform its commanded rotations. The RVDT was mounted directly to the drive shaft of the stepper motor and tested as described in Section 4.7, Equipment Limitations.

4.6.2 Software

The software required for data measurement was minimal. All readings were made using the 3497 Data Acquisition/Control Unit. The unit had to be cleared of all previous readings prior to new readings being taken. The measurement of transducer output was then accomplished by the computer commanding the 3497 to output the value from the appropriate channel(s).

The 3497 is cleared by the command CLEAR 709. The number 709 is the address of the data acquisition unit. The subsequent command dictates the channel(s) which are to be read. When more than one channel is read, the requested information is transmitted from the 3497 to the computer as a string variable instead of individual readings. This speeds up the data transmission when a significant number of channels must be read quickly. Refer to Gill and Kofoed, 1988.

4.7 Equipment Limitations

The placement device designed for and used in this research was made to drive and push piles which modeled the Hunter's Point Pile Group

at test g-levels between 59 and 66 g's. However, it was designed to provide the user a great deal of versatility and is capable of placing a wide variety of model piles without modifying the device. This section presents the limitations of the centrifuge and placement device in general terms and also in specific terms where use of the equipment beyond those limits would cause damage to or destruction of the device. The limitations imposed by the centrifuge will be discussed first followed by a discussion of the limitations of the placement device.

The centrifuge is limited to a rotational speed of 250 rpm. Rotation of the arms at this speed results in the tops of the platforms (radius equals 63.5 in.) being subjected to approximately 115 g's. Assuming a soil specimen of 6.0-in. height (average radius equals 60.5 in.), the specimen is subjected to an average g-level of approximately 110 g's. The weight of the payload on one arm is then governed by the maximum static capacity of the platform and arms and the factor of safety the user is comfortable with. Figure 4-56 shows the maximum payload weight based on the limiting strength of the pillow block bearings. Also shown are the payload weight and rotational speed combinations used in this research. The weight of the platform and support pins (26 lbs) has already been included in the computations. Weights shown are for payload only.

The eight channel on-board bridge completion unit restricts the number of strain gages which can be mounted on an individual model (group). Fifty-six of the available eighty electric slip ring channels were used. The twenty four remaining channels could provide the capability of reading an additional twelve strain gages if the appropriate

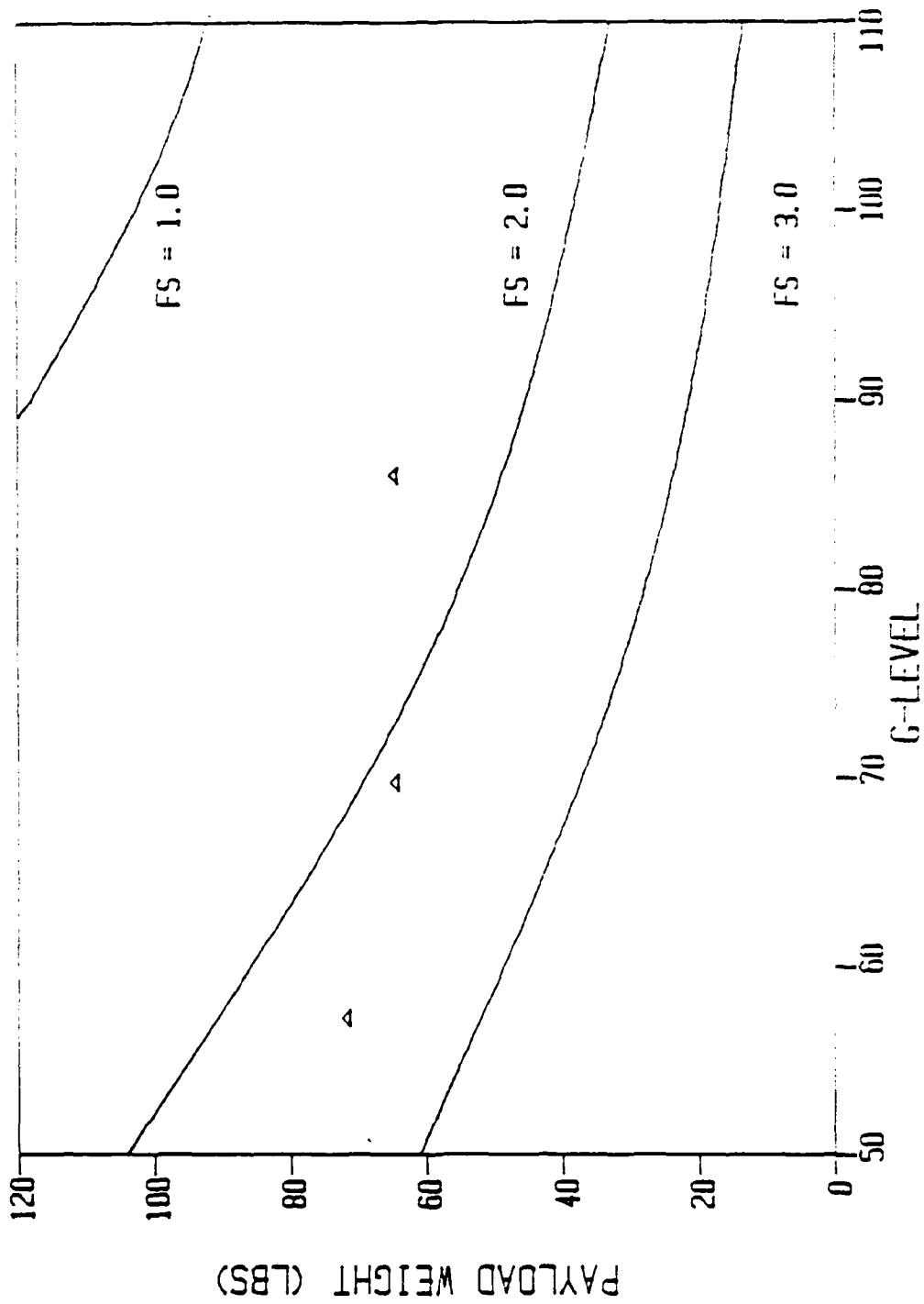


Figure 4-56 Maximum Payload Operating Capacities vs. RPM

on-board bridge completion unit were constructed. Increasing the number of strain gage circuits available for use on the models represents the most efficient use of the remaining channels.

The most significant concerns about the equipment designed for this research arise from the misuse of the placement device. There are not many safeties built in to protect the user from damaging the device through misunderstanding or unintentional error in the initialization of the pile placement programs. The device was designed to place piles which were 35.0 scale feet long and driven or pushed to a scale depth of 30.0 ft at g-levels above 69.8 g's. Consider the placement of a model pile at 69.8 g's as this is the worst case scenario with the least clearance between payload and centrifuge top. If the pile is driven, there is approximately 0.5 in. clearance between the top of the ball screw and centrifuge roof at the start of the test. This is adequate clearance to permit the centrifuge to start safely. Problems can arise during the early portion of the driving sequence in which the ball screw (and electromagnet and hammer) must be raised to the specified lift height. Should the stepper motor or multiprogrammer devices fail with the ball screw in the raised position there will no longer be adequate clearance between the top of the ball screw and the centrifuge roof when the centrifuge is spun down. Decelerating the centrifuge with the ball screw in the raised position will cause severe damage to the placement device. The only option in this situation is to continue rotating the centrifuge arms at some minimum speed to maintain clearance until the stepper motor or its support devices can be repaired. If the failure is a result of programming failure or computer malfunction, it might still

be possible to turn the stepper motor over to manual control and push the ball screw downward far enough to achieve the necessary clearance. The centrifuge could then be safely spun down.

Significant damage could also be caused to the placement device if there is insufficient clearance between the top of the electromagnet and bottom of the c-channel support to permit the electromagnet and hammer to be raised the desired amount. The stepper motor will complete its commanded rotation even after the electromagnet has been pulled up far enough to contact the c-channel. This will most likely result in the soft brass teeth of the driving or driven gear (or both) being shorn off. The available clearance must be determined by the user prior to conduct of any model driving to ensure the electromagnet can be raised the necessary amount. Remember, the program determines the hammer lift height based on the g-level at the midheight of the hammer and not the nominal test g-level. DRIVEPILE displays the initial lift height. This value should be compared with the distance between the electromagnet and c-channel measured during specimen setup. Obviously, the program should be continued only if there is sufficient clearance for the proposed lift height. If there is insufficient clearance, the hammer should be replaced by a heavier hammer thereby decreasing the required lift height, or the pile should be inserted some distance which would provide the necessary clearance.

The pushing process can culminate in the separation of the ball screw from the ball nut if the proper consideration is not given to the length (height) of the pile cap and load cell. The ball screw is not long enough to reach the top of the soil with the screw still properly

housed within the nut. Thus, at some point, the screw will fall out of the nut if the nut is rotated far enough. Even if the nut is not rotated far enough to permit separation, ball bearings will be dislodged from their race if the top of the screw sinks below the top of the nut. This can result in damage to the device when the screw (and load cell) is lifted back off of the model as the ball bearings can be lodged between the screw and nut. The model cap and load cell must be long enough to ensure the top of the screw will remain above the top of the nut after final penetration has been achieved. Figure 4-1 shows how the pile caps were constructed for initial push tests bearing in mind the need to keep the screw high enough from the soil surface after final penetration to prevent dislodging the ball bearings in the ball screw. This is not a concern in the driving tests as the electromagnet, hammer, and cap assembly are sufficiently long to preclude the ball screw from being lowered too far.

The size of the model pile is limited only by the depth of the specimen container and the desired clearance between the pile tip and container base after penetration. The specimen container was designed to provide 10 scale feet of clearance between the pile tip and specimen container base after placement of a scale 35-foot pile was complete at the 69g test level. Subsequent tests of this prototype at higher g levels are possible using this container as the model becomes smaller and the clearance between tip and base larger. In general, the size of the modeled prototype must become smaller as the test scale decreases if this container is used. The suitability of the container and centrifuge being used for a specific test is the decision of the user.

A second specimen container was manufactured and provided sufficient depth to test the chosen prototype at no less than 57 g's, assuming the 10 scale feet of tip clearance was still required. Being taller than the first container, the canister rested higher above the platform, and the extended ball screw higher still. This resulted in insufficient clearance for the payload between the platform base and centrifuge roof. Two alternatives are available. The user can either insert the pile far enough that the ball screw has sufficient clearance or tilt the specimen container far enough to ensure the ball screw top will clear the roof support beams during initial spin up. If the pile is inserted prior to flight, the potential for developing skin friction is reduced along the portion of the shaft which has been inserted. This alters the total capacity, unit skin friction determination, and distribution of residual stress. In general, it makes the verification of modeling of models more difficult. If the specimen container is tilted prior to spin up, as can be done with mechanical stops similar to those which prevent over rotation, the soil character may be altered by the vibration experienced during spin up. The specimen may have to be tilted as much as 25 degrees depending on the size of the prototype and depth of model insertion. This degree of tilt approaches the angle of repose of the sand creating a significant potential for the soil to shift if vibrated. If it is necessary to test models of the chosen prototype in this (tilted) configuration, the harmonic response of the arms should be altered to reduce vibrations during spin up.

Within reason, the diameter of the model pile is not restricted by the size of the specimen container. Assuming the minimum clearance between the pile and container wall is 10 diameters, the container must be at least 21 pile diameters across. Given the 8.0-in. diameter of the containers, the largest model pile tested is limited to 0.38 in. This model diameter represents prototypes of 19.0-, 26.6-, and 34.2-in. diameter at 50, 70, and 90 g's, respectively. The length of the model is again restricted by the depth of bottom clearance desired after penetration.

The scale lift capacity of the placement device is unlimited within the boundaries of the weights commonly in use. The electromagnet is capable of lifting 120 pounds. Halving this capability results in the electromagnet having a lift capacity of 75, 147, and 243 scale tons at 50, 70, and 90 g's, respectively. Thus, the placement device can be used to model any single-acting impact pile driver currently available. Rather, the size of weight used for driving is limited only by the dynamic stress capacity of the model.

The rate of penetration during the pushing process is controlled by the rotational speed of the stepper motor. This rate of rotation was fixed at 1.065 revolutions per second (213 pulses per second) by placement of a 50,000 ohm resistor across the R3 terminals of the stepper motor card. This rate of rotation results in 0.132 in. of ball screw translation (penetration) per second. The scale rate of model penetration was thus different for the different g-levels. At 69.8 g's, the model was pushed in at 9.214 in. per second. At 86.0 g's, the rate of penetration was 11.352 in. per second. This variation in the rate of

penetration may or may not affect the total capacity of and distribution of residual stresses in the models pushed into Reid-Bedford sand. However, the potential for altering the capacity and stress distribution of a model pile pushed into a cohesive soil with deformation-rate dependent response is significantly greater. This response can be investigated by the addition of a readily available variable resistance card to the multiprogrammer. Using this card in tandem with the stepper motor card permits the rate of rotation of the stepper to be varied during the course of a test. Thus, rate of penetration can be altered. Furthermore, having this capability lends itself to development of a model cone which can then be pushed into soils at scale speeds depending on the gravity level of the test.

The length of time required to complete one lift cycle of the hammer is controlled by the frequency of pulses output by the stepper motor controller card. Increasing the frequency of output pulses reduces the time needed to raise the magnet and hammer and lower the magnet in search of the hammer after impact. This was the limiting factor in the amount of time required to drive a pile after the hammer size had been determined. Driving time can be minimized by finding the optimum rate of rotation of the stepper motor. This is most readily accomplished by experimentation with a variable resistance card.

Two tests were conducted to verify the positioning capability of the stepper motor at test gravity levels. The first test proved the stepper motor drive shaft could be made to return to a predetermined starting position after commanded rotations in either direction in a high gravity environment. The second test proved the ball screw

displaced an equal and repeatable distance for each step of the stepper motor. An outline of the test procedures and full results are presented.

The first test involved mounting the stepper motor horizontally on the centrifuge platform and measuring the response of the stepper motor to commanded rotations at test g-levels between 20 and 90 g's. Response to the commands was monitored by a rotational variable differential transformer (RVDT) mounted directly to the driveshaft as shown in Figure 4-57. The stepper motor response was tested by commanding the drive shaft to rotate 16 steps (28.8 degrees) in each direction from a preset starting position prior to returning to the starting position. The motor shaft was first commanded to rotate 28.8 degrees clockwise, then 28.8 degrees counterclockwise, 28.8 more degrees counterclockwise, and finally 28.8 degrees clockwise to return to the starting position. The RVDT response was linear over ± 30 degrees. Results are provided in Table 4-5. All readings are in millivolts.

The stepper motor and RVDT were mounted at a radius of 61.0 in. One step changed the RVDT output by 0.24 millivolts. Subsequent rotation of the stepper motor drive shaft by one complete rotation (200 steps) in each direction at every test g-level showed the stepper motor was performing as commanded and precisely returning to the starting point.

The second test involved mounting a linear variable differential transformer (LVDT) to the top of the ball screw shaft after the placement device had been completed. The connections to the placement device

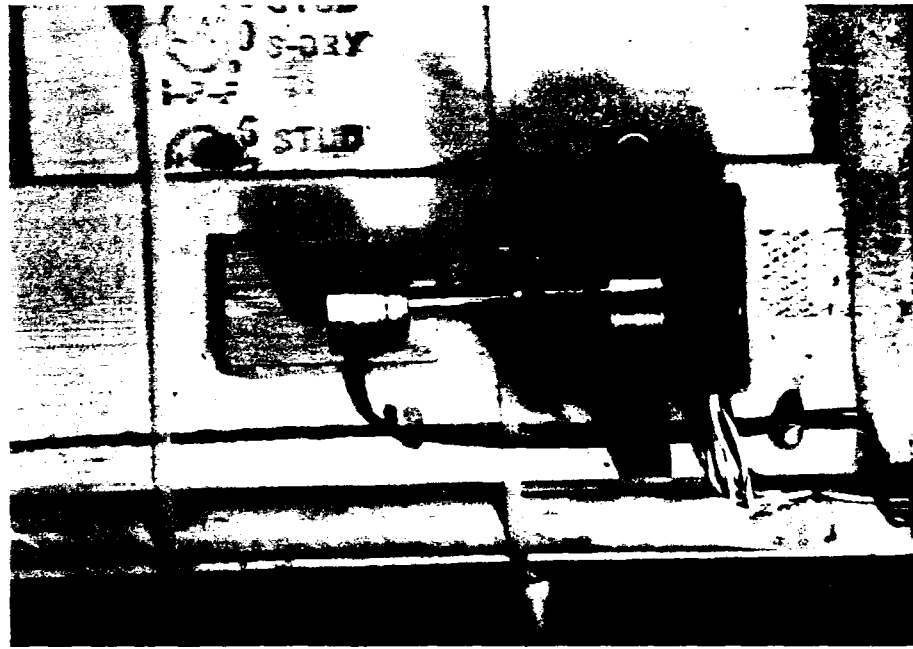


Figure 4-57 Stepper Motor and RVDT in Test Position

Table 4-5 Stepper Motor Response to Commanded Rotation at Test g-Levels

G-Level	RPM	Drive Shaft Position				
		0	+28.8°	0	-28.8°	0
20	107.6	0.00	+3.78	0.00	-3.80	0.00
30	131.8	0.00	+3.77	0.00	-3.80	0.00
40	152.2	0.00	+3.78	0.00	-3.80	0.00
50	170.1	0.00	+3.78	0.00	-3.80	0.00
60	186.3	0.00	+3.79	0.00	-3.80	0.00
70	201.3	0.00	+3.79	0.00	-3.80	0.00
80	214.4	0.00	+3.80	0.00	-3.81	0.00
90	225.8	0.00	+3.81	0.00	-3.81	0.00

NOTE: All readings are in millivolts

and LVDT were made through the slip rings as this was to be the configuration during testing. Figure 4-58 shows the LVDT in-place atop the placement device. The LVDT was adjusted to be in the middle of its 2.0-inch range of motion and the stepper motor was commanded to rotate 1600 steps counterclockwise, 3200 steps clockwise, and then 1600 steps counterclockwise returning to the starting position. All rotational displacements were conducted in 40 step increments. Figure 4-59 depicts the displacement of the ball screw for the commanded rotations of the stepper motor drive shaft. An additional test was conducted by commanding a rotation of 200 steps in both directions (-200, +400, -200) with readings being taken from the LVDT after each step. Results of that test are provided in Figure 4-60. Both tests demonstrate the ability of the ball screw displacement to be precisely controlled and the suitability of using the stepper motor-ball screw assembly as a position measuring device. Furthermore, both tests confirmed the ball screw displaced 0.0006217 in. for each commanded step.

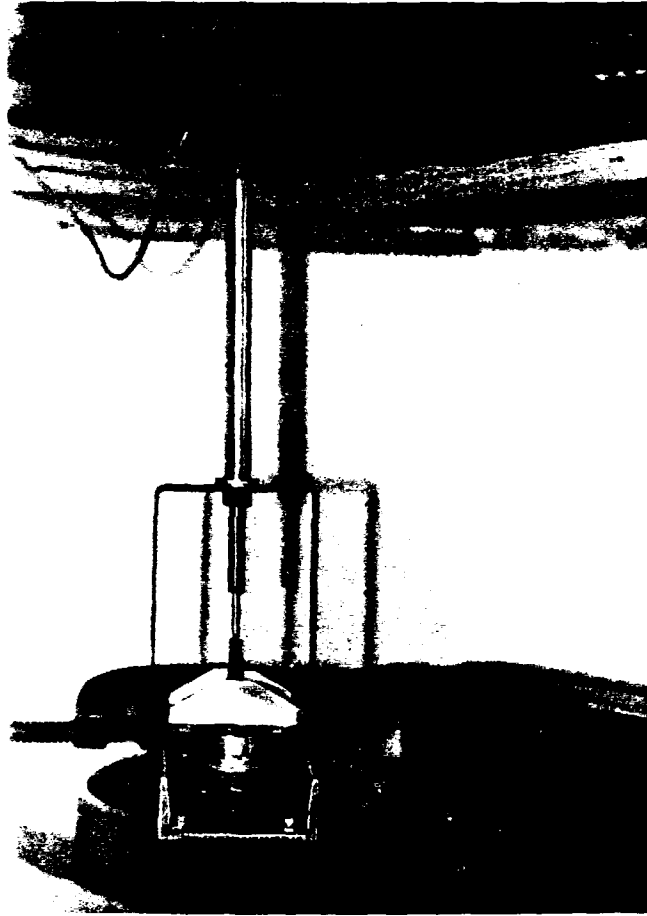


Figure 4-58 Placement Device and LVDT in Test Position

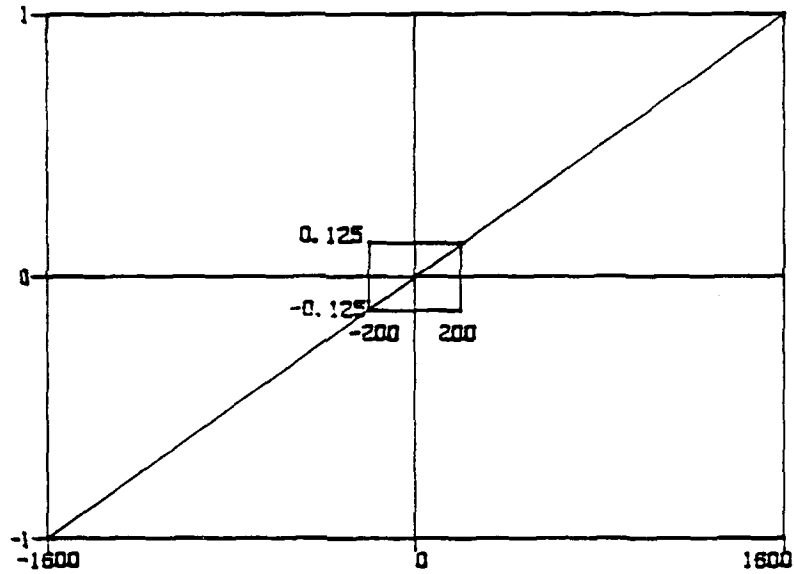


Figure 4-59 Ball Screw Response to Stepper Motor Drive Shaft Rotational Displacement (± 1600 Step Displacement, 40-Step Displacement Increment)

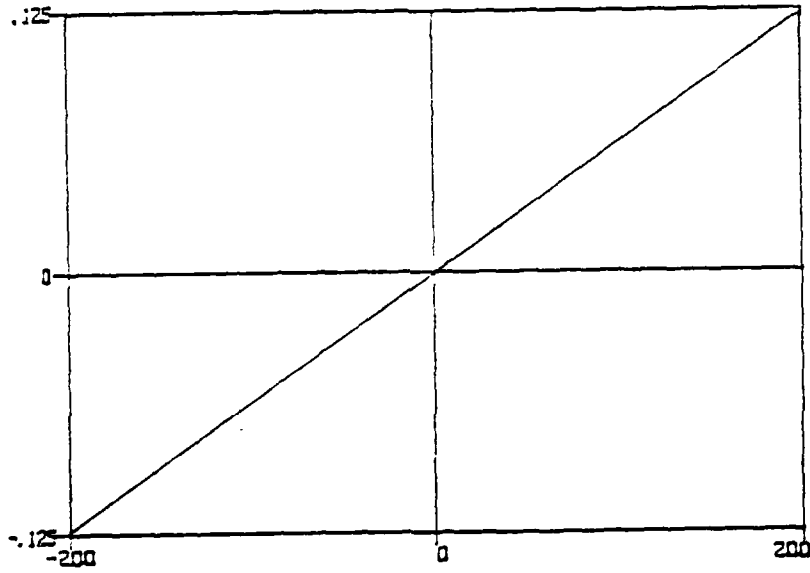


Figure 4-60 Ball Screw Response to Stepper Motor Drive Shaft Rotational Displacement (± 200 Step Displacement, 1-Step Displacement Increment)

CHAPTER 5
SPECIMEN PREPARATION, TEST RESULTS, AND DISCUSSION

This chapter presents the method used to prepare all specimens, results of all tests conducted on those specimens, and discussion of the results. Discussion is divided into qualitative and quantitative sections. Discussion of the results in a qualitative manner provides insight into the operation of the placement device and an understanding of its capabilities. The quantitative discussion presents the initial findings regarding scale capacities of the modeled piles. Section 5.2 presents the results of tests in which the models were pushed into the specimen. Results of individual pile and group tests are presented. Each plot of penetration versus load is followed by the associated load test plot. Load test results are analysed using the deBeer method of capacity determination and presented in the quantitative discussion section. This section also includes the results of tests in which the model piles were pulled from the soil in an attempt to separate skin friction forces from the tip end bearing capacity without the use of strain gages. Section 5.3 presents the results of the tests in which model piles were driven into the specimen. The inability of the bridge completion circuit and chosen strain gages to measure model strain is discussed at the end of this chapter (Section 5.7, Strain Measurement). Several causes are suggested.

All pushing and driving tests are designated by a 10 digit alphanumeric notation. The first letter is either a D or P corresponding to

the model pile (group) either being driven or pushed into the specimen. The second letter, always a G, indicates the models are scaled based on the geometry of the prototype. The following three digits designate the g-level at which the test was conducted, for example, 698 for 69.3 g's or 360 for 36.0 g's. The next two pair of digits denote the month (first pair) and day (second pair) on which the test was conducted. The last digit denotes the order in which tests were conducted on a specific day. The following test designation is provided as an example.

DG69803273--This model was geometrically scaled to represent the prototype and driven into the specimen. The test was conducted at 69.3 g's. It was the third test conducted on the 27th of March. The data sheet associated with the conduct of each test provides information regarding whether the test involved an individual pile or group. Furthermore, each data sheet includes notes regarding any unique aspects of the test. Load test plots are designated by the date and number of the test with the suffix LOAD. Thus, the load test for the example above is designated 03273LOAD.

5.1 Soil Description and Specimen Characterization

Reid Bedford sand was used exclusively in this test program because of its availability and well documented behavior. It has been used in several recent investigations involving centrifugal modeling at the University of Florida (Tabatabai, 1986, Gill, 1985) and many efforts pertaining to determination of its constitutive properties (Seereeram, 1983, 1986, Linton, 1986). Additionally, information is available from the

extensive research conducted with this sand at the Corps of Engineers Waterways Experiment Station in Vicksburg, Mississippi. The following soil description is a consolidation of the detailed presentations from the above-listed authors. More detailed descriptions can be found in Davidson et al. (1983) and Gupta (1983).

Color and type: light brown, clean, fine sand

Grain shape: subrounded to subangular.

Mineralogy: 89% quartz, 9% feldspar, 2% ferromagnesian and "heavies"

Specific Gravity: 2.66

All specimens were prepared by raining soil through a "chimney" as shown in Figure 5-1. The fall height was kept constant at 40.0 inches with the first 6.0 inches being taken up by four sieves. Variation in the overall density of the specimen was controlled by changing the number of stacked sieves and altering the size of the sieve openings. A spreader plate was placed in the top sieve for the preparation of all specimens to promote uniform raining through the cross section of the chimney. There were nine holes in the spreader plate (3 by 3 matrix pattern) which were 0.25 inches in diameter. Relatively loose specimens were created by allowing the sand to pour through the openings unobstructed. Denser specimens were obtained by placing tape over the openings partially obstructing the flow of the sand. Trial and error was necessary to create specimens with the desired dry unit weight. However, specimens can be created within ± 1.0 pcf once the tape obstructing the nine openings has been fixed in the desired position. Specimens with dry unit weights of 96.0 to 102.0 pcf (relative densities of 44.25% to 76.17%) were produced routinely without vibration or additional equipment. The

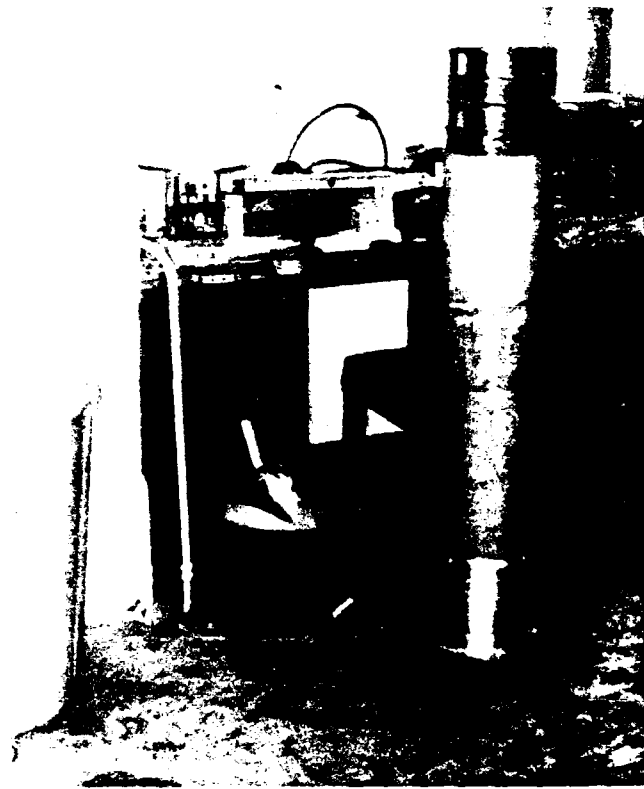


Figure 5-1 Specimen Preparation "Chimney" and Associated Tools

specimens appeared quite uniform with regard to depth based on the pushing and driving results which will be presented.

Two specimen containers were used in the conduct of this research. Both are shown in Figure 5-2. The dry unit weight and relative density of each specimen was determined based on the known volume and weight of the containers as follows.

The empty volume and weight of each container is shown below:

	Small Container	Large Container
Depth (in.)	6.9	9.7
Volume (cu. ft.)	0.199	0.279
Empty Weight (lbs.)	7.21	9.42

After raining the sand into the specimen container, the chimney was removed from the top of the container and the sand screeded off in multiple passes. A straightedge was used to level the sand surface. The excess sand was cleaned from the base of the container. The container and specimen were then weighed. Subtracting the weight of the container from the total weight provided the sand weight in the container. Dividing the specimen (sand only) weight by the cubic foot capacity of the container rendered the dry unit weight. This value was requested during the initialization of each program in which a pile (group) was placed. The computer then calculated the void ratio (e) and relative density (D_r).

The value for relative density was determined using the relationship provided in Perloff and Barron, 1976.

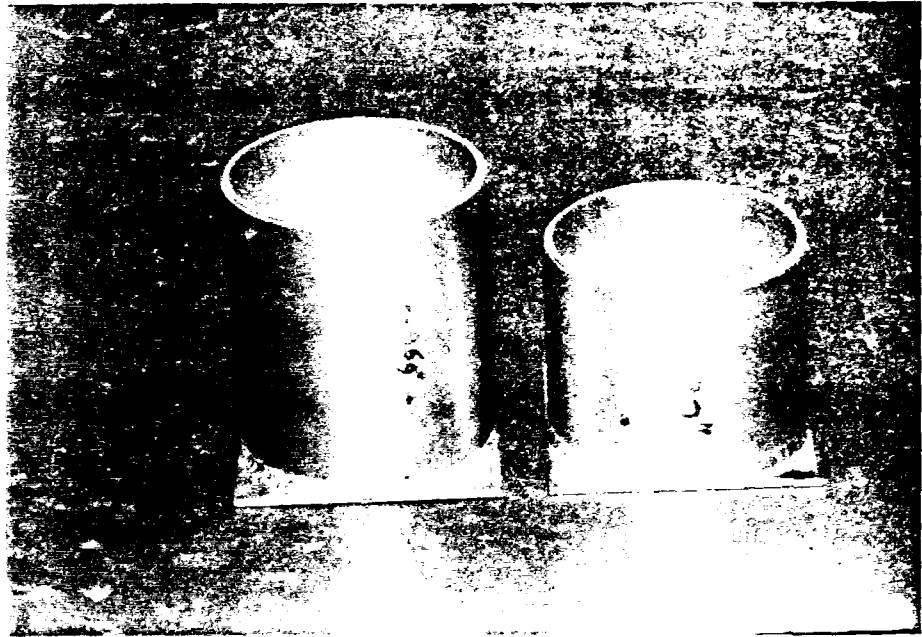


Figure 5-2 Specimen Containers

$$D_r = \frac{e_{\max} - e}{e_{\max} - e_{\min}} \quad \text{Eq. 5-1}$$

The values for e_{\max} and e_{\min} were taken from Seereeram, 1983.

$$e_{\max} = 0.871$$

$$e_{\min} = 0.550$$

Therefore, the relationship used to determine the relative density of the specimens was

$$D_r = \frac{0.871 - e}{0.321} \quad \text{Eq. 5-2}$$

5.2 PUSHPILE and PUSHGROUP Test Results

5.2.1 Qualitative Discussion of Pushed Model Pile Test Results

Several tests were performed with the intent of determining the operating characteristics of the placement device and a general understanding of the magnitude of output loads expected during model placement. The ability of the placement device to push piles from different initial insertion depths down to the desired depth of total penetration was verified. No load tests were conducted during this phase.

The following conclusions were drawn from the tests; the device can precisely record and reproduce the pile's resistance to penetration

versus depth when like tests are conducted on the same specimen and interrupting the flight of the centrifuge one or more times during insertion of the pile does not appear to adversely affect the ultimate resistance to penetration of the pile. The tests substantiating the above conclusions are now presented.

Tests PG69812072 and PG69812073 (Figure 5-3) demonstrate both the reproducibility of the load versus penetration curve for like tests in the same specimen and the insensitivity of the result to the interruption of the flight of the centrifuge during the pushing sequence. Both tests were performed on the same specimen. The piles were spaced at 10d. Test PG69812072 depicts the load versus penetration curve with the centrifuge being stopped every five scale feet of penetration after the first scale ten feet. The large reduction in load at ten scale feet is due to the stepper motor being turned off in conjunction with the stopping of the centrifuge. The stepper motor remained energized for the next three times the centrifuge was stopped. Each stop permitted the specimen to rest five minutes. There were no major discontinuities in the plot after the ten scale feet of penetration and it is concluded neither the specimen nor the load carrying capacity of the model pile is adversely affected by momentary pauses in the rotation of the centrifuge if penetration and loading are accomplished at the test g level.

Test PG69812073 was conducted to determine the load versus penetration response for a model pile pushed into the same specimen without interrupting the flight. The response duplicated that of PG69812072 indicating the pile soil interaction during penetration is modeled precisely by the placement device. These two tests are not conclusive

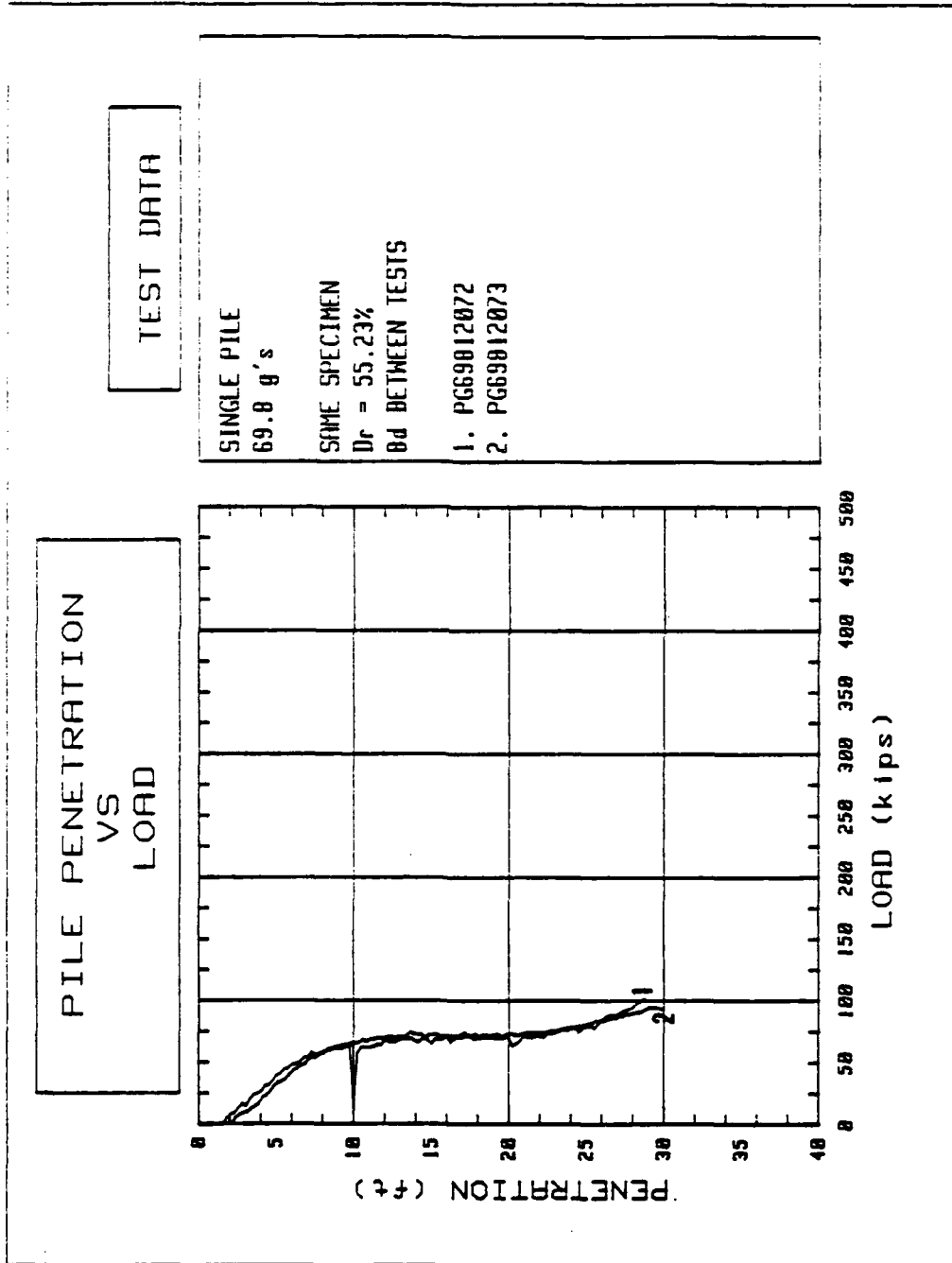


Figure 5-3 Pile Penetration vs. Load, Single Pile, PG698120/2, PG698120/3

by themselves. Rather, they are presented as two of many investigations conducted which displayed the same similarities.

Tests PG69812151 and PG69812154 (Figure 5-4) involve the buckling failure of a model pile (test 1) and reproduction of the test to help determine the cause (test 4). PG69812151 was conducted on a specimen with 73.42% relative density. The model buckled under a scale load of 350 kips after the pile had penetrated to 26 scale feet. The second test was conducted on a specimen with 73.92% relative density. The model buckled under a scale load of 350 kips after the pile had penetrated 25 scale feet. The response of the models indicate the breakage of the first was not the fault of the device but the true response of the model to the loading conditions as verified by the second test.

A like specimen (69.89% relative density) was used in test PG86012153 (Figure 5-5). The purpose was to recreate the failure of the previous two tests in a different scale model. The model's load versus penetration curve indicates slightly less resistance than the two tests conducted at 69.8 g's, however this can be attributed to the slight decrease in dry unit weight. The model withstood being pushed to a scale depth of 30 feet due to the relatively higher axial stiffness of the 86.0 g model (95.4% of the axial stiffness of the prototype for the 86.0 g model versus 73.8% for the 69.8 g model). The same model was subsequently tested in a specimen with a 72.12% relative density and buckled under a scale load of 425 kips after penetrating 26 scale feet (PG86012181, Figure 5-5). The tests conducted in the higher range of relative densities, greater than 64%, suggest penetration should be limited to 20 scale feet when testing models of relatively low axial

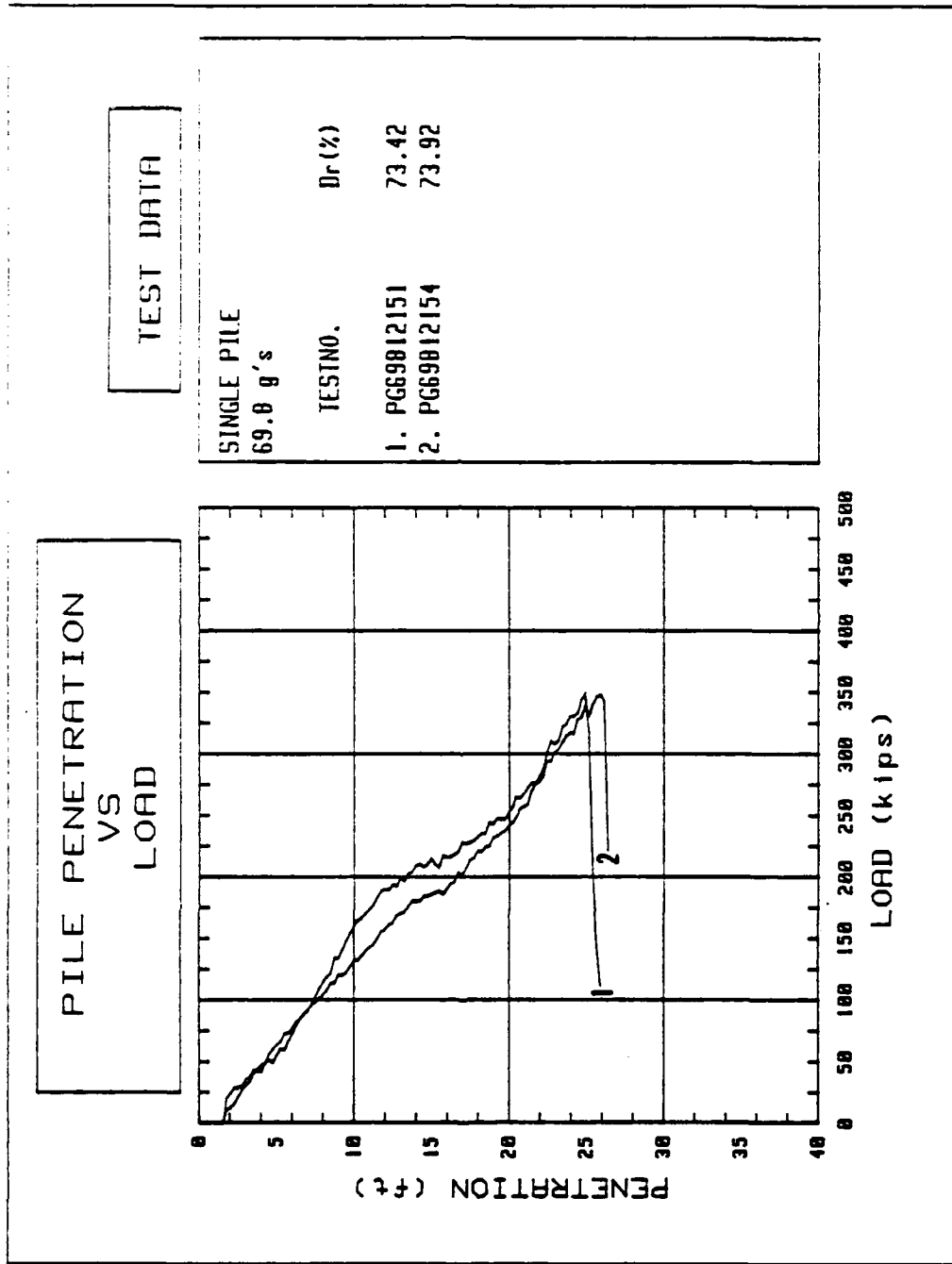


Figure 5-4 Pile Penetration vs. Load, Single Pile, PG69812151, PG69812154

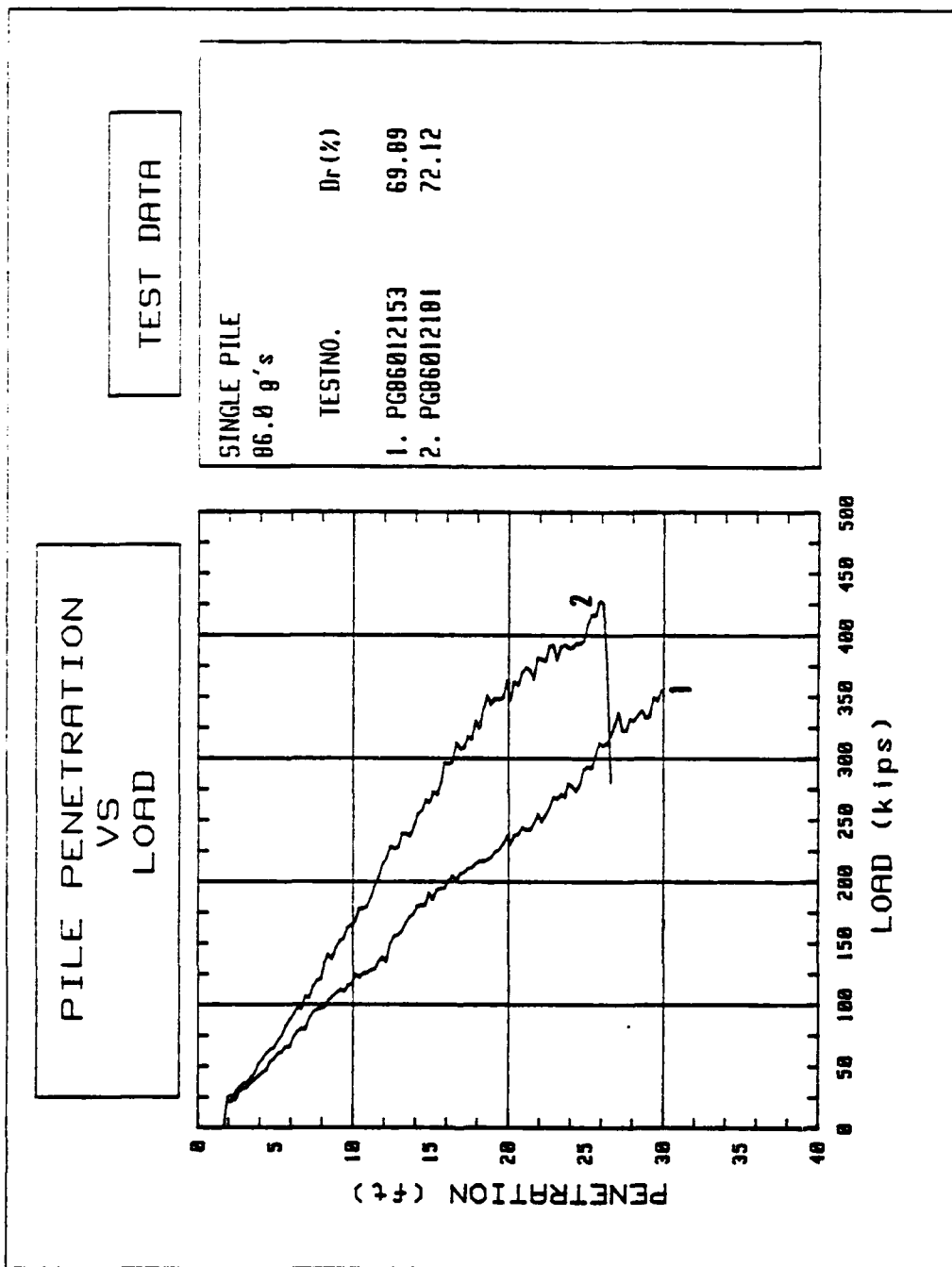


Figure 5-5 Pile Penetration vs. Load, Single Pile, PG86012153, PG86012181

stiffness. No models were destroyed during tests conducted with specimens having a relative density of less than 64%.

Load tests were conducted on all successfully pushed model piles (groups) after the performance of the placement device and associated programs was deemed acceptable. The following is a summary of the tests conducted. Scaled models of individual piles, groups of four (same pattern as the group of five, but with the center pile removed), and groups of five were tested at 69.8 and 86.0 g's. Three tests were conducted on each model at each g level. The plots of penetration versus load and the associated load tests are provided in the order shown in Table 5-1. Quantitative results of those tests will be discussed in the following section.

Table 5-1 Pushed Pile (Group) Model Test Series

Type	Unit Wgt. (pcf)	Dr (%)	
Individual Piles			
Figure 5-6	PG69804013	97.7	53.61
	PG69804011	98.6	58.44
	PG69804021	99.5	63.18
Figure 5-7	PG86004014	97.7	53.61
	PG86004012	98.6	58.44
	PG86004022	99.5	63.18
	PG86012172	100.5	68.35
Group of Four			
Figure 5-8	PG69802251	96.6	47.58
	PG69802252	97.3	51.43
	PG69802253	98.0	54.96
Figure 5-9	PG86002244	97.2	50.89
	PG86002243	98.3	56.84
	PG86002242	98.5	57.91
Group of Five			
Figure 5-10	PG69804023	96.5	47.03
	PG69804051	97.2	50.89
	PG69802254	97.9	54.69
Figure 5-11	PG86002231	97.7	53.61
	PG86002232	98.6	58.44
	PG86002241	98.6	58.44

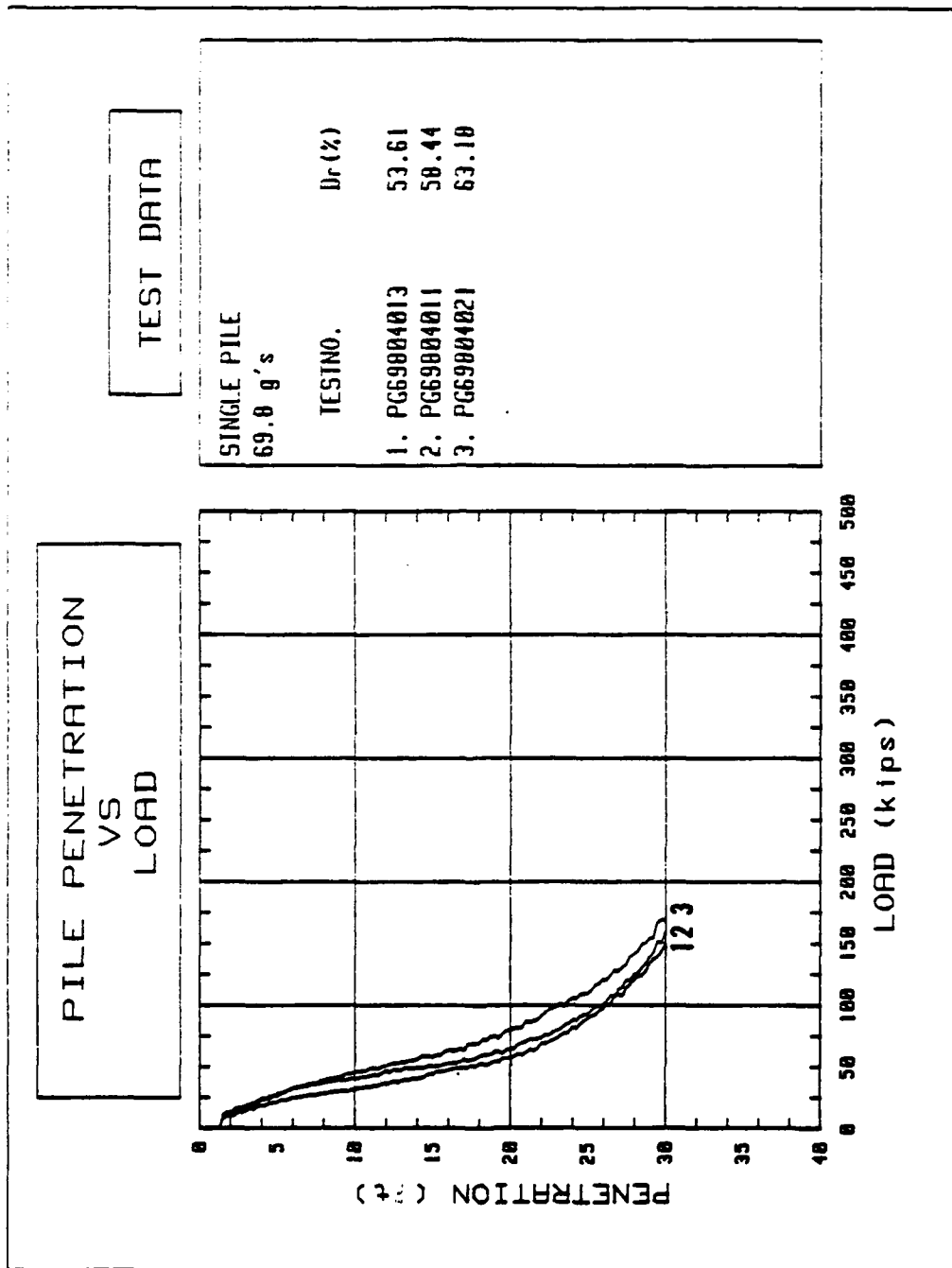


Figure 5-6 Pile Penetration vs. Load, Single Pile, PG69804013, PG69804011, PG69804021

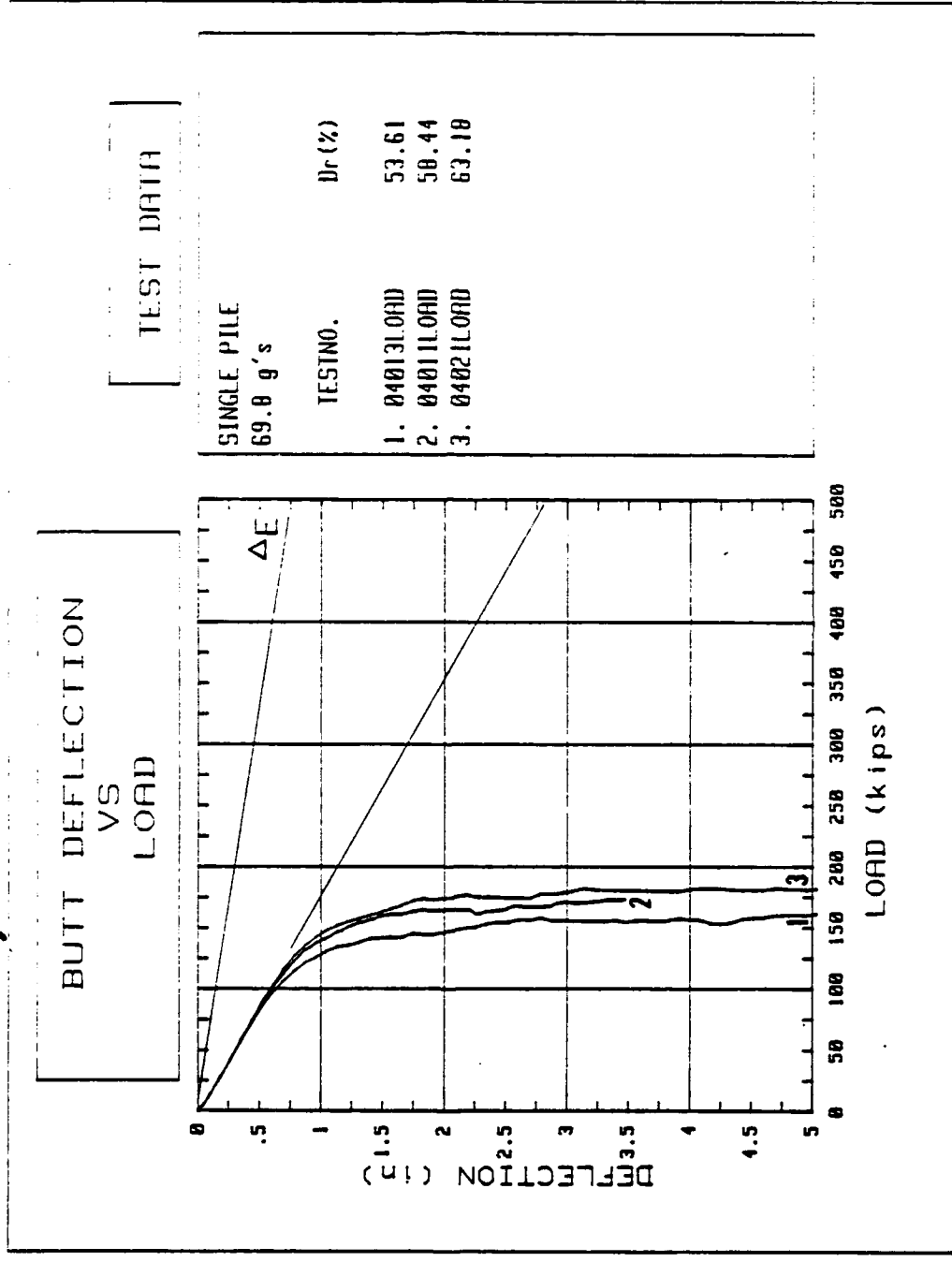


Figure 5-6--continued

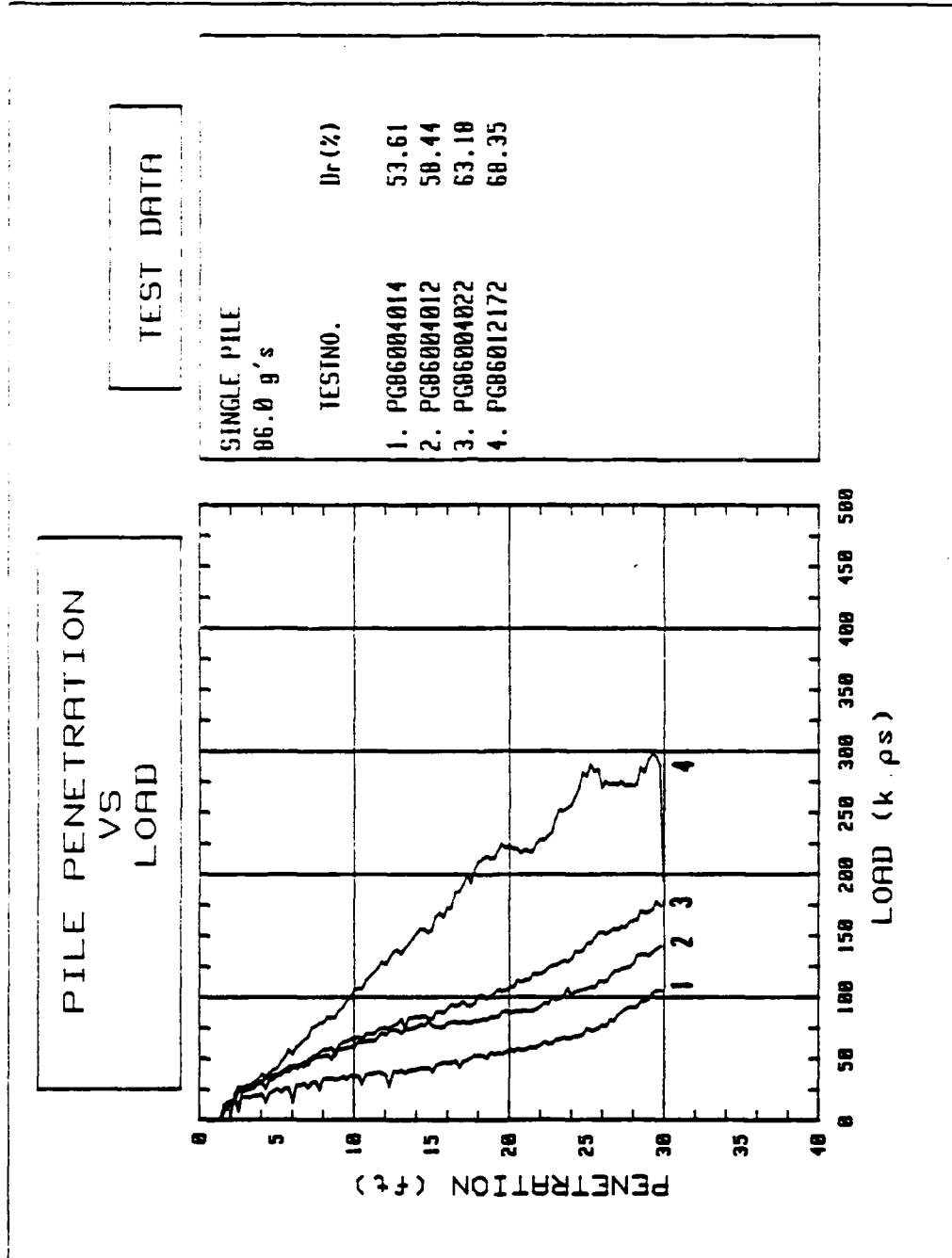


Figure 5-7 Pile Penetration vs. Load, Single Pile, PG86004014, PG86004012, PG86004022, PG86012172

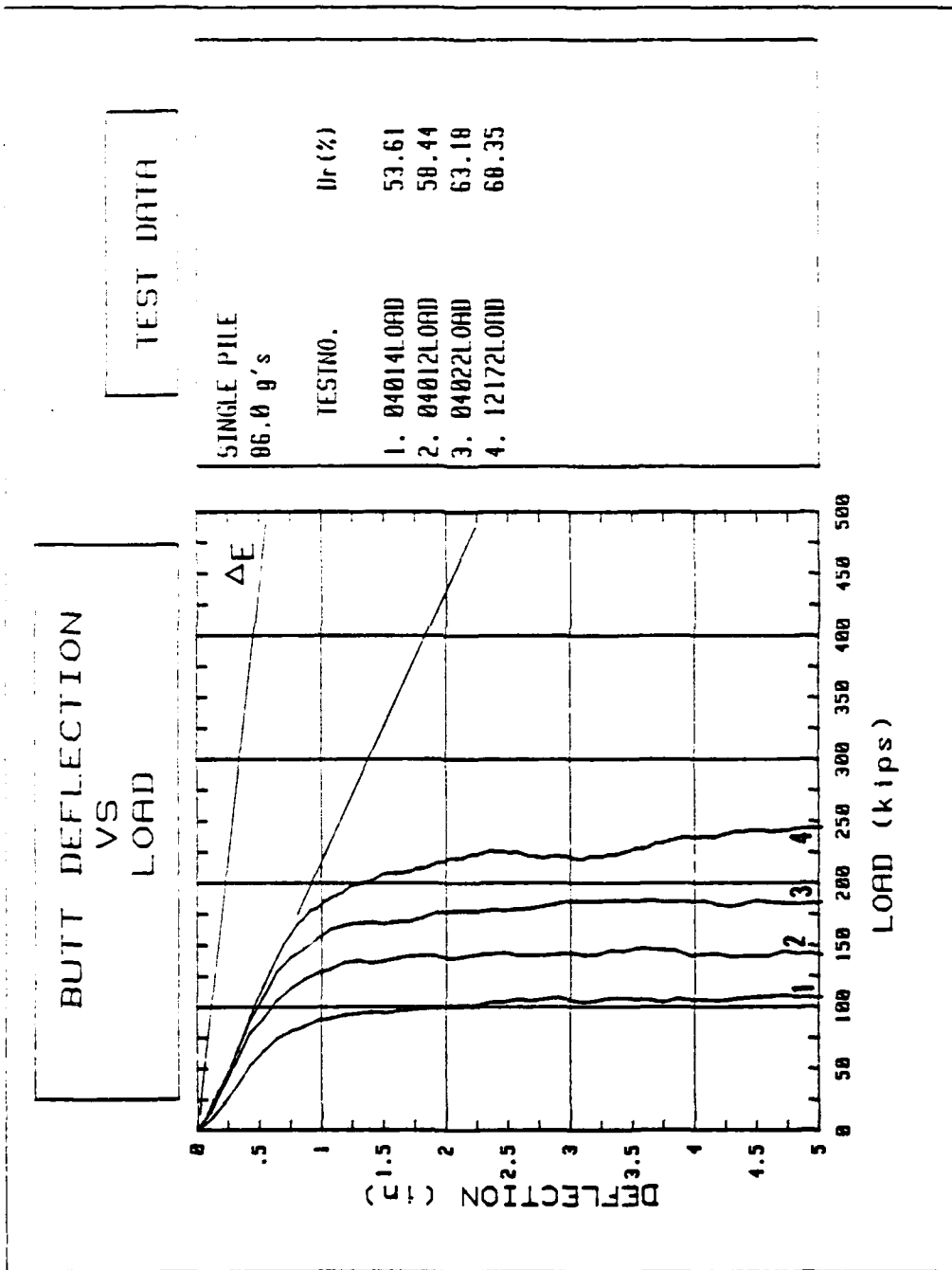


Figure 5-7--continued

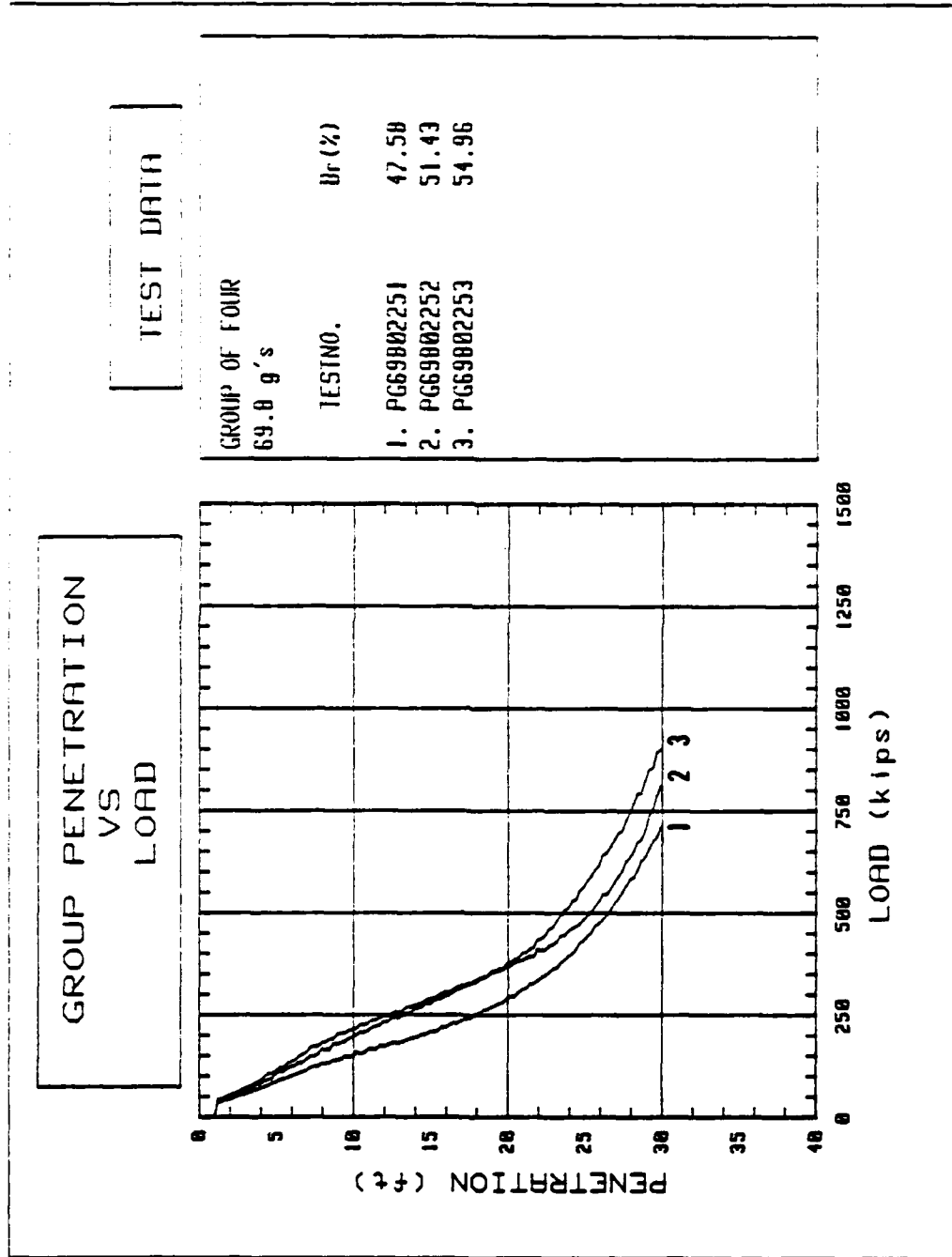


Figure 5-8 Group Penetration vs. Load, Group of Four PG69802251, PG69802252, PG69802253

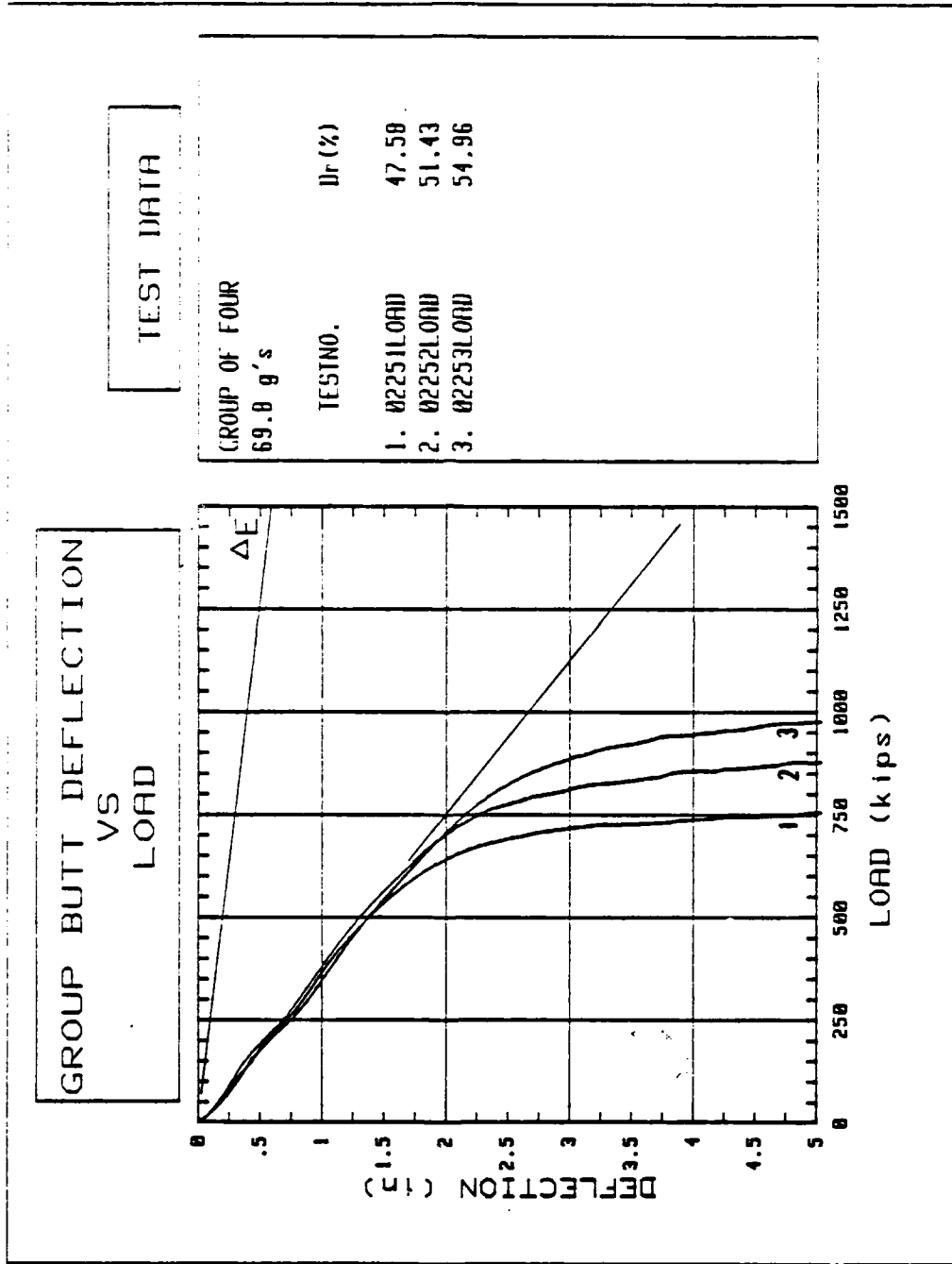


Figure 5-8--continued

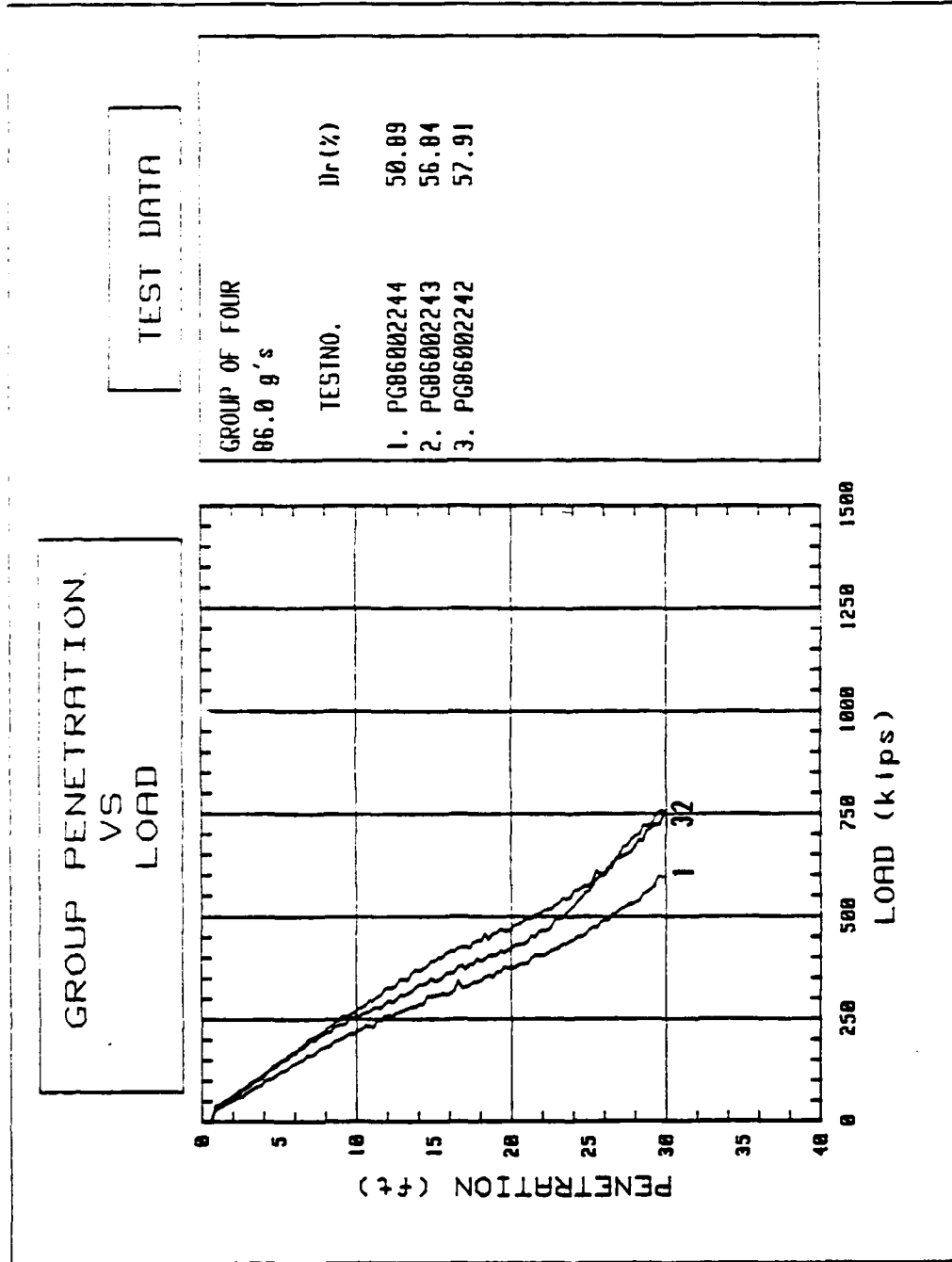


Figure 5-9 Group Penetration vs. Load, Group of Four, PG86002244, PG86002243, PG86002242

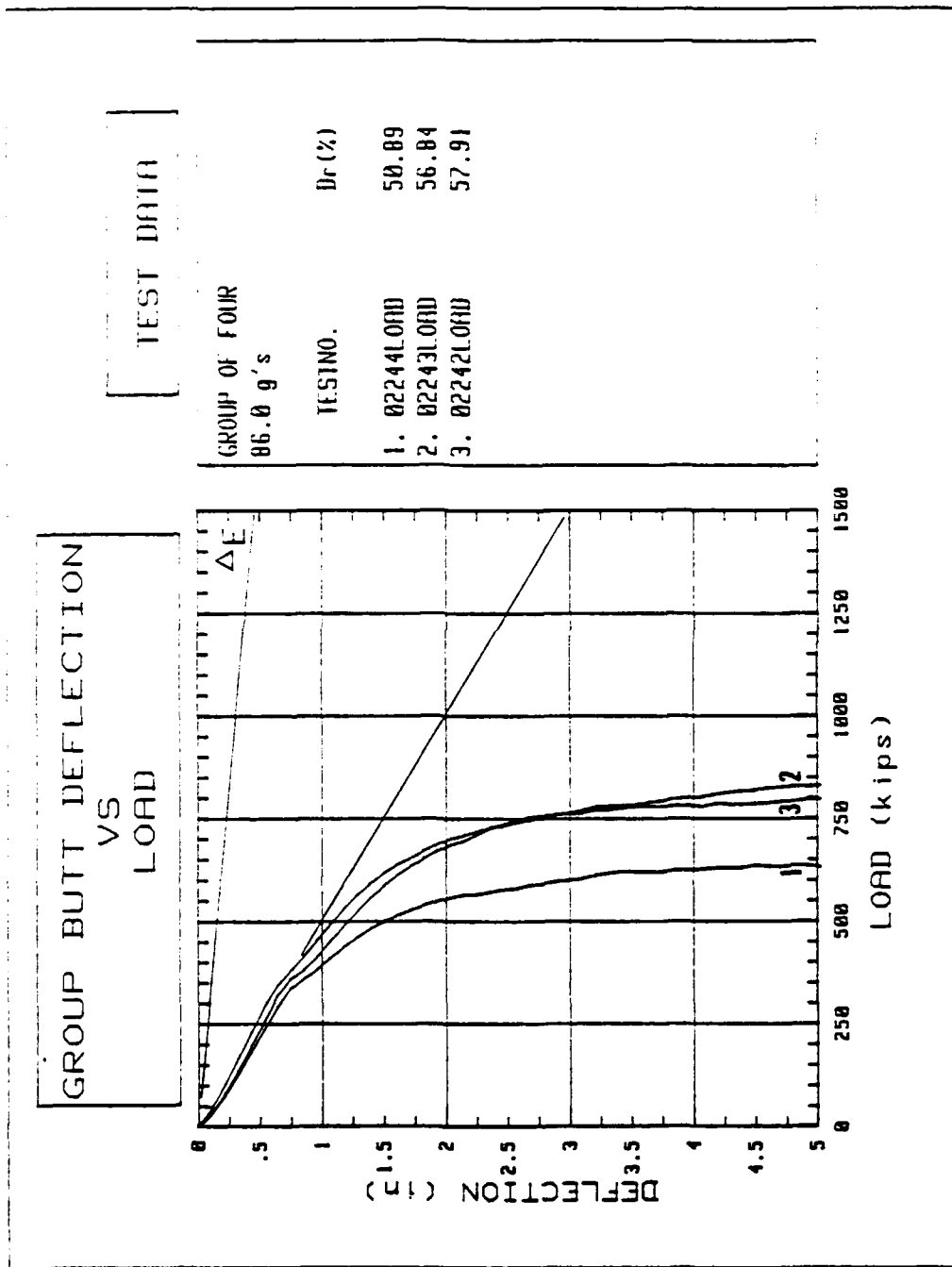


Figure 5-9--continued

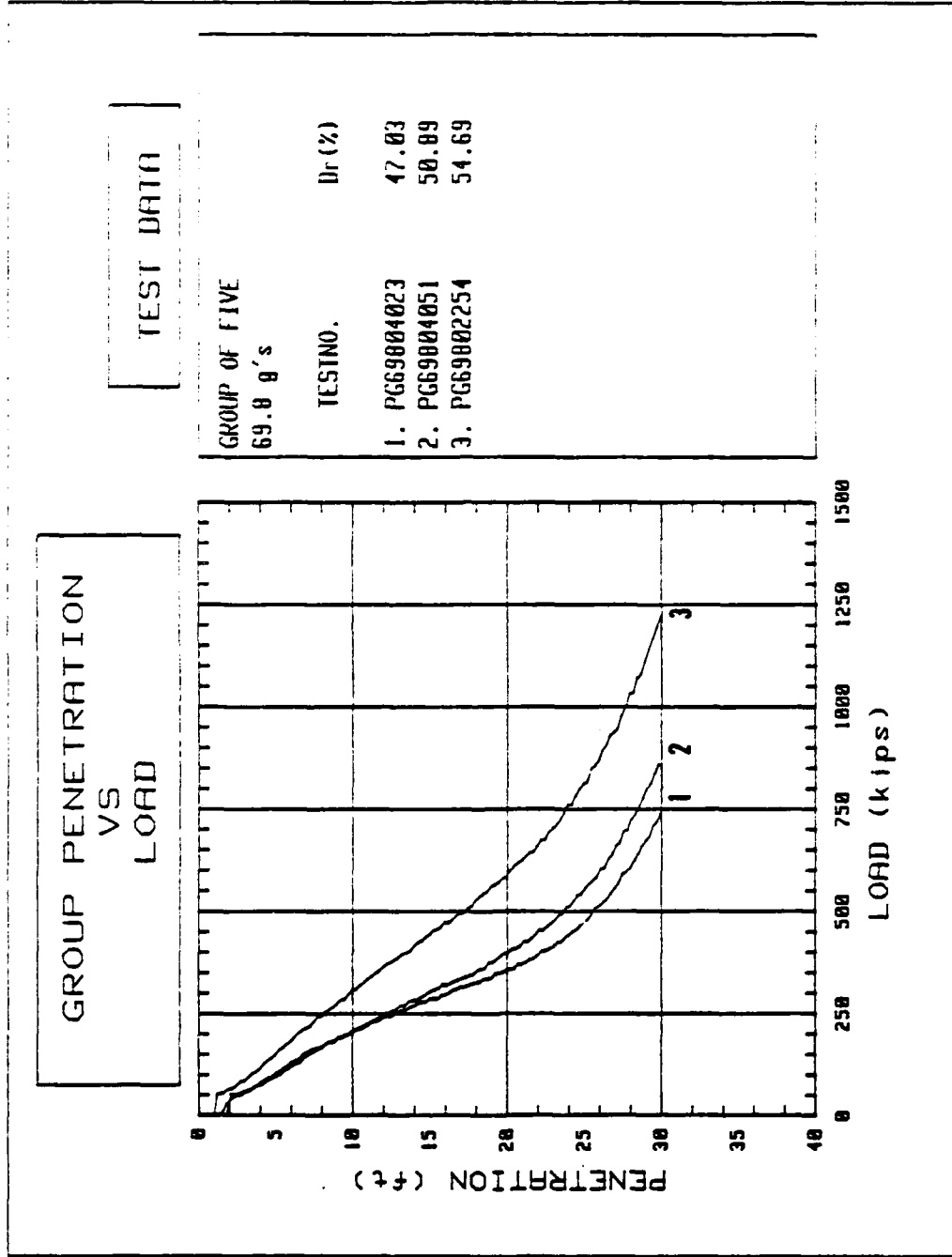


Figure 5-10 Group Penetration vs. Load, Group of Five, PG69804023, PG69804051, PG69802254

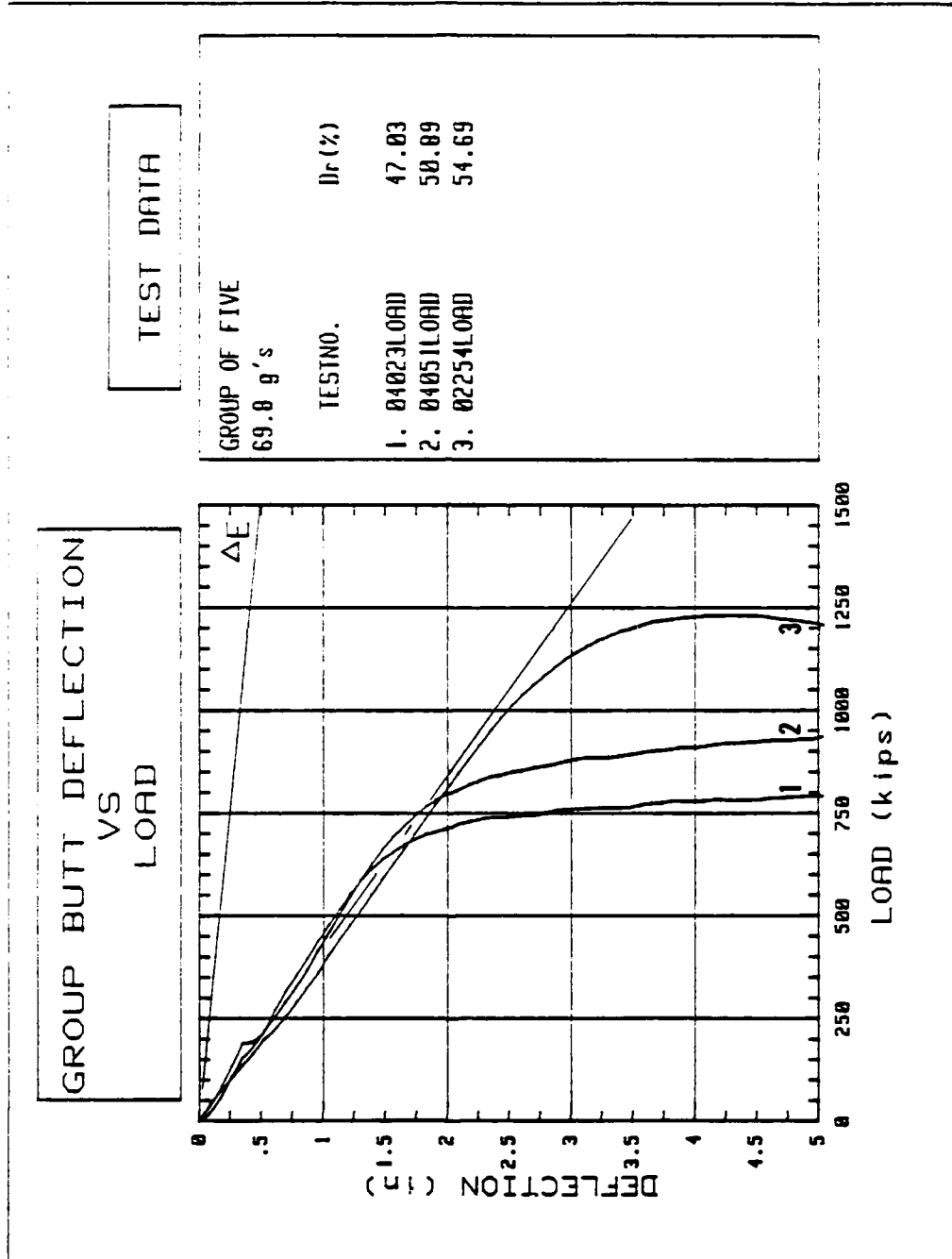


Figure 5-10--continued

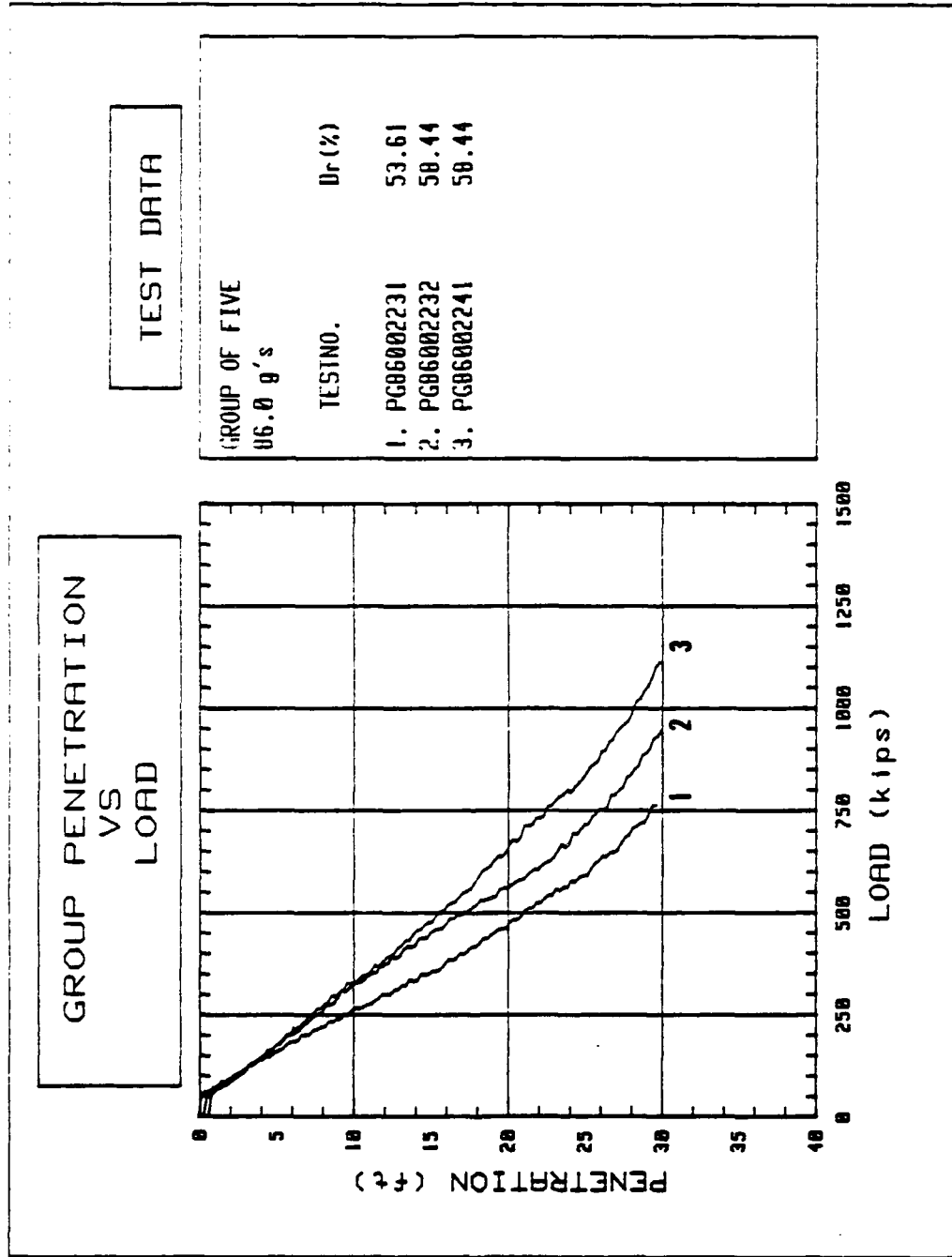


Figure 5-11 Group Penetration vs. Load, Group of Five, PG86002231, PG86002232, PG86002241

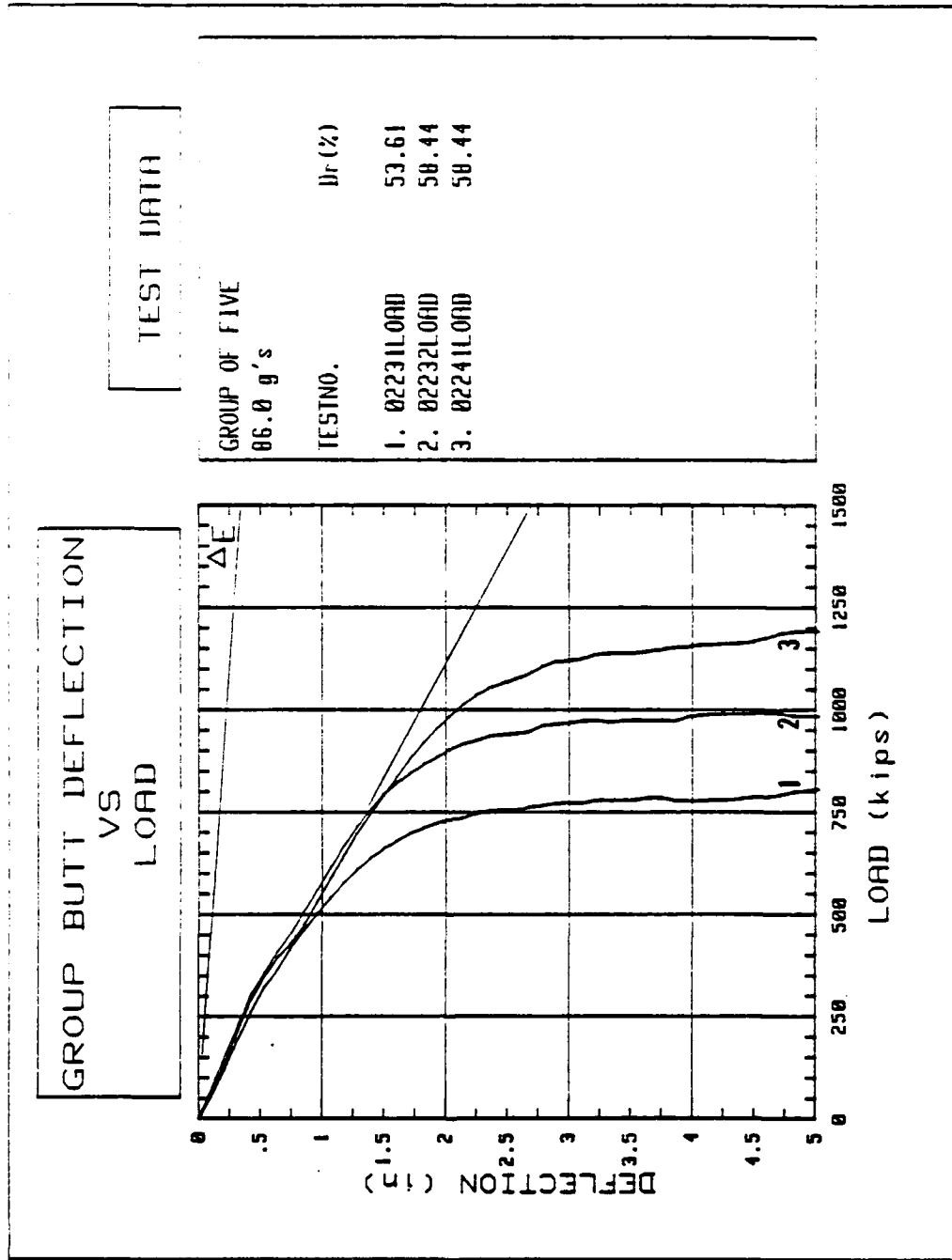


Figure 5-11--continued

All plots demonstrate the expected increase in resistance to penetration by the pile (group) in response to an increase in the relative density of the specimen. Furthermore, most of the plots of Pile (Group) Penetration vs. Load indicate a tendency for the resistance of the soil to increase noticeably in the last five to ten scale feet of penetration.

This tendency is most pronounced in the 69.8 g model tests. Boundary effects were suspected as the tip of the pile was 1.72 inches (ten scale feet) from the specimen container base. However, tests conducted in the large specimen container on the same models also showed the tendency. The pile tip was 4.54 inches (26.5 scale feet) from the container base in these tests. The tendency was first noticed after failure of a group of five test which exerted a significant lateral force at the bottom end (near the soil) of the slotted cast acrylic guide tube. Apparently, the connection between the tube and supporting c-channel was weakened which subsequently permitted the tube base to move sideways during heavy axial load applications. This tendency became more pronounced as testing continued indicating the connection was becoming progressively weaker. The tendency was most pronounced when 69.8 g models were tested because these models were the least stiff and require application of a relatively large axial force compared to the 86.0 g models.

Correction of this weakness requires that the connection between the supporting c-channel and the top of the support tube be stiffened. Alternatively, the bottom of the support tube could be restricted using an appropriate attachment to the c-channel. Tests were conducted at relative densities which kept the tendency of the model piles to

displace laterally to an acceptable level. It is recommended the device be fitted with additional support before further tests are conducted. This may increase the range of relative densities which may be tested with the aluminum models.

The looseness of the support tube is not thought to have influenced the results of tests on individual piles at 86.0 g's. However, all of the individual and group tests at 69.8 g's, PG86002243, and PG86004023 appear to have been influenced to varying degrees. The significant effects of the looseness of the support tube are more pronounced differences between the ultimate capacity of the group models (higher axial loads) at the two test g levels and an increase in the apparent efficiency of the groups as will be explained.

Three tests were conducted in which the pushed individual model pile was slowly pulled from the soil in an attempt to determine how much skin friction resistance might be acting on the model and contributing to total ultimate capacity. One test each was conducted at 57.5, 69.8, and 86.0 g's with the results as presented below.

Test No.	Dr(%)	Tension (kips)
PG57501161	60.03	20*
PG69801162	57.91	5
PG86001291	55.77	3

* Tension based on the 13.3 kip tensile capacity of the 20-foot portion of the pile pushed from ten feet to thirty feet (scale magnitudes)

The tests indicate the frictional forces resulting from the pullout of the model pile may be influenced by the g level at which the test is conducted. The same effect may appear when the piles are pushed into

the specimen, however, this determination cannot be made on models unless the frictional forces are separated from the tip loads. The above data may also indicate the influence of the specimen relative density on its ability to mobilize resistive frictional forces, however, the change in relative density is minimal compared to the resulting change in unit skin friction. Rather, the change is attributed to scale effects. Figure 5-12 shows the change (%) in total frictional resistance with respect to the change (%) in model pile-soil contact area using the 86.0 g model as a reference.

5.2.2 Quantitative Discussion of Pushed Model Pile Test Results

The deBeer method (Sharp, 1987) was used in the interpretation of the capacity of the pushed models. This method involves the plotting of the load test results (deflection vs. load) on log-log scales. The capacity of the pile (group) is highlighted as being the intersection of two approximately straight lines. Figures 5-13 through 5-18 depict the deBeer plots of the load test results. The capacities determined by the deBeer method are presented in Table 5-2.

Results of the deBeer capacity determinations are plotted with respect to specimen relative density in Figure 5-19. This plot includes a failure envelope beyond which the aluminum models will fail if loaded under the respective combination of axial force and specimen relative density. Conclusions based on the results of the capacity determinations are presented below.

The following trends are observed regarding the capacities determined by the deBeer method (Figure 5-19). Ultimate capacities for the single piles agree very closely; the average difference between the 69.8 and 86.0 g model capacities being only 12.0%. These capacities are

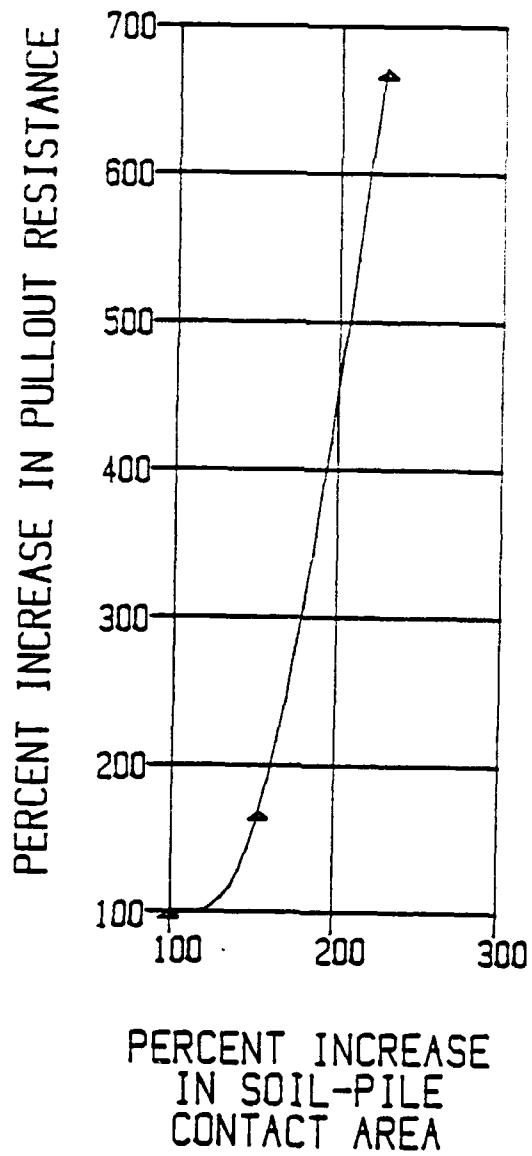


Figure 5-12 Change (%) in Total Frictional Resistance to Pull-Out With Respect to the Change (%) in Model Pile-Soil Contact Area (Referenced to Single 86.0 g Model)

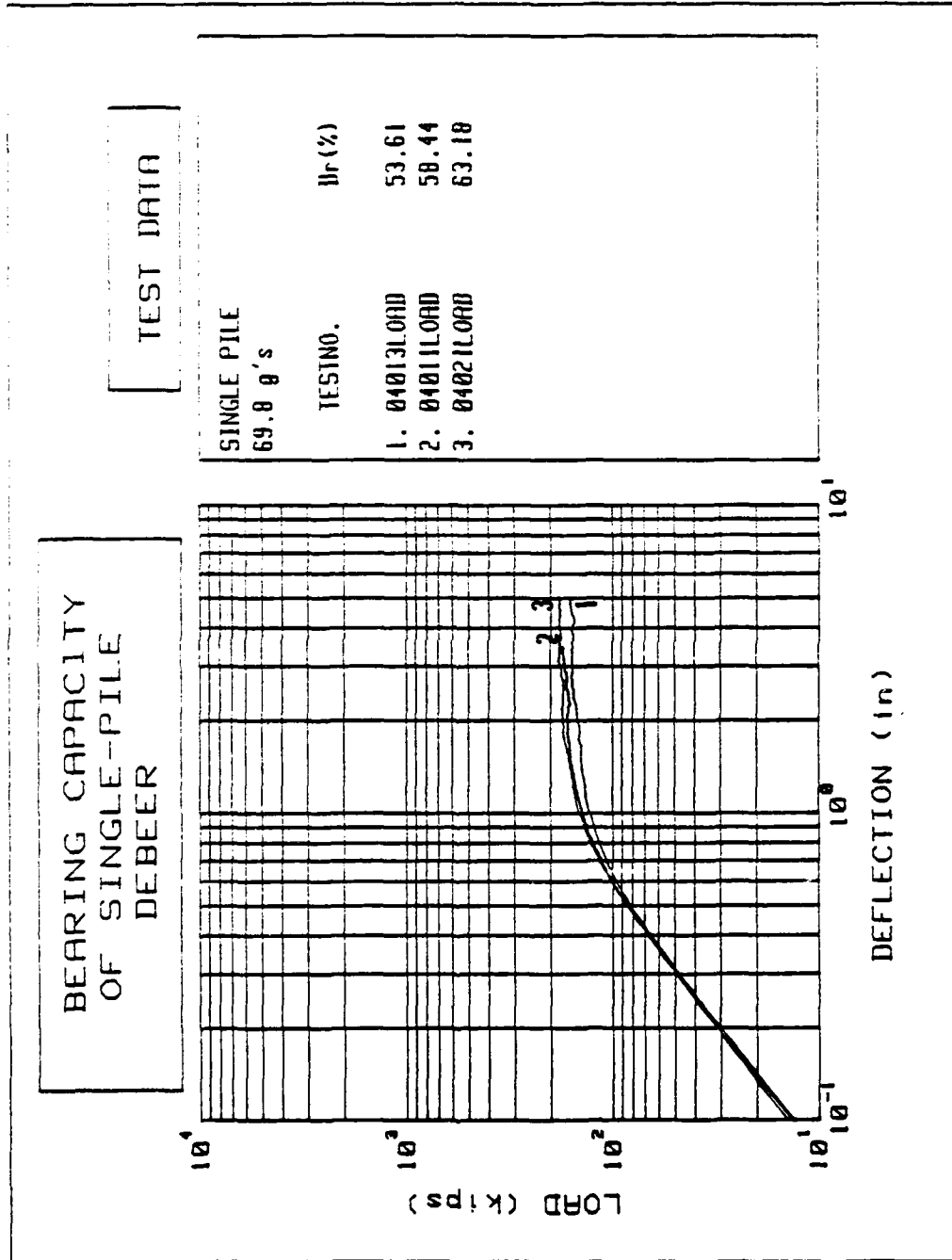


Figure 5-13 Bearing Capacity of Single Pile, deBeer, 04013LOAD, 04011LOAD, 04021LOAD

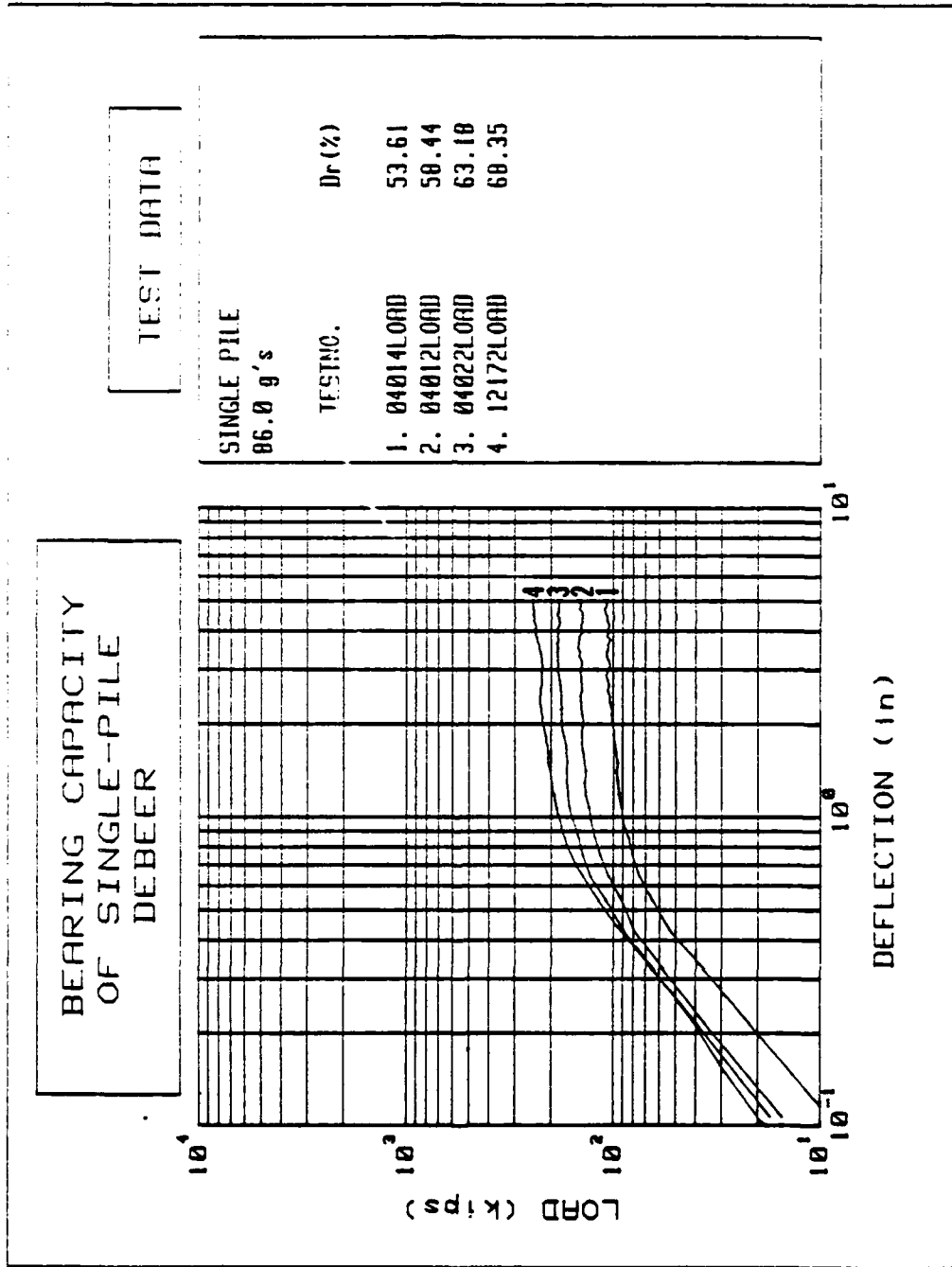


Figure 5-14 Bearing Capacity of Single Pile, deBeer, 04014LOAD, 04012LOAD, 04022LOAD, 12172LOAD

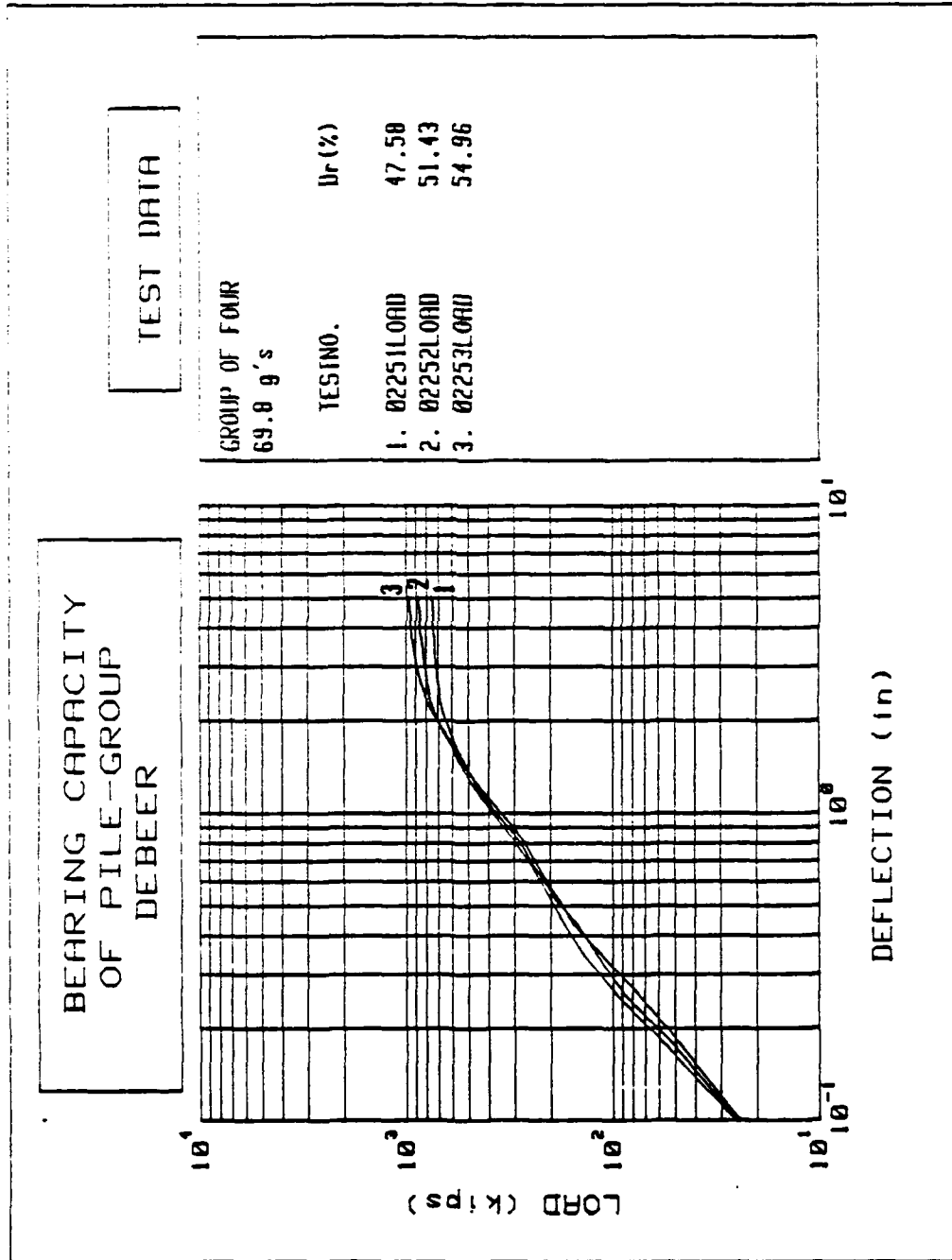


Figure 5-15 Bearing Capacity of Pile Group, deBeer, Group of Four, 02251LOAD, 02252LOAD, 02253LOAD

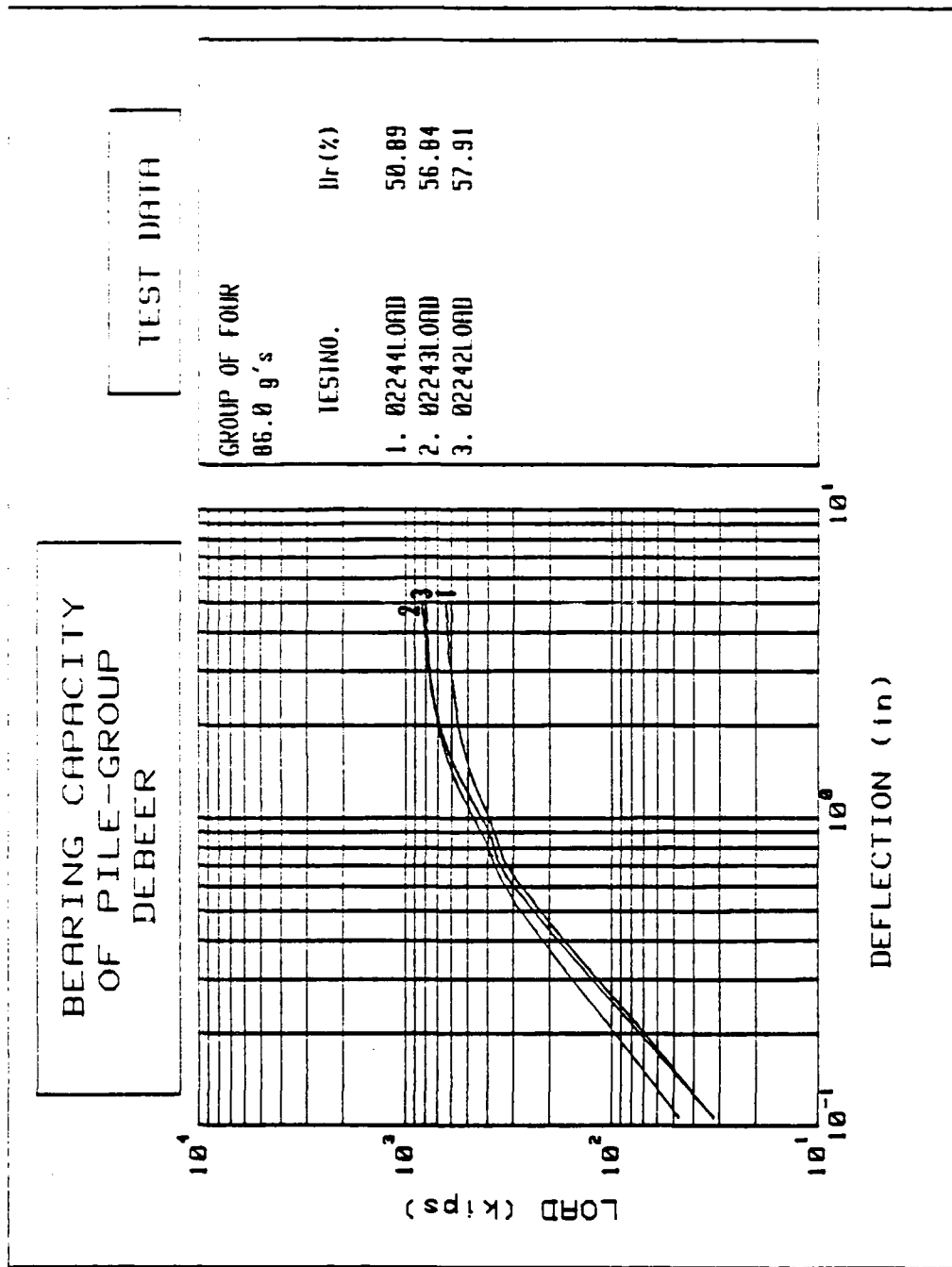


Figure 5-16 Bearing Capacity of Pile Group, deBeer, Group of Four, 022441.0AD, 022431.0AD, 022421.0AD

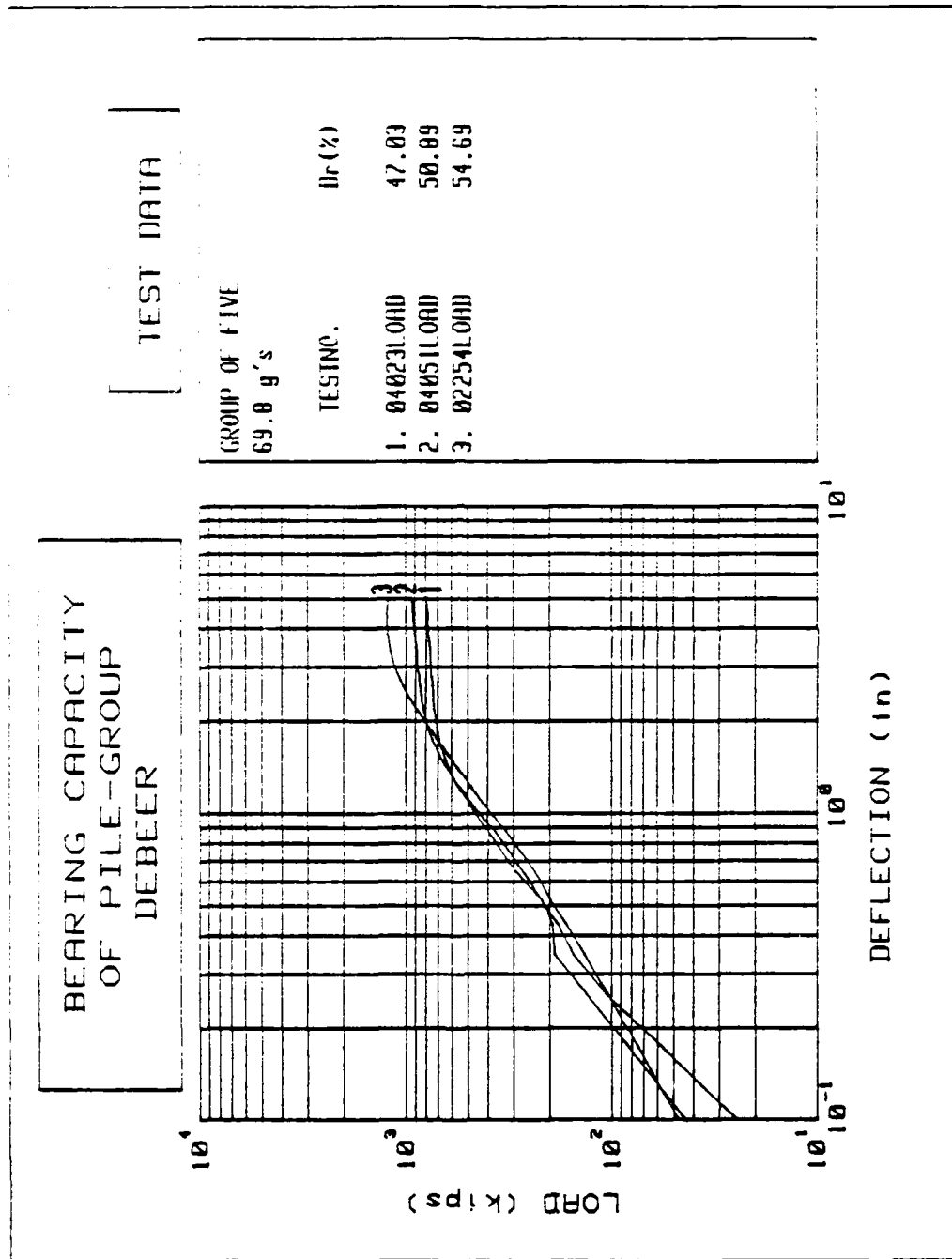


Figure 5-17 Bearing Capacity of Pile Group, deBeer, Group of Five, 040231.0AD, 040511.0AD, 022541.0AD

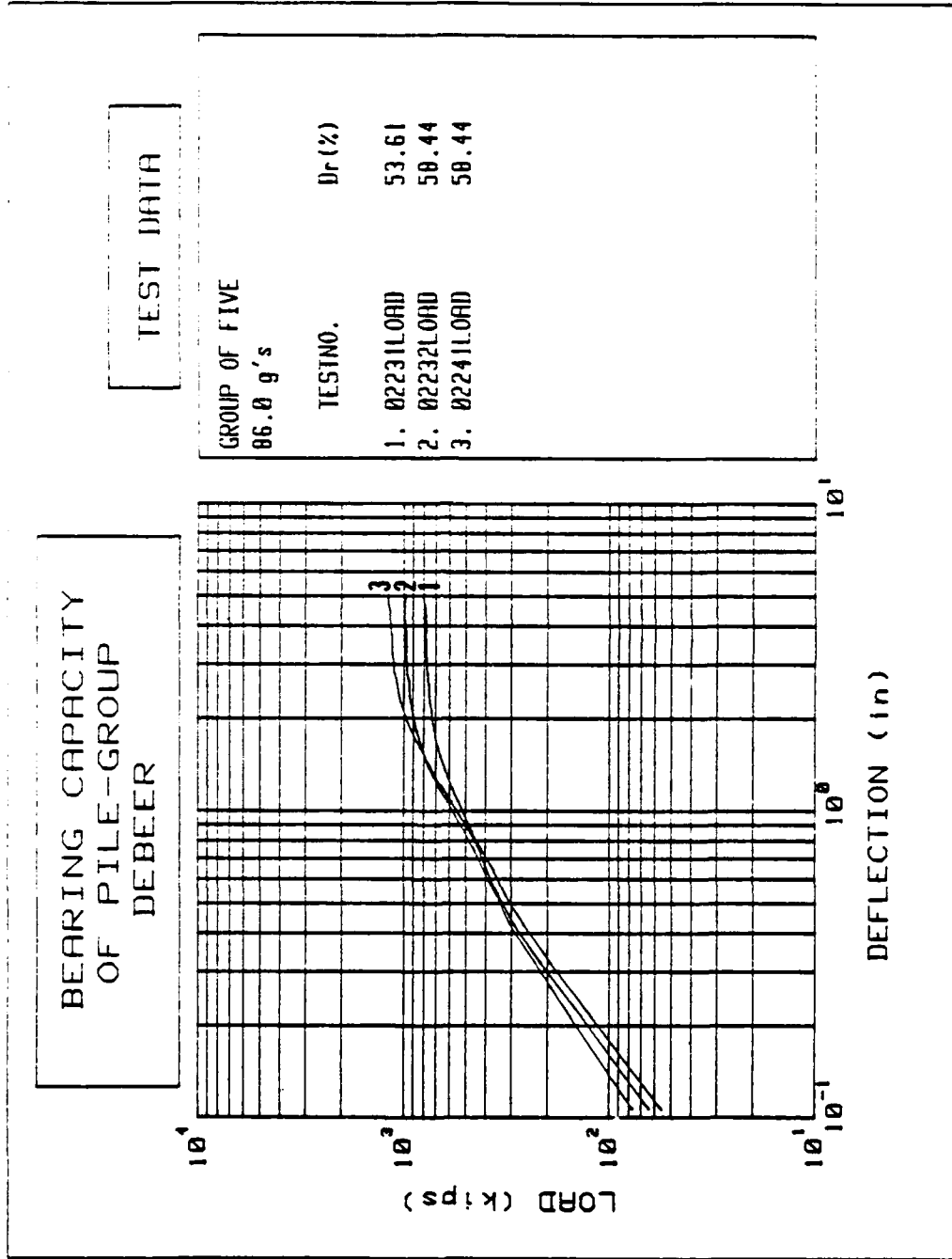


Figure 5-18 Bearing Capacity of Pile Group, deBeer, Group of Five, 02231LOAD, 02232LOAD, 02241LOAD

Table 5-2 Pushed Pile (Group) Load Test Results

Type		Dr (%)	Scale Capacity (kips)
Individual Piles			
Figure 5-13	PG69804013	53.61	112
	PG69804011	58.44	130
	PG69804021	63.18	150
Figure 5-14	PG86004014	53.61	83
	PG86004012	58.44	111
	PG86004022	63.18	140
	PG86012172	68.35	170
Group of Four			
Figure 5-15	PG69802251	47.58	660
	PG69802252	51.43	710
	PG69802253	54.96	811
Figure 5-16	PG86002244	50.89	500
	PG86002243	56.84	700
	PG86002242	57.91	720
Group of Five			
Figure 5-17	PG69804023	47.03	700
	PG69804051	50.89	815
	PG69802254	54.69	1050
Figure 5-18	PG86002231	53.61	710
	PG86002232	58.44	930
	PG86002241	58.44	1010

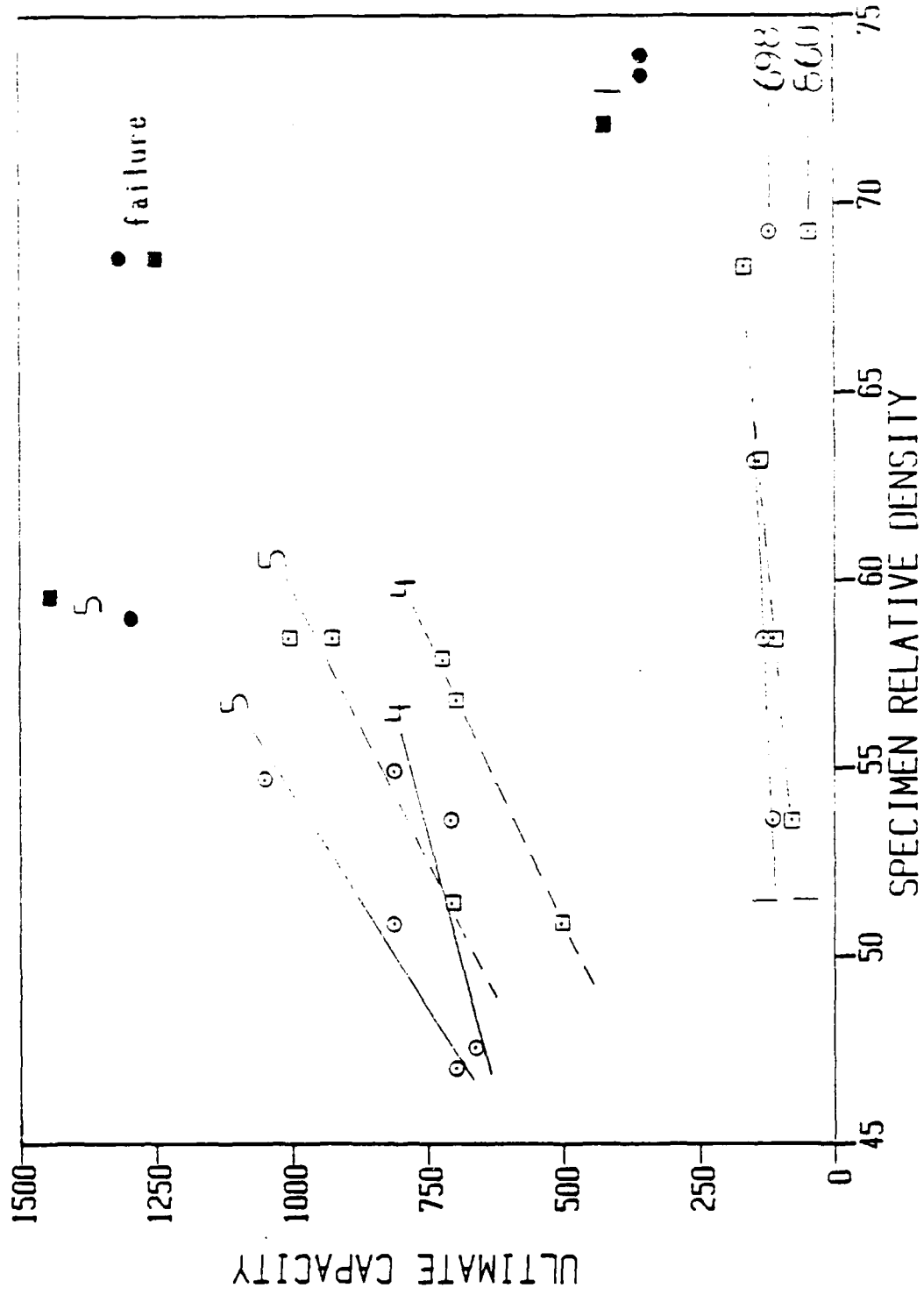


Figure 5-19 deBeer Method Model Pile Capacity vs. Specimen Relative Density

expected to give the closest agreement as the axial loads exerted by the placement device are the least of all of the tests conducted. Therefore, there is the least tendency for the cast acrylic guide tube to be pushed to the side. The capacities of the groups show greater divergence as the number of piles in the group increases. This is possibly due to the greater axial load needed to push the piles to full penetration. It may also indicate scale effects with the 86.0 g models developing lesser capacities as a result of their relatively smaller pile-soil contact areas. The group factors are presented below in Table 5-3 to aid in the understanding of which effect is controlling. The following relationship is used in the determination of the group factors.

$$\text{Group Factor} = \frac{\text{Group Ultimate Capacity}}{\text{Single Pile Capacity} \times \# \text{ of Piles in Group}} \quad \text{Eq. 5-3}$$

Group factors are determined at 52.0 and 57.0% relative density to discern the influence relative density may have on the group factor.

Within the accuracy of the pile capacities measured, the group factors are equal for all groups. There appears to be no tendency for the group factor to increase in response to an increase in specimen relative density. Nor does there appear to be any tendency for the group factor to decrease as the test g level increases as might be expected if there were scale effects. It is concluded the scale effects influence the friction forces only (as discussed in the previous section) and not the bearing capacity of the tip. Since these models derive a significant portion of their capacity from end bearing, scale effects are minimal.

Table 5-3 Pile Group Factors Based on deBeer Capacities

69.3 g's	Capacity (kips)		Group Factor	
	52% Dr	57% Dr	52% Dr	57% Dr
Single Pile	105	125	-	-
Group of Four	725	835	1.73	1.67
Group of Five	915	1175	1.74	1.38
86.0 g's	Capacity (kips)		Group Factor	
	52% Dr	57% Dr	52% Dr	57% Dr
Single Pile	75	105	-	-
Group of Four	535	710	1.78	1.69
Group of Five	650	915	1.73	1.74

The group factors are all significantly higher than 1.0. This indicates the looseness of the guide tube, as suspected, may have contributed to the apparent strength of the groups. Lateral displacement of the guide tube tip permits the pile to tilt at the point of insertion which results in a larger cross sectional area being presented to the soil (greater resistance to penetration). This increases the tendency of the piles to break and may even cause the piles to "grab" the guiding template thus deriving additional apparent strength from the friction between the template and pile(s). Excessive bending-induced strain will be recorded from the piles which are flexing at the soil surface compared to those which are inserted straight into the soil. Thus, it is important to monitor development of strain in the models before this determination can be made.

The initial slope of the loading curve for the individual and group piles at both g levels was determined from the butt deflection vs. load plots (Figures 5-6 through 5-16, even numbered figures). The plot of

elastic deformation (PL/AE) of the piles (groups) is also shown on those figures (Δ_E). The difference between the two (initial slope of the loading curve minus the slope of the elastic deformation curve) is attributed to the soil response and possible group effects. The slopes are listed below (Table 5-4) with the values of butt deflection (inches) at failure versus failure load being plotted in Figure 5-20. The values of ultimate capacity and deflection at failure are based on the deBeer method.

Table 5-4 compares the soil's response to loading for the individual, group of four, and group of five models at each g level as well as the response at the two test g levels for each of the models. The group effect becomes evident in the first comparison as the pile group responses to loading show an average efficiency of 1.17 for the group of four and 1.18 for the group of five. The models at each g level display efficiencies within 2.0% of one another indicating again the scale effects for axial loading of model piles placed in granular soils may be insignificant (Figure 5-21).

Comparing the soil response for each of the model types at the two g levels indicates the soil is 130% more stiff at 86.0 g's than 69.8 g's. The relative increase in the stiffness of the soil at 86.0 g's is to be expected as moduli for model materials are scaled one-to-one. Based on the ratio of the g levels (86.0/69.8, or 1.23), the model soil for the 69.8 g tests appears 7.0% less stiff than one might expect, or the soil used in the 86.0 g tests 7.0% stiffer. The difference is most reasonably attributed to the relative axial stiffnesses of the models with the 69.8 g models being only 77.4% as stiff as the 86.0 g models.

Table 5-4 Initial Loading Curve Slope, Elastic Deformation Curve Slope, and Resulting Soil Response for Individual and Group Model Piles

69.8 g's	Single Pile	Group of Four	Group of Five
Elastic Deformation Curve Slope (kips/in.)	644	2,577	3,221
Initial Loading Curve Slope (kips/in.)	<u>177</u>	<u>375</u>	<u>417</u>
Δ Slope (Soil Response)	467	2,202	2,804
Efficiency*		1.18	1.20

36.0 g's	Single Pile	Group of Four	Group of Five
Elastic Deformation Curve Slope (kips/in.)	833	3,332	4,165
Initial Loading Curve Slope (kips/in.)	<u>217</u>	<u>484</u>	<u>555</u>
Δ Slope (Soil Response)	616	2,848	3,610
Efficiency		1.16	1.17

	Single Pile	Group of Four	Group of Five
Δ Modulus _{86.0}			
<u>Δ Modulus _{69.8}</u>	1.32	1.29	1.29

$$* \text{ Efficiency} = \frac{\Delta \text{ Slope (Group Piles)}}{\Delta \text{ Slope (Single Pile)} \times \text{number of piles in group}}$$

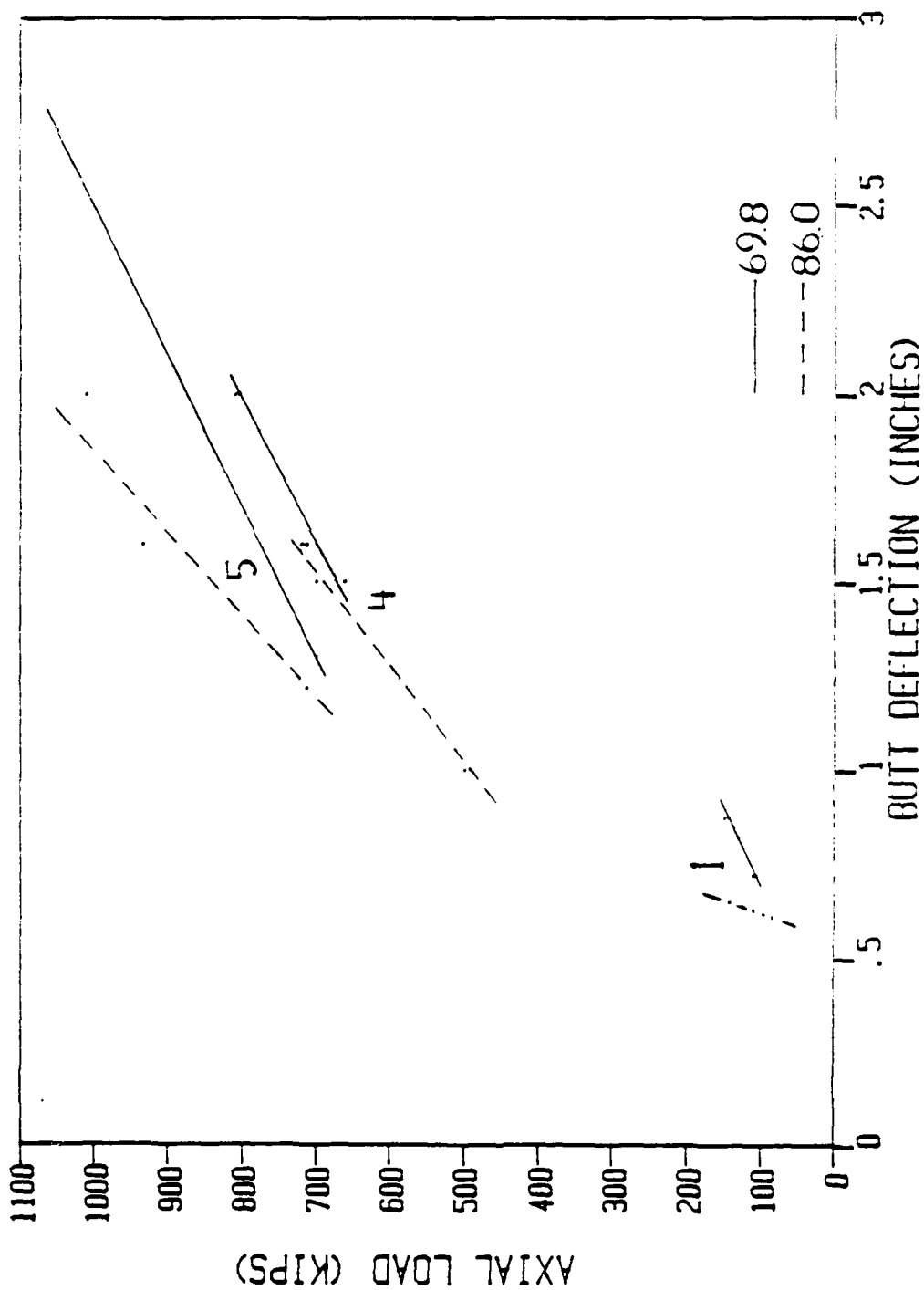


Figure 5-20 Butt Deflection (inches) at Failure vs. Failure Load (kips) Using the deBeer Method of Capacity Determination

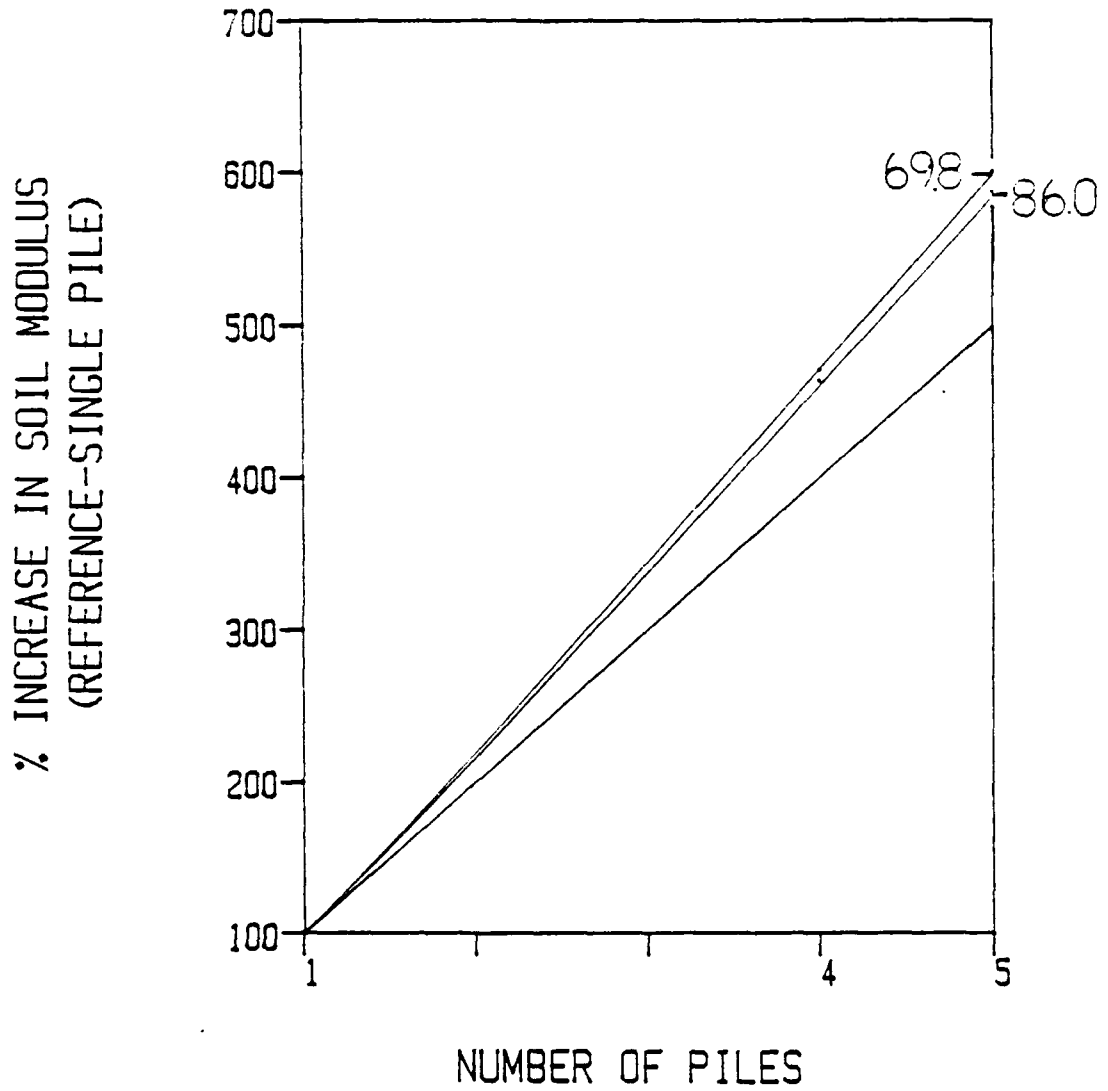


Figure 5-21 Per Cent Increase in Soil Stiffness vs. Increase in Number of Piles

Better agreement can be expected when the axial stiffness of the pile is modeled exactly instead of choosing models from available stock.

5.3 DRIVEPILE Test Results

5.3.1 Qualitative Discussion of Driven Model Pile Test Results

Five tests were conducted but terminated before reaching full penetration. The reasons for stopping the test provide insight into the two most important considerations in the operation of the placement device in the driving mode. Test DG68903171 (Figure 5-22) was the first successful use of the device as a driver. The pile was pushed in at one g to a scale depth of fifteen feet prior to starting the driving process. This permitted the electromagnet, hammer, and pile cap to be viewed by closed circuit television during the entire driving cycle. Penetration stopped at 24 scale feet because the electromagnet had not been powered sufficiently to lift the hammer. Increasing the electromagnet voltage (and current) alleviated the problem. The electromagnet then continued to lift and drop the hammer until full penetration was achieved. This test demonstrated the capability of driving model piles in the centrifuge by the use of a falling hammer. Surprisingly, the resistance to penetration from the initial blows of the hammer was relatively weak compared to that at the end of penetration. The pile penetrated easily during the first five impacts even though the soil's unit bearing capacity and lateral stresses were already significant. It appears the insertion at one g does little to develop the overall bearing capacity of the model. Bearing capacity in the model is developed only by the penetration of models (either by driving or pushing) at the appropriate g level. This is in agreement with the findings of Ko et al. (1984) and

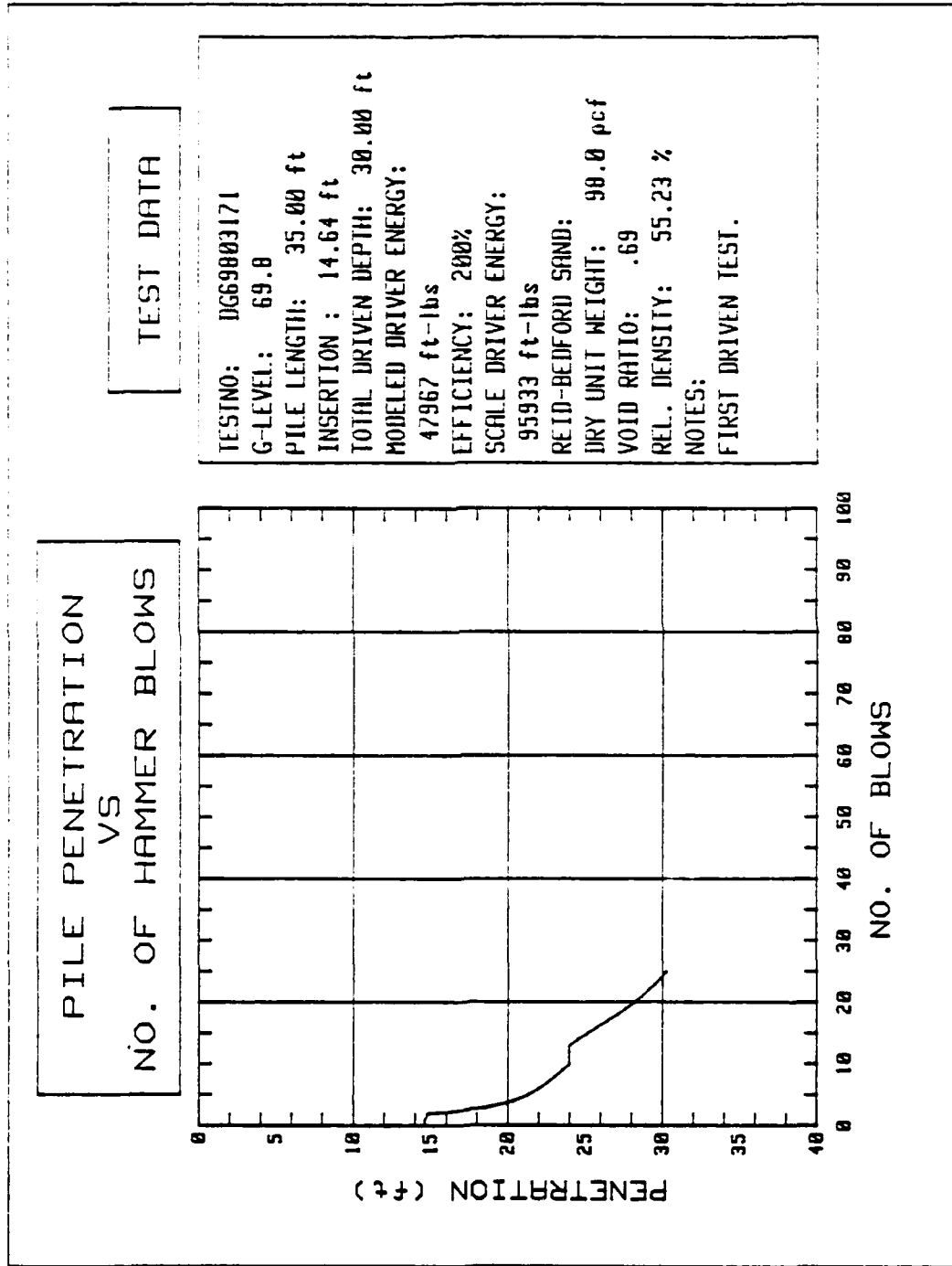


Figure 5-22 Pile Penetration vs. Number of Hammer Blows, Single Pile, DG69803171

the USDOT/FHWA reports (1984a, 1984c). Both reports concluded the portion of the model inserted at one g contributed little to the ultimate bearing capacity, and thus, resistance to penetration of the model pile.

Tests DG69803131 and DG69803282 (Figure 5-23) were terminated because the pile cap separated from the guide rod. Two causes are suggested regarding separation of the two; friction between the guide rod and the insulating sleeve in the magnet and improper connection of the guide rod to the model cap. The guide rod had been lubricated prior to testing so it could travel freely within the insulated hole through the center of the magnet. This did not appear to be a cause contributing to the separation. Rather, the connection between the guide rod and hammer was incapable of withstanding the repeated impacts of the hammer. Each impact served to pull the cap off of the end of the guide rod. Special care was taken in the manufacture of later caps to ensure separation would not occur.

Tests DG69803251 and DG69803281 (Figure 5-24) were terminated because the model pile failed by buckling at the connection between the cap and butt. The caps were manufactured with a 0.125 inch recess which encased the pile butt. However, this type of connection was insufficient to prevent stress concentrations. Minor eccentricities developed in the way the hammer struck the cap and these eccentricities resulted in deformation of the butt. This type of failure was evidenced by the tilting of the hammer as it rested on the cap waiting to be picked up again. The tilt of the hammer was sufficient to prevent the electromagnet from being able to pick it up. This is evident in the lack of penetration even though "blows" have been recorded. The electromagnet simply raised itself to the appropriate lift height but the hammer was

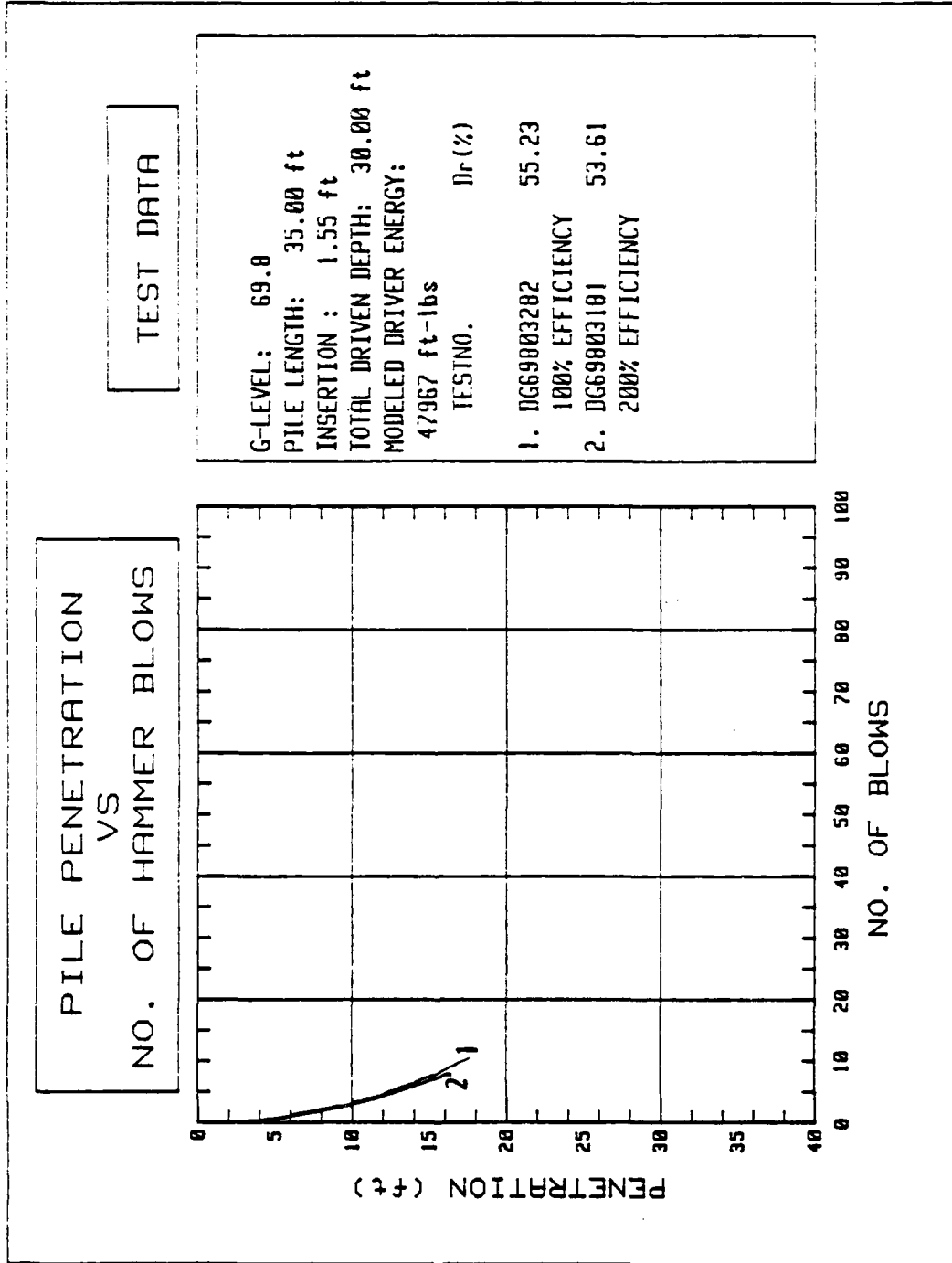


Figure 5-23 Pile Penetration vs. Number of Hammer Blows, Single Pile, DGG9803282, DGG9803181

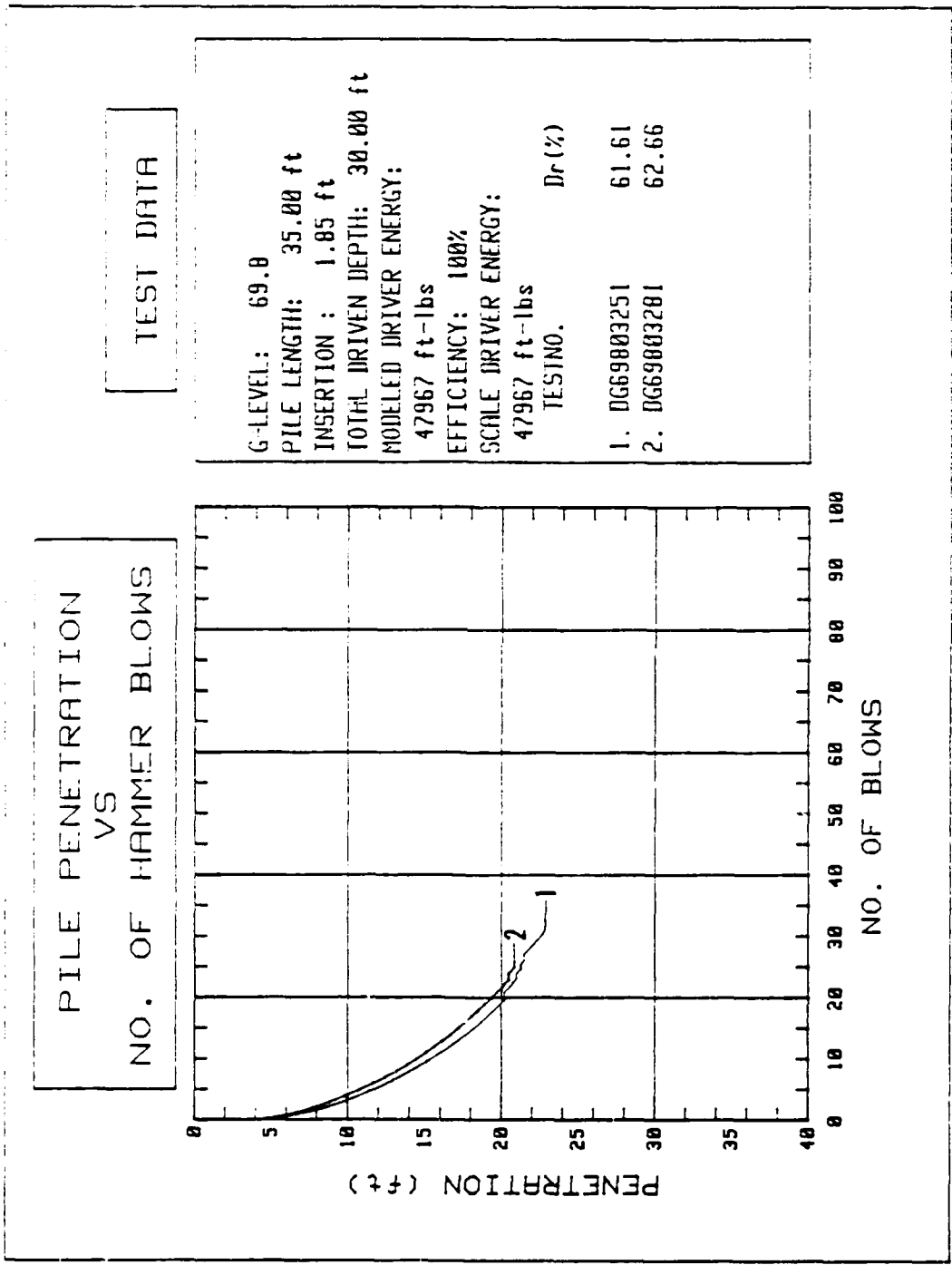


Figure 5-24 Pile Penetration vs. Number of Hammer Blows, Single Pile, DG69803251, DG69803281

not attached. The tilt of the hammer did not appear to adversely affect the performance of the proximity device.

Tests DG69803291, DG69803292, and DG69803182 (Figure 5-25) demonstrate the effect of increasing resistance to penetration per blow with respect to depth. Furthermore, the tests show an increasing number of blows are required to drive the pile to depth as the relative density of the specimens is increased. This relationship is developed in Section 5.3.2, Quantitative Discussion of Driven Model Pile Test Results. The tests which were terminated exhibit the same tendency for increased number of blows for a given penetration with respect to an increase in the relative density of the specimen.

The pile driven in test DG69803292 was the first driven pile to be successfully load tested. The pile demonstrated a significantly different load curve shape (Figure 5-26) and ultimate capacity compared to model piles which had been pushed in. The pile developed no strength until the butt had been deflected 1.5 scale inches. The butt had to be deflected a total of 5.0 scale inches before the resistance to load equaled 100 scale kips. Manipulation of the Load Test portion of the main program permitted the butt to be deflected an additional 3.5 scale inches resulting in an ultimate resistance of 120 kips. Pushed model piles with an ultimate resistance to penetration of 120 kips can be expected to develop an ultimate capacity of approximately 100 kips based on the results of pushed individual piles.

This performance bears no resemblance to the loading curve of the pushed piles although the ultimate resistance to pushing is equal in magnitude. Several causes are suspected: disturbance of the pile during placement of the load cell, release of some of the residual stresses

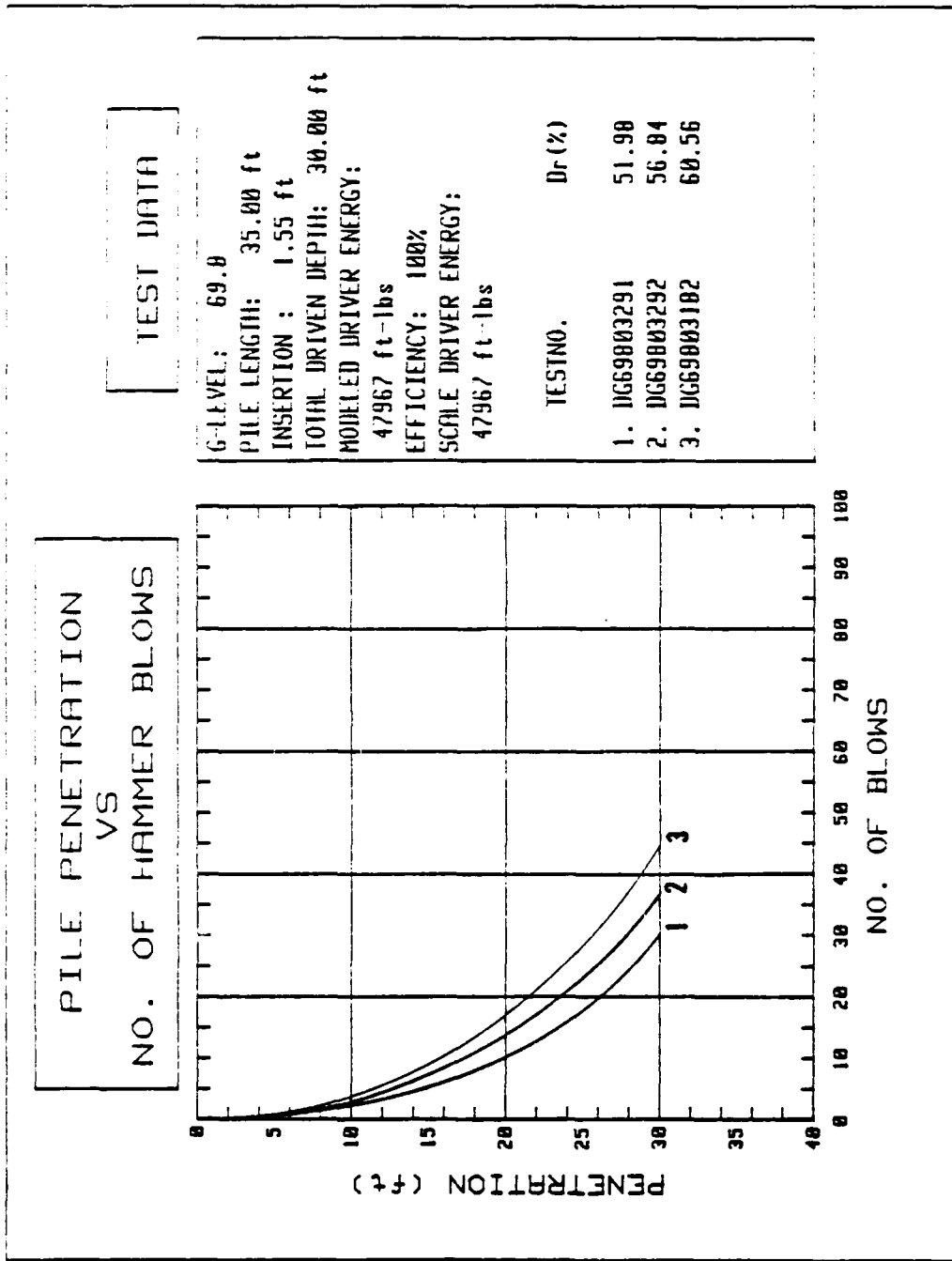


Figure 5-25 Pile Penetration vs. Number of Hammer Blows, Single Pile, DG69803291, DG69803292, DG69832182

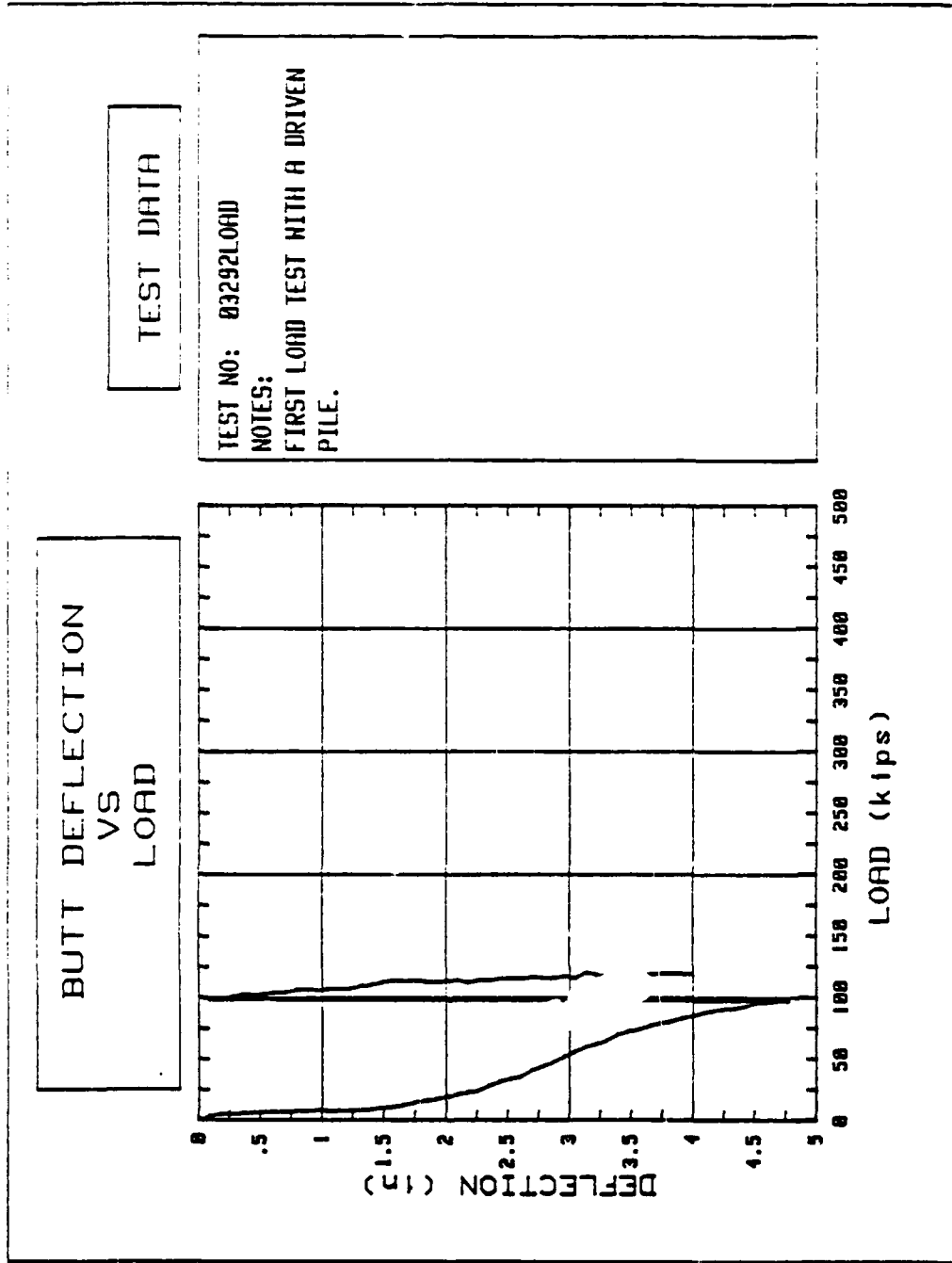
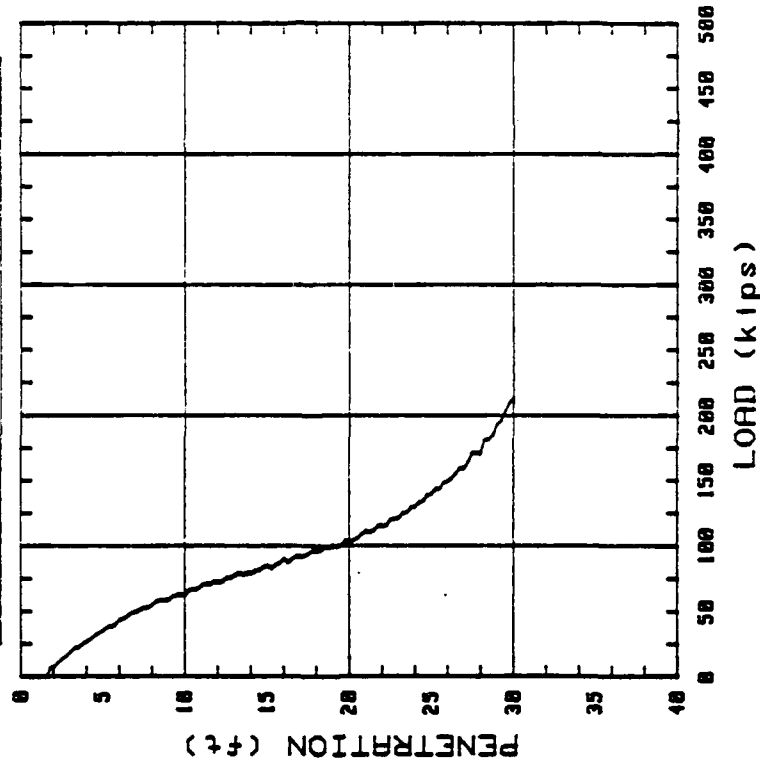


Figure 5-26 Butt Deflection vs. Load, Single Pile, DG69803293

PILE PENETRATION
VS
LOAD



TEST DATA

TESTNO: PG69003293
G-LEVEL: 69.0
PILE LENGTH: 35.00 ft
INSERTION : 1.55 ft
TOTAL DRIVEN DEPTH: 30.00 ft
REID-BEDFORD SAND:
DRY UNIT WEIGHT: 90.3 pcf
VOID RATIO: .69
REL. DENSITY: 56.84 %
NOTES:
SAME SPECIMEN AS DG69003292

Figure 5-26--continued

resulting from the driving process, and improper seating of the load cell adaptor on the pile butt. Each will be discussed briefly.

Placement of the load cell requires the pile cap be lifted off the butt leaving the pile free-standing in the specimen. Typically, the pile is restrained by a holding device inserted through the slotted guide tube and the cap lifted off. However, after being struck 50 times, the cap is rather firmly attached to the butt. The connection between the cap and butt must be "broken" before the cap can be removed.

Therefore, it is suggested the soil particles at the pile soil interface may be disturbed if the butt is moved back and forth or the pile pulled even slightly out of the ground during removal of the cap. The slight retraction of the pile may account for the sluggish increase in load bearing capacity of the model. The ultimate capacity of the driven pile approaches that of a pushed model because the driven pile was pushed in almost nine scale inches during load testing. The important considerations in the conduct of the load test on the driven model are then to test the model immediately after placement, without disturbing the model.

Residual stresses may have been released during the cycling of the centrifuge for load cell placement. More research is suggested to better understand the development of such stresses and their possible release by interrupting the flight of the centrifuge. The placement of strain gages at the pile butt and development of a suitable bridge completion circuit will permit the load test to be conducted immediately following the driving of the pile without removing the cap. This will provide the most accurate information regarding residual stresses and their contribution to bearing capacity.

Lastly, the adaptor which is connected to the load cell and slips over the pile butt may not have seated properly on the butt. The receptacle on the bottom of the adaptor was formed by drilling an oversize hole. The conical depression left by the drill bit may not be suitable for seating the butt unless the butt happens to be exactly centered in the adaptor. The hole was drilled oversize to lessen the possibility of the adaptor exerting a lateral stress on the butt.

Test PG69803293 (Figure 5-26) was conducted on the same specimen as DG69803292 to determine the bearing capacity of a pile pushed into the same soil. The tests were conducted 10 pile diameters apart. The pile was successfully pushed in, but the load test was not conducted due to a separation of the load cell wires from their housing in the centrifuge. Capacity of this pile was estimated at 125 kips based on the performance of other pushed piles at this relative density.

5.3.2 Quantitative Discussion of Driven Model Pile Test Results

Tests DG69803291, DG69803292, and DG69803181 were conducted with a hammer weight of 20.0 grams and a hammer input efficiency of 100%. Figure 5-27 presents the number of blows required for full penetration versus the relative density of the soil. The plot verifies the increasing resistance to penetration as the relative density increases within the range tested. The linearity of the plot is a coarse indication of the quality of the specimens, both in relative density and uniformity, and the ability of the hammer to impart equal energy with each blow.

The number of impacts required to drive the pile to depth is significantly less than that of a prototype pile. This may be attributed to four factors; hammer weight, hammer shape, model cap weight, and contact area between the model pile and soil. Considering the hammer properties,

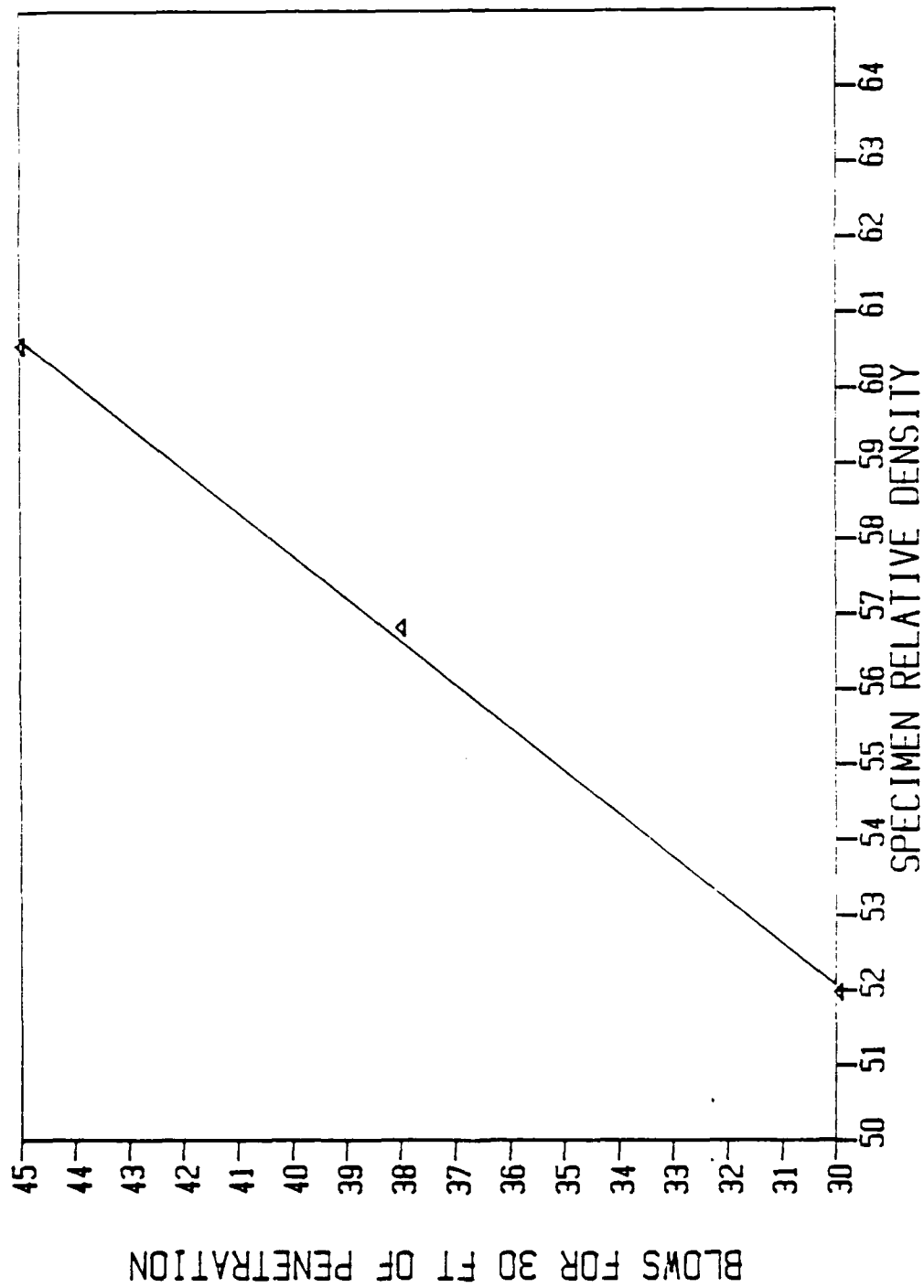


Figure 5-27 Hammer Blows (100% Efficiency, 20 Gram Hammer) for 30 Scale Feet of Penetration vs. Specimen Relative Density

the weight and shape both contribute to efficient transfer of energy to the pile. The model hammer weight is 2.4 times the weight suggested by the program DRIVEPILE. The heavier hammer has more momentum than the suggested lighter hammer for the specific weight and fall height combination. The flatness of the hammer imparts a relatively high percentage of the available energy (Figure 2.5) to the cap and butt resulting in more set per blow of the hammer. Regarding the cap weight, the relatively massive size of the cap ensures the cap and butt remain in contact permitting more complete transfer of energy. Lastly, the relatively larger size of the soil particle with respect to the pile decreases the contact area of the soil particles with the piles. This effect may be further amplified at higher g-levels as the potential for soil arching around the model increases. Arching would tend to decrease even further the contact area between model pile and soil resulting in relatively easier penetration. All of the above factors contribute to a decrease in the number of blows required for a given penetration, with specimen relative density being held constant.

The improved cap design may permit higher "efficiencies" during driving. This is expected to lead to an exponential decrease in required number of blows rather than linear due to the way efficiency of the input energy is computed. The efficiency is considered to double as a result of doubling the lift height. However, efficiency will be more than doubled as the kinetic energy ($0.5 mv^2$) of the hammer is increased by a factor of 3.30 when the lift height is doubled. The product of the lift height and hammer weight gives the work done in lifting the hammer, but, the available energy is dependent on the kinetic energy of the hammer at impact.

5.4 Reproducibility of Results

Both the pushing and driving test results indicated a high degree of reproducibility once the process of manufacturing a uniform specimen had been established. Use of the placement device in the driving mode provided very precise results in that differences of approximately 0.5% relative density were sufficient to result in a greater or lesser number of blows required for a given penetration depending on the shift of the density. This tendency is borne out by the linearity of the plot in Figure 5-27.

Conduct of a sufficient number of tests with the hammer weight and efficiency being held constant may permit the driving of a model pile (or cone) to become a method of determining specimen characteristics in flight. More significantly, the influence of one model pile being driven near a previously placed model can be investigated simply by monitoring the blows required to drive the second and subsequent models. The ability to accurately measure residual stresses with appropriately positioned strain gages is of paramount importance in this endeavor as it is just as important to measure the effect the pile being driven has on the already driven pile. Using strain gages, the determination can be made as to whether the residual stresses in the first pile relieve themselves due to the disturbance caused by the driving of the second pile or whether the stresses and lateral forces on the pile are somehow augmented. The placement device is well suited for this type of research when used in the driving configuration because of the inherent reproducibility of the energy being imparted from the hammer to the pile cap.

The placement device has the prospect of producing very repeatable results when used in the pushing configuration once the guide tube attachment is stiffened. Although the results of the push tests indicated a variation between the scale capacities of the same type of models at the different test g levels, the capacities of the 69.3 g models were consistently higher than those of the same type models tested at 36.0 g's. This difference is attributed to the progressive weakening of the guide tube combined with the relatively greater force needed to push the 69.3 g models to depth. This determination is made pending the development of a sufficiently sensitive strain gage bridge completion circuit which would permit the effect of the guide tube to be quantified.

An accurate strain measuring system would fulfill two purposes in the investigation of the guide tube effects. First, the gages would indicate the development of excessive bending stresses in the model. This information would precede the failure of the pile giving an indication before the destruction of the model. Second, the strain gages would aid in determining the source of the pile's resistance to penetration. If, as currently suspected, the models displace laterally under increasing axial loads, the bending stresses at the top of the soil surface will be significantly greater than the stresses due solely to axial load. However, if the source of resistance to penetration is due to the contributions of the tip and imbedded portion of the pile with no undue bending stresses, then the current design of the guide tube may be sufficient. A very important benefit of refining the placement device by strengthening of the guide tube and development of

usable strain gage circuitry will be the accurate determination of the magnitudes of sidewall friction mobilized during placement of the model.

The friction forces acting on the pile are considered to be affected by the gravity level at which testing is done. This was demonstrated by pulling model piles from the soil at three different g levels with the lower g level models developing significantly greater resistance to movement. The same effect is expected when the models are pushed into the soil. Thus, strengthening the guide tube in an effort to lessen the suspected lateral freedom of the pile and development of a working strain gage circuit to help quantify any improvement will tend to increase the accuracy, and thus, the repeatability of the results.

As mentioned, the reproducibility of results is dependent on the ability to create uniform specimens and accurately determine their relative density. The method of raining soil into the specimen container worked well and should continue to be used. However, improvement may result if a device can be made to more precisely meter the "flow" of the sand through the stacked sieves. Specimen creation was the most operator-dependent aspect of this research and, as such, has a significant potential for improvement.

5.5 Modeling of Models

Given the high degree of similarity between the model pile (group) responses to loading with respect to efficiency and the proportionate increase in the model responses between the two g levels, the two models are essentially in agreement. Strict modeling of models requires the scale axial stiffness be the same in all models. This was not accomplished and has been suggested as the cause for the minor differences

between the response of like models at the two g levels. Likewise, the inability of modeling the soil grain sizes may have contributed to the slight differences in model response.

Considering that a pile driven into granular soils may develop 25 to 30% of its capacity from sidewall friction, this aspect of modeling requires further attention. The determination must be made as to the g level and model pile size combination at which the sidewall frictional forces are not being modeled correctly. Combined research involving the accurate modeling of scale axial stiffness and soil grain size will improve the reproducibility of results.

5.6 Comparison with a Prototype

The loading curves of the individual and group of five model piles have the same characteristic shapes as those of prototype piles. The model responses to loading exhibit easily distinguished break points making the model capacity easily and accurately determined by the deBeer method. However, two significant differences appear when the model is compared to the prototype. The initial slope of the loading curve of all model piles is substantially less than the prototype and the scale capacities greater. The differences can be attributed to several causes, among them, inaccurate modeling of the scale axial stiffness, the possible loss of unit sidewall friction forces at progressively higher g levels as discussed previously, differences between the model and prototype soil conditions, and alteration of the load test procedure in the centrifuge.

The relatively low axial stiffnesses of the models is considered to be a direct cause of the low initial loading curve slope. The 69.8 g

model's responses were altered more significantly than those of the 36.0 g model's as evidenced by Figure 5-20. The unique effect of the lower axial stiffnesses on the model's responses are masked by the still undetermined effects caused by not modeling the soil grain size. Quantifying the different effects can most easily be accomplished by manufacturing a variety of model piles with the same axial stiffness. Testing model piles which are scaled based on the outer diameter of available stock tubing can be made more accurate by honing (or reaming) the inside of the appropriate models until the axial stiffness of all models is equal to that of the least stiff model. The honing process will leave the interior of the pile model well suited for the application of strain gages. Naturally, the range of relative densities available for testing decreases as the models are weakened; likewise, the initial loading modulus. However, it will be easier to distinguish the ratio of model pile size to specimen grain size at which the unit side friction begins to be altered.

Roughening the exterior of the model piles should also be investigated as an alternative in increasing the initial loading modulus of the pile (group). Circumferential scoring (as opposed to longitudinal) is recommended as this may induce an element of bearing capacity along the sidewall which can be adjusted (by varying the depth and spacing of the scores) to be the equivalent of a true frictional resistance. Likewise, the unit sidewall friction of the model may be enhanced by a covering of grit or abrasive powder glued in place. Each of the above techniques leaves the interior of the model available for the placement of strain gages.

Regarding the differences between the model and prototype soil conditions, the model capacity may be higher due to it being tested in a dry soil whereas the suggested prototype was driven into hydraulic fill with the water level being seven feet below the ground surface. The lower effective stresses at the tip of the driven piles contribute to a marked decrease in the ultimate capacity. Testing in saturated soils may shift the model capacity more in line with that of the prototype.

Lastly, the response of the models may be altered by the technique used to conduct the load test. The butt was deflected and then force measured as opposed to the application of a constant force with the measurement of resulting settlement being measured over time. This permits the soil around the model to relax resulting in a decrease in the apparent load on the model over time. Load readings were taken almost instantaneously by the data acquisition unit, however, the potential exists for error if too much time is permitted between deflection and reading. It is suggested the readings from the load cell be read at a relatively high frequency to determine if static forces are maintained on the butt or if a peak force develops and then dissipates after each deflection of the butt. Furthermore, a higher frequency data collection system would permit the stepper motor to load the pile with a more continuous push potentially altering the shape of the load curve.

5.7 Strain Measurement

The chosen strain gages and bridge completion circuit were not suitable for measuring strain in the models. Several causes are suspect. The gages were examined microscopically to ensure they were well bonded and it appeared the method of gage placement was satisfactory.

Resistance of the gages was checked and all gages which were used in the initial system checkout were within 0.5 ohms of the nominal 120 ohm resistance. Each of the gages was then checked for being insulated from the model pile. Again, all was satisfactory. A final gage was installed on the outside of the first test pile adjacent to the position of one of the gages inside the pile to determine if it was the placement method or the bridge completion circuit at fault.

Each of the eight bridge completion circuits was checked out by placing a known working gage in the circuit and checking the system output in response to a known input strain. After balancing each circuit, the gage was subjected to various inputs of tensile and compressive forces. The tests were conducted through the slip rings of the centrifuge. Each circuit operated correctly.

The model piles, one 69.3 g model and one 86.0 g model, were then independently connected to the appropriate bridge completion channels and tested. Stable zeroed readings could not be obtained for any of the gages. Finger pressure on the gages sites caused erratic readings and the gages responded very poorly to axial compressive strain. Readings were not stable or repeatable. The gage mounted on the outside of the 69.8 g model responded as poorly as did the gages on the inside. All gages responded in the proper sense regarding compression or tension, however, no accurate value of strain could be determined. The 69.8 g model was calibrated over ten times using the calibration support and CALTEST program with the results being nonrepeatable. Slight changes in temperature at the gage site appeared to adversely affect the performance of the gage.

The chosen strain gages were temperature compensated for steel instead of the aluminum of the models. Temperature compensation is necessary in a gage as the thermal coefficient of expansion of the gage alloys is matched to the expansion coefficient of the material to which the gage is bonded. This matching of coefficients ensures both gage and specimen material expand (strain) the same amount in response to changes in temperature. Mismatching of the temperature compensation characteristics can lead to erratic readings and an inability to balance the circuit prior to testing as was experienced. This type of gage has been reported to perform adequately in prior research efforts, however, it is recommended all strain measurements be taken using gages temperature compensated for aluminum.

Additional strain gages were purchased which were temperature compensated for aluminum, but the gages had a nominal resistance of 350 ohms and could not be used in the available bridge completion circuit. Therefore, a new bridge completion circuit must be built to test the suitability of the new gages. The 350 ohm gages are more suitable for this type of measurement for two reasons. The gages are more sensitive to strain by a factor of 2.92 (350/120) and the higher resistance means less current passes through the gage. Both of these responses can be explained using Ohm's law, $V = IR$. In a constant current (I) system, the voltage output (in response to strain) is directly related to the resistance (R) of the gage. Placing a higher resistance gage in the circuit provides a higher output voltage for a given strain. In a constant voltage system, increasing the gage resistance decreases the current passed through the resistive element. Since power (P) is dissipated by the element according to the relationship $P = I^2R$, the heat

generated by a strain gage is lessened as the nominal resistance of the gage is increased, all else being equal. Thus, the higher resistance gage may be found more suitable because of its temperature compensation, increased sensitivity, and decreased heat generation.

CHAPTER 6
CONCLUSIONS AND RECOMMENDATIONS

6.1 Conclusions

A placement device was designed and built for the purpose of driving and pushing model piles (groups) under a gravitational force of 90 g's. The capacities of individual piles, groups of four, and groups of five piles were studied to determine how well the device performed and also the feasibility of modeling group pile responses in the centrifuge. Scale models based on the Hunter's Point prototype were tested at 59.8 g's and 86.0 g's. The following conclusions were drawn.

1. The results of the driven model pile tests indicate a linear relationship between the number of blows required for the model to penetrate 30 scale feet and the relative density of the specimen over the range of 50 to 65% relative density. The pile driver delivers a uniform amount of energy throughout the travel of the pile which is made possible by the readjustment of the lift height after every impact of the hammer. The portion of the pile inserted at one g contributes little to the ultimate capacity of the model. Rather, capacity is developed by the driving penetration of the model at the appropriate test g level. The relatively massive weight of the model hammer, its flat shape, and the large model cap all act to improve the efficiency of the energy transfer from hammer to pile and result in a scale set of almost 1.0 feet per hammer blow (69.8 g's, 20 gram hammer weight, 100% driver efficiency). Adjustment of

the "efficiency" of the driver is an effective means of controlling the input energy and thus blows required for penetration.

2. The scaling effects introduced by not modeling the soil grain size have little effect on the bearing capacity of the pile tip(s), however, the friction on the shaft may be greatly influenced. Results are based on pullout tests in which the scale resistance to pullout decreased exponentially in relation to the decrease of the test g level. Results are inferred to apply to friction forces experienced during pushing of the pile(s) and must be verified through the use of strain gages mounted along the shaft.
3. Axial stiffness of the pile(s) must be precisely modeled to permit the direct comparison of results obtained from different g level tests. The relative axial strength of the models was apparent in the comparison of results between the same type of models at the two test g levels. The less axially stiff 69.8 g models consistently demonstrated lower initial strength moduli during load tests. The 86.0 g models (95.4% as axially stiff as the Hunter's Point prototype) are considered to have responded most like the prototype.
4. The deBeer method of pile capacity determination is well suited for interpreting the capacity of model piles. The method simply highlights the "break" in the load test curve instead of determining model capacity based on resistive forces which may exist only in the prototype (i.e., sidewall friction). Single model pile tests at 69.8 and 86.0 g's give close agreement with the group of four models and group of five models showing progressively more divergence as the relative density of the specimen is increased. This divergence has been attributed to the relatively low axial stiffness of the

69.3 g model and the lack of rigidity in the connection of the cast acrylic guide tube to the supporting c-channel.

5. The shape of the load versus deflection curves is generally similar to the shape of the prototype loading curve. However, the initial loading modulus of the model pile is significantly lower than that of the prototype and the ultimate capacity greater. The low initial modulus is thought to be the result of the method by which the load test is conducted, the relatively low axial stiffness of the models, and the progressive decrease in unit sidewall friction on the model at higher g levels.

The conduct of the model load test involves deflection of the butt and subsequent measurement of the resistive force developed by the pile. This is opposite from the method of conduct of the load test on prototype piles as they are loaded with a constant static force and the resulting deflection is measured over some specified time period. This difference in the method of load testing is thought to lower the initial loading modulus. Circumferential grooving of the model or the coating of the model with an abrasive, gritty material may improve this response.

The high scale model capacity is considered to be due to the models being pushed into a dry specimen, unlike the prototype, which is driven into hydraulic fill and rests in saturated soil.

6. The driving of the model pile is considered to result in the creation of different stresses, and thus, unit capacities at the tip and along the sidewall of the model. These factors contribute to the difference in the load curves of the driven model versus the pushed model. However, the residual stresses and soil structure around the

model are disturbed when the centrifuge is stopped to permit the load cell to be fixed to the butt of the driven pile. The effects of the different stresses created during driving can be quantified by the placement of strain gages at the butt. This will permit the driven model to be load tested immediately after placement and without being disturbed.

7. The pushed pile groups show efficiencies which increase in response to an increase in the relative density of the specimen and also to the introduction of the fifth pile in the center of the group of four. Both increases are very slight. Most significantly, the placement device is capable of accurately discerning these slight differences. Parametric studies of the change in efficiencies resulting from the variation of pile spacing and configuration within a group are warranted. A factor of safety of 1.0 for pile groups in dry granular soils appears to be conservative.
8. During the driving process, the rigidity of the connections between the guide rod, pile cap, and model pile butt appear to be the limiting factors in the driveability of the pile. Improper connections at these joints leads to stress concentrations and buckling failure of the butt. When models are pushed, the connection between the cast acrylic support tube and supporting c-channel appears to be a limiting factor in the amount of axial load a pile (group) can withstand. Looseness at the connection permits the tube to move sideways during axial loading causing premature failure of the model.
9. The inability to measure strain, and thus force, in the model pile during placement and loading is a severe limitation. Development of an accurate strain measuring circuit will permit the continuous

measurement of pile response to placement and loading to be recorded on the available digital recording oscilloscopes. This will permit more flexibility in the capabilities of the multi-programmer to control the placement device as progress of the placement (driving or pushing) routine will not have to be paused during the measurement of pile response. The use of the digital recording oscilloscope will also permit the high frequency response of the pile to driving forces to be investigated.

10. The pile placement device exceeds the capability of modeling any known single acting pile driver and can drive model piles up to scale depths of 30.0 feet at g-levels up to 90 g's. This capability is subject to the limitations presented in Section 4.7, Equipment Limitations, and may be expanded as the influence of container boundaries on the modeling process are better understood. The device has also demonstrated the capability of pushing model pile groups with a scale force in excess of 1,250 scale kips. The device can measure to within 0.053 scale inches at 69.3 g's and 0.043 scale inches at 86.0 g's.
11. The placement device can perform a variety of penetration routines and loading regimes with program changes being made simply by the rearrangement of a variety of subroutines. The complete computer control of all pieces of equipment used during testing and the recording of all data in scale units lessens the potential for the operator to influence the test result or their interpretation. Furthermore, initialization of the program with scale pile dimensions and actual specimen container dimensions permits the computer

to determine whether the proposed penetration is possible within the limitations of the device and act accordingly.

6.2 Recommendations

1. Development of a working strain gage circuit should be given the highest priority. The method of gage placement appears to be satisfactory and results in a model well suited for the measurement of response to driving forces. A working strain gage system will permit the measurement of residual stresses, their change with respect to time, and the measurement of transient waveforms associated with the driving of the model. Mounting a strain gage rosette inside the model may permit the determination of lateral stresses acting on the model. Strain gages are available which consist of ten separate miniature gages in a short length for measurement of high strain variation gradients. This type of gage mounted in the tip of the model would more clearly indicate the development of stresses around the tip during penetration than does the pair of single axis gages.
2. The capacity of driven models should be investigated upon completion of a working strain gage bridge. The immediate conduct of a load test on a driven pile without stopping the centrifuge and disturbing the soil around the model will provide the most accurate measure of its capacity. The determination can then be made as to whether the interruption of the flight during driving or between driving and loading affects the model capacity.
3. The available mini-cone should be tested in the centrifuge and results compared between the driving and pushing of the cone. This will aid in the determination of how much the development of

residual stresses around the cone (pile) is altered by the two methods of placement.

4. Saturated soils and clays should be used as specimens for both the driving and pushing of model piles. The larger model piles may even be suited for the placement of pore pressure meters at the tip and along the shaft. This will permit the measurement of transient pore pressures and their dissipation over time.
5. The effects of modeling the soil grain size should be investigated to determine the relative sizes at which the grains become too large and adversely affect the test results. This information may become available once the strain gage circuit is developed, however modeling of the grain sizes appears to be more beneficial as it may expand the range over which tests may be conducted.
6. Group effects should be studied to determine the optimum spacing and number of piles required for different soils and loads. Piled foundations should also be investigated in an effort to determine the minimum number of piles required for a given load and soil type. The placement device has the static capacity of loading a reasonably sized model foundation with approximately 1.5 million scale pounds.

APPENDIX A
PI TERM DERIVATION AND
SCALING LAW DEVELOPMENT

Table A-1 Pisets Input Matrix

	L	V	E	r	a	E_n	I	C	T	D	F	D	A
M	0	1	1	1	0	1	1	0	0	0	1	0	0
L	1	-3	-1	-1	1	2	1	-1	0	1	-1	1	2
T	0	0	-2	-2	-2	-2	-1	-2	1	-1	-2	0	0
π_1	0	0	-2	2	0	0	0	0	0	0	0	0	0
π_2	2	2	-2	0	2	0	0	0	0	0	0	0	0
π_3	-6	0	-2	0	0	2	0	0	0	0	0	0	0
π_4	-6	-1	-1	0	0	0	2	0	0	0	0	0	0
π_5	0	0	-2	0	0	0	0	2	0	0	0	0	0
π_6	-2	-1	1	0	0	0	0	0	2	0	0	0	0
π_7	0	1	-1	0	0	0	0	0	0	2	0	0	0
π_8	0	0	-2	0	0	0	0	0	0	0	2	0	0
π_9	-2	0	0	0	0	0	0	0	0	0	0	2	0
π_{10}	-4	0	0	0	0	0	0	0	0	0	0	0	2

Table A-2 Pi Terms

π_1	Stress	σ	=	$\frac{\sigma^2}{E^2}$	=	$\frac{(M/LT^2)^2}{(M/LT^2)^2}$
π_2	Acceleration	a	=	$\frac{a^2 D^2 \gamma^2}{E^2}$	=	$\frac{(L/T^2)^2 L^2 (M/L^3)^2}{(M/LT^2)^2}$
π_3	Impact Energy	E_n	=	$\frac{E_n^2}{E^2 D^6}$	=	$\frac{M^2 L^4 / T^4}{(M^2 / L^2 T^4) L^6}$
π_4	Impulse	I	=	$\frac{I^2}{\gamma D^6 E}$	=	$\frac{M^2 L^2 / T^2}{(M/L^3) L^6 (M/LT^2)}$
π_5	Cohesion	C	=	$\frac{C^2}{E^2}$	=	$\frac{(M/LT^2)^2}{(M/LT^2)^2}$
π_6	Dynamic Time	T	=	$\frac{ET^2}{D^2 \gamma}$	=	$\frac{M/LT^2 (T^2)}{(L^2) M/L^3}$
π_7	Wave Speed	P	=	$\frac{\gamma P^2}{E}$	=	$\frac{M/L^3 (L^2/T^2)}{M/LT^2}$
π_8	Yield Strength	F	=	$\frac{F^2}{E^2}$	=	$\frac{M^2/L^2 T^4}{M^2/L^2 T^4}$
π_9	Displacement	D	=	$\frac{D^2}{L^2}$	=	$\frac{L^2}{L^2}$
π_{10}	Area	A	=	$\frac{A^2}{D^4}$	=	$\frac{L^4}{L^4}$

Table A-3 Scaling Law Derivation

	Scale length factor	n	=	L _p /L _m	therefore, L _m	=	1/n L _p
	Gravity	n	=	g _m /g _p	therefore, g _m	=	n g _p
π ₁	Stress		=	$\frac{\sigma^2}{E^2}$			
				$\frac{\sigma_m^2}{E_m^2}$		=	$\frac{\sigma_p^2}{E_p^2}$
				σ_m^2		=	$\sigma_p^2 \frac{E_m^2}{E_p^2}$
							$\frac{E_m^2}{E_p^2} = 1$
				σ_m		=	σ_p
π ₂	Acceleration		=	$\frac{a^2(D^2)\gamma^2}{E^2}$			
				$\frac{a_m^2(D_m^2)\gamma_m^2}{E_m^2}$		=	$\frac{a_p^2(D_p^2)\gamma_p^2}{E_p^2}$
				a_m^2		=	$a_p^2 \frac{D_p^2(\gamma_p^2) E_m^2}{D_m^2(\gamma_m^2) E_p^2}$
							$\frac{D_p^2}{D_m^2} = 1$
							$\frac{\gamma_p^2}{\gamma_m^2} = 1$
							$\frac{E_m^2}{E_p^2} = 1$

Table A-3--continued

$$a_m^2 = a_p^2 n^2$$

$$a_m = n a_p$$

$$\tau_3 \text{ Impact Energy} = \frac{E_n^2}{E^2} (D^6)$$

$$\frac{E_n^2}{E_m^2 (D_m^6)} = \frac{E_n^2}{E_p^2 (D_p^6)}$$

$$E_n^2 = E_p^2 \frac{E_m^2 (D_m^6)}{E_p^2 (D_p^6)}$$

$$\frac{E_m^2}{E_p^2} = 1$$

$$\frac{D_m^6}{D_p^6} = \frac{1}{n^6}$$

$$E_n^2 = E_p^2 \left(\frac{1}{n^6} \right)$$

$$E_n = \frac{1}{n^3} E_p$$

Table A-3--continued

$$\pi_4 \quad \text{Impulse} \quad = \quad \frac{I^2}{\gamma(D^6)E}$$

$$\frac{I_m^2}{\gamma_m(D_m^6)E_m} \quad = \quad \frac{I_p^2}{\gamma_p(D_p^6)E_p}$$

$$I_m^2 \quad = \quad I_p^2 \frac{\gamma_m(D_m^6)E_m}{\gamma_p(D_p^6)E_p}$$

$$\frac{\gamma_m}{\gamma_p} \quad = \quad 1$$

$$\frac{D_m^6}{D_p^6} \quad = \quad \frac{1}{n^6}$$

$$\frac{E_m}{E_p} \quad = \quad 1$$

$$I_m^2 \quad = \quad I_p^2 \frac{1}{n^6}$$

$$I_m \quad = \quad \frac{1}{n^3} I_p$$

$$\pi_5 \quad \text{Cohesion} \quad = \quad \frac{C^2}{E^2}$$

$$\frac{C_m^2}{E_m^2} \quad = \quad \frac{C_p^2}{E_p^2}$$

Table A-3--continued

$$C_m^2 = C_p^2 \frac{E_m^2}{E_p^2}$$

$$\frac{E_m^2}{E_p^2} = 1$$

$$C_m^2 = C_p^2$$

$$C_m = C_p$$

π_6 Dynamic Time = $\frac{ET^2}{D^2\gamma}$

$$\frac{E_m T_m^2}{D_m^2 \gamma_m} = \frac{E_p T_p^2}{D_p^2 \gamma_p}$$

$$T_m^2 = T_p^2 \frac{E_p (D_m^2) \gamma_m}{E_m (D_p^2) \gamma_p}$$

$$\frac{E_p}{E_m} = 1$$

$$\frac{D_m^2}{D_p^2} = \frac{1}{n^2}$$

$$\frac{\gamma_m}{\gamma_p} = 1$$

Table A-3--continued

$$T_m^2 = T_p^2 \left(\frac{1}{n^2} \right)$$

$$T_m = \frac{1}{n} T_p$$

$$\pi_7 \quad \text{Wave Speed} = \frac{\gamma p^2}{E}$$

$$\frac{\gamma_m p_m^2}{E_m} = \frac{\gamma_p p_p^2}{E_p}$$

$$p_m^2 = p_p^2 \frac{\gamma_p E_m}{\gamma_m E_p}$$

$$\frac{\gamma_p}{\gamma_m} = 1$$

$$\frac{E_m}{E_p} = 1$$

$$p_m^2 = p_p^2$$

$$p_m = p_p$$

Table A-3--continued

$$\pi_3 \quad \text{Impact Energy} = \frac{E_n^2}{E^2 D^6}$$

$$\frac{E_n^2}{E_m^2 D_m^6} = \frac{E_n^2}{E_p^2 D_p^6}$$

$$E_n^2 = E_p^2 \frac{E_m^2 D_m^6}{E_p^2 D_p^6}$$

$$\frac{E_m^2}{E_p^2} = 1$$

$$\frac{D_m^6}{D_p^6} = 1$$

$$E_n^2 = E_n^2$$

$$E_n = E_n$$

$$\pi_9 \quad \text{Displacement} = \frac{D^2}{L^2}$$

$$\frac{D_m^2}{L_m^2} = \frac{D_p^2}{L_p^2}$$

$$D_m^2 = \frac{D_p^2 L_m^2}{L_p^2}$$

Table A-3--continued

$$\frac{L_m^2}{L_p^2} = \frac{1}{n^2}$$

$$D_m^2 = D_p^2 \frac{1}{n^2}$$

$$D_m = \frac{1}{n} D_p$$

$$\pi_{10} \text{ Area} = \frac{A^2}{D^4}$$

$$\frac{A_m^2}{D_m^4} = \frac{A_p^2}{D_p^4}$$

$$A_m^2 = A_p^2 \frac{D_m^4}{D_p^4}$$

$$\frac{D_m^4}{D_p^4} = \frac{1}{n^4}$$

$$A_m^2 = A_p^2 \frac{1}{n^4}$$

$$A_m = \frac{1}{n^2} A_p$$

NOTE: Scaling laws are formulated by equating model Pi terms to the prototype Pi terms using the scale length factor (n) and canceling like material properties.

APPENDIX B
NUMBER THEORY AND DIGITAL, OCTAL, AND DECIMAL
CONVERSION ALGORITHMS

Use of the Hewlett-Packard 6940B multiprogrammer requires a cursory understanding of number theory as all data transferred within the computer and between peripherals is accomplished using one of the three base number systems; Binary, base 2, Octal, base 8, and Decimal, base 10. All three of the systems share the characteristic that each digit is weighted by a power of the base and that power increases by one for each successive digit to the left with the right-most digit to the left of the decimal point being raised to the zero power.

$$b^4 \quad b^3 \quad b^2 \quad b^1 \quad b^0 \quad .b^{-1} \quad b^{-2} \quad b^{-3}$$

The decimal system has been used by mankind for thousands of years and is the system of preference in most economies. It is the base 10 system because it has 10 unique characters which can be used for counting (0 through 9). However, computers require a much simpler language with fewer characters in order to process information at high rates. Therefore, the binary language has been adopted as "machine language". Binary numbers are represented by only two unique characters (0 and 1) which are easily communicated by electronic devices as being either a low or high voltage state. Thus, any number value can be communicated by a string of low and high voltage pulses. However, these strings can be rather cumbersome when dealing with large numbers and quite difficult

to manipulate if programmers had to use binary coding in their communications with computers. Instead, Octal numbers are used in the programming of the multiprogrammer cards. The Octal system has eight unique characters (0 through 7) and there is a simple relationship between Octal, Decimal, and Binary numbers which makes the Octal system useful to humans as well as computers. Three Binary digits allow us to represent eight unique values, for example, 000 Binary equals 0 Decimal, 001 Binary equals 1 Decimal, 010 Binary equals 2 Decimal, etc. Since a single Octal digit may also represent any of eight unique values, a single Octal Digit can be used to represent a Binary triad. Conversion from Binary to Octal or the reverse is accomplished by inspection as shown below.

011000010101001	Binary
	to
3 0 2 5 1	Octal
6 1 4 7 5	Octal
	to
110001100111101	Binary

The Octal number is more easily understood and remembered by programmers than the Binary equivalent. It is also easily converted to or derived from its Binary counterpart and is therefore closely related to the machine language of computers. The Binary value transmitted in twelve digits (four triads) can be transmitted just as simply by four Octal digits and be easily understood by both programmer and computer. The relationship between the three systems is then complete once the conversion from Decimal to Octal and back is understood. The following methods can be used. The information above and algorithms presented below are as shown in Appendix A of the Hewlett-Packard 6940B

'Multiprogrammer User's Guide. Only the methods for dealing with positive number values will be introduced. The User's Guide should be consulted for a better understanding of negative Octal and Decimal numbers and their manipulation by digital electronic data calculating devices.

Conversion from Decimal to Octal:

1. Divide the Decimal number by 8 and write down the remainder.
2. Divide the quotient of step one by 8 and write down the remainder.
3. Repeat step 2 until the quotient is zero. The last remainder is also retained.
4. The reverse of the remainders obtained is the Octal representation of the Decimal number. See the example below.

Determine the Octal equivalent of 3,981 Decimal.

$$3,981/8 = 497, \text{ remainder } 5$$

$$497/8 = 62, \text{ remainder } 1$$

$$62/8 = 7, \text{ remainder } 7$$

$$7/8 = 0, \text{ remainder } 7$$

Therefore, the Octal representation is 7715. By inspection, this can easily be converted to its Decimal representation of 111111001101 if needed.

Conversion from Octal to Decimal:

1. Multiply the most significant Octal digit by 8.
2. Add the next most significant Octal digit and multiply the sum by 8.
3. Repeat step 2 until the least significant digit is reached.
4. Lastly, add the least significant Octal digit. Do not multiply the final sum by 8.

REFERENCES

- American Society of Civil Engineers Committee on Deep Foundations, Practical Guidelines for the Selection, Design, and Installation Piles, American Society of Civil Engineers, New York, 1984.
- C. R. Bard Incorporated, Coronary Balloon Dilatation Catheter, Product Information Pamphlet, Billerica, Massachusetts, 1985.
- Bradley, D. M., "Scaling Laws for Centrifugal Testing of GLCM Shelter," Master's Report, University of Florida, Gainesville, Florida, December, 1983.
- Bradley, D. M., Townsend, F. C., Fagundo, F. E., and Davidson, J. L., Centrifugal Scaling Laws for Ground Launch Cruise Missile Shelter, ESL-TR-84-07, Air Force Engineering and Services Center, Tyndall Air Force Base, Florida, April 1984.
- Brierly, G. S., Thompson, D. E., and Eller, C. W., "Interpreting End-Bearing Pile Load Test Results," Behavior of Deep Foundations, edited by R. Lundgren, ASTM Special Technical Publication 60, American Society for Testing and Materials, Philadelphia, Pennsylvania, 1979, pp. 42-67.
- Buchsbaum, W. H., "Buchsbaum's Complete Handbook of Practical Electronic Reference Data," Prentice-Hall Inc., Englewood Cliffs, New Jersey, 1973.
- Butterfield, R., and Banerjee, P. K., "The Problem of Pile Group-Pile Cap Interaction," Geotechnique, Vol. 21, No. 2, June 1971, pp. 135-142.
- Cheeks, J. R., "Analytical Methods to Predict Pile Capacities," Behavior of Deep Foundations, edited by R. Lundgren, ASTM Special Technical Publication 60, American Society for Testing and Materials, Philadelphia, Pennsylvania, 1979, pp. 310-317.
- Chellis, R. D., Pile Foundations Theory, Design, Practice, First Edition, McGraw-Hill Inc., New York, 1951.
- Cho, Y. Y., "Design Considerations Using SPT's," Proceedings, 13th Ohio River Valley Soils Seminar, Lexington, Kentucky, October 8, 1982, American Society of Civil Engineers, New York, 1982, pp. 102-107.
- Comptrol Incorporated, Comptrol Ball Screw Nut Assemblies Technical Handbook, Comptrol Bulletin C-30, Cleveland, Ohio, 1984.

- Coyle, H. M., and Castello, R. R., "New Design Correlations for Piles in Sand," Journal of the Geotechnical Engineering Division, American Society of Civil Engineers, Vol. 107, No. GT7, 1981, pp. 965-986.
- Dally, J. W., and Riley, W. F., Experimental Stress Analysis, McGraw-Hill Inc., New York, New York, 1973.
- Das, B. M., Principles of Foundation Engineering, Wadsworth, Inc., Brooks/Cole Engineering Division, Belmont, California, 1984.
- Davidson, J. L., and Boghrat, A., "Displacements and Strains Around Probes in Sands," Proceedings, ASCE Specialty Conference, Geotechnical Practice in Offshore Engineering, Austin, Texas, April 27-29, 1983, American Society of Civil Engineers, New York, 1983, pp. 131-202.
- Davisson, M. T., "Stresses in Piles, Behavior of Deep Foundations," Behavior of Deep Foundations, edited by R. Lundgren, ASTM Special Technical Publication 60, American Society for Testing and Materials, Philadelphia, Pennsylvania, 1979, pp. 183-193.
- Deep Foundations Institute, A Pile Inspector's Guide to Hammers, Springfield, New Jersey, 1979a.
- Deep Foundations Institute, Inspector's Manual for Pile Foundations, Springfield, New Jersey, 1979b.
- Desai, C. W., and Abel, J. F., Introduction to the Finite Element Method, Van Nostrand, New York, New York, 1972.
- Dismuke, T. D., "Behavior of Steel Piles During Installation and Service," Behavior of Deep Foundations, edited by R. Lundgren, ASTM Special Technical Publication 60, American Society for Testing and Materials, Philadelphia, Pennsylvania, 1979, pp. 194-205.
- Dove, R. C., and Adams, P. H., Experimental Stress Analysis and Motion Measurements, C. E. Merrill Books, Columbus, Ohio, 1964.
- Dwyer, T. A., and Kaufman, M. S., Computer Programming in Basic for Everyone, Houghton-Mifflin Corporation, Fort Worth, Texas, 1973.
- Ellison, R. D., "An Analytical Study of the Mechanics of Single Pile Foundations," Ph.D. Dissertation, Carnegie-Mellon University, Pittsburgh, Pennsylvania, 1969.
- Epsilonics Staff Writers, "The Three-Wire Quarter Bridge Circuit," Epsilonics, Vol. 3, No. 2, August 1983, pp. 1-3.
- Ferguson, K. A., "Centrifugal Modeling of the Quasi-Static Cone Penetrometer," Master's Report, University of Colorado, Boulder, Colorado, 1983.

- Fitzgerald H. K., Higginbotham, B. M., and Grabel, T. W., Basic Electrical Engineering, Fourth Edition, McGraw-Hill Inc., New York, New York, 1975.
- Gill, J. J., "Centrifugal Modeling of a Subterranean Structure Subjected to Blast Loading," Master's Report, University of Florida, Gainesville, Florida, 1985.
- Gill, J. J., and Kofoid, N., Programs Developed for Use in the University of Florida Geotechnical Centrifuge (GEOCENT), Internal Report, University of Florida, Gainesville, Florida, April 1988.
- Gupta, R. C., "Determination of the Insitu Coefficients of Consolidation and Permeability of Submerged Soils Using Electrical Piezocone Soundings," Ph.D. Dissertation, University of Florida, Gainesville, Florida, 1983.
- Harrison, F. R., "Centrifugal Monitoring of Axially and Laterally Loaded Piles and Pile Groups in Clay," Master's Report, University of Colorado, Boulder, Colorado, 1983.
- Hery, P., "Residual Stress Analysis in WEAP," Master's Report, University of Colorado, Boulder, Colorado, 1983.
- Hewlett-Packard Part Number 59500-90005, Hewlett-Packard 6940B "Multi-programmer User's Guide, Hewlett-Packard, Orlando, Florida, 1976.
- Holloway, D. M., Wave Equation Analysis of Pile Driving, Technical Report S-75-5, Soils and Pavements Laboratory, United States Army Engineer Waterways Experiment Station, Vicksburg, Mississippi, June 1975.
- Holloway, D. M., Clough, G. W., and Vesic, A. S., "A Rational Procedure for Evaluating the Behavior of Impact-Driven Piles," Behavior of Deep Foundations, edited by R. Lundgren, ASTM Special Technical Publication 60, American Society for Testing and Materials, Philadelphia, Pennsylvania, 1979, pp. 261-293.
- Hougnon, J. H., "Centrifugal Modeling of Axially Loaded Piles," Master of Science Thesis, University of Colorado, Boulder, Colorado, 1980.
- Ireland, H. O., Moretto, O., and Vargas, M., "The Dynamic Penetration Test: A Test that is Not Standardized," Geotechnical Journal, Vol. 20, No. 2, June 1970, pp. 185-192.
- Ko, H. Y., Atkinson, R. H., Goble, G. G., and Ealy, C. D., "Centrifugal Modeling of Pile Foundations," Analysis and Design of Pile Foundations, edited by J. R. Meyer, American Society of Civil Engineers Publications, New York, 1984, pp. 127-143.
- Kolsky, H., Stress Waves in Solids, Dover Publications, New York, 1963.

- Knapos, D. K., "Wave Equation Study and Recommended Specifications for the Impact Driving of Pre-Stressed Concrete Piles," Ph.D. Dissertation, University of Florida, Gainesville, Florida, June 1977.
- Lambe, T. W., and Whitman, R. V., Soil Mechanics, John Wiley and Sons, New York, New York, 1969.
- Langhaar, H. L., Dimensional Analysis and Theory of Models, John Wiley and Sons, New York, New York, 1951.
- Lenk, J. D., Handbook of Microcomputer-Based Instrumentation and Controls, Prentice-Hall Inc., Englewood Cliffs, New Jersey, 1984.
- Liao, S. S. C., and Whitman, R. V., "Overburden Correction Factors for SPT in Sand," American Society of Civil Engineers Journal, Vol. 112, No. 1, March 1986, pp. 373-377.
- Lundgren, R., (Ed.), Behavior of Deep Foundations, ASTM Special Technical Publication 60, American Society for Testing and Materials, Philadelphia, Pennsylvania, 1979.
- Lynch, J. E., and Higgins, C. J., "The Effects of Gravity on the Bearing Capacity of Cohesionless Soils," Master's Report, Air Force Institute of Technology, Wright-Patterson Air Force Base, Ohio, August 1964.
- Manzoori, M., "Centrifugal Testing of Model Piles and Pile Groups," Master's Report, University of Colorado, Boulder, May 1987.
- Marcuson, W. F., III, and Bieganousky, W. A., "Laboratory Standard Penetration Tests on Fine Sands," Journal of the Geotechnical Engineering Division, Vol. 103, June 1977a, pp. 565-588.
- Marcuson, W. F., III, and Bieganousky, W. A., "SPT and Relative Density in Coarse Sands," Journal of the Geotechnical Engineering Division, Vol. 103, November 1977b, pp. 1295-1309.
- Measurements Group Incorporated, Errors Due to Misalignment of Strain Gages, Technical Note 511, Raleigh, North Carolina, 1983a.
- Measurements Group Incorporated, Strain Gage Selection, Technical Note 505, Raleigh, North Carolina, 1983b.
- Measurements Group Incorporated, Techniques for Bonding Leadwires to Surfaces Experiencing High Centrifugal Forces, Technical Note 601, Raleigh, North Carolina, 1983c.
- Measurements Group Incorporated, Experimental Stress Analysis Notebook, Issue 7, The Strain Gage Measurement System, Raleigh, North Carolina, 1987.
- Meyerhoff, G. G., "Bearing Capacity and Settlement of Pile Foundations," Journal of the Geotechnical Engineering Division, American Society of Civil Engineers, Vol. 102, 1976, No. GT3, pp. 197-228.

- Micro-Measurements, Strain Gage Installations, Instruction Bulletin 3-100-2, July 1972.
- Millan, A. A., 'Centrifuge Modeling of Pile Groups in Sand,' Ph.D. Dissertation, University of Florida, Gainesville, Florida, August 1985.
- Montgomery, W. M., "Pile Load Tests to Evaluate Load Transfer," Behavior of Deep Foundations, edited by R. Lundgren, ASTM Special Technical Publication 50, American Society for Testing and Materials, Philadelphia, Pennsylvania, 1979, pp. 86-103.
- Nataraja, M. S., and Cook, B. E., "Increase in SPT n Values Due to Displacement Piles," American Society of Civil Engineers Journal, January 1983.
- Nielsen, J. P., The Centrifugal Simulation of Blast Parameters, ESL-TR-83-12, Air Force Engineering and Services Center, Tyndall Air Force Base, Florida, December 1983.
- O'Neill, M. W., "Hunters Point Pile Project," Draft Report, University of Houston-University Park, Houston, Texas, 1986.
- Palacios, A., "The Theory and Measurement of Energy Transfer During Standard Penetration Test Sampling," Ph.D. Dissertation, University of Florida, Gainesville, Florida, 1977.
- Peck, R., Hanson, W., and Thornburn, T., Foundation Engineering, John Wiley and Sons, New York, New York, 1974.
- Pokrovsky, G. I., and Fyodorov, I. S., "Centrifugal Model Testing in the Construction Industry, Vol. 1, Model Testing of Static Processes in Soils and Structures," Draft Translation prepared by Building Research Establishment Library Translation Service, August 1975.
- Reese, L. C., "Design and Evaluation of Load Tests on Deep Foundations," Behavior of Deep Foundations, edited by R. Lundgren, ASTM Special Technical Publication 60, American Society for Testing and Materials, Philadelphia, Pennsylvania, 1979, pp. 227-244.
- Richart, F. E., Hall, J. R., and Woods, R. D., Vibrations of Soils and Foundations, Prentice-Hall, Englewood Cliffs, New Jersey, 1970.
- Rocha, M., The Possibility of Solving Soil Mechanics Problems by the Use of Models, Fourth International Conference on Soil Mechanics and Foundation Engineering, Book 1, 1957.
- Rockford Ball Screw Company, Rockford Ball Screw Technical Handbook, Manual 101-B, Rockford Ball Screw Company, Rockford, Illinois, 1986.
- Ryan, W. F., "Centrifuge Modeling of Axially Loaded Piles in Sand," Master's Report, University of Florida, Gainesville, Florida, December, 1983.

- Saffery, M. R., and Tate, A. P. K., Model Tests on Pile Groups in a Clay Soil with Particular Reference to the Behavior of the Group When it is Loaded Eccentrically, Fifth International Conference on Soil Mechanics and Foundation Engineering, Book 2, 1961.
- Sands, L. G., and Mackenroth, D. R., Encyclopedia of Electronic Circuits, Parker Publishing Company Inc., West Nyack, New York, 1975.
- Sanglerat, G., Developments in Geotechnical Engineering; Interpretation of Penetration Diagrams - Theory and Practice, Elsevier Publishing Company, New York, New York, 1972.
- Schmertmann, J. H., and Palacios, A., "Energy Dynamics of SPT," Journal of the Geotechnical Engineering Division, Vol. 103, GT3, August 1977.
- Schofield, A. N., Centrifuge Studies, PB82-226592, Cambridge, England, 1982.
- Scott, R. F., Centrifuge Studies of Cyclic Lateral Load-Displacement Behavior of Single Piles, Report to American Petroleum Institute, OSAPR Project 8, 1977.
- Seereeram, D., "Plasticity Theory for Granular Media", Ph.D. Dissertation, University of Florida, Gainesville, Florida, 1987.
- Sharp, M., McVay, M., Townsend, F., and Basnett, K., Evaluation of Pile Capacity from Insitu Test, University of Florida Geotechnical Group handout for training conducted at the University of Florida, Gainesville, Florida, 1987.
- Shin, E. C., "On Pile-Soil Load Transfer," Master's Report, University of Colorado, Boulder, Colorado, April 1987.
- Smith, E. A. L., "Pile Driving Analysis by the Wave Equation," Soil Mechanics and Foundations Division, American Society of Civil Engineers Journal, Vol. 86, No. SM4, Proceedings Paper 2574, August 1960.
- Sowers, G. F., Martin, C. B., Wilson, L. L., and Fausold, M., The Bearing Capacity of Friction Pile Groups in Homogeneous Clay from Model Studies, Fifth International Conference on Soil Mechanics and Foundation Engineering, Book 2, 1961.
- Tabatabai, H., "Centrifugal Modeling of Underground Structures Subjected to Blast Loading," Ph.D. Dissertation, University of Florida, Gainesville, Florida, 1987.
- United States Department of Transportation/Federal Highway Administration, Report Number FHWA/RD-84-001, "Centrifugal Testing of Model Piles and Pile Groups," Executive Summary, November 1984a.

- United States Department of Transportation/Federal Highway Administration, Report Number FHWA/RD-84-004, "Centrifuge Tests in Clay," November 1984b.
- United States Department of Transportation/Federal Highway Administration, Report Number FHWA/RD-84-003, "Centrifuge Tests in Sand," November 1984c.
- United States Department of Transportation/Federal Highway Administration, Report Number FHWA/IP 86/19, "Wave Equation Analysis of Piles," General Users Manual, Vol. 2, 1986.
- Vesic, A. S., "Tests on Instrumented Piles, Ogeechee River Site," Journal of the Soil Mechanics and Foundation Division, Proceedings, American Society of Civil Engineers, March 1970.
- Vesic, A. S., "Design of Pile Foundations," National Cooperative Highway Research Program, Synthesis of Practice Number 42, Transportation Research Board, Washington, D. C., 1978.
- Whitaker, T., "Experiments With Model Piles in Groups," Geotechnique, No., 1957.
- Williams, M., and McFetridge, G., Unbalanced-Bridge Computational Techniques and Accuracy for Multichannel Strain-Measuring Systems, Experimental Techniques, April 1983, pp. 32-37.
- York, D. L., Miller, V. G., and Nabil, F. I., "Long Term Load Transfer in End Bearing Pipe Piles," Transportation Research Board, Record #517, 1974.
- Zienkiewicz, O. C., The Finite Element Method in Engineering Science, McGraw-Hill Inc., New York, 1971.

BIOGRAPHICAL SKETCH

The author [REDACTED]

[REDACTED] the age of 11 attending both public and private schools. Moving to Alexandria, Virginia, he continued his education until obtaining his Bachelor of Science degree in civil engineering at the University of Virginia, Charlottesville. He was subsequently commissioned a Second Lieutenant in the United States Air Force and served tours at Moody Air Force Base, Georgia, Ramstein Air Base, Germany, and Incirlik Air Base, Turkey. His most recent assignment to the Air Force Institute of Technology, serving at the University of Florida, Gainesville, was necessary to attain his Master of Engineering degree, awarded in May of 1986, and his doctorate, expected in August of 1988. Prior to attending the University, he had obtained his master's in business administration from Embry-Riddle Aeronautical University in August of 1981 and had become a private pilot with over 150 hours of flight time. Captain Gill is a graduate of the Air Force's Squadron Officer School and Air Command and Staff College. He is also a member of the Tau Beta Pi engineering honor society, Florida Alpha chapter, and a recipient of The Outstanding Young Men of America award.

[REDACTED]
[REDACTED] Subsequent to the award of this degree, he intends to pursue soil dynamics research at the Air Force Weapons Laboratory, Kirtland Air Force Base, Albuquerque, New Mexico.